http://researchcommons.waikato.ac.nz/

Research Commons at the University of Waikato

Copyright Statement:

The digital copy of this thesis is protected by the Copyright Act 1994 (New Zealand).

The thesis may be consulted by you, provided you comply with the provisions of the Act and the following conditions of use:

- Any use you make of these documents or images must be for research or private study purposes only, and you may not make them available to any other person.
- Authors control the copyright of their thesis. You will recognise the author's right to be identified as the author of the thesis, and due acknowledgement will be made to the author where appropriate.
- You will obtain the author's permission before publishing any material from the thesis.

An Investigation of the Multifunctional Alkylation Chemistry of $[Pt_2(\mu\text{-}S)_2(PPh_3)_4]$

Oguejiofo Theophilus Ujam

An Investigation of the Multifunctional Alkylation Chemistry of $[Pt_2(\mu\text{-}S)_2(PPh_3)_4]$

THE UNIVERSITY OF
WAIKATO
Te Whare Wānanga o Waikato

A thesis submitted in fulfilment
of the requirements for the degree of

Doctor of Philosophy in Chemistry

at

The University of Waikato

by

Oguejiofo Theophilus Ujam

The University of Waikato
2011

Dedication

To my father Chief Francis Ugwu Ujam

and

my late twin brother Uchenna Augustus Ujam whose fond memories I still live with.

Abstract

This thesis presents the studies on the multifunctional alkylation of the metalloligand $[Pt_2(\mu\text{-}S)_2(PPh_3)_4]$ **1.1**. Multifunctional organic groups which include semicarbazone and thiosemicarbazone, urea, isocyanate, guanidine, ketones and amides react with **1.1** to generate the corresponding functionalised derivatives containing thiolate ligands produced by alkylation of one or both sulfide centres. Polymers with suitable electrophilic branches also react to immobilise **1.1**. By using Electrospray Ionisation Mass Spectrometry (ESI-MS) as the monitoring technique, $[Pt_2(\mu\text{-}S)_2(PPh_3)_4]$ was employed as a productive template for structurally and chemically diverse thiolate-platinum complexes. Before this study, **1.1** was known to be one of the best building blocks for multimetallic molecules through the exceptional ligating ability of the two sulfide centres to virtually any transition and main group metal fragment. However, extension of the synthetic versatility of **1.1** to multifunctional non-metallic positive centres has only been explored to a lesser extent and thus far less developed.

This thesis is organised into five chapters. Chapter one is the review of literature on $[Pt_2(\mu\text{-}S)_2(PPh_3)_4]$ and the development of its chemistry from an efficacious metalloligand for multimetallic assembly to a powerful nucleophile for organic electrophiles. The main geometry and electronic features of **1.1** and analogous complexes were highlighted especially as it affects the dihedral angle (θ) between the two Pt_2S_2 planes in $[Pt_2(\mu\text{-}S)_2(PPh_3)_4]$. The variable reaction modes of **1.1** with different electrophiles were discussed especially as it may affect the less studied multifunctional alkylation. The effectiveness of the ESI-MS as a monitoring tool in the study of **1.1** chemistry is also discussed.

Chapter two details the study of the multifunctional monoalkylation reactions of the aforementioned array of multifunctional organic groups with $[Pt_2(\mu\text{-}S)_2(PPh_3)_4]$. Alkylation reaction of **1.1** with organo-halide of the type R–CH_2-X and R–CH_2CH_2-X (R= organic group and X = Cl or Br) formed thiolate-

bridged platinum complexes. The main discovery in this study is that any suitable organic functionality can be incorporated into an electrophile for **1.1**. By using the ESI-MS monitoring technique, they successfully reacted with **1.1** to give novel monoalkylated platinum complexes with μ-thiolate ligands of the type $[Pt_2(\mu\text{-}S)\{\mu\text{-}SR\}(PPh_3)_4](PF_6)$ which included $[Pt_2(\mu\text{-}S)\{\mu\text{-}SCH_2C(=NNHC(O)NH_2)R\}(PPh_3)_4](PF_6)$ in **2.1b·PF$_6$** (R = Ph) and **2.2b·PF$_6$** (R = CH_3) and $[Pt_2(\mu\text{-}S)\{\mu\text{-}SR\}(PPh_3)_4](PF_6)$ (R = $-CH_2C(=NOH)Ph$ **2.3b·PF$_6$**, $-CH_2C(=NNHC(NH_2)NH_2)Ph$ **2.4b·(PF$_6$)$_2$**, $-CH_2C(=NNHC(S)NH_2)CH_3$ **2.5b·PF$_6$**, $-CH_2CH_2NHC(O)NHPy$ **2.6b·PF$_6$** (Py = *o*-C_5H_4N), $-CH_2CH_2NHC(O)N(CH_2CH_2)_2S$ **2.7b·PF$_6$** and $-CH_2C(O)NHC(O)NHCH_2CH_3$ **2.8b·PF$_6$**. $-CH_2C(=NNHTs)Ph$ **2.9b·PF$_6$**, $-CH_2C(=NNHTs)CH_3$ **2.10b·PF$_6$** (Ts = $-SO_2C_6H_4CH_3$), $-CH_2C(=NHNC(O)Py)Ph$ (Py = *o*-C_5H_4N) **2.11b·PF$_6$** and $-CH_2C(=NNHC(O)NH_2)C_6H_4C_6H_5$ **2.12b·PF$_6$**. Geometrical isomers formed with $BrCH_2C(NNHAr)C_6H_4Ph$ **2.13a** (Ar = 2,4-dinitrophenyl) was studied and characterised with 2D NMR techniques. The X-ray crystal structures of **2.1b·PF$_6$**, **2.4b·(PF$_6$)$_2$**, **2.7b·PF$_6$** and **2.8b·PF$_6$** are also reported.

Chapter three reports an investigation of conditions that encourage the formation of homo- and heterodialkylated thiolate complexes of the type $[Pt_2(\mu\text{-}SR)_2(PPh_3)_4]^{2+}$ and $[Pt_2(\mu\text{-}SR)\{\mu\text{-}SR'\}(PPh_3)_4]^{2+}$ since these are currently not well understood. The factors were employed in the selective choice of alkylating agents used in the sequential syntheses of homodialkylated derivatives $[Pt_2(\mu\text{-}SCH_2COPh)_2(PPh_3)_4](PF_6)_2$ **3.1b·(PF$_6$)$_2$**, $[Pt_2(\mu\text{-}SCH_2C(O)pyr)_2(PPh_3)_4](PF_6)_2$ (pyr = pyrene) **3.2b·(PF$_6$)$_2$** and $[Pt_2(\mu\text{-}SCH_2C(O)cyl)_2(PPh_3)_4](PF_6)_2$ (cyl = coumaryl) (**3.4b·(PF$_6$)$_2$**. A major outcome of this study is the successful syntheses of the heterodialkylated derivatives $[Pt_2(\mu\text{-}SCH_2C(O)Ph)(\mu\text{-}SBu)(PPh_3)_4](PF_6)_2$ **3.5b·(PF$_6$)$_2$** and $\{Pt_2(\mu\text{-}SCH_2COPh)(\mu\text{-}SCH_2CH_3)(PPh_3)_4\}(PF_6)_2$ **3.6b·(PF$_6$)$_2$** through a sequential alkylation with organo-halide electrophiles. The X-ray crystal structures of **3.1b·(PF$_6$)$_2$** and **3.5b·(BPh$_4$)$_2$** are reported. The secondary products resulting from the displacement of a PPh_3 by Br^- in the synthesis of the heterodialkylated derivatives **3.5b·(PF$_6$)$_2$** and **3.6b·(PF$_6$)$_2$**, $[Pt_2(\mu\text{-}SCH_2C(O)Ph)(\mu\text{-}SBu)(PPh_3)_3Br](PF_6)$ **3.5c·PF$_6$** and $[Pt_2(\mu\text{-}SCH_2COPh)(\mu\text{-}SCH_2CH_3)(PPh_3)_3Br](PF_6)$ **3.6c·PF$_6$** were also isolated and characterised by ESI-MS and X-ray crystallography.

Chapter four describes the multifunctional intra- and intermolecular bridging dialkylation of **1.1**. The variable alkylation mode of α,ω-dialkylating electrophiles, which is dependent on the nature and the number of spacer atoms, was investigated with functionalised electrophiles, $ClCH_2C(O)CH_2Cl$ **4.1a**, $ClCH_2C(NNHC(O)NH_2)$ CH_2Cl **4.2a** and $ClCH_2C(O)NHNHC(O)CH_2Cl$ **4.3a**. A very important novel result is the stabilisation and isolation of an intramolecular bridged five-membered ring derivative **4.1b·PF_6** $[Pt_2\{\mu\text{-}SCH_2C(O)CHS\}(PPh_3)_4](PF_6)$. The reaction of **4.1a** with **1.1** in the presence of dilute aqueous NaOH aided the isolation of **4.1b·PF_6** resulting from intramolecular rearrangement of the four membered ring. The semicarbazone derivative **4.2a** and diamide **4.3a** dialkylated **1.1** by bridging the two sulfide centres to form stable $[Pt_2\{\mu\text{-}SCH_2C(NNHC(O)NH_2)CH_2S\text{-}\mu\}(PPh_3)_4](BPh_4)_2$ **4.2b·$(BPh_4)_2$** and $Pt_2\{\mu\text{-}SCH_2C(O)NHNH(O)CH_2S\}(PPh_3)_4(PF_6)_2$ **4.3b·$(PF_6)_2$**. Both **4.1b·PF_6** and **4.2b·$(BPh_4)_2$** were characterised by X-ray crystallography. The syntheses and X-ray crystal structure analysis of Pt_4 aggregates formed with amide α,ω-dialkylating agents with longer spacer atoms, *o*- and *p*-$ClCH_2C(O)NHC_6H_4NHC(O)CH_2Cl$ through the intermolecular linking of two $[Pt_2(\mu\text{-}S)_2(PPh_3)_4]$ complexes is also reported.

Chapter five is the investigation of the immobilisation of $[Pt_2(\mu\text{-}S)_2(PPh_3)_4]$ on electrophilic polymer supports. Following the reactivity of $[Pt_2(\mu\text{-}S)_2(PPh_3)_4]$ with electrophiles established in chapter two a monomeric electrophilic unit 3-chloropropyltetraethoxysilane **5.1a** reacted **1.1** to give **5.1b.BPh_4**. Further investigations to immobilised **1.1** on solid polymer supports through the alkylation of one of the sulfide centres with electrophilic polymers, Merrifield's resin **5.2a**, 3-bromopropylpolysiloxane **5.3a** 3-chloropropyl silica **5.4a** and 3-chloropropyl controlled pore glass **5.5a** were done. This gave the corresponding immobilised products which is generally represented as $[Pt_2(\mu\text{-}S)(\mu\text{-}SCH_2R\text{–}P)(PPh_3)_4]$ (where R = phenyl or $\text{-}CH_2CH_2\text{-}$ groups). The immobilisation of **1.1** was also achieved through phosphine exchange reactions on polymers, a polyethertriamine phosphine derivative **5.6a** and diphenylphosphine polystyrene **5.8a**. The products were characterised by Scanning Electron Microscopy, solid state $^{31}P\{H\}$ (CP MAS) NMR, Inductively Coupled Plasma Mass Spectrometry (ICP-MS) and X-ray Photoelectron Spectroscopy (XPS).

Acknowledgments

The completion of this research project is both a humbling experience and a daunting task. Thankfully, numerous talented people helped, and their collective efforts have greatly improved the final result. First and foremost I appreciate the privileged to enjoy excellent supervision by Professors William Henderson and Brian K. Nicholson with whom I consulted throughout the project. Their profound understanding of the chemical ideas and facts in the work helped in shaping every stage of this research.

In addition to supervision, a large number of other scientific professionals and institutions played important roles in this project. Their contributions of time and experiences added immeasurably to the relevance and accuracy of the outcome of this research. I owe special thanks to our collaborator Prof. T. S. A. Hor of the Chemistry Department, National University of Singapore for sharing his research ideas in this work; Pat Gread and Wendy Jackson of the Department of Chemistry, University of Waikato for all their assistance with ESI-MS; Steve Cameron for platinum analysis with ICP-MS; Prof. Alistair Wilkins for help with advanced and specialised NMR techniques; Assoc. Prof. Lyndsay Main for advice on organic synthesis; Dr. Michael Mucalo for assistance with Solid State $^{31}P\{H\}$ NMR and XPS data interpretation and my co-research students Stephen Gardyne, Narendra Prasad, Toshie Asamizu, Peter Wilson, Simon Addison and others whose different but encouraging laboratory behaviours propelled the eagerness to work through this research. I am also thankful to Assoc. Prof. Jadranka Travas-Sejdic and Dr. Lijuan Zhang of the Chemistry Department and Dr. Colin Doyle of the Department of Chemical and Materials Engineering University of Auckland for help with acquiring and interpreting XPS data.

My family were most supportive during this research. I am thankfully grateful to my wife Amarachi for her understanding and support; my son Uchenna for always waking me up in the middle of night with his cries to work on this

thesis; my parents for their encouragement and support; my brother, Ujam and my sister, Ngozi for their supportive concerns.

I am very grateful to Education New Zealand for a Study Abroad Scholarship, the Department of Chemistry, University of Waikato for financial support, and the University of Waikato for a University of Waikato Doctoral Scholarship.

Table of Contents

List of Tables

List of Figures

List of Schemes

List of General Abbreviations

Å	Angstrom
COSY	correlation spectroscopy
HSQC	Heteronuclear Single Quantum Coherence
calc	calculated
d	doublet (NMR)
ESI-MS	electrospray ionisation mass spectrometry
IR	infrared spectroscopy
J	coupling constant (NMR)
M	metal species
$[M]^{n+}$	molecular ion (ESI-MS)
m	multiplet (NMR)
m.p.	melting point
m/z	mass to charge ratio
NMR	nuclear magnetic resonance
o	*ortho*
p	*para*
ppm	part per million
s	singlet (NMR)
t	triplet (NMR)
X	halide
ν	stretch (IR)
δ	bend (IR)

List of Chemical Abbreviations

Ar	2,4-dinitrophenyl
Bu	butyl
$CDCl_3$	deuterated chloroform
CD_2Cl_2	deuterated dichloromethane
D_2O	deuterium oxide
$(CD_3)_2SO$	deuterated dimethyl sulfuroxide
cod	cycloocta-1,5-diene
CPG	controlled pore glass
cyl	coumaryl
DPP	diphenylpolystyrene
dppe	1,2-bis(diphenylphosphino)ethane
dppf	1,1'-bis(diphenylphosphino)ferrocene
dppm	bis(diphenylphosphino)methane
dppp	1,3-bis(diphenylphosphino)propane
dppy	2-diphenylphosphinopyridine
Et	ethyl
L	ligand
Me	methyl
MR	Merrifield’s Resin
P	polyether triamine-Merifield’s resin
Ph	phenyl
PPS	polypropyl siloxane
PS	propylsilica
pyr	pyreryl
Py	pyridyl
R	organic substituent
THF	Tetrahydrofuran
tolpy	4-(2-pyridyl)-3-tolyl

Ts	$-SO_2C_6H_4CH_3$
pap	2-(2-pyridylamino)phenyl
acac	2,4-pentanedionate
bipy	2,2'-bipyridine

Chapter 1

Review of the Literature on $[Pt_2(\mu\text{-}S)_2(PPh_3)_4]$

1.1 Introduction

The rich individual chemistries of platinum and sulfur have been the subject of extensive systematic studies since the discoveries of both elements. Both have retained the interest of many researchers due to the wide range of applications of the two elements and their compounds. Since its discovery in South America by Antonio de Ulloa in 1735, platinum and many of its compounds have been extensively used in catalysis[1-5], jewellery, wires[6, 7], synthesis of biologically active coordination compounds and antitumor drugs[8] e.g. *cis*-$PtCl_2(NH_3)_2$ {*cis*-diaminedichloridoplatinum(II)} and synthetic precursors e.g. *cis*-$PtCl_2(PPh_3)_2$[9, 10]. Platinum readily forms coordination compounds with interesting properties and exists in variable oxidation states ranging from 0 to +6, including non-even[11] with +1 and +3 found in dinuclear Pt-Pt bonded complexes.

Sulfur also exhibits interesting chemical properties particularly as a versatile coordinating ligand. The versatility of sulfur as a ligand is demonstrated by its ability to catenate forming polysulfido ligands (S_n^{2-}) where n is up to 8. It also has the tendency to extend its coordination from terminal groups e.g. $[Mo_2S_{10}]^{2-}$)[12], to μ-sulfido group e.g. $[Pt_2(\mu\text{-}S)_2(PPh_3)_4]$[10] and to an encapsulated form e.g. $[Rh_{17}(S)_2(CO)_{32}]^{3-}$ which consist of a S-Rh-S moiety in the cavity of a rhodium-carbonyl cluster[13]. The coordination chemistry of sulfur ligands is extensively manifested in the unique variety of structures it forms with most of the transition metals in different oxidation states[14].

The exceptional ability of sulfur to bind to heavy metals is not only evidenced by the extensive attention metal sulfide compounds have attracted but also because of their structural diversity[15] and applications. The ready combination of sulfur and metal centres can be exemplified by the occurrence of platinum (and its group congeners palladium and nickel) and sulfur in natural occurring ores e.g. Cooperite ($Pt_{0.6}Pd_{0.3}Ni_{0.1}S$)[16, 17] and Braggite ($Pt_{0.38}Pd_{0.50}Ni_{0.10}S_{1.02}$)[17]. Interest in platinum–sulfur complexes has been augmented by the use of platinum compounds like *cis*-platin as an anti-cancer drug. The high reactivity between sulfur and organo thiolate compounds with platinum is implicated in the studies of the nephrotoxicity and resistance associated with platinum based anti-cancer drugs[18]. It was found that the therapeutic drawbacks associated with platinum based drugs is largely associated with strong and irreversible binding of the platinum atom in the drugs to intracellular thiolate ligands such as glutathione[18]. Investigation for solutions to the problem also provided the drive for further studies into platinum sulfur complexes.

Considering that the first platinum-sulfur complex, $(NH_4)_2[Pt(\eta^2\text{-}S_5)_3]$, was isolated in 1903[19] and the essential role of metal sulfide compounds in catalysis[20], and rich solid-state and bioinorganic chemistry[21], the development of platinum sulfide complexes has not received much attention for many years. Enthusiastic studies in platinum sulfide chemistry and its development from simple co-ordination compounds to a unique class of binuclear chalcogenide metalloligand compounds containing the $\{Pt_2(\mu\text{-}S)_2\}$ core started with the pioneering work of Chatt and Mingos in 1970[9]. This was followed by Ugo *et al*[10] a year later in the study of the reactions of zerovalent platinum phosphine complexes with H_2S and elemental sulfur to give di-μ-sulfidotetrakis-(triphenylphosphine) diplatinum(II) $[Pt_2(\mu\text{-}S)_2(PPh_3)_4]$ **1.1**. This initial work initiated the emergence of **1.1** as a molecular "trap" for almost any metal fragment and organic electrophiles. In the past two decades, many investigations have been carried out into the reactivity of **1.1** as well as its selenide analogue $[Pt_2(\mu\text{-}Se)_2(PPh_3)_4]$ as a metalloligand towards a wide range of transition and main group metal fragments[22-33]. Other analogues with different terminal ligands include $[Pt_2(\mu\text{-}S)_2(PPh_2Py)_4]$[34] **1.2**, $[Pt_2(\mu\text{-}S)_2(dppf)_2]$[19] **1.3**, $[Pt_2(\mu\text{-}S)_2(dppe)_2]$[35] **1.4**, $[Pt_2(PMe_2Ph)_4(\mu\text{-}S)_2]$[36] **1.5** and $[Pt_2(\mu\text{-}S)_2(dppp)_2]$ **1.6** [37]. However, **1.1** is by far

the most extensively studied. The development of the chemistry of **1.1** and the other sulfide-bridged complexes with the $\{Pt_2(\mu\text{-}S)_2\}$ core, as well as the advances in the synthesis of its derivatives, structures, and reactivities have been highlighted in excellent reviews by Fong and Hor[38] and González-Duarte[39]. This review is therefore mainly focused on $[Pt_2(\mu\text{-}S)_2(PPh_3)_4]$ and associated compounds thereof.

1.2 Syntheses of $[Pt_2(\mu\text{-}S)_2(PPh_3)_4]$ and Other Analogues

$[Pt_2(\mu\text{-}S)_2(PPh_3)_4]$, as well as other closely related complexes, can be synthesised through a number of routes as shown in Scheme 1.1. The best known method of synthesising pure **1.1** is by the combination and displacement reactions between *cis*-$[PtCl_2(PPh_3)_2]$ and $Na_2S.9H_2O$ in benzene for at least 48 hours. Chlorinated compounds like CH_2Cl_2 are strictly avoided in the synthesis as they reacts to decompose **1.1** through alkylation of the sufides. *Cis*-$[PtCl_2(PPh_3)_2]$ is synthesised by replacing the 1,5-cyclooctadiene (cod) in $[PtCl_2(cod)]$ by 2 mol equivalent of triphenylphosphine. $[PtCl_2(cod)]$ is prepared by metathesis reaction between K_2PtCl_4 and 1,5-cylcooctadiene. K_2PtCl_4 can be made by the reaction of 2 mole equiv. of potassium hexachloroplatinate(IV) ($K_2[PtCl_6]$) and hydrazine dihydrochloride ($N_2H_4.2HCl$) in water.

Other routes to preparing $[Pt_2(\mu\text{-}S)_2(PPh_3)_4]$ **1.1** includes the oxidation reaction of $Pt(PPh_3)_4$ with S_8[10]. The method gives Ph_3PS as a secondary product in **1.1**. Alternatively, the synthesis is achieved through an initial reaction between *cis*-$[PtCl_2(PPh_3)_2]$ and NaSH[34]. This involves the formation of $Pt(SH)_2(PPh_3)_2$ which is further reacted with another 1 mol equivalent of *cis*-$[PtCl_2(PPh_3)_2]$ to yield $[Pt_2(\mu\text{-}S)_2(PPh_3)_4]$ **1.1** and HCl. The resulting HCl reacts with $[Pt_2(\mu\text{-}S)_2(PPh_3)_4]$ to give a secondary product $[Pt_2(\mu\text{-}S)_2(PPh_3)_4.HCl]$. This exists as an impurity in the final product which may not be easily separated and therefore it is not a convenient by-product in the reaction as it may cause the decomposition of $[Pt_2(\mu\text{-}S)_2(PPh_3)_4]$ **1.1** through the $\{Pt_2S_2\}$ core[40].

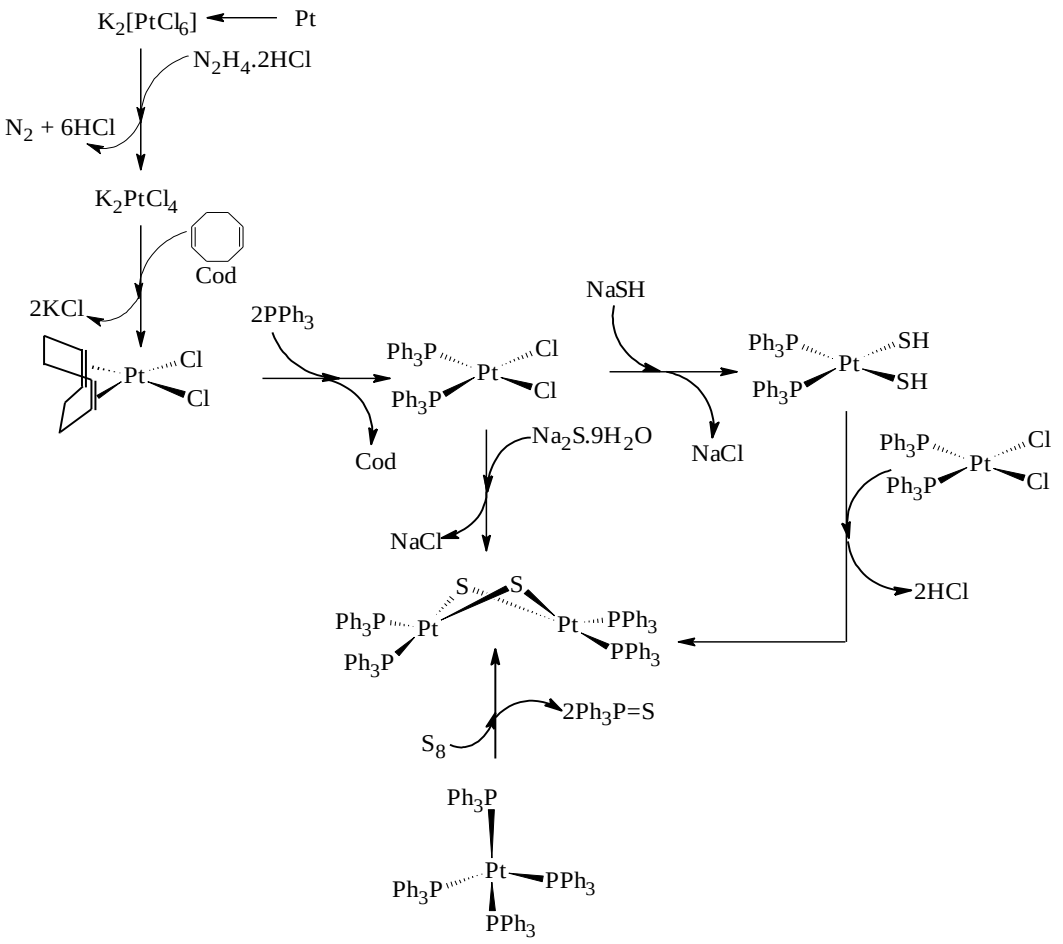

Scheme 1.1 Recommended synthetic routes to $[Pt_2(\mu\text{-}S)_2(PPh_3)_4]$ complex starting from platinum metal. Adapted and modified from González-Duarte, *et al*, Eur. J. Inorg. Chem., 2004, 3585.

1.3 The Main Structural and Electronic Features of $\{Pt_2(\mu\text{-}S)_2\}$ Complexes.

In general the core of **1.1** consists of a four membered $\{Pt_2(\mu\text{-}S)_2\}$ ring with the platinum(II) centres in a square-planar arrangement. A feature of the $\{Pt_2S_2\}$ core is the flexibility of the Pt_1SS and Pt_2SS coordination planes along the S---S axis which adjusts the dihedral angle (θ).

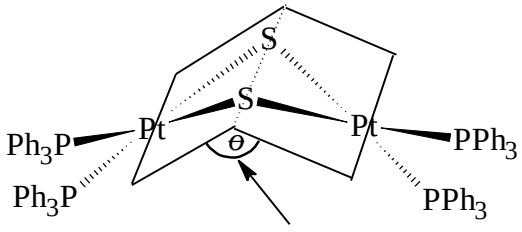

The dihedral angle (θ) as well as the Pt---Pt and S---S distances of separation allows for two possible structural forms. The planar geometry occurs when the angle between the Pt_1SS and Pt_2SS planes is 180^o. The hinged geometry occurs when the angle is less than 180° (Scheme 1.2).

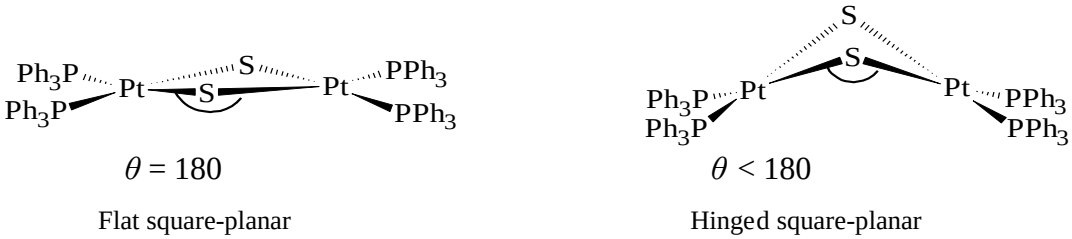

Scheme 1.2 The two possible geometries for complexes with a $\{Pt_2(\mu\text{-}S_2\}$ core.

The reported structural determination of $[Pt_2(\mu\text{-}S)_2(PPh_3)_4]$ **1.1**[41] was erroneous and has been proven to be $[Pt_2(\mu\text{-}OH)_2(PPh_3)_4]^{2+}$ [42]. The actual structure of free **1.1** is therefore not known. The alcohol solvates of **1.1** through hydrogen bond with solvents like ethanol, n-butanol, methanol and hexafluoropropan-2-ol[43] are also known. Other known analogues of **1.1** with different bridging and terminal ligands include; $[Pt_2(\mu\text{-}S)_2(PPh_2Py)_4]$[34] **1.2**, $[Pt_2(\mu\text{-}S)_2(dppf)_2]$[19] **1.3**, $[Pt_2(\mu\text{-}S)_2(dppe)_2]$[35] **1.4**, $[Pt_2(\mu\text{-}S)_2(PMe_2Ph)_4]$[36] **1.5**, $[Pt_2(\mu\text{-}S)_2(dppp)_2]$[37] **1.6** $[Pt_2(\mu\text{-}Se)_2(PPh_3)_4]$[44] **1.1a** and $[Pt_2(\mu\text{-}Te)_2(PPh_3)_4]$[45] **1.1b.** A comparison of some their structural parameters are summarised in Table 1.1 shows a variation in the dihedral angles and other parameters due to different terminal ligands and non- rigid PtX_2 planes.

Table 1.1 Comparison of some structural parameters of compounds with $\{Pt_2(\mu\text{-}X)_2\}$ cores (X = S, Se and Te)

Complex	θ(º)	Pt-X-Pt (º)	Pt---Pt (Å)	X---X (Å)	Ref.
$[Pt_2(\mu\text{-}S)_2(PPh_2Py)_4]$	180.0	99.6	3.55	3.01	34
$[Pt_2(\mu\text{-}S)_2(dppe)_2]$	140.2	88.9	3.29	3.13	35
$[Pt_2(\mu\text{-}S)_2(dppp)_2]$	134.8	87.4	3.23	3.10	37
$[Pt_2(\mu\text{-}S)_2(PMe_2Ph)_4]$	121.0	85.5	3.17	3.06	36
$[Pt_2(\mu\text{-}Se)_2(PPh_3)_4]$	180.0	100.4	3.13	3.76	44
$[Pt_2(\mu\text{-}Te)_2(PPh_3)_4]$	180.0	102.7	3.25	4.10	45

Many compounds derived from **1.1** have been characterised by X-ray crystallography. They show considerable structural diversity as a direct consequence of a non-rigid dihedral angle (*θ)*. The main distinguishing structural feature within this family of compounds is the degree of hinging of the $\{Pt_2(\mu\text{-}S)_2\}$ core. Theoretical studies by Aullón *et al* [46] and Capdevila *et al* [47] on S^{2-} and SR^- bridging ligands show that the degree of bending in $\{M_2(\mu\text{-}X)_2\}$ (X = S, Se, Te; M= metal) complexes is dependent on a number of factors. In general, the bending is driven by the attractive metal---metal interaction between the d_z^2 and p_z orbitals of two metal atoms, which is controlled by the nature of the metal atom, the terminal ligand and the bridging atom. Generally, the bending decreases down a group of the bridging atoms (S, Se and Te). Complexes with Se^{2-} and Te^{2-} as the bridging ligands are planar when compared with S^{2-} as the bridging atom. This is because of the larger atomic size of Se^{2-} and Te^{2-} and consequently increased steric repulsion of the terminal PPh_3 ligands. Consequently, the reduction in the folding of the $\{Pt_2(\mu\text{-}X)_2\}$ ring increases the dihedral angle.

The tendency to form bent structures also increases with the diffuseness of the metal atomic orbitals and the σ-donor ability of the terminal ligands and with decreasing electronegativity of the bridging atoms[39]. On the basis of these general rules complexes derived from $\{Pt_2(\mu\text{-}S)_2\}$ core with phosphine terminal ligands are therefore expected to adopt hinged structures. However, steric interactions between terminal ligands may limit the extent of folding of the $\{Pt_2(\mu\text{-}S)_2\}$ core. A trend with an increase in the size of the terminal ligand as can be seen in Table 1.1. The dihedral angle in **1.1** is therefore expected to be increased due to the bulkiness of the terminal PPh_3 ligands.

1.4 Effect of Metallation or Alkylation on the Geometry of $\{Pt_2(\mu\text{-}S)_2\}$ core

Metallation or alkylation of **1.1** affects the geometry of the $\{Pt_2(\mu\text{-}S)_2\}$ core. In monoalkylated derivatives, electronic factors rather than the nature of organic R group attached to the bridging sulfur ligands in **1.1** influence the geometry of the $\{Pt_2(\mu\text{-}S)_2\}$ ring[47]. The conformation is dependent on the attaching position and size of the metal fragment or the incorporated thiolate

group (SR). The various conformations that could be adopted are in Scheme 1.3. When both sulfur atoms are metallated or alkylated (homo- or heterodialkylated), the attached groups could be on the opposite side of the $\{Pt_2(\mu\text{-}S)_2\}$ ring and adopt *anti*- conformation (**a**) which results in a planar geometry (hinge angle = 180º) as in $[Pt(\mu\text{-}SAuCl)_2(PPh_3)_4]$[48], $[Pt(\mu\text{-}SAgCl)_2(PPh_3)_4]$[49] and $\{[(dppp)Pt\{\mu\text{-}S(CH_2)_2NHC(=O)NHEt\}]_2\}^{2+}$ [50]. In addition, in the *anti* configuration the through-ring antibonding interaction is weaker and thus the geometry is planar. When the incorporated group is attached on the same sides of the ring system and adopt the *syn*- conformation which results increased sterric repulsion between the incorporated group and the terminal ligands resulting in the hinged geometry and reduced dihedral angle (< 180º) e.g. $[Pt_2(\mu\text{-}SC_{10}H_{10}N_2)_2(PPh_3)_4]^{2+}$[51]. The *syn*-configuration also gives rise to stronger through-ring antibonding interaction and folding of the $\{Pt_2(\mu\text{-}S)_2\}$ core[47]. The *syn*- conformations (**b**) - (**f**) (Scheme 1.3) are common and there are many reported examples of these conformations among the metallated and alkylated $\{Pt_2(\mu\text{-}S)_2\}$ complexes.

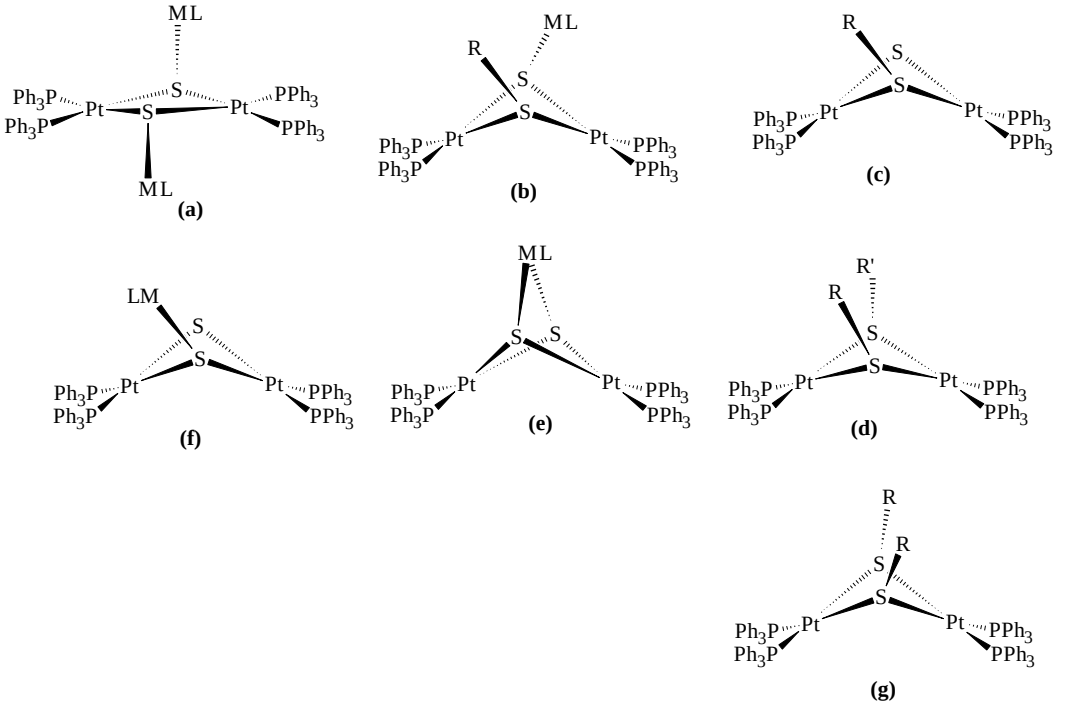

Scheme 1.3 Conformational preferences of the metallated and alkylated derivatives of $[Pt_2(\mu\text{-}S)_2(PPh_3)_4]$ complexes.

Selected examples of the $[Pt_2(\mu\text{-}S)_2(PPh_3)_4]$ derived complexes and their dihedral angles are listed in Tables 1.2 and 1.3 respectively. There are no definite trends in the size of the dihedral angle among the metallated and alkylated derivatives. This may be due to crystal packing and electronic forces. However, among the metallated derivatives the dihedral angle increases with increase in atomic radius of the incorporated metal atoms[52]. Among the fragments of the same metal atom as arranged in Table 1.2, the trend also varies with the size of the ligand(s) attached to the incorporated metal centre. For instance the dihedral angle of the $[Pt_2(\mu_3\text{-}S)_2](PPh_3)_4HgCl_2]$[53], $[Pt_2(\mu_3\text{-}S)_2(PPh_3)_4HgPh](BPh_4)$ and $[Pt_2(\mu_3\text{-}S)_2(PPh_3)_4HgPPh_3](PF_6)_2$[53] are 131º, 132º and 133º respectively, showing a progressive increase in the size of the dihedral angle with the size of the attached metal fragments.

Among the alkylated derivatives, θ increases with the bulkiness and spatial conformation of the incorporated organic groups. This is obvious when monoalkylated complexes are compared with dialkylated complexes, e.g. the dihedral angle of $[Pt_2(\mu\text{-}S)(\mu\text{-}SCH_3)(PPh_3)_4](PF_6)$[36] is 138º while for $[Pt_2(\mu\text{-}SCH_3)_2(PPh_3)_4](PF_6)_2$[54] it is 157º. This is understandable as varying degrees of repulsion between the terminal PPh_3 ligands is required to accommodate the attached groups. Among intramolecular bridged alkylated derivatives, it appears that an interplay of steric repulsion forces either between the incorporated group and the terminal PPh_3 or between the four terminal PPh_3 adjust the size of θ. In general, the dihedral angle tends to increase with the length and bulkiness of the bridging electrophile. For example the dihedral angles for $[Pt_2(\mu\text{-}SCH_2CH_2S)(PPh_3)_4](PF_6)_2$, $[Pt_2(\mu\text{-}SCH_2CH{=}CHCH_2S)(PPh_3)_4](BPh_4)_2$, $[Pt_2(\mu\text{-}SCH_2C_6H_4CH_2S)_2(PPh_3)_4](PF_6)_2$ and $[Pt_2(\mu\text{-}S\text{-}o\text{-}CH_2C_6H_4\text{-}C_6H_4CH_2S)(PPh_3)_4](PF_6)_2$ are 124°, 135°, 140° and 147° respectively. The intermolecular bridged derivatives have a similar trend in the size of the dihedral angles as the monoalkylated derivatives since only one of the sulfide is alkylated at each end of the molecule.

Table 1.2 Dihedral angles (θ^o)of selected metallated derivatives of $[Pt_2(\mu\text{-}S)_2(PPh_3)_4]$.

No.	Complex	θ^o	Ref.
	$[Pt_2(\mu_3\text{-}S)(PPh_3)_4Tl](PF_6)$	136	55
	$[Pt_2(\mu_3\text{-}S)_2(PPh_3)_4\}Pd(C_6F_5)_2]$	104	56
	$[Pt_2(\mu_3\text{-}S)_2(PPh_3)_4]Pb(NO_3)_2]$	132	57
	$[Pt_2(\mu_3\text{-}S)_2(PPh_3)_4Pb(NO_3)](PF_6)$	134	57
	$[Pt_2(\mu\text{-}S)_2(PPh_3)_4PbPh_2I](PF_6)$	127	58
	$[Pt_2(\mu_3\text{-}S)_2(PPh_3)_4PdPh(PPh_3)](PF_6)$	126	23
	$[Pt_2(\mu_3\text{-}S)_2(PPh_3)_4Pd(bipy)](PF_6)_2$	131	59
	$[Pt_2(\mu_3\text{-}S)_2(PPh_3)_4PtH(PPh_3)](PF_6)$	131	23
	$[Pt_2(\mu_3\text{-}S)_2(PPh_3)_4Pt(cod)](BF_4)_2$	130	59
	$[Pt_2(\mu_3\text{-}S)_2(PPh_3)_5PtCl](PF_6)$	128	60
	$[Pt_2(\mu_3\text{-}S)_2(PPh_3)_4GaCl_2](GaCl_4)$	123	61
	$[Pt_2(\mu_3\text{-}S)_2(PPh_3)_4InCl_3]$	128	61
	$[Pt_2(\mu_3\text{-}S)_2(PPh_3)_4Ru(\eta^6\text{-p -cymene})](BPh_4)_2$	132	28
	$[Pt(\mu\text{-}SAuCl)_2(PPh_3)_4]$	180	48
	$[Pt(\mu\text{-}SAgCl)_2(PPh_3)_4]$	180	49
	$[Pt_2(\mu_3\text{-}S)_2(PPh_3)_4]Au(pap\text{-}C^1,N)](BF_4)_2$	126	24
	$[Pt_2(PPh_3)_4(\mu_3\text{-}S)_2Au(tolpy)](BF_4)_2$	127	62
	$[Pt_4(\mu_3\text{-}S)_4(PPh_3)_8Hg](PF_6)_2$	118	53
	$[Pt_2(\mu_3\text{-}S)_2](PPh_3)_4HgCl_2]$	131	53
	$[Pt_2(\mu_3\text{-}S)_2(PPh_3)_4HgPh](BPh_4)$	133	24
	$[Pt_2(\mu_3\text{-}S)_2(PPh_3)_4HgPPh_3](PF_6)_2$	134	53
	$[Pt_2(\mu_3\text{-}S)_2(PPh_3)_4HgFc](PF_6)$	147	26
	$[Pt_4(\mu_3\text{-}S)_4(PPh_3)_8Hg](ClO_4)_2$	135	53
	$[Pt_2(\mu_3\text{-}S)_2(PPh_3)_4SnMeCl_2](PF_6)$	129	24
	$[Pt_2(\mu_3\text{-}S)_2(PPh_3)_4SnMe_2Cl](PF_6)$	135	24
	$[Pt_2(\mu_3\text{-}S)_2(PPh_3)_4SnPhCl_2](PF_6)$	128	24
	$[Pt_2(\mu_3\text{-}S)_2(PPh_3)_4Sn(CH_2Ph)_2Br](PF_6)$	126	24
	$[Pt_2(\mu_3\text{-}S)_2(PPh_3)_4\}Ni(C_6F_5)_2]$	128	56
	$[Pt_2(\mu\text{-}S)_2(PPh_3)_4Ni(NCS)(PPh_3)]PF_6$	128	27
	$[Pt_2(\mu_3\text{-}S)_2(PPh_3)_4Cu(PPh_3)]PF_6$	137	63

	$[Pt_2(\mu_3\text{-}S)_2(PPh_3)_4Cu(bipy)](PF_6)_2$	137	64
	$[Pt_2(\mu_3\text{-}S)_2(PPh_3)_4Cu(CH_3COCHCOCH_3)](PF_6)$	136	64
	$[Pt_2(\mu_3\text{-}S)_2(PPh_3)_4Cu(CF_3COCHCOthienyl)](PF_6)$	129	64
	$[Pt_2(\mu_3\text{-}S)_2(PPh_3)_4CoCl_2]$	126	65
	$[Pt_2(\mu_3\text{-}S)_2(PPh_3)_4Co(acac)](BPh_4)$	131	66
	$[Pt_2\ (\mu_3\text{-}S)_2(PPh_3)_5RhCO](PF_6)$	130	60
	$[Pt_2(\mu_3\text{-}S)_2(PPh_3)_4Rh(cod)](PF_6)$	129	67
	$[Pt_2(\mu_3\text{-}S)_2(PPh_3)_4Rh(2,6\text{-}Me_2C_6H_3NC)_2](PF_6)$	131	68
	$[Pt_2(\mu_3\text{-}S)_2(PPh_3)_4Rh(CO)_2][Rh(CO)_2Cl_2]$	130	68
	$[Pt_2(\mu_3\text{-}S)_2(PPh_3)_4ZnCl_2]$	130	69
	$[Pt_2(\mu_3\text{-}S)_2(PPh_3)_4]_2[ZnSO_4]_2$	126	69
	$[Pt_2(\mu_3\text{-}S)_2(PPh_3)_4ZnCl(bipy)(](PF_6)$	128	70
	$[Pt_2(\mu_3\text{-}S)_2(PPh_3)_4Zn(acac)](BPh_4)$	131	66
	$[Pt_2(\mu_3\text{-}S)_2(PPh_3)_4]_2[CdSO_4]_2$	131	69
	$[Pt_4(\mu_3\text{-}S)_4(PPh_3)_8Cd][ClO_4]_2$	131	69
	$[Pt_2(\mu_3\text{-}S)_2(PPh_3)_4CdCl_2]$	131	69
	$[Pt_2(\mu_3\text{-}S)_2(PPh_3)_4CdCl(bipy)](PF_6)$	133	70
	$[Pt_2(\mu_3\text{-}S)_2(PPh_3)_5IrCO](PF_6)$	130	60
	$[Pt_2(\mu_3\text{-}S)_2(PPh_3)_4Re(CO)_3][Re_3(\mu_3\text{-}OMe)(\mu\text{-}OMe)_3(CO)_9]$	130	71
	$[Pt_2\ (\mu_3\text{-}S)_2(PPh_3)_4\ Re\ (CO)_3](BF_4)$	130	71
	$[Pt_2\ (\mu_3\text{-}S)_2(PPh_3)_4VO(OMe)_2](PF_6)$	130	25
	$[Pt_2\ (\mu_3\text{-}S)_2(PPh_3)_4UO_2(\eta^2\text{-}NO_3)_2]$	132	25
	$[Pt_2(\mu_3\text{-}S)_2(PPh_3)_4Bi(S_2CNEt_2)_2](PF_6)$	132	72
	$[Pt_2\ (\mu_3\text{-}S)_2(PPh_3)_4BiCl_3](PF_6)$	129	52
	$[\{Pt_2(\mu_3\text{-}S)_2(PPh_3)_4\}_2(\mu\text{-}1,4\text{-}C_6Me_4Hg_2)](BPh_4)_2$	133	73
	$[Pt_2(PPh_3)_4(\mu_3\text{-}S)_2Ag(PPh_3)](PF_6)$	142	74
	$[Pt_2(\mu\text{-}SCH_2Ph)(\mu\text{-}SHgFc)(PPh_3)_4](PF_6)_2$	144	75

*The standard deviation of the dihedral angles is not avalaible from the CSD but is usually less than1°.

Table 1.3 Dihedral angles (θ^o) of selected alkylated derivative of $[Pt_2(\mu\text{-}S)_2(PPh_3)_4]$.

	Complex	θº	Ref.
	$Pt_2(\mu\text{-}S)(\mu\text{-}SCH_3)(PPh_3)_4](PF_6)$	138	36
	$[Pt_2(\mu\text{-}S)(\mu\text{-}SCH_2C(O)Ph)(PPh_3)_4](PF_6)$	134	76
	$[Pt_2\mu\text{-}S)(\mu\text{-}SCH_2Ph)(PPh_3)_4](PF_6)$	140	51
	$[Pt_2(\mu\text{-}S)\{\mu\text{-}S(CH_2)_5Br\}(PPh_3)_4]BPh_4$	137	77
	$[Pt_2(\mu\text{-}S)\{\mu\text{-}SCH_2C(=NNHC(O)NH_2)Ph\}(PPh_3)_4]PF_6$	133	76
	$[Pt_2(\mu\text{-}S)\{\mu\text{ -}SCH_2CH_2NHC(O)N(CH_2CH_2)_2S\}(PPh_3)_4]PF_6$	139	76
	$[Pt_2\mu\text{-}S)(\mu\text{-}SCH_2CH_2CN)(PPh_3)_4](PF_6)$	144	51
	$[Pt_2\mu\text{-}S)(\mu\text{-}SCH_2CH_2CO_2Et)(PPh_3)_4](PF_6)$	157	51
	$[Pt_2(\mu\text{-}SCH_2CH{=}CH_2)(\mu\text{-}SCH_3)(PPh_3)_4](PF_6)_2$	148	54
	$[Pt_2(\mu\text{-}SCH_2C_6H_5)(\mu\text{-}SCH_3)(PPh_3)_4](PF_6)_2$	155	54
	$[Pt_2(\mu\text{-}SC_5H_{10}CO_2Et)(\mu\text{-}SCH_3)(PPh_3)_4](PF_6)_2$	149	54
	$[Pt_2(\mu\text{-}SCH_2CH_2SPh)(\mu\text{-}SCH_3)(PPh_3)_4](PF_6)_2$	150	54
	$[Pt_2(\mu\text{-}SCH_3)_2(PPh_3)_4](PF_6)_2$	157	54
	$[Pt_2(\mu\text{-}SC_{10}H_{10}N_2)_2(PPh_3)_4](PF_6)_2$	140	51
	$[Pt_2(\mu\text{-}SCH_2CH_2S)(PPh_3)_4](PF_6)_2$	124	78
	$[Pt_2(\mu\text{-}SCH_2CH{=}CHCH_2S)(PPh_3)_4](BPh_4)_2$	135	79
	$[Pt_2(\mu\text{-}S(CH_2)_5S\}(PPh_3)_4](BPh_4)_2$	147	77
	$[Pt_2(\mu\text{-}SCH_2C_6H_4CH_2S)_2(PPh_3)_4](PF_6)_2$	140	80
	$[Pt_2(\mu\text{-}S\text{-}o\text{-}CH_2C_6H_4\text{-}C_6H_4CH_2S)(PPh_3)_4](PF_6)_2$	147	81
	$[(PPh_3)_4Pt_2(\mu\text{-}S)(\mu\text{-}S\text{-}m\text{-}CH_2C_6H_4CH_2S)(\mu\text{-}S)Pt_2(PPh_3)_4](PF_6)_2$	132	81
	$[(PPh_3)_4Pt_2(\mu\text{-}S)(\mu\text{-}S\text{-}p\text{-}CH_2C_6H_4CH_2S)(\mu\text{-}S)Pt_2(PPh_3)_4](PF_6)_2$	138	81

1.5 Metallation of $[Pt_2(\mu\text{-}S)_2(PPh_3)_4]$

The efficacy of the use of $[Pt_2(\mu\text{-}S)_2(PPh_3)_4]$ **1.1** as a synthetic precursor to multimetallic aggregates makes it an excellent metalloligand towards main group, early and late transition metals. This exceptional reactivity is attributed to the Pt---Pt and S---S nonbonding distances, electron rich sulfide centres and flexibility of the dihedral angle (θ) between the two PtSS planes. In addition, the sulfide centres are capable of forming strong bonds with almost all metal fragments. The

significant number of known homo- and heterometallic sulfide aggregates[38] derived from **1.1** is a testimony that this complex is one of the most effective metalloligands identified to date. The knowledge of the metallation chemistry of $\{Pt_2(\mu\text{-}S)_2\}$ is well known and reasonably developed to maturity and well documented in excellent reviews[29, 38, 39]. Thus, it will not be extensively discussed herein. However, in addition to these reviews, the recent developments on the metallation chemistry of $\{Pt_2(\mu\text{-}S)_2\}$ complexes will be included in this discussion.

The reaction of **1.1** with main group, transition metals and actinide centres where one or the two sulfur atoms acts as donor ligands is shown in Scheme 1.4.

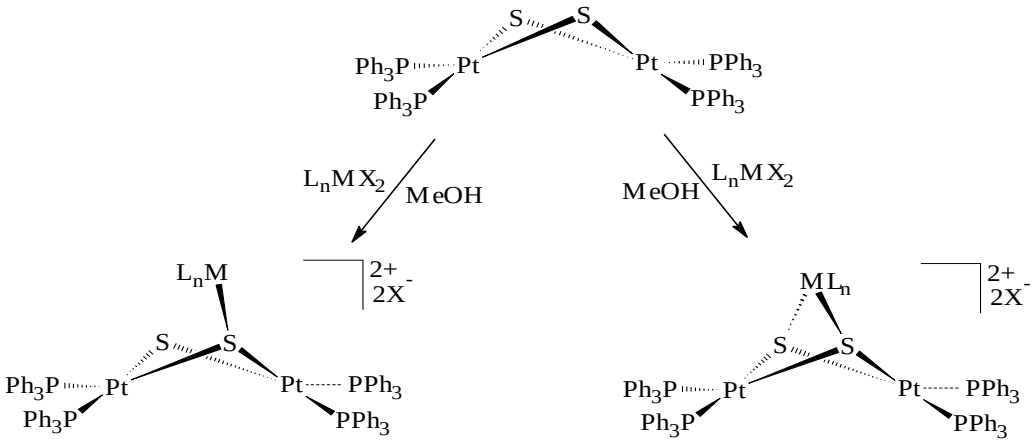

Scheme 1.4 Typical reaction of $[Pt_2(\mu\text{-}S)_2(PPh_3)_4]$ with metal-halide or –psuedohalide complex L_nMX_2.

The reactivity of metal groups with **1.1** simply involves a one step addition of one or in exceptional case two metal centres to the $\{Pt_2(\mu\text{-}S)_2\}$ core. It is noteworthy that the synthetic usefulness of **1.1** as a building block for polynuclear aggregate was unknown until Mingos and co-workers synthesised a series of heterometallic complexes of general formula $[\{Pt_2(PPh_3)_4(\mu_4\text{-}S)_2\}_xML_y]^{n+}$ in the early 1980s. The report propelled the interests in the use of complexes with $\{Pt_2(\mu\text{-}S)_2\}$ cores particularly $[Pt_2(\mu\text{-}S)_2(PPh_3)_4]$ **1.1** as a metalloligand precursor to multimetallic assemblies. The sustained considerable interest in the study of multinuclear complexes derived from **1.1** could be attributed to their rich chemistry in addition to the diverse structural features and applications of transition metal complexes with bridging sulfide ligands[15],

The metallic aggregates are readily formed by **1.1** due its nucleophilicity but are stabilised by the variable electron donation ability, variable non-bonding separating of the sulfide ligands and flexibility of the $\{Pt_2(\mu\text{-}S)_2\}$ core. In addition, the wide coordination ability offered by main group and transition metals in combination with the coordinating mode of the sulfide centres enhances the structural geometric diversity of the metallated derivatives. Virtually any organic fragment that can coordinate to a metal centre can be incorporated into **1.1** through coordination of the sulfur ligands to the metal. Homotrimetallic complexes based on **1.1** in which the two sulfur atoms are coordinated to different platinum metal fragments are known. Examples include $[Pt_3(PPh_3)_6(\mu_3\text{-}S)_2]^{+}$[82], $[Pt_3Cl_2(PPh_3)_6(\mu_3\text{-}S)_2]$[82] and $[Pt_3(C_6F_5)_2(PPh_3)_4(\mu_3\text{-}S)_2]$[56] formed through nucleophilic attack on $[PtCl_2(MeCN)_2]$, $[Pt(MeCN)_2(PPh_3)_2]^{2+}$ and $[Pt(C_6F_6)_2(PhCN)_2]$ respectively. In addition to the ready formation these derivatives they form many structurally diverse geometries (Scheme 1.5) in which the nucleophilic sulfide centres in **1.1** are coordinated directly to other metal fragments in homo– or heterometallic polynuclear aggregates; *viz* linear[48] $[Pt_2(\mu\text{-}S)(\mu\text{-}SAuPPh_3)(PPh_3)_4]^{+}$, angular[55] $[Pt_2Tl(\mu_3\text{-}S)_2(PPh_3)_4]X$ (X = NO_3, PF_6), tetrahedral[15] $[Pt_2(\mu_3\text{-}S)_2GaCl_2(PPh_3)_4][GaCl_4]$, square planar[83] $[\{Pt_2(\mu\text{-}S)_2(PPh_3)_4\}_2Pd](BF_4)_2$, square pyramidal[70, 84] $[Pt_2(\mu_3\text{-}S)_2InCl_3(PPh_3)_4]$ and $[Pt_2MCl(bipy)(\mu_3\text{-}S)_2(PPh_3)_4](PF_6)$ (M = Zn, Cd) respectively, trigonal bipyramidal[60] $[PdPt_2Cl(\mu_3\text{-}S)_2(PPh_3)_5](PF_6)$, distorted trigonal prismatic[57] $[Pt_2(\mu_3\text{-}S)_2Pb(NO_3)_2(PPh_3)_4]$, hexagonal-bipyramidal $[Pt_2(\mu_3\text{-}S)_2UO_2(\eta^2\text{-}NO_3)_2(PPh_3)_4]$[25], T-shaped,[85] $[Ag_2Pt_2(\mu\text{-}S)(PPh_3)_8](BF_4)_2$ and Y-shaped,[86] $[CuPt_2(\mu_3\text{-}S)_2(PPh_3)_5](PF_6)$.

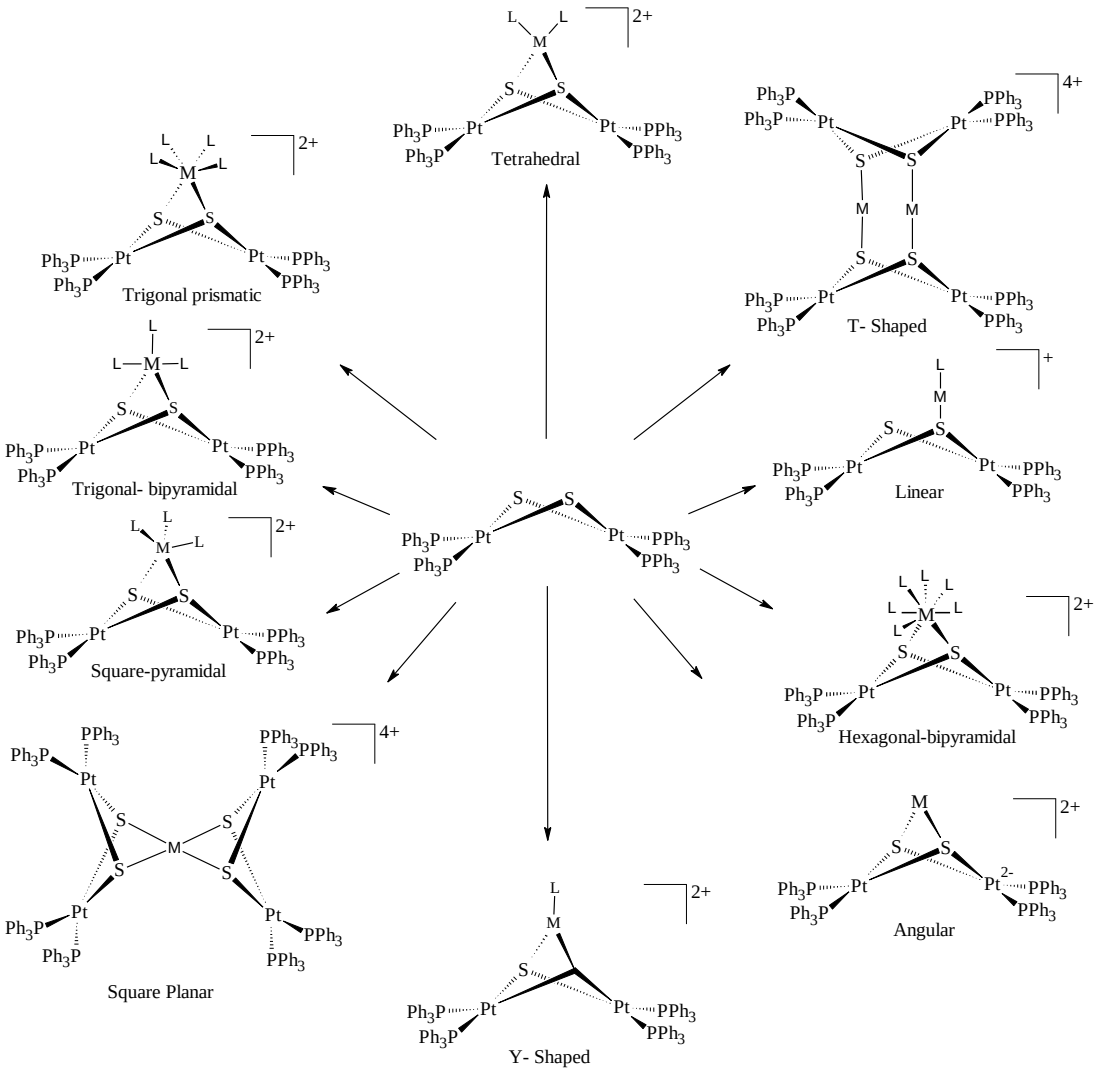

Scheme 1.5 Different structures of metallated products of $[Pt_2(\mu\text{-}S)_2(PPh_3)_4]$ in which the two sulfur atoms are coordinated to the metal centre. Adapted and modified from González-Duarte *et. al*. Eur. J. Inorg. Chem. 2004, p. 3592.

1.6 Syntheses of Di-μ-Thiolate Complexes with $\{Pt_2(\mu\text{-}S)_2\}$ core

Many metal thiolate complexes can be made by methods described in a review by Blower and Dilworth[87]. However, syntheses of dithiolate platinum compound with a $\{Pt_2(\mu\text{-}S)_2\}$ core can be achieved through a limited number of currently available methods. The methods included ligand addition and or displacement reaction of platinum chloride complexes e.g. $[PtCl_2(dppm)]$ and platinum thiolate complexes {equation (**a**)}[88]. The terminal bis(diphenyl phosphino)methane (dppm) ligand can be substituted by another suitable ligand[89].

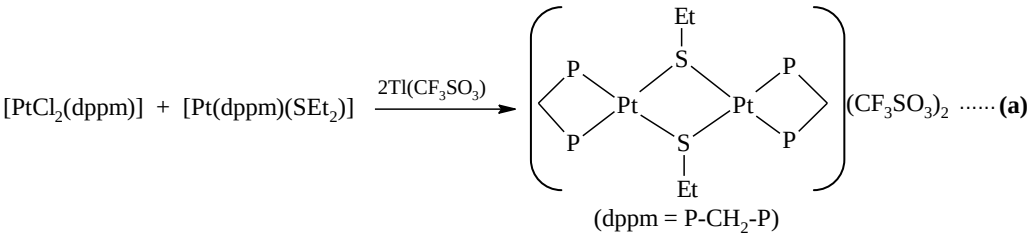

In another method, terminal ligands on platinum can also be moderated with the choice of the platinum chloride complex {equation (**b**)}[90].

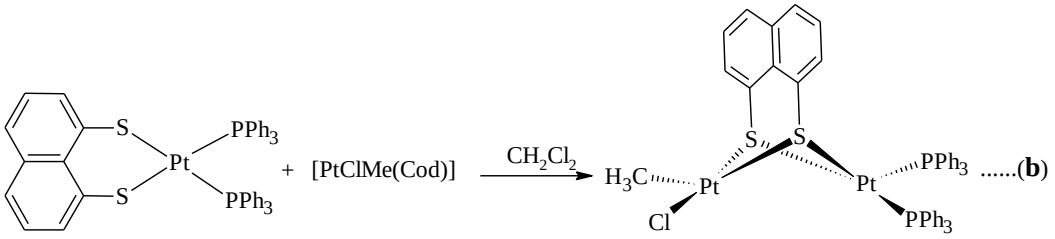

An alternative route is the reaction of a thiol and Pt(dppp)triflate complex, using piperazomethyl polystyrene (PP) as a base {equation (**c**)}[50].

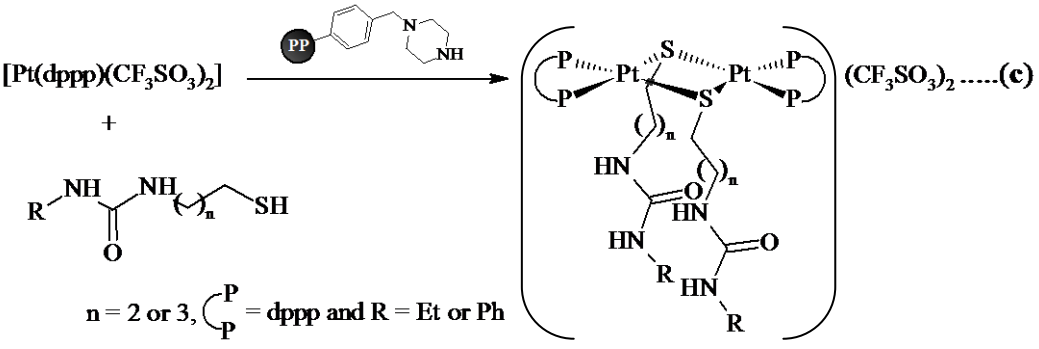

Syntheses of dithiolate platinum with a $\{Pt_2(\mu\text{-}S)_2\}$ core can also be achieved by the thiaplatinacyles with a strong acid e.g. HBF_4. An example is the reaction of thiaplatinacycle, $[(Et_3P)_2Pt(C_{12}H_8S\text{-}C,S)]$ with HBF_4 {equation (**d**)}[91].

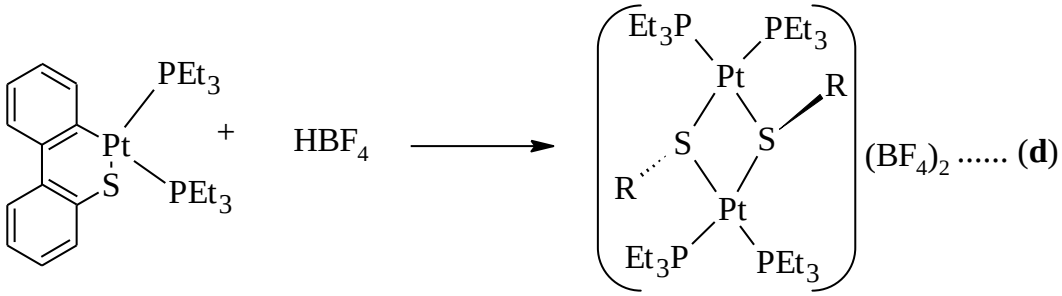

Another method utilises the reactivity of alkylthiols e.g. EtSH with halogen-bridged diplatinum(II) complexes in acetone[92] {equation (**e**)}. The reaction involves the deprotonation of the thiol and dehalogenation of the platinum-halogen complex to give either *cis*- or *trans*- $[PtCl(\mu\text{-}SEt)PEt_3]_2$ and HCl.

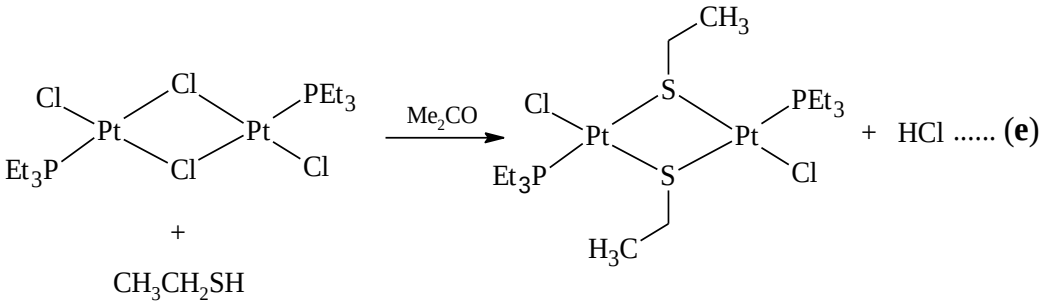

Diplatinum complexes with di-μ-thiolate core and halogen terminal ligands can also be made through the reaction of acetylplatinum (II) complexes with diorganodisulfide compounds[93] {equation (**f**)}.

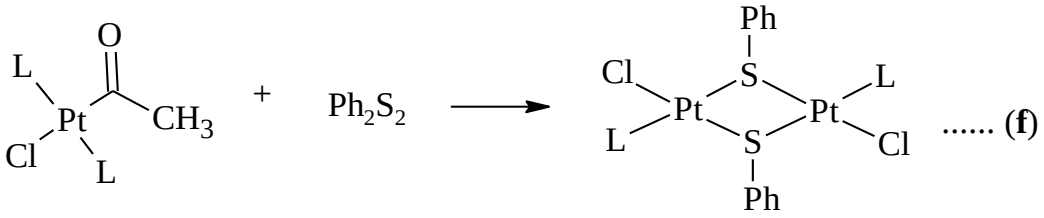

L = PPh_3, $P(4\text{-}FC_6H_4)_3$ or AsPPh

Kinetic analysis of the reaction of *cis*-platin with cysteine showed that *cis*-platin reacts with excess cysteine (a biological thiols) to predominantely generate $[Pt(NH_3)_2(cys)_2]_2$ [94] {equation (**g**)}. Thus, this is another synthetic route to prepare di-μ-thiolate platinum complexes.

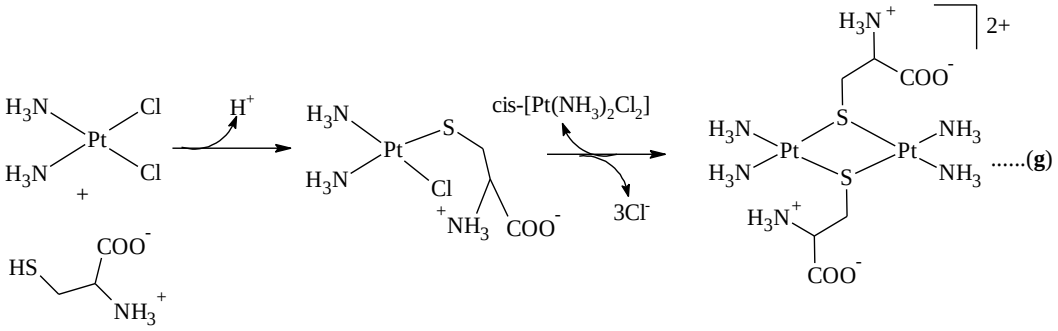

The synthetic methods mentioned above involved the synthesis of precursor(s) with displaceable atom or group and/or reactive thiol. This could be cumbersome and without any predictability of obtaining the desired thiolate compound. However, through simple alkylation reactions of the sulfide centres in $[Pt_2(\mu\text{-}S)_2(PPh_3)_4]$ thiolate substituent of any organic functionality can be made[76]. Thus, further investigation of the alkylation chemistry of $[Pt_2(\mu\text{-}S)_2(PPh_3)_4]$ with multifunctional organic electrophiles would be helpful to develop viable synthetic routes to new di-μ-thiolate compounds.

1.7 Protonation, Mono-, Homo- and Heterodialkylation of $[Pt_2(\mu\text{-}S)_2(PPh_3)_4]$

The strong nucleophilicity of the sulfide centres in $[Pt_2(\mu\text{-}S)_2(PPh_3)_4]$ **1.1** is evident from its exceptional readiness to couple with virtually any positive species including the smallest known positive species, the proton (hydrogen ion). The reactions of **1.1** with H^+ to form a single or diprotonated species **1.7** or **1.8** (Scheme 1.6) has been confirmed by Electrospray Ionisation Mass Spectrometry (ESI-MS)[24] and the monoprotonated species isolated and characterised by X-ray crystallography[62]. The diprotonated species is unstable in solution and has eluded isolation[40].

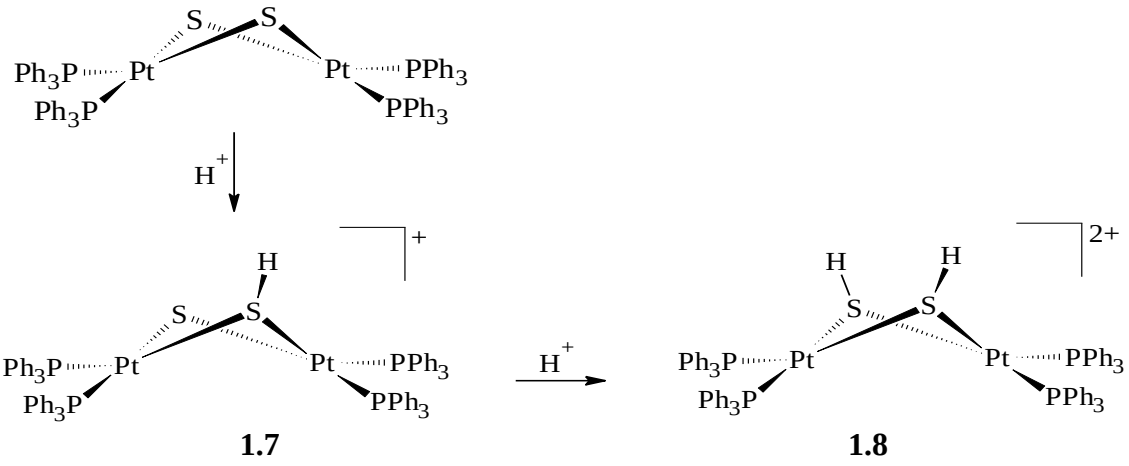

Scheme 1.6 Single and double protonation of $[Pt_2(\mu\text{-}S)_2(PPh_3)_4]$.

It is therefore not surprising that alkylation reactions with organic electrophiles were among the first set of rudimentary reactions to be demonstrated on **1.1**. This included the reactions of mild electrophiles like CH_3I, $PhCH_2Br$ and CH_2Cl_2 to synthesis alkylated derivatives $[Pt_2(\mu\text{-}S)(\mu\text{-}SCH_2Ph)(PPh_3)_4]^{+}$[9] **1.9**, $[Pt_2(\mu\text{-}S)(\mu\text{-}SCH_3)(PPh_3)_4]^{+}$[10 36] **1.10** and $[Pt_2(\mu\text{-}S)(\mu\text{-}SCH_2Cl)(PPh_3)_4]^{+}$[95]. This provided the initial evidence of the reactivity of **1.1** towards organic electrophiles. Surprisingly, this interesting feature has not been amply exploited as a route to functionalised metal bonded thiolate derivatives of **1.1**.

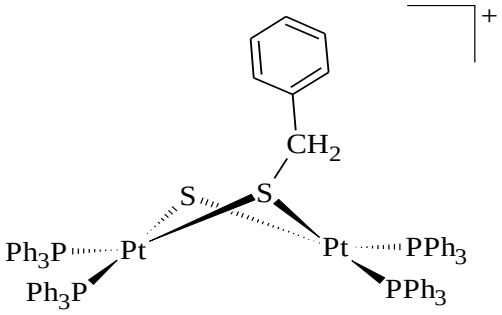

1.9

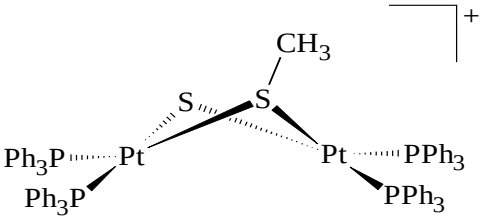

1.10

It is facile to prepare alkylated monocations $[Pt_2(\mu\text{-}S)(\mu\text{-}SR)(PPh_3)_4]^{+}$ with virtually any appropriate electrophilic aliphatic or aromatic halide[76, 96, 97]. Most alkylation and arylation reactions of **1.1** result in predominant conversion of only one of the sulfide ligands to a thiolate ligand[97], as illustrated in Scheme 1.7.

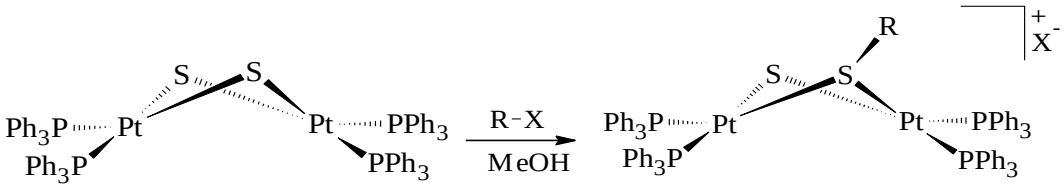

1.1 **1.11**

Scheme 1.7 Formation of thiolate derivative via alkylation of a single sulfur atom in **1.1**.

The interest in the alkylation studies of **1.1** increased with the report on the ESI-MS alkylation survey by Henderson *et al*[97] which brought to the fore broader possibilities of designing and generating a diverse range of multifunctional thiolate ligands bonded to platinum through alkylation reactions. Many of the

products which were only identified spectroscopically have subsequently been isolated or fully characterised by our group[76]. The report indicated that any organic functionality can be incorporated into any suitable electrophile for **1.1**.

The homo- and hetero-dialkylation of **1.1** is less common and not well understood. Homo- and heterodialkylation of **1.1** appeared unachievable after the initial misidentification of $[Pt_2(\mu\text{-}S)(\mu\text{-}SCH_3)(PPh_3)_4]I$ as the dialkylated complex $[Pt_2(\mu\text{-}SCH_3)_2(PPh_3)_4]I_2$[10]. The first observation of the possible formation of homodialkylated complexes with $\{Pt_2(\mu\text{-}SR)_2\}$ core was the formation of $\{Pt_2(\mu\text{-}SCH_2Cl)_2\}$ species reported in the studies on the reaction of $[Pt_2(\mu\text{-}S)_2(PPh_3)_4]$ **1.1** and other analogous complexes $[Pt_2(\mu\text{-}S)_2(PPh_2Py)_4]$[34] **1.2**, $[Pt_2(\mu\text{-}S)_2(dppf)_2]$[19] **1.3**, $[Pt_2(\mu\text{-}S)_2(dppe)_2]$[35] **1.4**, $[Pt_2(PMe_2Ph)_4(\mu\text{-}S)_2]$[36] **1.5** and $[Pt_2(\mu\text{-}S)_2(dppp)_2]$ **1.6** [37] with chlorinated solvents (CH_2Cl_2). The dialkylated intermediate species $\{Pt_2(\mu\text{-}SCH_2Cl)_2\}$ and $\{Pt_2(\mu\text{-}S_2CH_2)\}$ are very unstable and disintegrate rapidly to form mononuclear products (route (**1**) and (**2**), Scheme 1.8). The reason for the decomposition is not known but was primarily attributed to instability of the $\{Pt_2(\mu\text{-}S)_2\}$ core caused by electronic changes upon dialkylation.

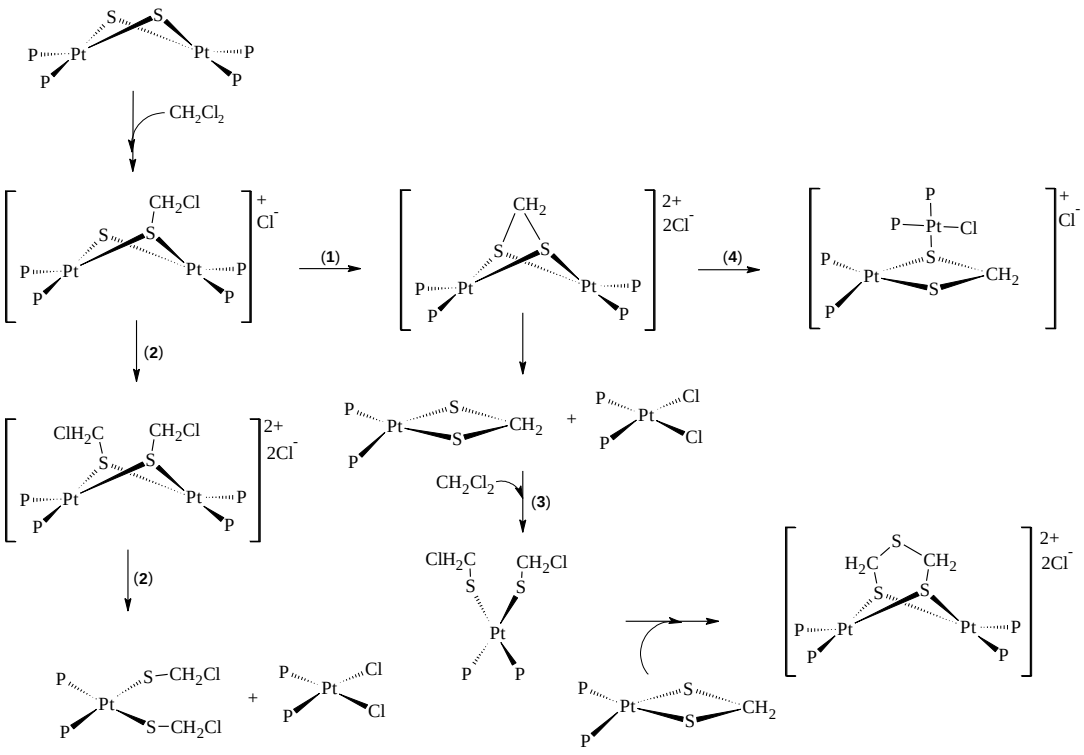

Scheme 1.8 Reaction pathways and products of the reaction of $\{Pt_2(\mu\text{-}S)_2\}$ complexes with CH_2Cl_2. Adapted and modified from Ref [38] .

The study also found that the nature of the terminal ligand has an effect on the extent and nature of the final species formed from the reaction of $\{Pt_2(\mu\text{-}S)_2\}$ complexes and CH_2Cl_2. While the reaction involving **1.1** and **1.6** with the terminal ligands PPh_3 and dppp gives $[\{Pt(S_2CH_2)(PPh_3)_2\}Pt(PPh_3)_2Cl]Cl$ and $Pt_2\{\mu\text{-}[S_3(C\text{-}H_2)_2]\}(dppp)_2](Cl)_2$ (route (**4**)and (**3**)) respectively, the reactions of **1.2**, **1.4** and **1.5** with terminal ligands, dppy, dppe and PMe_2Ph respectively terminates after the formation of the corresponding $\{Pt(S_2CH_2)P_2\}$ and $\{P_2PtCl_2\}$ (route (**1**). The reaction of $[Pt_2(\mu\text{-}S)_2(dppf)_2]$ with CH_2Cl_2 follows the breakdown of the dialky- lated intermediate $\{Pt_2(\mu\text{-}SCH_2Cl)_2\}$ that is $[Pt_2(\mu\text{-}SCH_2Cl)_2(dppf)_2]^{2+}$ route (**2**), resulting in the formation of the mononuclear complexes, $[Pt(SCH_2Cl)_2(dppf)]$ and $[PtCl_2(dppf)]$. The compound $[PtCl_2(P\text{-}P)_2]$ is known for a wide range of terminal ligands and can be recycled to the starting complex (see Scheme 1.1) by reacting with sodium sulfide.

Though the dialkylated species $\{Pt_2(\mu\text{-}SCH_2Cl)_2\}$ eluded isolation, its formation as an intermediate homodialkylated species to mononuclear end products is one of the earliest indications that dialkylation of **1.1** may be achieved under appropriate conditions. Neverthless, successful synthesis of the homo- and hetero-dialkylkated derivatives remained elusive until the synthesis of homodialkylated derivative $[Pt_2(\mu\text{-}SCH_3)_2(PPh_3)_4]^{2+}$ was achieved with a powerful non alkyl halide methylating agent, dimethyl sulfate (Me_2SO_4)[54]. Subsequently, the synthesis of heterodialkylated derivative $[Pt_2(\mu\text{-}SR)(\mu\text{-}SR')(PPh_3)_4]^{2+}$ **1.12** (R = $-CH_3$ from Me_2SO_4) was also achieved through a sequential two stage alkylation of **1.1**.[54]. Though the leaving group in the second alkylation to form heterodialkylated derivative is not the common halide ion from alkyl halide but $CH_3SO_4^-$, it provided stimuli for further investigation into the dialkylation chemistry of **1.1**.

Reaction of some alkyl halides e.g. CH_3I and $ClCH_2C_6H_4CH_2Cl$ with **1.1** results in homodialkylation but a secondary process then leads to a rapid displacement of the terminal PPh_3 ligands by the resulting halide (iodide) ion[78, 97] giving asymmetric products $[Pt_2(\mu\text{-}SRS)(PPh_3)_3X]^+$, $[Pt_2(\mu\text{-}SR)_2(PPh_3)_3I]^+$ and $[Pt_2(\mu\text{-}SR)(\mu\text{-}SR')(PPh_3)_3I]^+$. An example is $[Pt_2(\mu\text{-}SCH_3)_2(PPh_3)_3I]$ which was initially misidentified as the dialkylated compound $[Pt_2(\mu\text{-}SCH_3)_2(PPh_3)_4]I_2$. The tendency of the resulting halide ions from an halogeno electrophile to displace

the terminal PPh_3 increases in ascending order within the halogen group $F^- < Cl^- < Br^- < I^-$. The displacement reaction has not been observed with a bulky aromatic conjugated electrophile probably because of the greater stability of the alkylated product due to conjugation, electron resonance and better steric shielding of the platinum atoms[51]. This is an indication that deshielded or unevenly shielded platinum atoms may be the driving force for the displacement of PPh_3 as the halide ion is more likely to attack from the less shielded side of the platinum atom. This is exemplified by the synthesis of $[Pt_2(\mu\text{-}SC_{10}H_{10}N)_2(PPh_3)_4](PF_6)_2$ and $[Pt_2(\mu\text{-}SCH_2C(O)C_6H_4C_6H_5)_2(PPh_3)_4](PF_6)_2$[51] without traces of a PPh_3-displaced products. However, there are no established factors to determine the homo- and hetero- electrophilic dialkylation of **1.1**. Thus, a detailed study of the reaction conditions that influence the dialkylation of $[Pt_2(\mu\text{-}S)_2(PPh_3)_4]$ and the stability of the resulting alkylated products is imperative.

The generation of a monocation and the consequent electronic changes that occur upon monoalkylation may discourage alkylation of the second sulfide centre. However, suitable electrophiles and organohalides undergo a two stage reaction with **1.1** to give dialkylated product $[Pt_2(\mu\text{-}SR)_2(PPh_3)_4]^{2+}$ **1.13** as in Scheme 1.9.

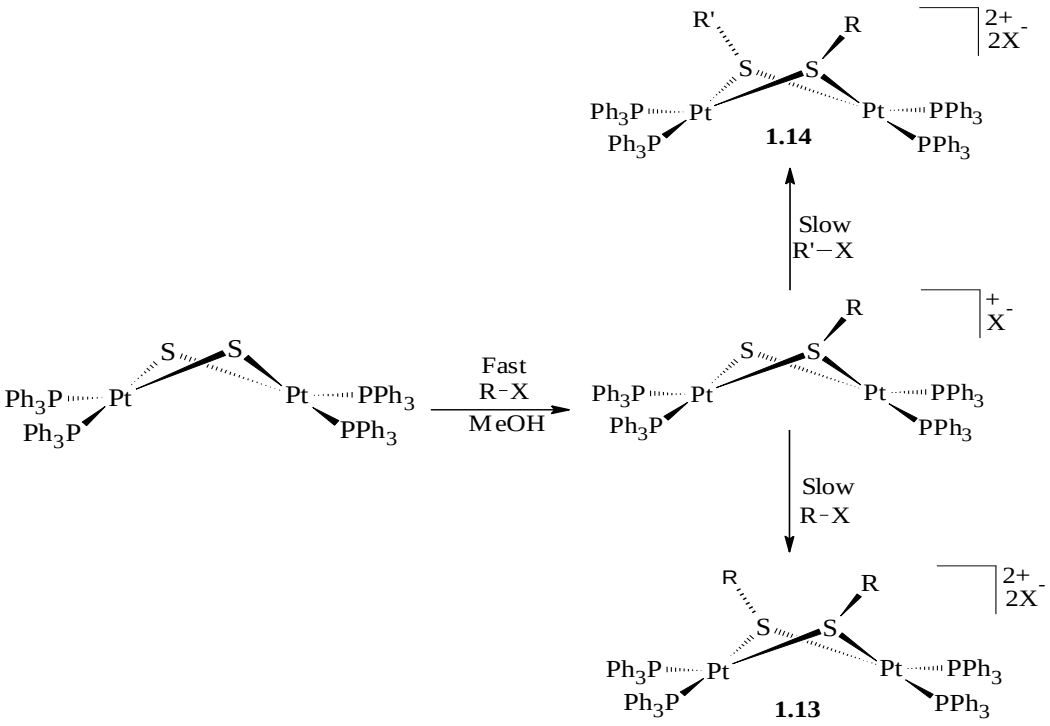

Scheme 1.9 Two stage homo- or heterodialkylation of $[Pt_2(\mu\text{-}S)_2(PPh_3)_4]$ with suitable electrophiles.

The first stage of the reaction is fast yielding a monocation, $[Pt_2(\mu\text{-}S)(\mu\text{-}SR)(PPh_3)_4]^+$ **1.11** followed by a slower second stage to give a dication $[Pt_2(\mu\text{-}SR)_2(PPh_3)_4]^{2+}$ **1.13** or $[Pt_2(\mu\text{-}SR)(\mu\text{-}SR')(PPh_3)_4]^{2+}$ **1.14**. Complete double alkylation of **1.1** has been achieved with selected bromo-organoelectrophiles. Reactions with chloro-organo compounds often result in incomplete dialkylation. Substantial decomposition of the products occurs on application of harsher reaction conditions or prolonged stirring. A report by Chong *et al* [51] suggests that alkylating agents with conjugated aromatic residual parts encourages homodialkylation. However, excess conjugated aromatic electrophiles e.g. $ClCH_2Ph$[97] and $ClCH_2C(O)Ph$[96] exclusively form monoalkylated derivatives with **1.1**. This strongly suggests that the conjugated residual part of an electrophile is not the only driving force to the formation of homo- and heterodialkylated derivatives. It is noteworthy that the absence of a detailed study of the factors influencing homo- and hetero-dialkylation has hindered the design and synthesis of the products and the overall development of the dialkylation chemistry of **1.1**.

1.8 Intra- and Intermolecular Bridging Dialkylation of $[Pt_2(\mu\text{-}S)_2(PPh_3)_4]$

Scheme 1.10 shows the two different alkylated derivatives that can be formed by α,ω- electrophiles. Flexible α,ω-dialkylating electrophiles with the appropriate number of spacer atoms dialkylate **1.1** by bridging the two sulfur atoms to give $[Pt_2(\mu\text{-}S\text{-}R\text{-}S)(PPh_3)_4]^{2+}$ **1.15**. Formation of this type of dialkylated derivative is limited by the number of spacer atoms in the electrophile. Appropriate organo dihalides with fewer than six atoms can dialkylate **1.1** by intramolecular bridging of the two sulfur atoms while dihalides with more than six spacer atoms tend to form bridged Pt_4 aggregates with two molecule of $[Pt_2(\mu\text{-}S)_2(PPh_3)_4]$, each attached to one end of the dihalide electrophile. The limitation imposed by the number of spacer atoms could be expected as steric hindrance due to repulsion between the bulky terminal electron rich PPh_3 of **1.1** is reduced with longer electrophile with more spacer atoms. Monofunctional α,ω-dialkylating agents with general formula XRX with rigid spacers groups e.g. α,α'-dibromo-*p*-xylene and 4,4'-bis(chloromethyl)-1,1'-biphenyl react with **1.1** to give Pt_4

aggregate frameworks with overhead dithiolate bridges, $[PPh_3)_4Pt_2(\mu\text{-}S)(\mu\text{-}S\text{-}R\text{-}S)(\mu\text{-}S)Pt_2(PPh_3)_4]^{2+}$ **1.16** [81]. This type of aggregate is also limited by the type of the alkylating agent especially when the rigidity is imposed by spacer atoms within a phenyl groups.

α,ω-Dialkylating agents with strong electron-withdrawing groups (e.g. $ClCH_2C(=NNAr)CH_2Cl$) close to the two alkylating carbons dialkylated **1.1** by bridging the sulfide centres. However, intramolecular rearrangement may occur upon dialkylation with this type of alkylation agent. Preliminary studies attributed this to the loss of H^+ from one of the methylene hydrogen atoms ($-CH_2-S-$) bonded to sulfur atoms. This lead to opening of the four membered $\{Pt_2(\mu\text{-}S_2\}$ ring into a five membered ring followed by the loss of one PPh_3 ligand[96].

In general, interest in the alkylation chemistry of $[Pt_2(\mu\text{-}S)_2(PPh_3)_4]$ **1.1** and related complexes has further motivated a study of their reactivity towards different multifunctional organohalides[76, 97] and dihalides[77]. In addition, a theoretical study of the reaction mechanism of the complexes with organodihalides[98] found that the reaction with dihalides of the type XRX followed an S_N2 mechanism where a sulfide replaces the halide ion. It was also discovered that the presence of excess halides reduces the activation energy barrier for the alkylation reaction. This explained why excess organohalide helps to achieve alkylation and the bridging sulfide centres in **1.1**. An exception is the formation of bridged alkylated products where stoichiometric control of the reactants is required.

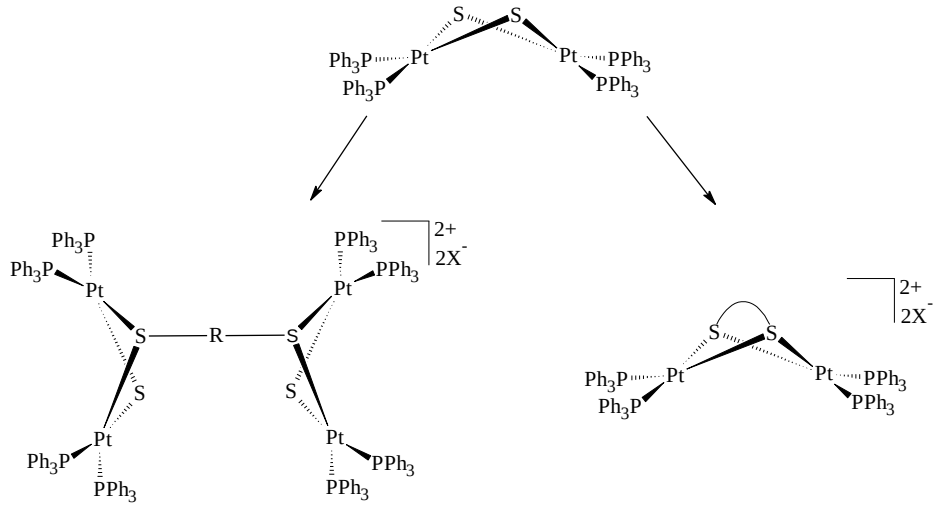

Scheme 1.10 Different products of alkylation of $[Pt_2(\mu\text{-}S)_2(PPh_3)_4]$ depending on the length of the α,ω-alkylating electrophile and the reaction ratio.

1.9 Metallation of $[Pt_2(\mu\text{-}S)(\mu\text{-}R)(PPh_3)_4]^+$

Upon reaction of a monoalkylated complex $[Pt_2(\mu\text{-}S)(\mu\text{-}SCH_2Ph)(PPh_3)_4]^+$ with an electrophile the reactivity of the second sulfide is reduced towards another weak electrophile but in some cases is strong enough to act as a cationic metalloligand towards metal fragments e.g. Ph_3PAu^+, $FcHg^+$ (Fc = Ferrocenyl) to form heterometallic aggregates $[Pt_2(\mu\text{-}SAuPPh_3)(\mu\text{-}SCH_2Ph)(PPh_3)_4]^{2+}$ **1.17** and $[Pt_2(\mu\text{-}SHgFc)(\mu\text{-}SCH_2Ph)(PPh_3)_4]^{2+}$ **1.18** respectively[75] (Scheme 1.11). The isolation of this type of derivative of **1.1** is indicative that the strength of the "positive" centre could enhance the reactivity of the second sulfide centre towards further reaction.

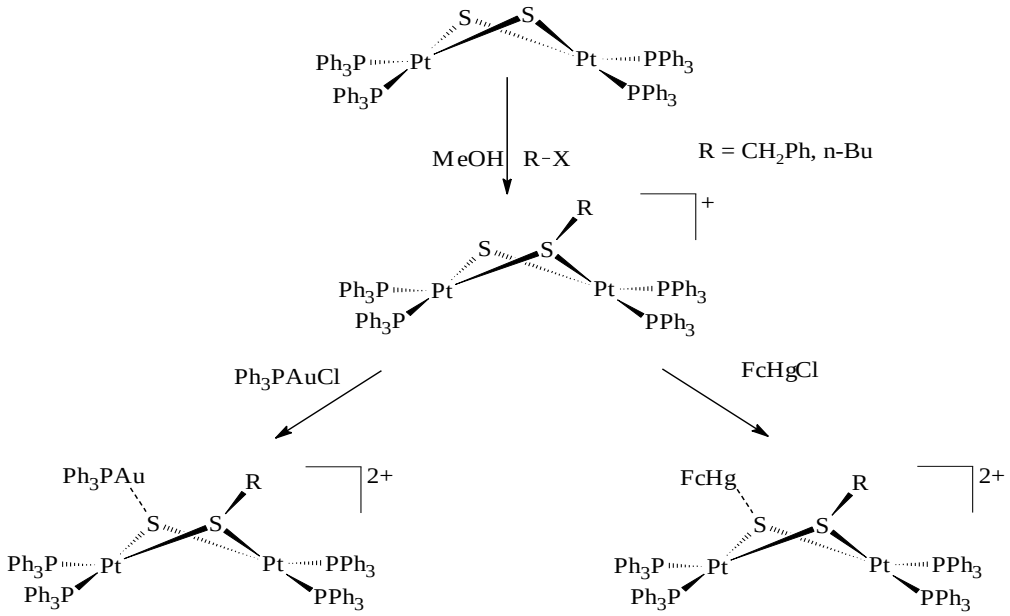

Scheme 1.11 The formation of multimetallic structure where the alkylating metal fragment is bonding to one sulfur atom of **1.1**.

The uniqueness of these types of multimetallic derivative of **1.1** is that the unalkylated sulfide centre is metallated in a monoalkylated derivative. This type of reactions of **1.1** is limited but could be a possible route to generating chemically diverse multimetallic molecules. This is more possible considering that multifunctional organic molecules with good ligating properties which can potentially coordinate to metal centres can initially be incorporated into **1.1**.

1.10 Research Methodology

1.10.1 Electrospray Ionisation Mass Spectrometry (ESI-MS)

Electrospray Ionisation Mass Spectrometry (ESI-MS) is a technique developed from the electrospray process. This involves creation of a fine spray of highly charged droplets of a solution by an atomiser or aerosol of charged droplets in the presence of strong electric field. The process has been known for over ninety years[99] and utilised in industries for painting, fuel atomisation etc for over ninety years[100]. The significance and utilisation of electrospray in science was fully understood by the late 1930s[101] but its use for ionisation of intact chemical species in mass spectrometry for chemical analysis was developed by the pioneering work of Dole and co-workers in the late 1960s[102, 103].

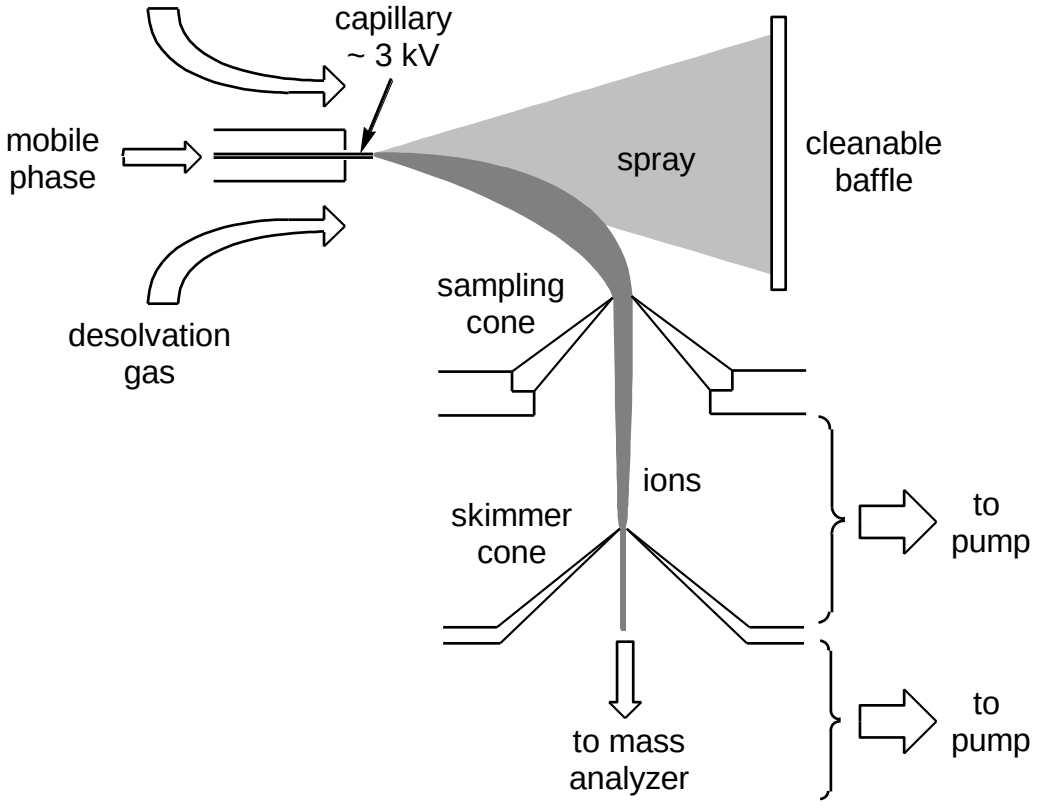

Figure 1.1 A schematic diagram of ESI-MS coupled to a mass analyser. Adopted from Ref.[104]

The technique was significantly developed by M. Yamashita and J. B. Fenn in the 1980s who coupled an electrospray source to a quadrupole mass analyser[105] making it easier for use as an analytical instrument in chemical analysis. J. B.

Fenn was recognised for his contribution by the award of the 2002 Nobel Prize for Chemistry. A schematic diagram of the basic features of ESI-MS is shown in Figure 1.1

ESI-MS is robust and employs a gentle ionisation technique that allows the analysis of large, involatile and also sensitive molecules *in solution*. In practice the **mobile phase** is a polar solvent, usually methanol. A very dilute solution of the analyte is prepared with suitable solvent such as water, methanol, ethanol, acetonitrile, dichloromethane, chloroform etc or a combination thereof. The solution is introduced into the main flow of the mobile phase by a loop or an injection pump through a hypodermic needle between a high voltage (about 2-5 kV) source at a flow rate of about 1µl min^{-1}. The analyte solution is dispersed as a spray of highly charged fine droplets as it flows through to the tip of the needle under high voltage (with respect to the ground state counter electrode) and applied pressure (Figure 1.2).

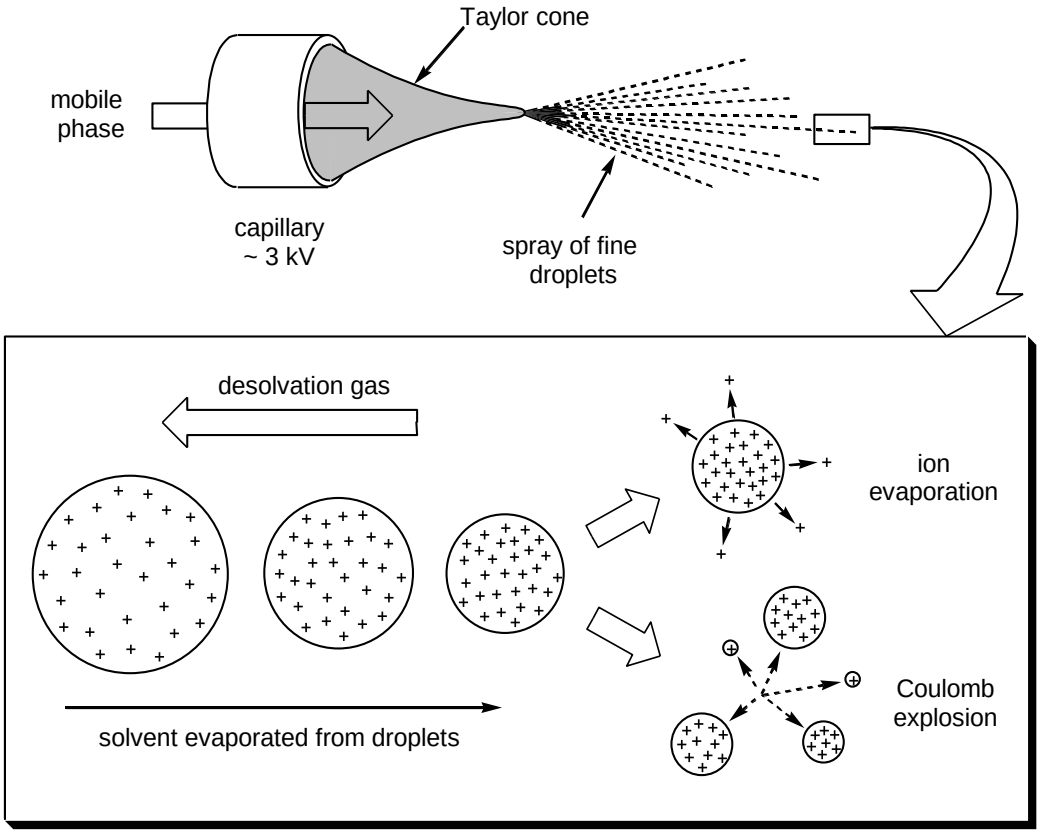

Figure 1.2 A schematic diagram of the mechanism of ion formation in ESI-MS. Adopted from Ref[104].

Because the charged droplets from the needle will have a surface charge of the same polarity as the charge on the needle, the droplets are repelled from the needle towards the source sampling cone on the counter electrode. The mist of charged droplets flows through an evacuated channel which is warmed to prevent condensation and continuously pumped down to modest vacuum. As the droplets move through this region and with continuous flow of the desolvation gas, the solvent evaporates from the surface of the droplets. The droplet shrinks until the surface tension can no longer sustain the charge (the Rayleigh limit) at which point a "Coulombic explosion" occurs and the droplet is ripped apart. This produces smaller charged droplets that can repeat the process as well to give naked charged analyte molecules. After passing through this region the ions travel through two more evacuated regions through the skimmer electrodes which refines the separation of the ions from the solvent molecules. Finally, the sample ions enter into the mass analyser where the mass-charge ratios are measured. This is a very soft ionisation process as very little residual energy is retained by the analyte upon ionisation.

1.10.2 Application of ESI-MS in Chemical Analysis

ESI-MS detects cationic or anionic singly or multiply charged molecular species in solution. Thus, in screening of chemical synthesis it is capable of identifying single or multiple charged species that may result from variable combination of the reactants and/or the products formed. ESI-MS employs a soft ionisation technique and small and large charged molecular species can be transferred to the gas phase and detected with minimal or no fragmentation. The soft ionisation in ESI-MS had its initial major impact in biochemical studies where it was used to observe mass spectra for very large and thermally fragile molecules such as peptides and proteins[106]. Its use in peptide and protein analysis led to an explosion of interest in the technique. It was specifically employed for the determination of the molecular weight of large peptides and protein molecules where the process involves multiple protonation of the species. The protonation of a compound of molecular weight say (M) by the (ESI-MS) mobile phase e.g. H_2O, MeOH etc gives rise to peaks in the mass spectrum equal to $[M + H_n]^{n+}$ which allows for the calculation of the molecular weight. Today the applications of ESI-

MS as an analytical tool is in use in all disciplines involved with chemical analysis.

ESI-MS has been conveniently employed by organometallic and coordination and polymer chemists in characterising large inorganic compounds and synthetic polymers[107]. It is employed in screening micro-syntheses to identify promising reactions, monitoring the progress of promising reactions on laboratory scale, accurate determination molecular mass, structural information of complexes and solving reaction mechanism problems.

1.10.3 ESI-MS Technique – an Indispensible Tool in the Probing of Reactivity of $[Pt_2(\mu\text{-}S)_2(PPh_3)_4]$ and Related Complexes.

Electrospray Ionisation Mass Spectrometry (ESI-MS) has been proven to be an effective technique for probing and directing the micro and macro reaction of $[Pt_2(\mu\text{-}S)_2(PPh_3)_4]$ [24, 59, 78, 97] towards metal halides, organohalides and related compounds. It is especially useful in solution chemistry and has the ability to analyse reaction mixtures and provide useful information on the species therein so that promising reactions can be identified for subsequent macroscopic study. It is a very sensitive technique and as a result it detects compounds in solutions of very low concentration. Small amounts of material can therefore be used in micro-syntheses and analysis. ESI-MS aided micro-synthesis is a simple experiment which helps to conserve expensive reactant starting materials such platinum - based starting compounds.

ESI-MS detects higher molecular masses and therefore well situated for studies on **1.1**. Neutral $[Pt_2(\mu\text{-}S)_2(PPh_3)_4]$ is not detected by ESI-MS but is ionised by protonation on dissolution in methanol to give in the ESI-MS the ion $[Pt_2(\mu\text{-}S)_2(PPh_3)_4 + H]^+$ which has a mass/charge ratio of *m/z* 1503. Metallation and/or alkylation reactions of **1.1** invariably involve the formation of charged products which makes it easy for detection in ESI-MS. In the absence of decomposition and side reactions the alkylation or metallation product is usually detected. Most of the recently reported work on $[Pt_2(\mu\text{-}S)_2(PPh_3)_4]$ involves the use of this

technique to monitor and accurately predict the outcome of promising reactions of **1.1** with metal centres or electrophiles.

The ionisation technique in ESI-MS is soft and by adjusting the cone voltage gives strong parent ions with little or no fragmentation. Because the ESI-MS detects single and multiple charged ions, the monocations or dications resulting from incorporation of metal and organic groups on one or both sulfur atoms in **1.1** are easily detected. In cases where there is a side reaction like the displacement of PPh_3 by halogen ion leaving the group, rearrangement of the products[54] or decomposition, ESI-MS has proved its usefulness in predicting the reaction mechanisms and structures of the resulting products[24, 97].

In its application to monitor synthesis, ESI-MS allows the generation of experimental molecular ion isotope patterns. This is used in the correct identification of the species as the experimental isotope pattern can be compared with the expected theoretical computer generated isotope pattern[108]. A typical example is the positive ESI-MS of the product $[Pt_2(PPh_3)_4(\mu_3\text{-}S)_2Au(pap)]$ (pap = 2-(2-pyridylamino)phenyl) from a 1:1 mixture of $[Pt_2(\mu\text{-}S)_2(PPh_3)_4]$ and $AuCl_2(pap)$ in MeOH reported by Fong *et al*[24, 62] shown in Figure 1.3.

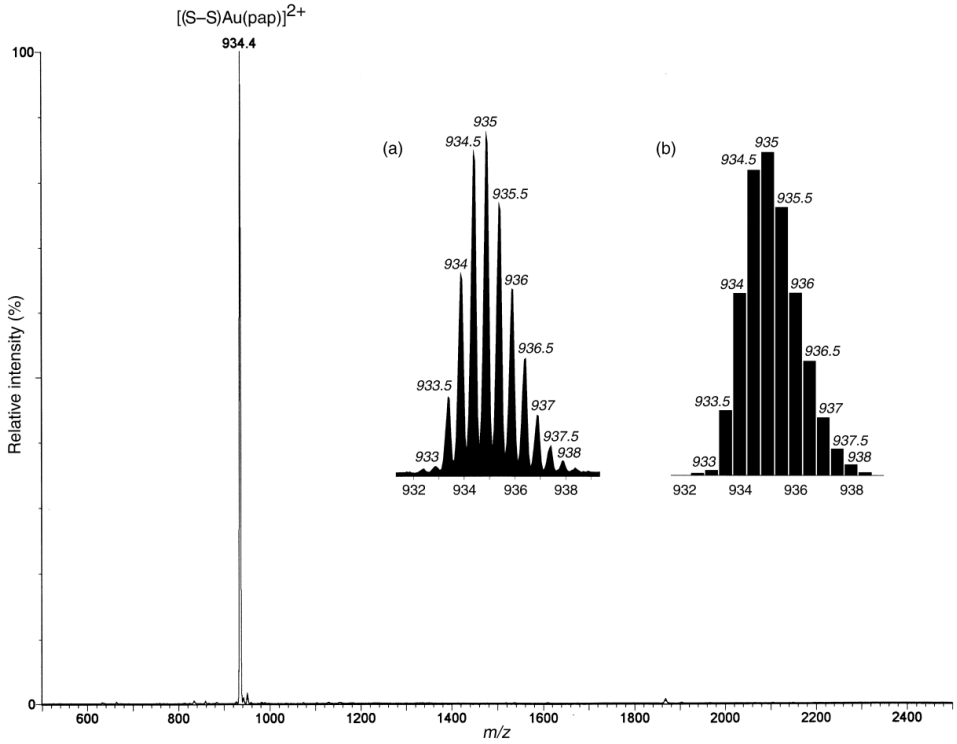

Figure 1.3 Positive ion electrospray mass spectrum of an approx. 1 : 1 mixture of **1.1** and $AuCl_2(pap)$ in MeOH. The inset shows the (a) observed and (b) calculated isotope distribution patterns for the principal ion $[(Pt_2(PPh_3)_4(\mu_3\text{-}S)_2Au(pap)]^{2+}$. Adapted from Ref.[24]

It affords the rapid determination of molecular mass accurately with high sensitivity. It is rapid and simple, therefore large number of systems can be analysed within a short period of time. The ionizability of different charged molecules in the same solution is effective in ESI-MS, therefore the peak intensities in the spectrum can be correlated directly to the quantities of the molecules in solution. This advantage of ESI-MS found application in clinical biochemistry where it is used to determine the quantities of metabolites in biological specimens[109]. In the same way, equimolar solution of different monocationic derivatives of **1.1** shows approximately equal peak intensities in ESI-MS spectra (Figure 1.4). The spectrum from the reports of Henderson *et al* [97] show the spectra of an equimolar solutions of $[Pt_2(\mu\text{-}S)(\mu\text{-}S)(PPh_3)_4]$ and $[Pt_2(\mu\text{-}S)(\mu\text{-}SCH_2Ph)(PPh_3)_4]^+$.

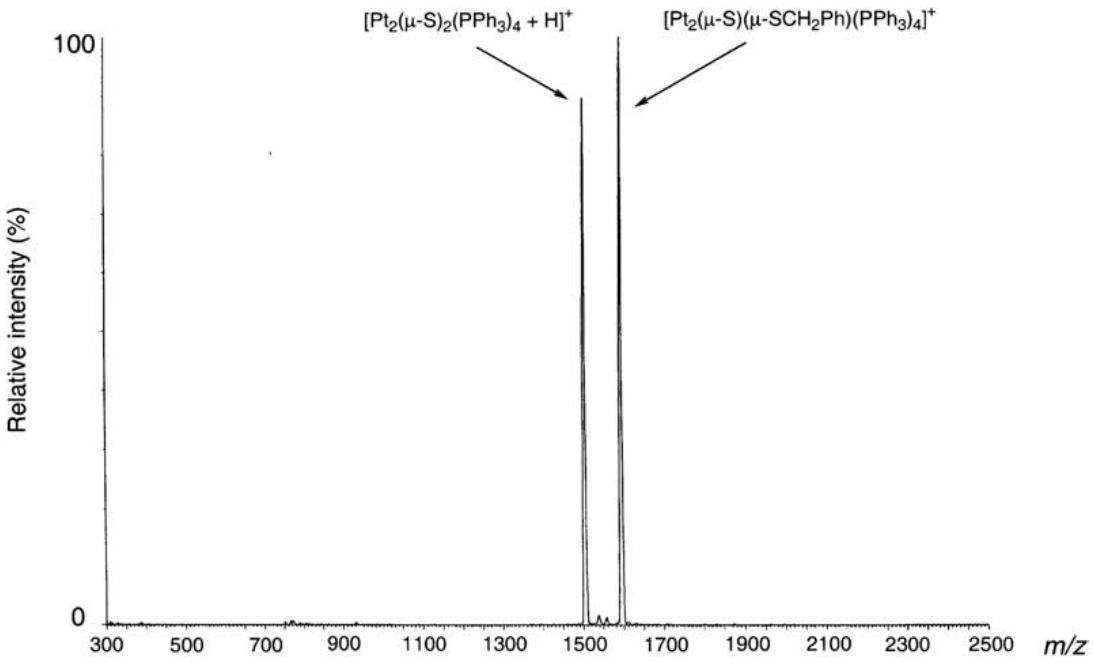

Figure 1.4 ESI-MS of an equimolar solution of $[Pt_2(\mu\text{-}S)_2(PPh_3)_4]$ and $[Pt_2(\mu\text{-}S)(\mu\text{-}SCH_2Ph)(PPh_3)_4]PF_6$ showing approximately equal intensity ions. Adopted from Ref. [97]

The fact that ESI-MS spectra of a solution containing monocations do not just give an indication of the species therein but also their relative quantities makes it suitable for monitoring possible side reactions of the alkylation reactions of **1.1**. It is not known if it would still be quantitative for solutions containing a mixture dicationic and monocationic derivatives. However, in practice the ESI-

MS peaks intensities will presumably depend on the formation (ionisation) of each species and thus could represent the actual quantities in solution. Both dicationic and monocationic derivatives of **1.1** have been observed side-by-side as products of alkylation reactions of **1.1**[97]. The effect of the number of charges on the species in solution on the ionisation process has not been studied.

1.10.4 Structural Information

ESI-MS can also be used to generate structural information. ESI-MS is normally operated with adjustable potential difference (cone voltage) applied across the two sampling cones which accelerate the generated gas phase ions. The ions can easily be subjected to a fragmentation process by increasing the cone voltage. The cone voltage at which fragmentation occurs can be fine-tuned to acquire appropriate data to elucidate the structure of the analyte. The main advantage of this method is that the degree of fragmentation can be carefully tuned to generate the data.

1.11 Objectives of the Present Research

The nvestigation of the alkylation chemistry of **1.1** has been limited to simple alkyl, aryl and very few functionalised organic electrophiles. There are still many functionalised organic substrates whose reactivity with **1.1** are not known and yet to be investigated. Also only little progress has been made in understanding the chemistry and synthesis of the derivatives of the type $[Pt_2(\mu\text{-}SR)_2(PPh_3)_4]^{2+}$, $[Pt_2(\mu\text{-}SR)(\mu\text{-}SR')(PPh_3)_4]^{2+}$ and the bridged derivatives. The prospect of the reactivity of **1.1** with functionalised organic electrophiles has been documented in an ESI-MS survey[97]. Therefore, there is a good prospect of generating an interesting valuable chemistry and compounds of this system. However, this opportunity has not been amply explored. Thus, the main target of this research work is therefore to employ ESI-MS as a monitoring tool in the study of the multifunctional alkylation chemistry of **1.1**. The chemistry of this investigation will be interesting considering the observed variable reactivity of **1.1** with different electrophiles. For instant, the donor atoms of a multifunctional organic moiety in the alkylated derivatives of **1.1** or the resulting halide ion

(leaving group) react with the platinum atom in the $\{Pt_2(\mu\text{-}S)_2\}$ core leading to displacement of the PPh_3 terminal ligand(s), intramolecular rearrangement and other secondary reactions. This chemistry of **1.1** is yet to be fully studied.

The applications of multifunctional organic molecules in coordination chemistry and as synthestic template or precusors is replete in literature. Therefore, the applicability of any multifunctionalised derivatives is therefore very extensive. Multifuctional organic groups that are known to have good ligating properties towards metal centers, e.g amides, ketones, semi-, and thiosemicarbazide ($H_2NHNC(X)NH_2$) (X= S or O) etc. will be selectively incoporated into suitable electrophiles for **1.1**.

In view of the above, the objevctives of the the current research are;

1. To design, synthesise and characterise functionalised monoalkylated derivatives of **1.1** that can potentially be employed in the construction of multimetallic molecules either through coordination with the donor atoms of the newly incorporated group and/or the unalkylated sulfur atoms; Investigate and detailed study of any unusual chemistry resulting form the reaction of the electrophiles with **1.1**.

2. To investigate the factors/properties of electrophiles that encourage the homo- and heterodialkylation chemistry of **1.1** which to date is not well understood; Use the factors in predetermining the electrophiles in investigating the dialkylation reactions of **1.1**, characterise any isolated product(s) and investigate any unsual chemistry; Develop viable synthetic routes to new di-μ-thiolate compounds of **1.1**.

3. To investigate the multifunctional bridging dialkylation reactions of **1.1** with the aim of identifying and studying in detail any unusual chemistry that may result from the electrophiles employed for further studies.

4. To employ alkylation and any other likely reactions of **1.1** to immobilise it on polymer supports and to characterise resulting products with suitable techniques.

1.12 Methodology

The ESI-MS directed synthetic methodology outlined by Henderson *et al* [97], and schematically summarised in Scheme 1.12 will be employed to identify promising reactions of **1.1** and the electrophiles for macroscopic study. The reactions will be carried out on a preparative scale and the resulting products further characterised by more traditional techniques (NMR, IR, Elemental Analysis and X-ray Crystallography where possible).

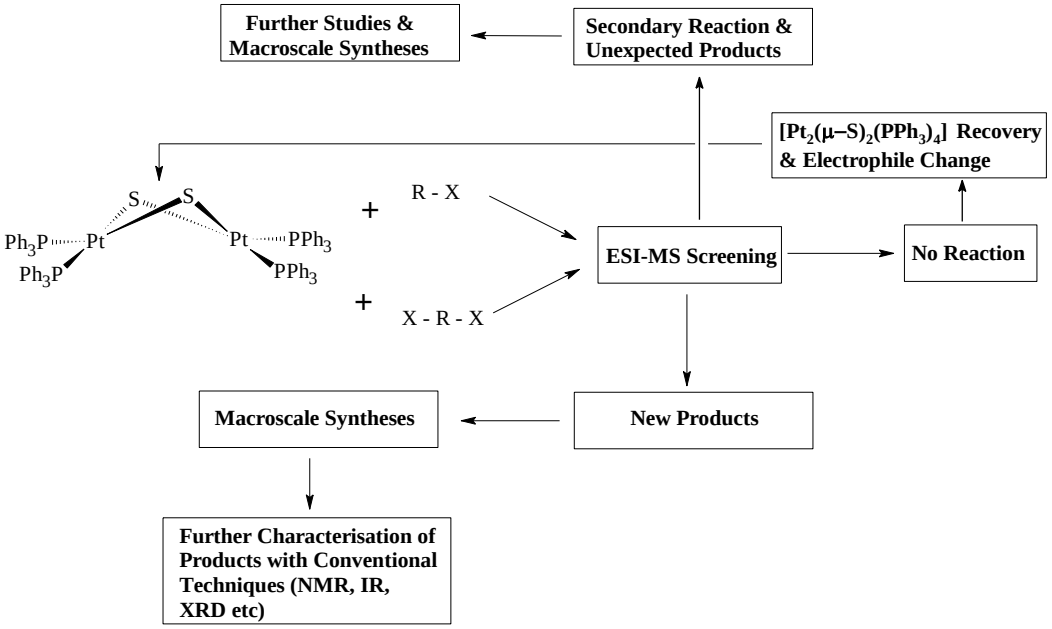

Scheme 1.12 Schematic diagram showing the use of ESI-MS to direct alkylation reactions (R = any organic group)

1.13 References

1. G. C. Bond, *J. Phys. Chem.*, 1956, **60**, 702.
2. M. Arai, K. Usui and Y. Nishiyama, *J. Chem. Soc., Chem. Comm.*, 1993, 1853.
3. G. Ovejero, J. L. Sotelo, A. Rodríguez, C. Díaz, R. Sanz and J. García, *Ind. Eng. Chem. Res.* , 2007, **46**, 6449.
4. E. L. Weaver and R. N. Bose, *J. Inorg. Biochem.*, 2003, **95**, 231.
5. S. Dey and V. K. Jain, *Platinum Metals Review*, 2004, **48**, 16.
6. P. J. Yang, V. V. Halbach, R. T. Higashida and G. B. Hieshima, *Am. J. Neuroradiol.*, 1988, **9**, 547.

7. H. A. Laitinen and I. M. Kolthoff, *J. Phys. Chem.*, 1941, **45**, 1061.
8. L. R. Kelland and N. P. Farrell, eds., *Platinum-based Drugs in Cancer Therapy*, Humana Press Inc., New Jersey, 2000.
9. J. Chatt and D. M. P. Mingos, *J. Chem. Soc. A*, 1970, 1243.
10. R. Ugo, G. La Monica, S. Cenini, A. Segre and F. Conti, *J. Chem. Soc. (A)*, 1971, 522.
11. M. Melnik and C. E. Holloway, *Coord. Chem. Rev.*, 2006, **250**, 2261.
12. W. Clegg, G. Christou, C. D. Garner and G. M. Sheldrick, *Inorg. Chem.*, 1981, **20**, 1562.
13. J. L. Vidal, R. A. Fiato, L. A. Cosby and R. L. Pruett, *Inorg. Chem.*, 1978, **17**, 2574.
14. J. C. Bayo´n, C. Claver and A. M. Masdeu-Bulto´, *Coordination Chemistry Reviews*, 1999, **193-195**, 73.
15. I. Dance and K. Fisher, *Prog. Inorg. Chem.*, 1994, **41**, 637.
16. A. F. Wells, *Structural Inorganic Chemistry, 5th edition*, Clarendon Press, Oxford, 1984.
17. L. J. Carbri, J. H. Gilles Laflamme, J. M. Stewart, K. Tunner and B. J. Skinner, *American Mineralogist*, 1978, **63**, 832.
18. H. Wei, X. Wang and Z. Guo, in *Metal Compounds in Cancer Chemotherapy* eds. J. M. Pérez, M. A. Fuertes and C. Alonso, Research Signpost, Kerala, India, Editon edn., 2005, p. 241.
19. K. A. Hofmann and F. Höchlen, *Ber. Dtsch. Chem. Ges.*, 1903, **36**, 3090.
20. T. B. Rauchfuss, *Inorg. Chem.*, 2004, **43**, 14.
21. E. I. Stiefel, *ACS Symp. Ser.*, 1996, **2**, 653.
22. S.-W. A. Fong and T. S. A. Hor, *J. Chem. Soc., Dalton Trans.*, 1999, 639.
23. B. C. White, W. Henderson, T. S. A. Hor, D. Harrison and B. K. Nicholson, *Inorg. Chim. Acta*, 2010, **363**, 2387.
24. S.-W. A. Fong, W. T. Yap, J. J. Vittal, T. S. A. Hor, W. Henderson, A. G. Oliver and C. E. F. Rickard, *J. Chem. Soc., Dalton Trans.*, 2001, 1986.
25. S.-W. A. Fong, W. T. Yap, J. J. Vittal, W. Henderson and T. S. A. Hor, *J. Chem. Soc., Dalton Trans.*, 2002, 1826.
26. X. Xu, S.-W. A. Fong, Z. Li, Z.-H. Loh, F. Zhao, J. J. Vittal, W. Henderson, S.-B. Khoo and T. S. A. Hor, *Inorg. Chem.*, 2002, **41**, 6838.

27. S.-W. A. Fong, T. S. A. Hor, J. J. Vittal, W. Henderson and S. Cramp, *Inorg. Chim. Acta*, 2004, **357**, 1152.

28. S.-W. A. Fong, T. S. A. Hor, W. Henderson, B. K. Nicholson, S. Gardyne and S. M. Devoy, *J. Organomet. Chem.*, 2003, **679**, 24.

29. Z. Li, S.-W. A. Fong, J. S. L. Yeo, W. Henderson, K. F. Mok and T. S. A. Hor, in *Modern Coordination Chemistry: The legacy of Joseph Chatt* eds. G. J. Leigh and N. Winterton, Royal Society of Chemistry, Cambridge, Editon edn., 2002, p. 355.

30. J. S. L. Yeo, J. J. Vittal, W. Henderson and T. S. A. Hor, *J. Chem. Soc. Dalton Trans.*, 2002, 328.

31. J. S. L. Yeo, J. J. Vittal, W. Henderson and T. S. A. Hor, *J. Chem. Soc. Dalton Trans.*, 2001, 315.

32. J. S. L. Yeo, J. J. Vittal, W. Henderson and T. S. A. Hor, *Inorg. Chem.*, 2002, **41**, 1194.

33. J. S. L. Yeo, J. J. Vittal, W. Henderson and T. S. A. Hor, *J. Organomet. Chem.* , 2002, **659**, 92.

34. V. W.-W. Yam, P. K.-Y. Yeung and K.-K. Cheung, *J. Chem. Soc. Chem Commun.*, 1995, 267.

35. M. Capdevila, Y. Carrasco, W. Clegg, R. A. Coxall, P. González-Duarte, A. Lledós, J. Sola and G. Ujaque, *Chem. Commun.*, 1998, 597.

36. C. E. Briant, C. J. Gardner, T. S. A. Hor, N. D. Howells and D. M. P. Mingos, *J. Chem. Soc., Dalton Trans.*, 1984, 2645.

37. R. Mas-Balleste´, M. Capdevila, P. A. Champkin, W. Clegg, R. A. Coxall, A. Lledo´ s, C. Me´gret and P. Gonza´lez-Duarte, *Inorg. Chem.*, 2002, **41**, 3218.

38. S.-W. Audi-Fong and T. S. Andy Hor, *J. Chem. Soc., Dalton Trans.*, 1999, 639.

39. P. González-Duarte, A. Lledós and R. Mas-Ballesté, *Eur. J. Inorg. Chem.*, 2004, 3585.

40. R. Mas-Balleste´, G. Aullo´ n, P. A. Champkin, W. Clegg, C. Me´gret, P. Gonza´lez-Duarte and A. Lledo´s, *Chem. Eur. J.* , 2003, **9**, 5023.

41. H. Li, G. B. Carpenter and D. A. Sweigart, *Organometallics*, 2000, **19**, 1823.

42. A. Ienco, M. Caporali, F. Zanobini and M. Mealli, *Inorg. Chem.*, 2009, **48**, 3840.
43. W. Henderson, S. Thwaite, B. K. Nicholson and T. S. A. Hor, *Eur. J. Inorg. Chem.*, 2008, 5119.
44. A. Bencini, M. Di Varia, R. Morassi, P. Stoppioni and F. Mele, *Polyhedron*, 1996, **15**, 2079.
45. R. D. Adams, T. A. Wolfe, B. W. Eichhorn and R. C. Haushalter, *Polyhedron* 1989, **8**, 701.
46. G. Aullón, G. Ujaque, A. Lledós, S. Alvarez and P. Alemany, *Inorg. Chem.*, 1998, **37**, 804.
47. M. Capdevila, W. Clegg, P. González-Duarte, A. Jarid and A. Lledós, *Inorg. Chem.*, 1996, **35**, 490.
48. W. Bos, J. J. Bour, P. P. J. Schlebos, P. Hageman, W. P. Bosman, J. M. M. Smits, J. A. C. van Wietmarschen and P. T. Beurskens, *Inorg. Chim. Acta*, 1986, **119**, 141.
49. H. Liu, A. L. Tan, C. R. Cheng, K. F. Mok and T. S. A. Hor, *Inorg. Chem.*, 1997, **36**, 2916.
50. C. Mendoza, J. Benet-Buchholz, M. A. Perciás and R. Villar, *Dalton Trans.*, 2009, 2974.
51. S. H. Chong, W. Henderson and T. S. A. Hor, *J. Chem. Soc. Dalton Trans.*, 2007, 4008.
52. M. S. Zhou, A. L. Tan, Y. Xu, C.-F. Lam, P.-H. Leung, K. F. Mok, L.-L. Koh and T. S. A. Hor, *Polyhedron*, 1997, **16**, 2381-2386.
53. Z. Li, X. Xu, S.-B. Khoo, K. F. Mok and T. S. A. Hor, *J. Chem. Soc. Dalton Trans.*, 2000, 2901.
54. S. H. Chong, L. L. Koh and W. Henderson, *Chem. Asian J.*, 2006, 264.
55. M. Zhou, Y. Xu, L. L. Koh, K. F. Mok, P. H. Leung and T. S. A. Hor, *Inorg. Chem.*, 1993, **32**, 1875.
56. J. Ruiz, V. Rodríguez, A. Pérez, G. López and D. Bautista, *J. Organomet. Chem.*, 2004, **689**, 2080.
57. M. Zhou, Y. Xu, C.-F. Lam, L.-L. Koh, K. F. Mok, P. H. Leung and T. S. A. Hor, *Inorg. Chem.*, 1993, **32**, 4660.

58. K. Pham, W. Henderson, B. K. Nicholson and T. S. A. Hor, *J. Organomet. Chem.*, 2007, **692**, 4933.

59. S.-W. A. Fong, T. S. A. Hor, S. M. Devoy, B. A. Waugh, B. K. Nicholson and W. Henderson, *Inorg. Chim. Acta*, 2004, **357**, 2081.

60. Z. Li, H. Liu, A. S. Batsanov, J. A. K. Howard and T. S. A. Hor, *J. Organomet. Chem.*, 1999, **575**, 223.

61. M. Zhou, Y. Xu, C.-F. Lam, P.-H. Leung, L.-L. Koh, K. F. Mok and T. S. A. Hor, *Inorg. Chem.*, 1994, **33**, 1572.

62. S.-W. A. Fong, J. J. Vittal, W. Henderson, T. S. A. Hor, A. G. Oliver and C. E. F. Rikard, *J. Chem. Soc., Chem. Commun.*, 2001, 421.

63. L. Huang, A. L. Tan, X. Yan, K. F. Mok and T. S. A. Hor, *Polyhedron*, 1997, **16**, 377.

64. S. M. Devoy, W. Henderson, B. K. Nicholson, J. Fawcett and T. S. A. Hor, *J. Chem. Soc. Dalton Trans.*, 2005, 2780.

65. L. Huang, A. L. Tan, K. F. Mok and T. S. A. Hor, *J. Chem. Soc., Dalton Trans.*, 1996, 4023.

66. J. H. Bridson, W. Henderson, B. K. Nicholson and T. S. A. Hor, *Inorg. Chim. Acta.*, 2005, **359**, 680.

67. C. E. Briant, D. I. Gilmour, M. A. Luke and D. M. P. Mingos, *J. Chem. Soc., Dalton Trans.*, 1985, 851.

68. D. I. Gilmour, M. A. Luke and D. M. P. Mingos, *J. Chem. Soc. Dalton Trans.*, 1987, 335.

69. Z. Li, W. Zheng, Z. Liu, K. F. Mok and T. S. A. Hor, *Inorg. Chem.*, 2003, **42**, 8481.

70. Z. Li, Z.-H. Loh, S.-W. A. Fong, Y.-K. Yan, W. Henderson, K. F. Mok and T. S. A. Hor, *J. Chem. Soc., Dalton Trans.* , 2000, 1027.

71. H. Liu, C. Jiang, J. S. L. Yeo, K. F. Mok, L. K. Liu, T. S. A. Hor and Y.-K. Yan, *J. Organomet. Chem.*, 2000, **595**, 276.

72. Z. Li, K. F. Mok and T. S. A. Hor, *J. Organomet. Chem.*, 2003, **682**, 73.

73. N. E. Cameron, R. A. Linklater, W. Henderson, B. K. Nicholson and T. S. A. Hor, *J. Organomet. Chem.*, 2008, **693**, 3711.

74. H. Liu, A. L. Tan, K. F. Mok, M. T. C. W., A. S. Batsanov, J. K. A. Howard and T. S. A. Hor, *J. Am. Chem. Soc.*, 1997, **119**, 11006.

75. W. Henderson, B. K. Nicholson, S. M. Devoy and T. S. A. Hor, *Inorg. Chim. Acta.*, 2008, **361**, 1908.

76. O. T. Ujam, S. M. Devoy, W. Henderson, B. K. Nicholson and T. S. A. Hor, *Inorg. Chim. Acta*, 2010, **363**, 3558.

77. S. M. Devoy, W. Henderson, B. K. Nicholson and T. S. A. Hor, *Inorg. Chim. Acta*, 2010, **363**, 25.

78. S. H. Chong, A. Tjindrawan and T. S. A. Hor, *J. Mol. Catal. A*, 2003, **204**, 267.

79. S. M. Devoy, W. Henderson, B. K. Nicholson and T. S. A. Hor, *Inorg. Chim. Acta*, 2009, **362**, 1194.

80. S. H. Chong, D. J. Young and T. S. A. Hor, *J. Organomet. Chem.*, 2006, **691**, 349.

81. S. H. Chong, W. Henderson and T. S. A. Hor, *Eur. J. Inorg. Chem.*, 2007, 4958.

82. B. H. Aw, K. K. Looh, H. S. O. Chan, K. L. Tan and T. S. A. Hor, *J. Chem. Soc., Dalton Trans.*, 1994, 3177.

83. C. E. Briant, T. S. A. Hor, N. D. Howells and D. M. P. Mingos, *J. Chem. Soc., Chem. Commun.*, 1983, 1118.

84. M. Zhou, Y. Xu, C.-F. Lam, P. H. Leung, L.-L. Koh, K. F. Mok and T. S. A. Hor, *Inorg. Chem.*, 1992, **33**, 1572.

85. C. E. Briant, T. S. A. Hor, N. D. Howells and D. M. P. Mingos, *J.Organomet. Chem.*, 1983, **256**, C15.

86. H. Liu, A. L. Tan, Y. Xu, K. F. Mok and T. S. A. Hor, *Polyhedron*, 1997, **16**, 377.

87. P. J. Blower and J. R. Dilworth, *Coord. Chem. Rev.*, 1987, **76**, 121.

88. A. Singhal, V. K. Jain, A. Klein, M. Niemeyer and W. Kaim, *Inorg. Chim. Acta*, 2004, **357**, 2134.

89. P. S. Braterman and V. A. Wilson, *J. Organomet. Chem.*, 1971, **31**, 123.

90. S. M. Aucott, D. Duerden, Y. Li, A. M. Z. Slawin and J. D. Woollins, *Chem. Eur. J*, 2006, **12**, 5495.

91. J. J. Garcia, A. Arevalo, V. Montiel, F. Del Rio, B. Quiroz, H. Admas and P. M. Maitlis, *Organometallics*, 1997, **16**, 3216.

92. H. C. Clark, V. K. Jain and G. S. Rao, *J. Organomet. Chem*, 1985, **279**, 181.

93. C. Albrecht, S. S., C. Bruhn, C. Wagner, R. Kluge, H. Schmidt and D. Steinborn, *J. Am. Chem. Soc.*, 2007, **129**, 4551.

94. R. N. Bose, S. K. Ghosh and S. Moghaddas, *J. Inorg. Biochem*, 1997, **65**, 199.

95. R. R. Gukathasan, R. H. Morris and A. Walker, *Can. J. Chem.*, 1983, **61**, 2490.

96. S. M. Devoy, M.Sc. Thesis, The University of Waikato, 2005.

97. W. Henderson, S. H. Chong and T. S. A. Hor, *Inorg. Chim. Acta.*, 2006, **359**, 3440.

98. A. Nova, P. González-Duarte, A. Lledós, R. Mas-Ballesté and G. Ujaque, *Inorg. Chim. Acta*, 2006, **359**, 3736.

99. J. Zeleny, *Phys. Rev.*, 1917, **10**, 1.

100. S. A. Hofstadler, R. Bakhtiar and R. D. Smith, *J. Chem. Educ.*, 1996, **73**, A82.

101. S. Chapman, *Phys. Rev.*, 1937, **10**, 184.

102. M. Dole, L. L. Mack, R. L. Hines, R. C. Mobley, L. D. Ferguson and M. B. Alice, *J. Chem. Phys.*, 1968, **49**, 2240.

103. L. L. Mack, P. Kralik, A. Rheude and M. Dole, *J. Chem. Phys.*, 1970, **52**, 4977.

104. W. Henderson and J. S. McIndoe, *Mass Spectrometry of Inorganic, Coordination and Organometallic Compounds: Tools - Techniques - Tips*, John Wiley & Sons, Ltd, England, 2005.

105. M. Yamashita and J. B. Fenn, *J. Phys. Chem.*, 1984, **88**, 4451.

106. R. Bakhtiar, S. A. Hofstadler and R. D. Smith, *J. Chem. Educ*, 1996, **73**, A118.

107. C. E. C. A. Hop and R. Bakhtiar, *J. Chem. Educ*, 1996, **73**, A162.

108. L. J. Arnold, *J. Chem. Educ*, 1992, **69**, 811.

109. C. S. Ho, C. W. K. Lam, M. H. M. Chan, R. C. K. Cheung, L. K. Law, L. C. W. Lit, K. F. Ng, M. W. M. Suen and H. L. Tai, *Clin. BioChem. Rev*, 2003, **24**, 3.

Chapter 2

Multifunctionalised Monoalkylated Derivatives of $[Pt_2(\mu\text{-}S)_2(PPh_3)_4]$

2.1 Introduction

$[Pt_2(\mu\text{-}S)_2(PPh_3)_4]$ **1.1** is well known to exhibit exceptional reactivity towards organic electrophiles[1] leading to formation of a thiolate ligand bonded to platinum (see Scheme 1.7). The sulfide centres in **1.1** are highly nucleophilic and can readily react with even very mild electrophiles[2-5] (see section 1.6). The alkylation of a sulfide ligand in **1.1** has therefore been clearly established as a facile way to the generation of thiolate ligands (SR). However, a limited number of functionalised thiolate complexes have, to date, been synthesised using this method.

A recent ESI-MS study using weak alkylating agents such as *n*-butyl chloride, $Me_2NCH_2CH_2Cl{\cdot}HCl$, bromoethylphthalimide, $PhNHCOCH_2Cl$, and 2,4-dinitrophenylhydrazones $PhC(=NNHAr)CH_2Br$ and $CH_3C(=NNHAr)CH_2Cl$ (Ar = 2,4-dinitrophenyl) by Henderson *et al*[6] pointed to selective monoalkylation of $[Pt_2(\mu\text{-}S)_2(PPh_3)_4]$ and highlighted the possibility of constructing and generating novel and diverse multifunctional thiolate ligands bonded to platinum. Many of the products have only been identified spectroscopically and only a limited number has been successfully isolated and fully characterised. This section of the research project focused on the preparation, isolation and characterisation of a range of multifunctionalised monoalkylated derivatives of **1.1**, some of which have only been identified by mass spectrometry by Henderson *et al.* The same synthetic method used by Henderson *et al* was also employed in the present

investigation of the alkylation reactions of **1.1** with additional organic electrophiles with other functionalities.

2.2 Results and Discussion

This chapter describes the syntheses of a number of monoalkylated derivatives of $[Pt_2(\mu\text{-}S)_2(PPh_3)_4]$ **1.1** using multifunctional electrophiles which include halogeno-hydrazone electrophiles derived from semicarbazide, thiosemicarbazide and isonicotinic acid hydrazide. Functionalised electrophiles derived from guanidine carbonate, 2,4-dinitrophenyl hydrazine, isocyanate and tosylhydrazide were also used and the isolated products were characterised.

2.2.1 Syntheses

A similar method was used in the reactions between **1.1** and the electrophiles to prepare monoalkylated derivatives (Scheme 2.1 and 2.2). Slight variations in reaction time and temperature were required to effect complete reaction and formation of the products. Before the actual preparation of the derivatives, the reactions between the electrophiles and **1.1** were initially screened with ESI-MS using a miniscule amount of the reactants in methanol as solvent. Promising reactions were carried out on preparative scale and also monitored by ESI-MS. Figure **2.1** below shows an example; the ESI-MS of the reaction mixture of **1.1** with excess of $ClCH_2C(O)NHC(O)NHCH_2CH_3$ **2.8a**. The insert shows the experimental and theoretical isotope patterns of the product ion at *m*/*z* 1632.

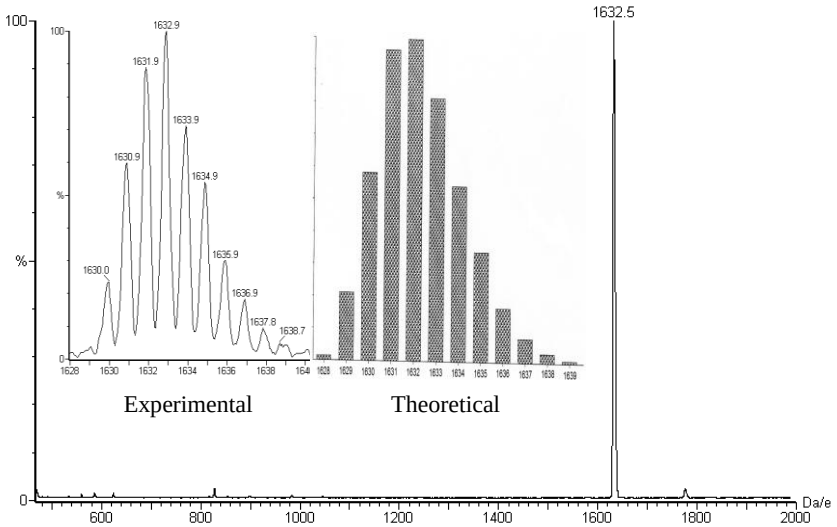

Figure 2.1 The ESI-MS, actual and theoretical isotope patterns of the reaction mixture of $[Pt_2(\mu\text{-}S)_2(PPh_3)_4]$ with excess $ClCH_2C(O)NHC(O)NHCH_2CH_3$ **2.8a**.

Complete alkylation was often indicated by the changing of the original orange suspension of **1.1** in methanol to a clear, pale yellow solution and the disappearance of $[M + H]^+$ peak of **1.1** in the ESI-MS of the reaction mixture. As soon as complete alkylation was confirmed, the solution was filtered to remove traces of solid impurity. The alkylated product was precipitated from the filtrate as its hexafluorophosphate salt with the addition of excess NH_4PF_6. The results from the reactions showed that all the electrophiles selectively alkylate one of the sulfide centres in **1.1**.

The reaction of **1.1** with multifunctionalised Schiff base alkylating agents derived from semicarbazide $ClCH_2C(=NNHC(O)NH_2)Ph$ **2.1a**, $ClCH_2C(=NNHC(O)NH_2)CH_3$ **2.2a**, hydroxylamine $ClCH_2C(=NOH)Ph$ **2.3a**, guanidine $ClCH_2C(=NNHC(NH)NH_2)Ph$ **2.4a** and thiosemicarbazide $ClCH_2C(=NNHC(S)NH_2)CH_3$ **2.5a** were carried out in this series of reactions to investigate the monoalkylation of **1.1** with functionalised alkylating agents. Complete reaction of **1.1** with the alkylating agents was achieved by stirring **1.1** with about 1.2 mole equivalent of **2.1a**, **2.2a**, **2.3a**, **2.4a** and **2.5a** in methanol at room temperature for between 30 and 75 minutes.

The characterisation of the isolated solid products by ESI-MS, NMR and elemental analysis showed the products to be monoalkylated derivatives of **1.1** $[Pt_2(\mu\text{-}S)(\mu\text{-}SR)(PPh_3)_4](PF_6)$ in **2.1b·PF$_6$** (R = Ph) and **2.2b·PF$_6$** (R = CH_3), $[Pt_2(\mu\text{-}S)\{\mu\text{-}SCH_2C(=NOH)Ph\}(PPh_3)_4](PF_6)$ **2.3b·PF$_6$** and $[Pt_2(\mu\text{-}S)\{\mu\text{-}SCH_2C(=NNHC(S)NH_2)CH_3\}(PPh_3)_4](PF_6)$ **2.5b·PF$_6$**. The reaction between **2.4a** and **1.1** gave a dicationic product $[Pt_2(\mu\text{-}S)\{\mu\text{-}SCH_2C(=NNHC(NH_2)_2)Ph\}(PPh_3)_4](PF_6)_2$ **2.4b·(PF$_6$)$_2$** resulting from spontaneous protonation of the highly basic guanidine group $=NNHC(NH)NH_2$ (pK_a = 13.6) to form a guanidinium cation in complex **2.4b·(PF$_6$)$_2$**.

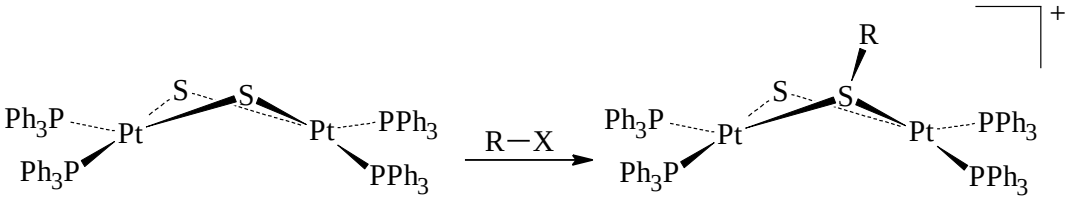

Scheme 2.1. The synthesis of monoalkylated complexes $[Pt_2(\mu\text{-}S)(\mu\text{-}SR)(PPh_3)_4]^+$ and the range of functionalised substituents R (see next page).

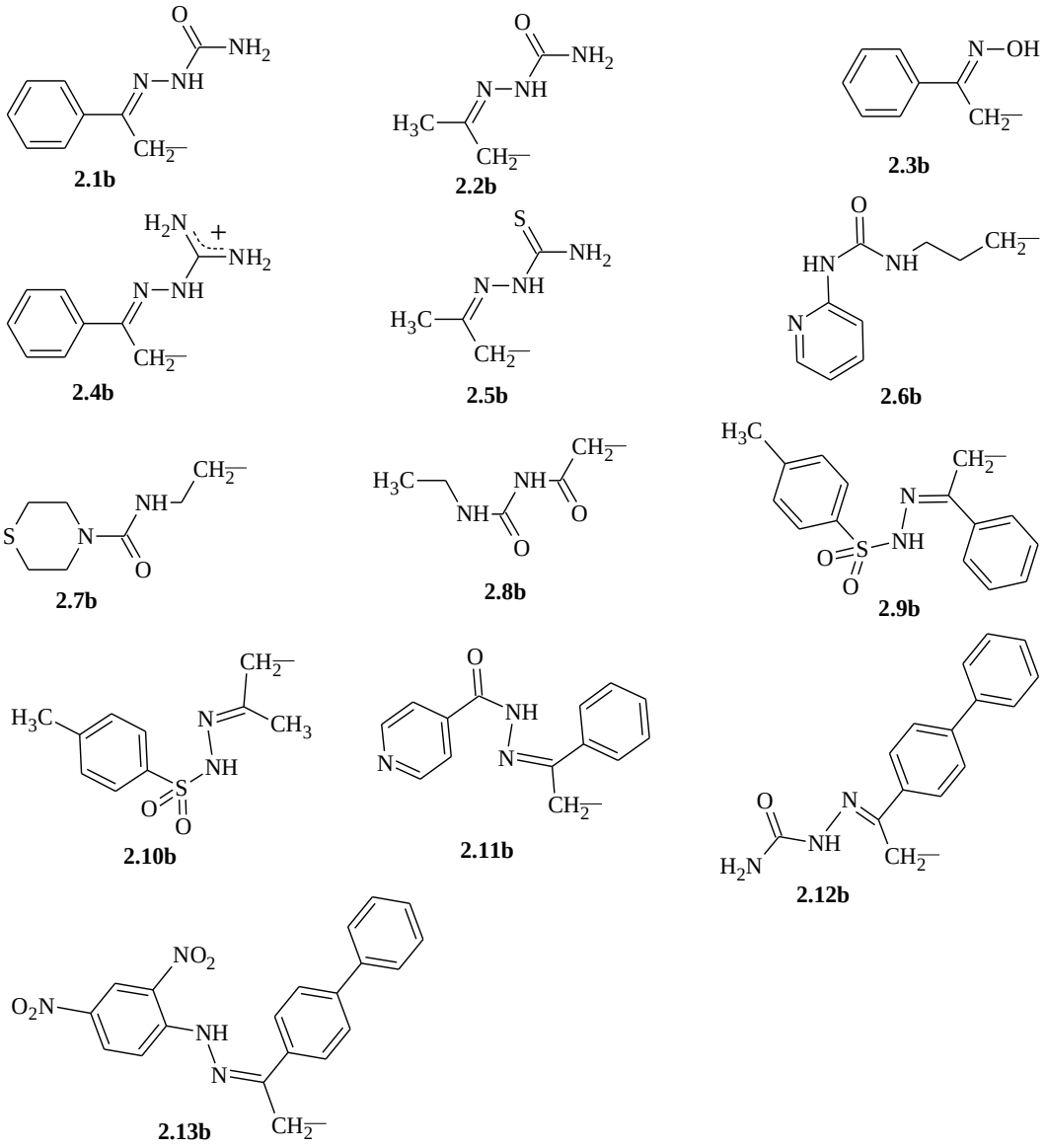

Scheme 2.2 Multifunctional organic groups R in the alkyated derivatives of **1.1**, viz **2.1b·PF$_6$**, **2.2b·PF$_6$**, **2.3b·PF$_6$** etc.

The synthesis of $ClCH_2C(=NNHC(S)NH_2)Ph$ from phenacyl chloride and thiosemicarbazide was not possible because of a cyclisation reaction leading to the formation of 1,3,4-thiadiazin-2-hydrohalide derivative[7, 8] as shown in Scheme 2.3.

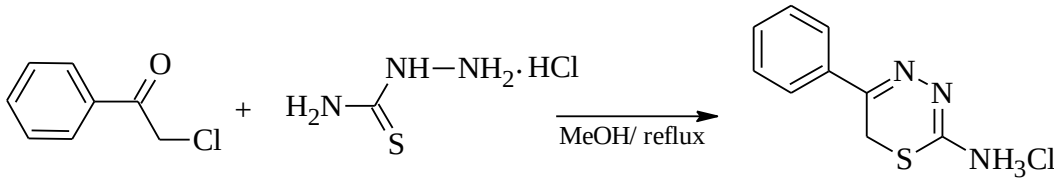

Scheme 2.3 Formation of 1,3,4-thiadiazin-2-hydrohalide derivative

An attempt to synthesis the target $[Pt_2(\mu\text{-}S)_2(PPh_3)_4]$ derivative by reacting thiosemicarbazide with $[Pt_2(\mu\text{-}S)\{\mu\text{-}SCH_2C(O)Ph\}(PPh_3)_4](PF_6)$[9] was unsuccessful as no peak attributable to the target product was identified in the ESI-MS spectrum of the reaction mixture.

The reactions of three alkylating agents containing the urea functional group, $ClCH_2CH_2NHC(O)NHPy$ **2.6a** (Py = C_5H_4N, (Scheme 2.2 above), $ClCH_2CH_2NHC(O)N(CH_2CH_2)_2S$ **2.7a** and $ClCH_2C(O)NHC(O)NHCH_2CH_3$ **2.8a** with **1.1** yielded the corresponding monoalkylated derivatives **2.6b·PF$_6$**, **2.7b·PF$_6$** and **2.8b·PF$_6$** as identified by peaks at *m/z* 1667, 1675 and 1632 corresponding to $[M]^+$ ion in the ESI-MS spectra of the reaction mixtures. The synthesis of **2.6b·PF$_6$** was completed after 24 hours of stirring at room temperature, while **2.7b·PF$_6$** was completed after 24 hours of stirring at room temperature and 24 hours of refluxing in methanol at 65^{o}C. The longer time applied for the synthesis of **2.6b·PF$_6$** and the higher temperature applied for **2.7b·PF$_6$** was to effect a complete reaction. This is because **2.6a** and **2.7a** are relatively weak alkylating electrophiles presumably because the electron releasing effect of the second alkyl $-CH_2-$ group weakened the positive charge generated on the first $-CH_2Cl$ by the electron withdrawing effect of the chlorine atom. The reaction of **2.8a** also gave purely monoalkylated derivative after 90 mins. Crystals of **2.7b·PF$_6$** and **2.8b·PF$_6$** suitable for X-ray crystallographic analysis were isolated by vapour diffusion of diethyl ether into the dichloromethane solutions of the corresponding PF_6^- salts.

The reactions of the hydrazones $ClCH_2C(=NNHTs)Ph$ **2.9a**, $ClCH_2C(=NNHTs)CH_3$ **2.10a** and $BrCH_2C(=NHNC(O)Py)Ph$ **2.11a** (Ts = $-SO_2C_6H_4CH_3$) with **1.1** proceeded very quickly with the solubilisation and change of the orange colour of **1.1** into a clear pale yellow solution. The corresponding monoalkylated derivatives **2.9b·PF$_6$**, **2.10b·PF$_6$** and **2.11b·PF$_6$** was formed in within 20 mins, 25 mins and 30 mins of stirring at room temperature respectively. The ESI-MS of each reaction mixture indicated a simple spectrum with peaks at *m/z* 1787, 1735 and 1740 respectively, due to the presence of $[M]^+$ cations.

The hydrazone $BrCH_2C(=NNHC(O)NH_2)C_6H_4Ph$ **2.12a** derived from the biphenyl conjugated aromatic electrophile $BrCH_2C(O)C_6H_4Ph$ yielded purely a monoalkylated derivative after 60 mins of stirring. Electron rich conjugated aromatic systems reportedly encourage homodialkylation[10] but the ESI-MS of the reaction mixture of excess **2.12a** with **1.1** showed purely a monoalkylated

derivative even after stirring at room temperature for 24 hours and further refluxing at 65°C for another 24 hours. The ESI-MS of the isolated product also indicated purely an $[M]^+$ ion at *m/z* 1753. Further characterisation by NMR and elemental analysis proofed it to be $[Pt_2(\mu\text{-}S)\{\mu\text{-}SCH_2C(=NNHC(O)NH_2)C_6H_4C_6H_5\}(PPh_3)_4](PF_6)$ **2.12b·PF$_6$**. The result of this reaction gave an indication that the presence of a conjugated aromatic system is not the only factor which contributes to the ability of an electrophile to dialkylate **1.1**.

2.2.2 Geometrical Isomerism in Monoalkylated Derivative of {Pt$_2$ (μ-S)$_2$} Containing 2,4-Dinitrophenylhydrazone

The reaction of $BrCH_2C(NNHAr)C_6H_4Ph$ **2.13a** (Ar = 2,4-dinitrophenyl) with **1.1** formed a monoalkylated product **2.13b** containing *Z*- and *E*- geometrical isomers. The formation of 2,4-dinitrophenyl hydrazone derivatives by the condensation reaction of the amino group (NH_2) in 2,4-dinitrohydrazine with the carbonyl (C=O) group to form an azomethine (C=N) group is the most widely used method for the quantitative and qualitative analytical determination of aldehydes and ketones[11, 12]. However, the outcome of this method is usually quantitatively complicated due to the simultaneous formation of *Z*- and *E*-geometrical isomers[13] shown in Scheme 2.4.

Z-isomer *E-isomer*

Scheme 2.4 The *Z*- and *E*- isomers formed from the reaction of 2,4-dinitrophenylhydrazine and carbonyl (ketone and aldehyde) compounds

Both isomers which were formed because of the free rotation of the bond between the azomethine (C=N) and amine (NH) nitrogen atoms are retained upon incorporation into another moiety. Thus, reaction of 1.2 molar equivalents of $BrCH_2C(NNHAr)C_6H_4Ph$ **2.13a** (Ar = 2,4-dinitrophenyl) [derived from phenyl-hydrazine and 2-bromo-4'-phenylacetophenone] with **1.1** gave a bright yellow-orange cloudy solution after 30 min. The ESI-MS spectrum recorded after 1 hour (Figure 2.2) showed only a single $[M]^+$ ion at *m/z* 1876 indicating the formation of

the expected product $[Pt_2(\mu\text{-}S)(\mu\text{-}SCH_2C(NNHAr)C_6H_4Ph)(PPh_3)_4]^+$ **2.13b** which was isolated as the PF_6^- salt $[Pt_2(\mu\text{-}S)(\mu\text{-}SCH_2C(NNHAr)C_6H_4Ph)(PPh_3)_4](PF_6)$ **2.13b·PF$_6$** on addition of excess NH_4PF_6. Further characterisation of the compound by NMR indicated two species which suggested the formation of isomers. It is worth noting that the formation of isomeric products was not observed with other alkylating agents used in this study. A detailed study of the geometric isomerisation in **2.13b·PF$_6$** with NMR spectroscopy was carried out and is reported in Sections 2.2.3.1 and 2.2.3.2.

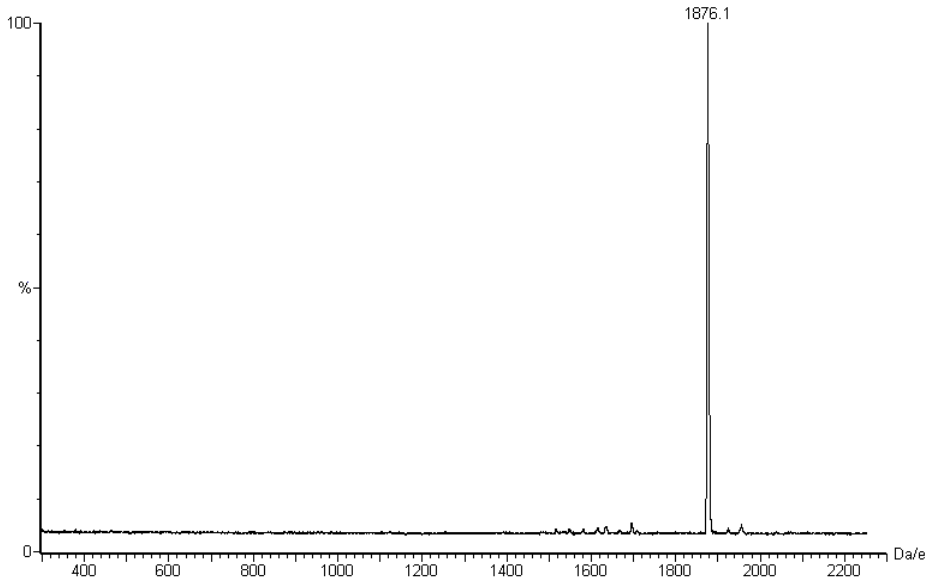

Figure 2.2 ESI-MS of the reaction mixture of **1.1** with $BrCH_2C(NNHAr)C_6H_4Ph$ showing a single peak for $[Pt_2(\mu\text{-}S)(\mu\text{-}SCH_2C(NNHAr)C_6H_4Ph)(PPh_3)_4]^+$ **2.13b** at *m/z* 1876

2.2.3 X-ray Crystal Structures

X-ray structure determinations of $[Pt_2(\mu\text{-}S)\{\mu\text{-}SCH_2C(=NNHC(O)NH_2)\text{-}Ph\}(PPh_3)_4](PF_6)$ **2.1b·PF$_6$**, $[Pt_2(\mu\text{-}S)\{\mu\text{-}SCH_2C(=NNHC(NH_2)_2Ph\}(PPh_3)_4]\text{-}(PF_6)_2$ **2.4b·(PF$_6$)$_2$**, $[Pt_2(\mu\text{-}S)\{\mu\text{-}SCH_2CH_2NHC(O)N(CH_2CH_2)_2S\}(PPh_3)_4](PF_6)$ **2.7b·PF$_6$** and $[Pt_2(\mu\text{-}S)(\{\mu\text{-}SCH_2C(O)NHC(O)NHCH_2CH_3\}(PPh_3)_4](PF_6)$ **2.8b·-PF$_6$** were carried out to confirm the structures of the complexes and to provide comparison with structures of the few monoalkylated derivatives that have been reported. Selected bond lengths and angles are presented in Tables 2.1 - 2.4. Crystal structure refinement data are given in the tables in Section 2.5. The molecular structures along with the atom numbering schemes are shown in Figures 2.3 - 2.6.

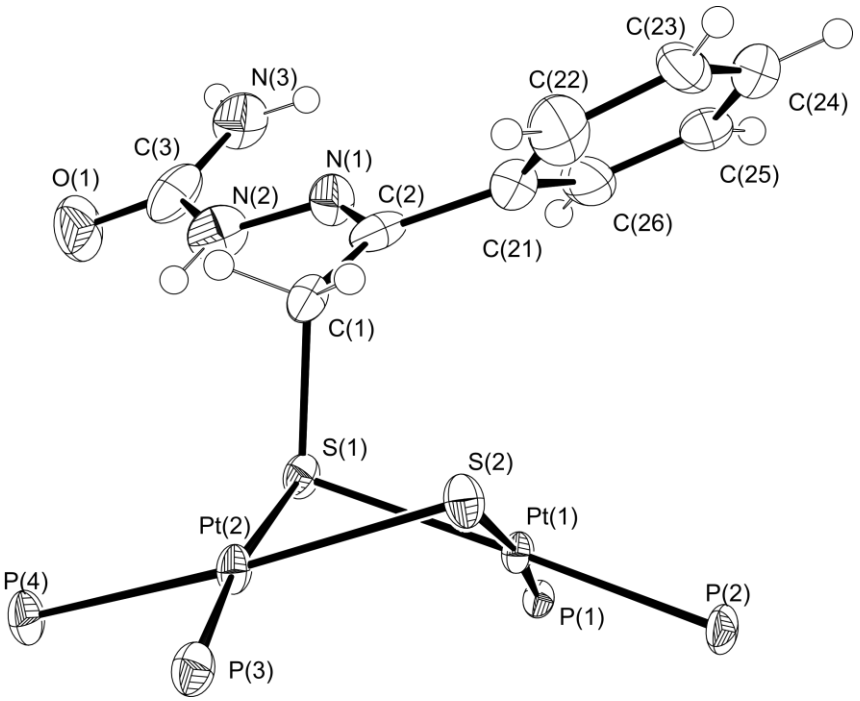

Figure 2.3 Molecular structure of the complex $[Pt_2(\mu\text{-}S)\{\mu\text{-}SCH_2C(=NNHC(O)NH_2)Ph\}(PPh_3)_4](PF_6)$ **2.1b·PF$_6$** showing the atom numbering scheme, with thermal ellipsoids at the 50% probability level. The PF_6^- and the phenyl rings of the PPh_3 ligands have been omitted for clarity.

Table 2.1 Selected bond lengths and atomic distances (Å) and bond angles (°) for $[Pt_2(\mu\text{-}S)\{\mu\text{-}SCH_2C(=NNHC(O)NH_2)Ph\}(PPh_3)_4](PF_6)$ **2.1b·PF$_6$**. (Estimated standard deviations are in brackets).

Bond lengths and atomic distances (Å)					
Pt(1)-P(2)	2.310(3)	Pt(2)-S(2)	2.333(3)	S(1)-C(1)	1.853(10)
Pt(1)-P(1)	2.315(3)	Pt(2)-S(1)	2.401(3)	C(1)-C(2)	1.486(15)
Pt(1)-S(2)	2.344(3)	C(3)-N(3)	1.328(15)	C(3)-N(2)	1.388(14)
Pt(1)-S(1)	2.379(3)	N(1)-N(2)	1.359(13)	C(2)-C(21)	1.525(16)
Pt(2)-P(3)	2.281(3)	C(3)-O(1)	1.245(15)	C(2)-N(1)	1.298(13)
Pt(2)-P(4)	2.316(3)	Pt(1)---Pt(2)	3.297	S(1)---S(2)	3.071

Bond angles (°)			
S(2)-Pt(1)-S(1)	81.14(9)	Pt(1)-S(1)-Pt(2)	87.23(8)
S(2)-Pt(2)-S(1)	80.80(9)	Pt(2)-S(2)-Pt(1)	89.65(9)
N(1)-C(2)-C(1)	126.1(11)	C(1)-S(1)-Pt(2)	102.2(3)
O(1)-C(3)-N(2)	118.6(13)	C(1)-S(1)-Pt(1)	104.7(3)
N(3)-C(3)-N(2)	116.7(12)	C(1)-C(2)-C(21)	121.0(9)
C(2)-N(1)-N(2)	119.9(10)	O(1)-C(3)-N(3)	124.7(12)
N(1)-N(2)-C(3)	119.0(11)	C(2)-C(1)-S(1)	113.7(7)

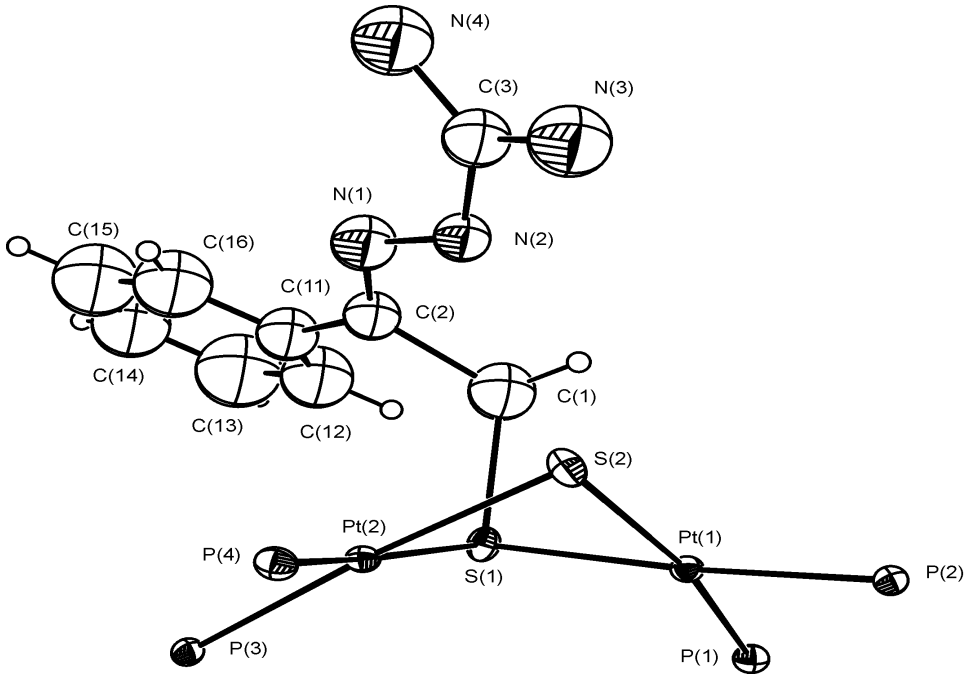

Figure 2.4 Molecular structure of the complex $[Pt_2(\mu\text{-}S)\{\mu\text{-}SCH_2C(=NNHC(NH_2)_2)Ph\}(PPh_3)_4](PF_6)_2$ **2.4b·$(PF_6)_2$** showing the atom numbering scheme, with thermal ellipsoids at the 50% Probability level. The PF_6^- and the phenyl rings of the PPh_3 ligands have been omitted for clarity.

Table 2.2 Selected bond lengths (Å) and bond angles (°) for $[Pt_2(\mu\text{-}S)\{\mu\text{-}SCH_2C(=NNHC\text{-}(NH_2)_2Ph\}(PPh_3)_4](PF_6)_2$ **2.4b·$(PF_6)_2$**. (Estimated standard deviations are in brackets).

Bond lengths and atomic distances (Å)					
Pt(1)-P(2)	2.291(2)	Pt(2)-S(2)	2.353(2)	S(1)-C(1)	1.934(17)
Pt(1)-P(1)	2.293(2)	Pt(2)-S(1)	2.354(2)	C(1)-C(2)	1.687(15)
Pt(1)-S(2)	2.353(2)	C(3)-N(3)	1.26(2)	C(3)-N(2)	1.398(19)
Pt(1)-S(1)	2.363(2)	N(1)-N(2)	1.357(16)	C(2)-C(11)	1.608(18)
Pt(2)-P(3)	2.295(2)	C(3)-N(3)	1.41(2)	C(2)-N(1)	1.215(17)
Pt(2)-P(4)	2.297(2)	Pt(1)---Pt(2)	3.305	S(1)---S(2)	3.064
Bond angles (°)					
S(2)-Pt(1)-S(1)	81.01(8)	Pt(1)-S(1)-Pt(2)	88.96(7)		
S(2)-Pt(2)-S(1)	81.20(7)	Pt(2)-S(2)-Pt(1)	89.23(7)		
N(1)-C(2)-C(1)	126.1(14)	C(1)-S(1)-Pt(2)	105.6(5)		
N(4)-C(3)-N(2)	116.5(15)	C(1)-S(1)-Pt(1)	96.9(5)		
N(3)-C(3)-N(2)	117.5(16)	C(1)-C(2)-C(11)	102.7(11)		
C(2)-N(1)-N(2)	117.4(13)	N(4)-C(3)-N(3)	126.0(17)		
N(1)-N(2)-C(3)	121.0(12)	C(2)-C(1)-S(1)	113.7(11)		

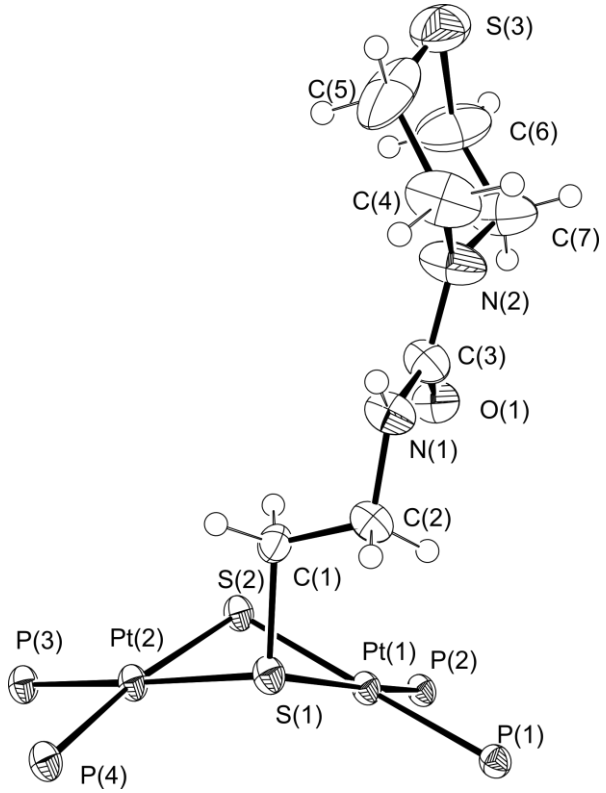

Figure 2.5 Molecular structure of $[Pt_2(\mu\text{-}S)\{\mu\text{-}SCH_2CH_2NHC(O)N(CH_2CH_2)_2S\}(PPh_3)_4](PF_6)$ **2.7b·PF$_6$** showing the atom numbering scheme, with thermal ellipsoids at the 50% probability level. The PF_6^-, CH_2Cl_2 and the phenyl rings of the PPh_3 ligand have been omitted for clarity.

Table 2.3 Selected bond lengths (Å) and bond angles (°) for $[Pt_2(\mu\text{-}S)(\mu\text{-}SCH_2CH_2NHC(O)N(CH_2CH_2)_2S(PPh_3)_4](PF_6)$ **2.7b·PF$_6$**. (Estimated standard deviations are in brackets).

Bond lengths and atomic distances (Å)			
Pt(1)-P(2)	2.2907(17)	Pt(2)-P(3)	2.2694(18)
Pt(1)-P(1)	2.2981(18)	Pt(2)-P(4)	2.3081(17)
Pt(1)-S(2)	2.3433(17)	Pt(2)-S(2)	2.3252(16)
Pt(1)-S(1)	2.3621(16)	Pt(2)-S(1)	2.3720(17)
S(1)-C(1)	1.827(7)	C(3)-O(1)	1.246(9)
C(1)-C(2)	1.516(10)	C(2)-N(1)	1.466(9)
Pt(1)---Pt(2)	3.325	S(1)---S(2)	3.077
Bond angles (°)			
S(2)-Pt(1)-S(1)	81.68(6)	C(1)-S(1)-Pt(1)	104.9(2)
S(2)-Pt(2)-S(1)	81.84(6)	C(1)–S(1)–Pt(2)	103.1(2)
P(2)–Pt(1)–P(1)	98.10(6)	Pt(2)-S(2)-Pt(1)	90.83(6)
Pt(1)-S(1)-Pt(2)	89.23(6)	N(1)-C(2)-C(1)	113.1(6)
C(2)-C(1)-S(1)	109.0(5)	O(1)-C(3)-N(2)	120.9(7)

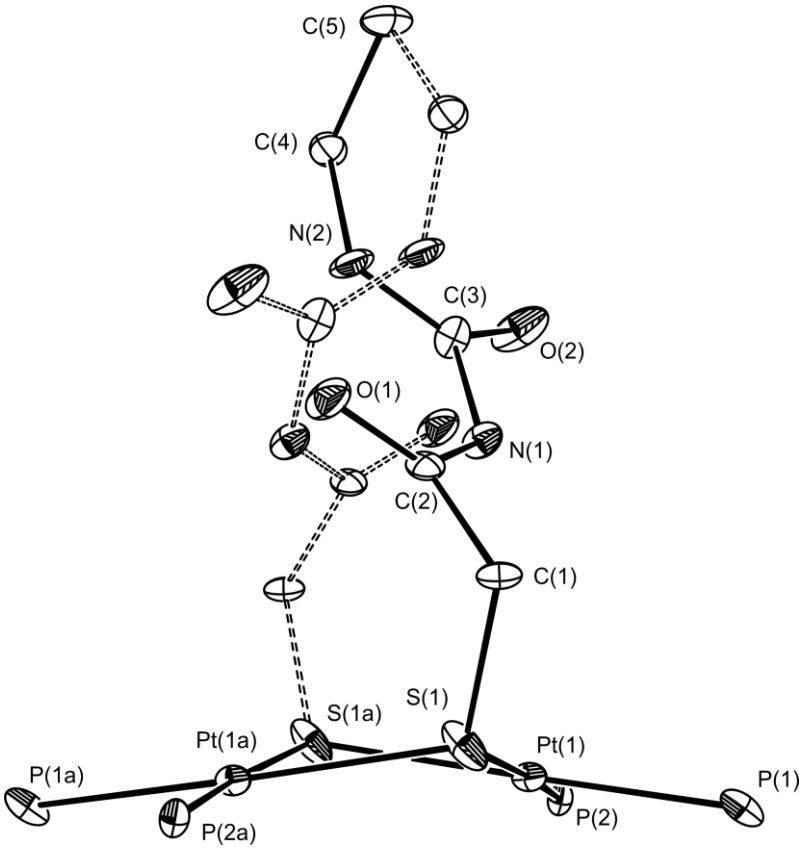

Figure 2.6 Molecular structure of the complex $[Pt_2(\mu\text{-}S)(\mu\text{-}SCH_2C(O)NHC(O)NHCH_2CH_3)(PPh_3)_4](PF_6)$ **2.8b·PF$_6$** showing the atom numbering scheme, with thermal ellipsoids at the 50% probability level and the pseudo symmetry generated disordered substituent on the second sulfur. The PF_6^- and the phenyl rings of PPh_3 ligands have been omitted for clarity.

Table 2.4 Selected bond lengths (Å) for $[Pt_2(\mu\text{-}S)(\mu\text{-}SCH_2C(O)NHC(O)NHCH_2CH_3)(PPh_3)_4]$-$(PF_6)$ **2.8b·PF$_6$** (Estimated standard deviations are in brackets).

Bond lengths and atomic distances (Å)			
Pt(1)-P(2)	2.276(10)	Pt(1a)-P(1a)	2.293
Pt(1)-P(1)	2.2954(13)	Pt(1a)-P(2a)	2.274
Pt(1)-S(1a)	2.3371(11)	Pt(1a)-S(1a)	2.338
Pt(1)-S(1)	2.3304(14)	Pt(1a)-S(1)	2.332
S(1)-C(1)	1.782(8)	N(1)-C(3)	1.422(11)
C(1)-C(2)	1.506(12)	C(3)-O(2)	1.194(11)
C(2)-O(1)	1.2010(11)	C(3)-N(2)	1.332(12)
C(2)-N(1)	1.365(11)	N(2)-C(4)	1.465(11)
C(4)-C(5)	1.675 (13)	Pt(1)---Pt(2)	3.479
S(1)---S(2)	3.034		

The structures of **2.1b·PF$_6$**, **2.4b·(PF$_6$)$_2$**, **2.7b·PF$_6$** and **2.8b·PF$_6$** as determined by X-ray crystallography revealed that the complexes have the typical hinged square-planar conformation on the $\{Pt_2(\mu\text{-}S)_2\}$ ring. Table 2.5 shows a comparison of the geometric parameters of the ethanol solvate of **1.1** $[Pt_2(\mu\text{-}S)(PPh_3)_4]\cdot 2EtOH$[14] **2.0** with $[Pt_2(\mu\text{-}S)\{\mu\text{-}SCH_2C(=NNHC(O)NH_2)Ph\}(PPh_3)_4](PF_6)$ **2.1b·PF$_6$**, $[Pt_2(\mu\text{-}S)\{\mu\text{-}SCH_2C(=NNHC(NH_2)_2)Ph\}(PPh_3)_4](PF_6)_2$ **2.4b·(PF$_6$)$_2$**, $[Pt_2(\mu\text{-}S)\{\mu\text{-}SCH_2CH_2NHC(O)N(CH_2CH_2)_2S\}(PPh_3)_4](PF_6)$ **2.7b·PF$_6$** and $[Pt_2(\mu\text{-}S)\{\mu\text{-}SCH_2C(O)NHC(O)NHCH_2CH_3\}(PPh_3)_4](PF_6)$ **2.8b·PF$_6$** and the structures of previously reported complexes $[Pt_2(\mu\text{-}S)\{\mu\text{-}SCH_2C(O)Ph\}(PPh_3)_4](BPh_4)$[9] **2.14·BPh$_4$**, $[Pt_2(\mu\text{-}SMe)(\mu\text{-}S)(PPh_3)_4]PF_6\cdot MeOH$[5] **2.15**, $[Pt_2(\mu\text{-}S)(\mu\text{-}SCH_2C(=NNHAr)Ph)(PPh_3)_4](BPh_4)$[9] **2.16·BPh$_4$** and $[Pt_2(\mu\text{-}S)(\mu\text{-}SCH_2CH_2CN)(PPh_3)_4](PF_6)$[10] **2.17·PF$_6$**. The structures also revealed slightly different dihedral angles in the derivatives. The alkyl substituents adopt an *exo*- conformation and point away from the bulky triphenylphosphine ligands of the $\{Pt_2(\mu\text{-}S)_2\}$ core. This indicates a low intra-molecular attraction between the donor atoms of the incorporated groups and platinum.

The dihedral angles of the complexes, i.e. the angles between the two coordination planes Pt_1SS and Pt_2SS (Table2.5), vary between 133-158^o depending on the nature of the attached group. The dihedral angles of **2.7b·PF$_6$** (138.6^o) and **2.15** (138^o) are larger than **2.1b·PF$_6$** (133.1^o**)** and **2.14·BPh$_4$** (133.8^o). The smaller dihedral angles in **2.1b·PF$_6$** and **2.14·BPh$_4$** may be caused by the repulsion between the phenyl group of the attached groups and the PPh_3 rings of $\{Pt_2(\mu\text{-}S)_2\}$. This is also possible because of inevitably larger degrees of bending resulting from the intramolecular repulsion in order to accommodate the attached substituents and maximise the intramolecular separation between the attached groups and the terminal PPh_3[10]. The difference in dihedral angles of **2.4b·PF$_6$** (135^o) and **2.8b·PF$_6$** (158^o) also showed the same trend but cannot be easily compared due to the disordered substituent groups in the determined crystal structure.

Table 2.5 also shows that the Pt---Pt separations are shorter in **2.1b·PF$_6$** (3.297 Å) and **2.14·BPh$_4$ (**3.283 Å) than in **2.7b·PF$_6$** (3.325 Å) and **2.15** (3.306 Å). This is obviously due to the folding along the S---S axis due to increased steric effect which imposed a shorter Pt---Pt distance in complexes with phenyl group in the attached group. It also shows that the average of the Pt-S-Pt bond

angle in complexes **2.7b·PF$_6$** and **2.15** is 90.0^o while it is about 88.4^o for **2.1b·PF$_6$** and **2.14·BPh$_4$**. The bending caused by the repulsion between the attached groups in **2.1b·PF$_6$** and **2.14·PF$_6$** and the terminal PPh_3 rings may be responsible for the reduction in the Pt-S-Pt angles.

The structure of **2.1b·PF$_6$** (Figure 2.3) shows that the attached semicarbazone is not planar above the $\{Pt_2S_2\}$ ring. The plane N(2)-N(1)-C(2) of the semicarbazide moiety in the attached group is twisted away at an angle of 40.28^o from the plane of the phenyl group C(23)-C(26)-C(21). This twist may be due to crystal packing or steric hindrance between the attached semicarbazone and the triphenylphosphine group of **1.1**. This is evident from the angles made by S(1), C(1) and C(2) in complex **2.1b·PF$_6$** [113.7(7)^o] compared to the same angle in complex **2.7b·PF$_6$** [109.0(5)^o]. The difference in the angles in **2.1b·PF$_6$** and **2.7b·PF$_6$** is attributable to a greater intramolecular repulsion between the phenyl group of the attached semicarbazone than the extra -CH_2- in **2.7b·PF$_6$** and PPh_3 phenyl rings of $\{Pt_2S_2\}$. This repulsion, resulting in a large degree of bending of the Pt_1SS and Pt_2SS planes, may also be responsible for smaller Pt---Pt separation in **2.1b·PF$_6$**, 3.297 Å compared to **2.7b·PF$_6$**, 3.325 Å and $[Pt_2(\mu\text{-}SMe)(\mu\text{-}S)(PPh_3)_4]PF_6.MeOH$[5] **2.15**, 3.306 Å, where less repulsion is expected between the attached group and PPh_3. This is because of the absence of phenyl groups in the attached groups in **2.7b·PF$_6$** and **2.15**.

The Pt–P bonds *trans* to S^{2-} have longer distances than the Pt–P bond *trans* to thiolate SR in the complexes. For example, Table 2.1 shows that the Pt(1)-P(1) (2.315(3) Å) and Pt(2)-P(4) (2.316(3) Å) bond lengths are longer than the Pt(1)-P(2) (2.310(3) Å) and Pt(2)-P(3), (2.3281(3) Å) bond lengths in **2.1b·PF$_6$**. The sulfide bridging group has a greater *trans* influence than the thiolate bridging group, and thus the bonds positioned *trans* to S^{2-} are weakened and consequently lengthened relative to the bonds *trans* to the SR^- group. A more detailed analysis of the coupling constant data (see Table 2.7) reveals that the compounds containing the $SCH_2C(O)$ group (e.g. 3379 Hz for **2.8b·PF$_6$**) tend to have higher values of $^1J_{(Pt\text{-}P)}$ for the phosphines trans to the thiolate ligand, indicating that these thiolates have slightly lower *trans* influences than their counterparts with $SCH_2C(NR)$ groups (e.g. 3332 Hz in **2.3·PF$_6$**). Compounds with the SCH_2CH_2 (e.g. 3232 Hz for **2.7b·PF$_6$**) functionality have the lowest $^1J_{(Pt\text{-}P)}$ values for the phosphines *trans* to thiolates, indicating these ligands have slightly higher trans

influences. The dicationic guanidine-based compound **2.4b·PF_6** has a notably large $^1J_{(Pt\text{-}PA)}$ coupling constant for the phosphines *trans* to sulfide (2738 Hz), and a low $^1J_{(Pt\text{-}P)}$ coupling constant for the phosphines *trans* to thiolate (3287 Hz).

The reported structure parameters of **2.0** compare closely with the newly synthesised monoalkylated complexes and the previously reported ones. The mean Pt–S bond lengths in **2.0** [2.332(8) Å] compared to the newly prepared complexes show that the average Pt–S bond lengths in the alkylated complexes are about the same and within a narrow range, **2.15** [2.320(8) Å], **2.7b** [2.334(16) Å], **2.16** [2.335(7) Å], **2.14·BPh_4** [2.338(7) Å], **2.1b·PF_6** [2.339(3) Å] and **2.4b·$(PF_6)_2$** [2.353(2) Å]. Table 2.5 also shows that the average Pt-SR bond lengths in the complexes are within a narrow range from **2.4b·$(PF_6)_2$** [2.307(2) Å], **2.15** [2.363(11) Å], **2.7b·PF_6** [2.367(16) Å], **2.16·BPh_4** [2.369(7) Å], **2.14·BPh_4** [2.372(7) Å] to **2.1b·PF_6** [2.390(3) Å]. The S-Pt-S bond angle remains fairly constant from one compound to the next revealing that the torsion which may have been created within the ring by alkylation has no substantial effect on the S---S separation which would have affected the S-Pt-S bond angles. This may be because of the flexibility of the hinge angle in the $\{Pt_2S_2\}$ ring. [15]

Table 2.5 Comparison of the geometric parameters [distances and separations (Å) and angles (°)] for **2.0**, **2.1b·PF_6**, **2.4b·PF_6**, **2.7b·PF_6**, **2.8b·PF_6**, **2.14·BPh_4**, **2.15**, **2.16·BPh_4** and **2.17·PF_6** (Estimated standard deviations are in brackets where reported)

	2.0	**2.1b·PF_6**	**2.4b·$(PF_6)_2$**	**2.7b·PF_6**	**2.8b·PF_6**	**2.14·PF_6**	**2.15**	**2.16·BPh_4**	**2.17·PF_6**
Mean Pt-S	2.332(8)	2.339(3)	2.353(2)	2.334(16)	2.330(8)	2.338(7)	2.320(8)	2.335(7)	2.367(5)
Mean Pt-SR	2.349(8)	2.390(3)	2.307(2)	2.367(16)	2.337(13)	2.372(7)	2.363(11)	2.369(7)	2.345(17)
Mean Pt-P	2.283(9)	2.306(3)	2.294(2)	2.292(17)	2.286(6)	2.293(7)	2.276(7)	2.288(7)	2.299(18)
Pt---Pt	3.283	3.297	3.305	3.325	3.479	3.283	3.306	3.216	3.311
S---S	3.057	3.071	3.064	3.077	3.034	3.087	3.06	3.075	3.169
Mean Pt-S-Pt	88.1(3)	88.4(8)	84.1(7)	90.0(6)	96.39(3)	88.4(2)	90.0(10)	86.2(2)	89.3(12)
Mean S-Pt-P	87.8(3)	89.1(9)	89.8(8)	89.6(7)	89.71(11)	88.9(3)	88.8(18)	90.2(3)	87.23(9)
Mean S-Pt-S	81.6(3)	81.0(9)	81.1(7)	81.76(6)	81.09(9)	81.9(3)	81.6(1)	81.6(2)	84.28(12)
Dihedral angle	133	133.1	134.8	138.6	157.62	133.8	138	129.2	144

Dihedral angles = the measured angles between Pt(1)S(1)S(2) and Pt(2)S(1)S(2) planes.

2.2.4 Spectroscopic and Mass Spectrometric Characterisation

2.2.4.1 ^{1}H NMR

The ^{1}H NMR spectra of the alkylated derivatives gave complicated signals in the aromatic region which could not be easily assigned. This is because of the large number of phenyl rings in the complex. However the signals attributable to non-phenyl hydrogen atoms of the attached group are identifiable except in cases where the hydrogen(s) possess unusual features preventing its signal from being clearly observed. The signals due to SCH_2 protons in the monoalkylated complexes occurred between 2.84-3.95 ppm. The methylene SCH_2 protons are easily identifiable as a broad triplet signal with broad satellite peaks produced by coupling to the ^{31}P and ^{195}Pt atoms respectively[16] as shown for **2.8b·PF$_6$** in Figure 2.7. This observation was a good indication that not only was the alkyl group present, but it was also bonded to one of the sulfur atoms of **1.1**.

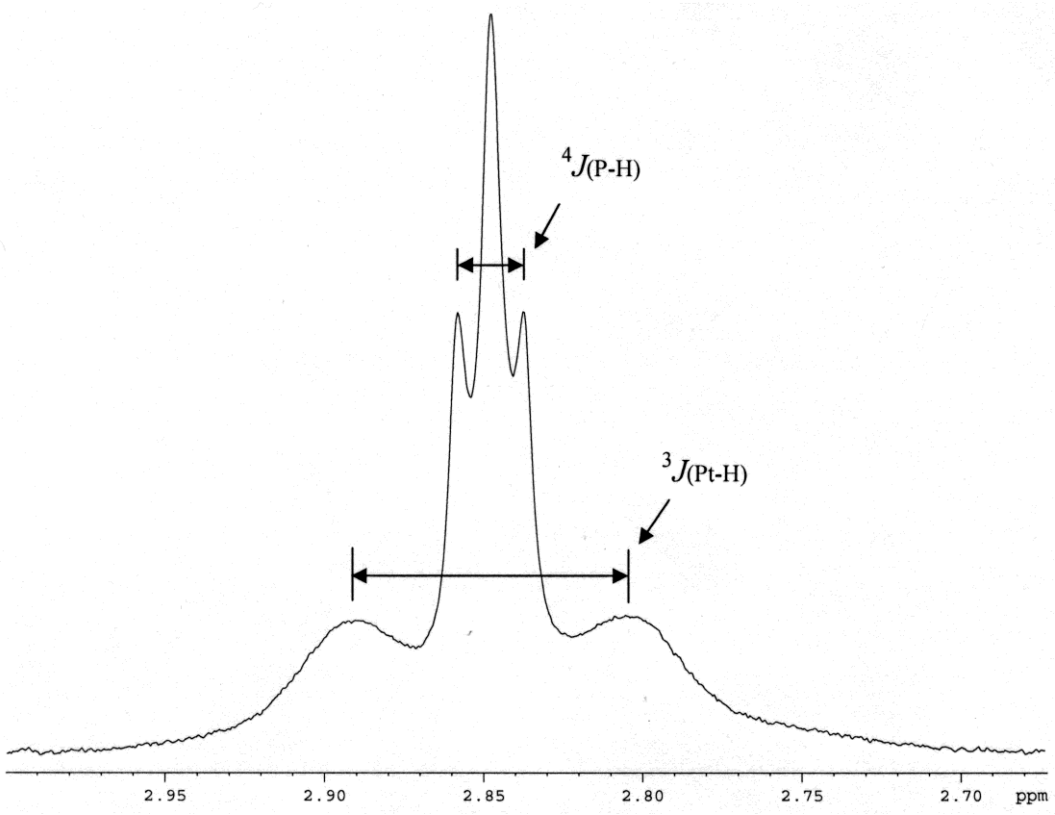

Figure 2.7 Part of the ^{1}H NMR spectrum of $[Pt_2(\mu\text{-}S)\{\mu\text{-}SCH_2C(O)NHC(O)NHCH_2CH_3\}(PPh_3)_4](PF_6)$ **2.8b·PF$_6$** showing the ^3J(Pt-H) coupling due to SCH_2 protons.

The ^{1}H NMR signal for the amide protons NH and NH_2 in the semicarbazones **2.1b·PF$_6$**, **2.2b·PF$_6$** and thiosemicarbazone **2.5b·PF$_6$** derivatives appeared broad

and less prominent than other signals. This is because the amide protons are likely to be exchanging. The same reason also applies for the -OH proton of the oxime derivative **2.3b·PF$_6$**.

The ^{13}C NMR spectra of the complexes also showed complicated signals around the aromatic region. The observed signals due to SCH_2, >C=N-, C=O and other carbon atoms of the attached groups are easily identifiable. The intensity of the carbon atoms of the attached groups to the PPh_3 carbons make them appear smaller, distinct and easily identifiable in the NMR spectra.

The initial ^{1}H NMR (Figure 2.8 (**A**)) of **2.13b·PF$_6$** showed signals attributable to the formation of *Z*- (*cis*-) (major product) and *E*- *(trans-)* (minor product) 2,4-dinitrophenylhyrazone adduct isomers of the product molecule (Scheme 2.5). A subsequent ^{1}H NMR (Figure 2.8 (**B**)) spectrum, recorded after the NMR solution of **2.13b·PF$_6$** had been stored for six months at -18 ºC, showed inversion in the intensities of the signals attributable to the *Z*- and *E*- isomers. Evidence for inversion of the isomer ratio was also observed in the ^{31}P NMR discussed in Section 2.2.2.

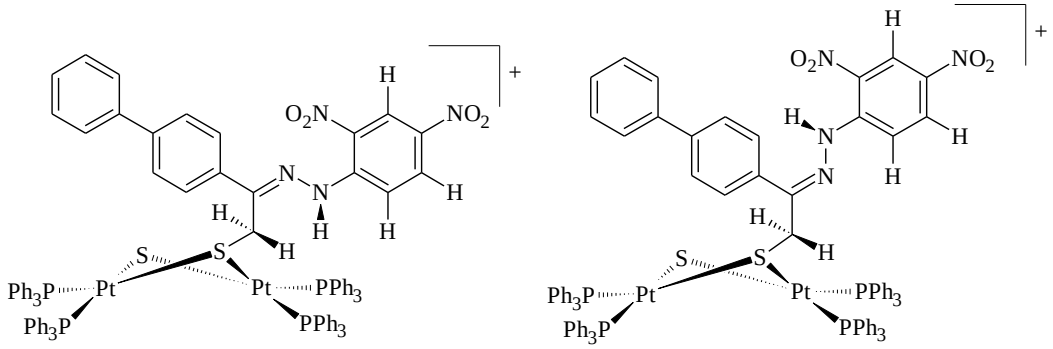

Scheme 2.5 Structures of the *Z*- and *E*- isomeric forms of **2.13b**, showing the relationship between the NH and S-CH_2 protons (*Z*-/*E*- or *cis*-/*trans*-)

Initially the ^{1}H NMR spectrum included dominant signals at 10.67 ppm (NH) and 4.40 ppm (-SCH_2), however after six months these signals showed much reduced intensities and signals at 11.19 ppm (NH) and 3.65 ppm (-SCH_2) were dominant.

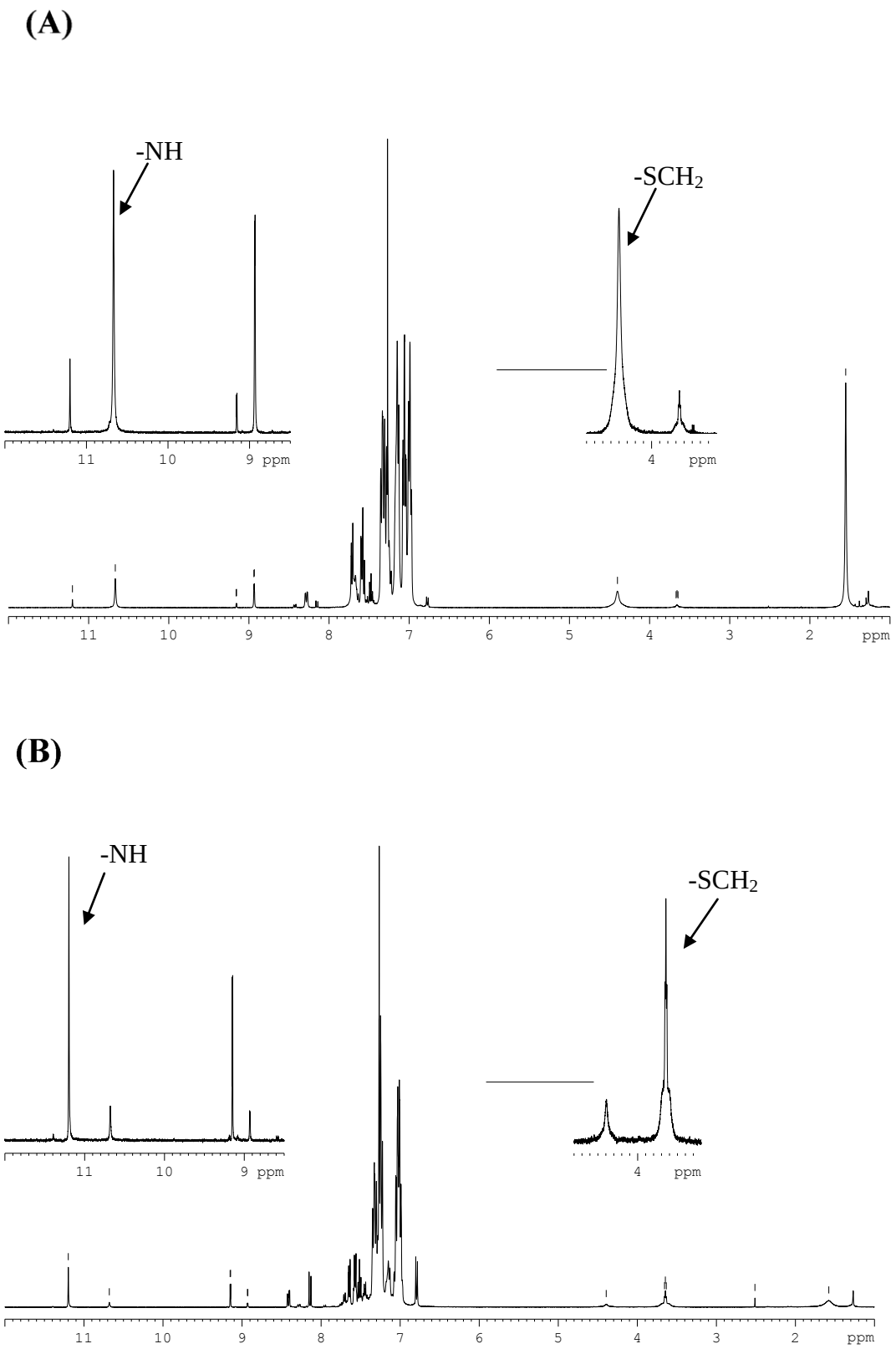

Figure 2.8 The (**A**) initial and (**B**) final ^{1}H NMR spectra (400 MHz) **2.13b·PF$_6$** showing the minor and major peaks from the two geometric isomers.

Signal assignments for protons in the vicinity of the C=N bond are presented in Table 2.6. The NMR atom labelling scheme is shown in Scheme 2.6. The stereochemistry and signal assignments for protons in the vicinity of the C=N bond of the *Z*- and *E*- isomers of **2.13b·PF$_6$** was established by an analyses of ROESY NMR data (the rotating frame equivalent of NOESY NMR data).

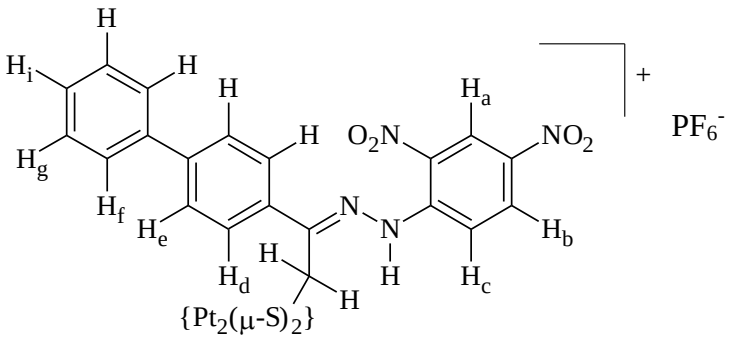

Scheme 2.6 The NMR atom numbering scheme of **2.13b·PF$_6$** (*Z*- isomer)

Table 2.6 The assignments of the ^{1}H NMR signals of *Z*- and *E*- isomeric forms of $[Pt_2(\mu\text{-}S)(\mu\text{-}SCH_2C(NNHAr)C_6H_4Ph)(PPh_3)_4](PF_6)$ **2.13b·PF$_6$**

	Z- isomer (ppm)	*E*- isomer (ppm)
NH	10.68	11.19 (s)
S-CH$_2$	4.40 (b s)	3.65 (b s)
H$_a$,	8.93 (*d, J* = 2.5 Hz*)*	9.15 (*d, J* = 2.5 Hz*)*
H$_b$,	8.29 (*dd, J* = 2.5Hz; *J* = 8.44 Hz)	8.42 (*dd, J* = 2.4Hz, J = 9.60Hz*)*
H$_c$,	7.94 (*d, J* = 8.44 Hz*)*	8.15 (*d, J* = 9.60 Hz*)*

The -SCH$_2$ signal which occurred at 4.40 ppm and the NH proton which occurred at 10.68 ppm exhibited mutual ROESY correlations (see Figure 2.9) consistent with a *Z*- relation between these protons (see Figure 2.8). On the other hand the -SCH$_2$ proton signal which occurred at 3.65 ppm showed ROESY correlations to a nearby aromatic proton which occurred at 6.79 ppm and not to the NH proton which occurred at 11.19 ppm (see Figure 2.10). Similarly this NH proton showed a ROESY correlation to an aromatic proton which occurred at 6.79 ppm and not to the -SCH$_2$ protons which occurred at 3.65 ppm. These observations are consistent with an *E*- relationship between the foregoing NH and SCH$_2$ protons.

The increased downfield shift of the S-CH$_2$ protons (4.40 ppm) in the *Z*-isomer compared to that of these proton in the *E*- isomer (3.65 ppm) can be

attributed to close proximity of the $-SCH_2$ and NH groups in the *Z*- isomer. The progressive increase in the level of the *E*- isomer ($-SCH_2$ signal at 3.65 ppm) can be attributed to its greater thermodynamic stability compared to the *Z*- isomer ($-SCH_2$ signal at 4.40 ppm), the kinetically favoured product due to reduce steric interaction between the $-SCH_2$ and NH protons in the *E*- isomer.

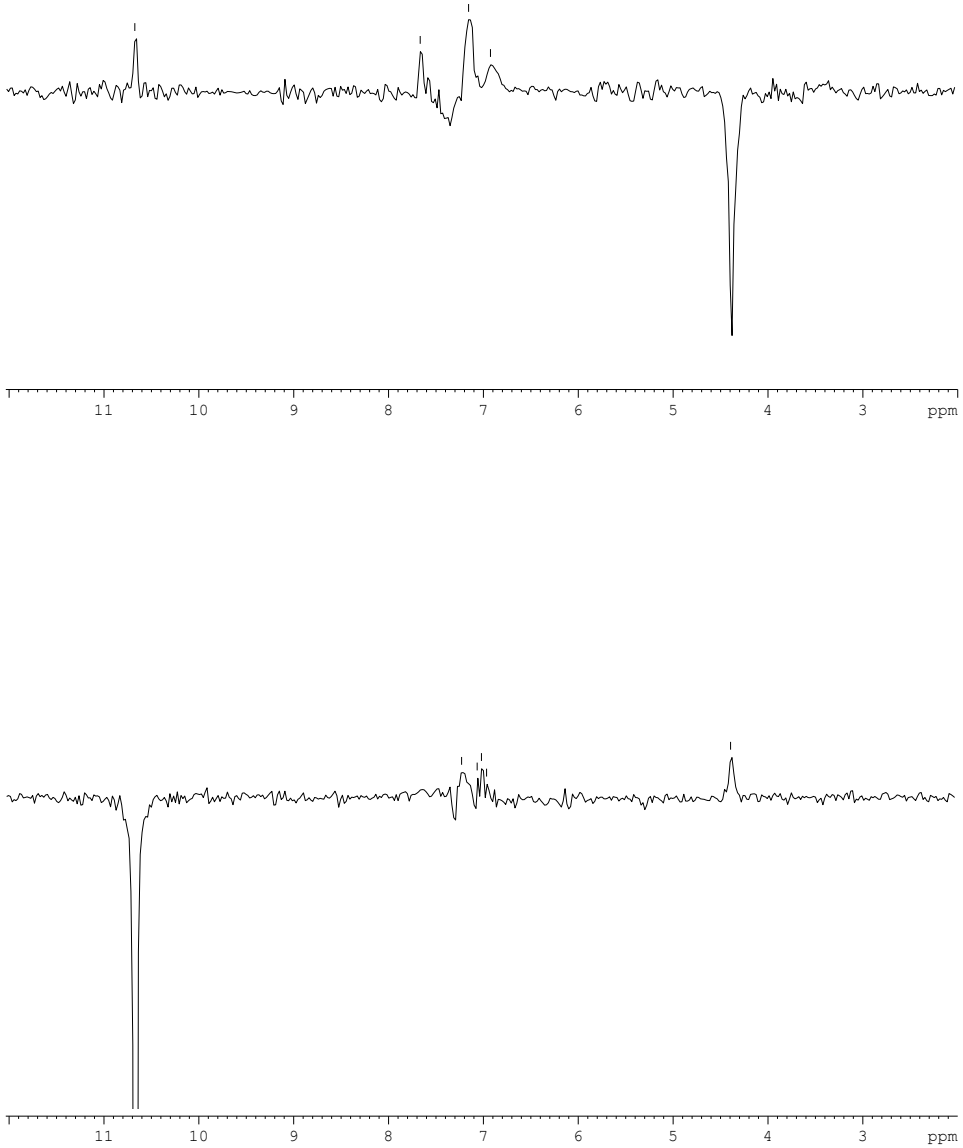

Figure 2.9 Slices from the 2D-ROESY NMR spectrum showing mutual correlations between the S-CH_2 (4.39 ppm) and NH (10.68 ppm) protons in the *Z*- isomer of **2.13b·PF_6**.

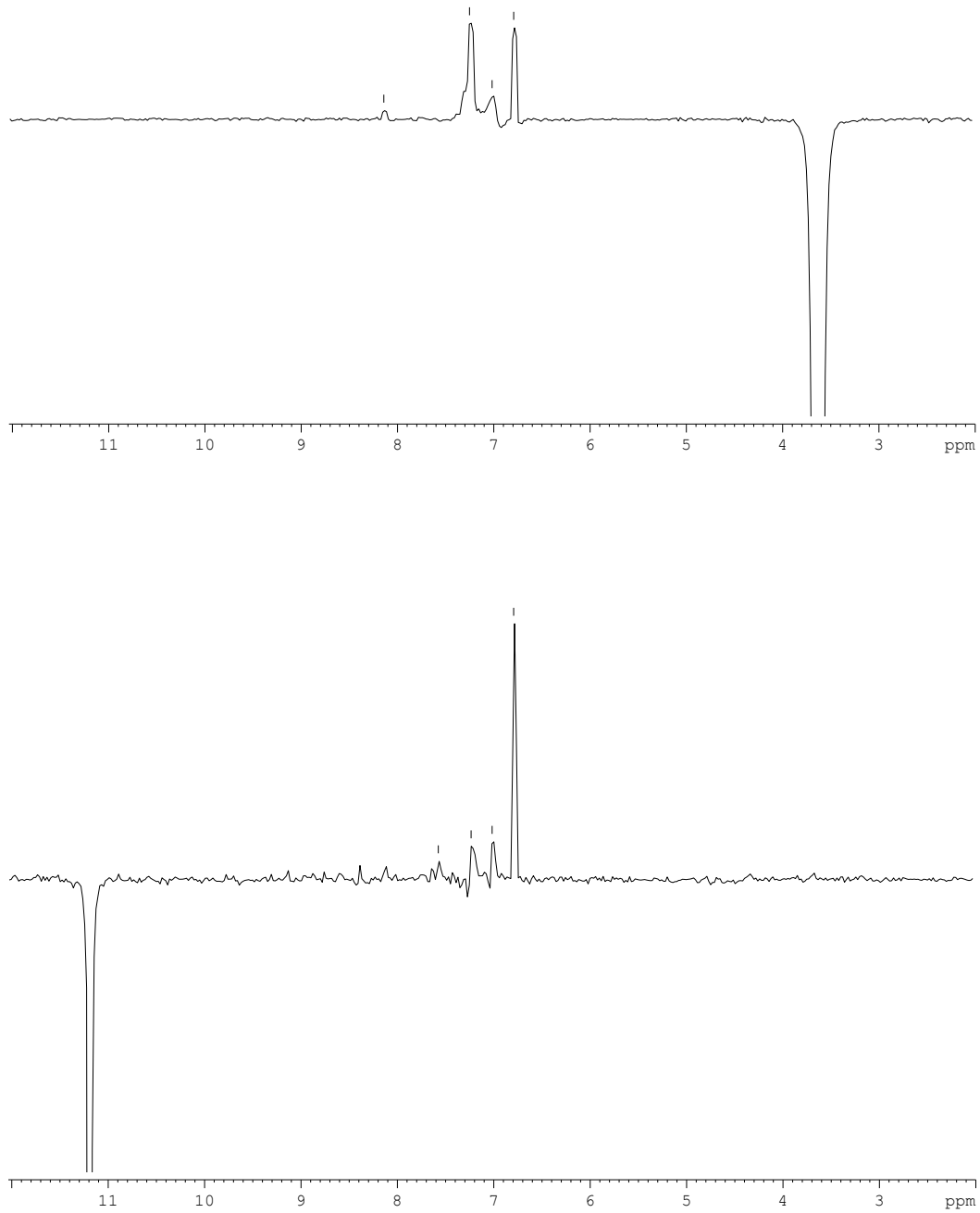

Figure 2.10 Slice from 2D-ROESY spectrum showing mutual correlations between the amide (NH) proton (11.19 ppm) and $-SCH_2$ and aromatic protons (6.79, 7.01 and 7.23 ppm) in the *E*-isomer.

2.2.4.2 $^{31}P\{^1H\}$ NMR

The ^{31}P NMR spectra of all the complexes show common features. The spectra of the complexes indicated two inequivalent phosphorus environments P_A and P_B, each giving rise to a doublet. In most of the complexes the signal due to the two different phosphorus environments appeared superimposed on one another. This is because the two sets of triphenylphosphine ligands, *cis*- or *trans*- to S^{2-} coincidentally have almost identical chemical shifts. The two signals were however, distinguished by their different $^1J_{(Pt\text{-}P)}$ coupling constants as shown in the illustration below (Scheme 2.7). An example is the $^{31}P\{^1H\}$ NMR of **2.8b·PF$_6$** in Figure 2.11. Table 2.7 shows a comparison of the coupling constant of complexes **2.1b·PF$_6$-2.12b·PF$_6$** and $[Pt_2(\mu\text{-}SMe)(\mu\text{-}S)(PPh_3)_4]PF_6$.MeOH **2.15**.

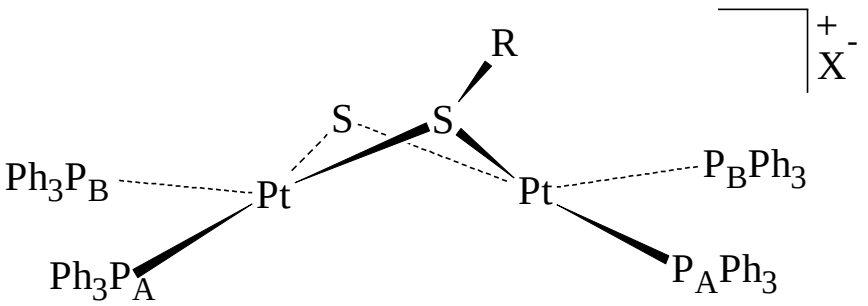

Scheme 2.7 The numbering scheme of the phosphorus environments P_B *trans*- to S^{2-} and P_A *cis*- to the thiolate SR

The two different phosphorus groups have different coupling constants to ^{195}Pt, with the phosphines *cis* to the SR ligand, P_A and P_B *trans* to the S^{2-}. The two phosphorus atoms *cis* to SR are expected to give rise to the smaller ^1J(Pt-P) coupling constant. This is because the higher *trans* influence of S^{2-}, relative to SR, lengthens the Pt-P_A bond, resulting in a smaller ^1J(Pt-P) value. The two chemically inequivalent ^{31}P nuclei were confirmed by ^{31}P NMR spectra of the complexes. The spectra showed that the signals for both P_A and P_B were flanked by two satellite peaks, one on each side. The ^1J(Pt-P_A) and ^1J(Pt-P_B) coupling constants for the complexes are in Table 2.7 below. The ^{195}Pt satellite peaks appear as pseudo triplets. The triplet was presumably due to further ^{31}P ^4J(P-P_{trans}) and ^4J(P-P_{cis}) coupling.

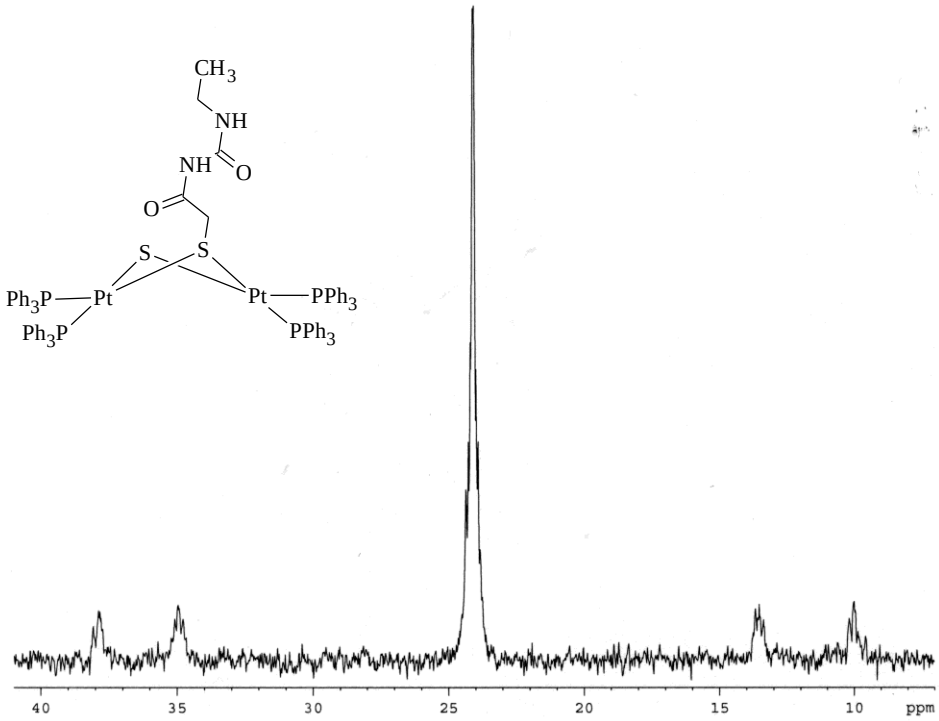

Figure 2.11 $^{31}P\{^1H\}$ NMR of $[Pt_2(\mu\text{-}S)\{\mu\text{-}SCH_2C(O)NHC(O)NHCH_2CH_3\}(PPh_3)_4](PF_6)$ **2.8b·PF$_6$** showing the near equivalence of the chemical shifts of the two P_A and P_B environments resulting in the appearance of a single central resonance, rather than the expected two.

Table 2.7 Comparison of the ^1J(Pt-P_A) and ^1J(Pt-P_B) coupling constants for the monoalkylated derivatives of complex **2.1b·PF$_6$**, **2.2b·PF$_6$**, **2.3b·PF$_6$**, **2.4b·PF$_6$**, **2.5b·PF$_6$**, **2.6b·PF$_6$**, **2.7b·PF$_6$**, **2.8b·PF$_6$**, **2.9b·PF$_6$**, **2.10b·PF$_6$**, **2.11b·PF$_6$**, **2.12b·PF$_6$** and for **2.15**.

Complex	^1J(Pt-P_A) coupling constant (Hz)	^1J(Pt-P_B) coupling constant (Hz)
2.15	2591	3220
2.1b·PF$_6$	2634	3379
2.2b·PF$_6$	2607	3332
2.3b·PF$_6$	2635	3332
2.4b·PF$_6$	2738	3287
2.5b·PF$_6$	2602	3322
2.6b·PF$_6$	2597	3281
2.7b·PF$_6$	2670	3232
2.8b·PF$_6$	2602	3379
2.9b·PF$_6$	2648	3375
2.10b·PF$_6$	2613	3330
2.11b·PF$_6$	2668	3319
2.12b·PF$_6$	2619	3381

The $^{31}P\{^1H\}$ NMR of **2.13b·PF$_6$** acquired after the compound was isolated and dried (Figure 2.12 (**A**)), initially gave two major signals at 24.5 ppm and 24.7 ppm and two minor signals at 22.4 ppm and 23.1 ppm with the corresponding satellite peaks due to coupling to ^{195}Pt. Similar spectrum has been previously observed in the ^{31}P NMR spectrum of $[Pt_2(\mu\text{-}S)(\mu\text{-}SCH_2C(NNHAr)Ph)(PPh_3)_4](BPh_4)$[9]. However, it was not completely clear whether the signals were due to the presence of two isomeric forms or is a unique characteristic spectrum of the 2,4-dinitrophenyl hydrazone derivative of **1.1** and thus required further investigative study to resolve the uncertainties.

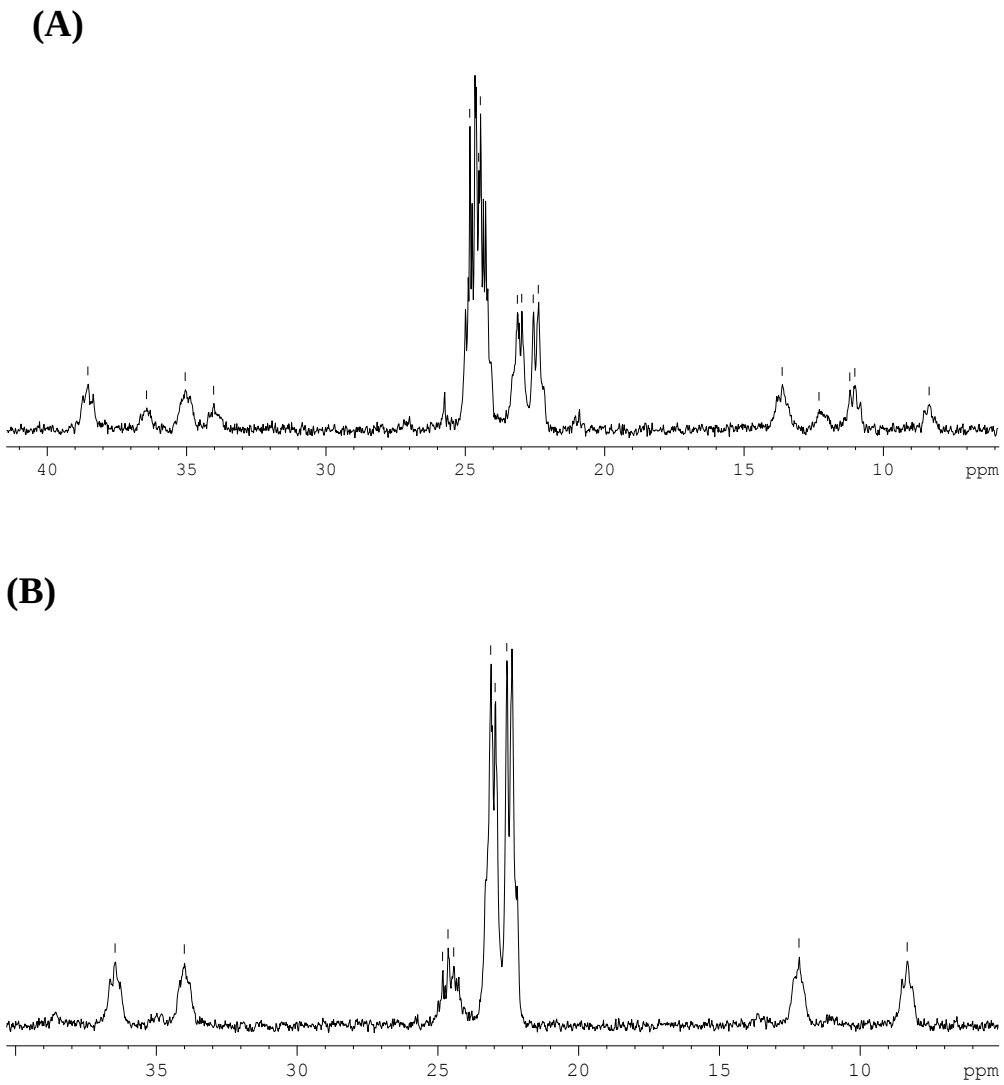

Figure 2.12 The initial (**A**) and later (**B**) $^{31}P\{^1H\}$ NMR of **2.13b·PF$_6$** showing almost complete conversion of the initial *Z*- major isomer to the *E*- minor isomer after six months of standing in $CDCl_3$ at -18^{o}C.

The smaller coupling constants in the *E* and *Z* (final major and minor isomers) 2639 Hz and 2602 Hz respectively are due to the phosphorus atoms *trans*- to the S^{2-} ligand and the large coupling constants 3411 Hz and 3344 Hz respectively for the phosphorus atoms *trans*- to the thiolate SR. The $^{31}P\{^1H\}$ NMR spectrum of the same sample left in the freezer at -18^{o}C for six months shown in Figure 2.12 (**B**) indicated almost a complete conversion of the initial major isomer to the initial minor isomer. The latter, which became the major isomer is presumably the more thermodynamically stable of the two isomers. The conversion was never completed after prolonged period of 9 months.

2.2.4.3 IR Spectroscopy

The infrared spectra of the complexes show peaks attributable to the characteristic functionalities of the attached groups. The peaks were assigned to confirm the presence of the functional groups in the alkylated products but did not give structural information about the complexes**.** Variable IR absorptions attributable to the C=O stretch were observed between 1700 -1638 cm^{-1} in the IR spectra of the complexes containing a carbonyl group. The absorption due to NH was also observed in all the complexes between 3000 and 3450 cm^{-1}.

2.3 Conclusion

The results obtained from the investigation in this section of the research show the successful construction of a range of multifunctionlised thiolate ligands bonded to platinum $[Pt_2(S)(SR)(PPh_3)_4]^+$. The two isomeric alkylated products formed upon incorporation of 2,4-dinitrophenylhydrazone moiety on **1.1** have been successfully characterised, resolving the previous uncertainties in the nature of the product from $BrCH_2C(NNHAr)Ph$. The multifunctional cationic ligand systems offer a potential template that could mediate the synthesis of diverse compounds tailored towards specific applications. Potentially, the study can be extended to the reactivity of the functionalised derivative towards metal fragments and in turn add to synthetic method of the heterometallic aggregate of **1.1**. The overall outcome of this study indicates that any suitable functional group can be incorporated into a suitable electrophile and incorporated into **1.1**. The ESI-MS technique is a very convenient and efficient screening and monitoring tool in the

study of alkylation reactions between the electrophiles and **1.1**. The application of this technique in monitoring the laboratory scale syntheses of promising reactions between the electrophiles and **1.1** and the ability of the instrument to detect charged species in the reaction mixtures successfully aided the synthesis and isolation of the monoalkylated derivatives of **1.1**. The isolated derivatives which were further characterised by NMR, elemental analysis, IR and X-ray crystallography perfectly correlated the ESI-MS data. However, the electrophiles used in this synthesis selectively monoalkylated one of the sulfide centres in **1.1** even when used in a large excess. This raises a research question as to why most of the electrophiles only alkylated one of the sulfide centres. A recent report by Chong *et al*[10] of homodialkylation of **1.1** by large conjugated aromatic systems indicates that there exists promising prospects of generating a range of dialkylated derivatives of **1.1**. The possibility of constructing and synthesising dialkylated derivatives lies in the appropriate choice of alkylating agent. An investigation into the factors that induce the required optimal electronic change upon monoalkylation of **1.1** for further alkylation of the second sulfide will be the focus of the subsequent chapter.

2.4 Experimental

Solvents used were generally drum grade as supplied. Complex $[Pt_2(\mu\text{-}S)_2(PPh_3)_4]$ **1.1** was synthesised by metathesis of *cis*-$[PtCl_2(PPh_3)_2]$ with $Na_2S.9H_2O$ in benzene[1] and obtained at a yield of 88%. ESI-MS; +20 V distilled MeOH : *m/z* 1503 $[M + H]^+$. Unless otherwise stated, all ^1H NMR ESI-MS mass spectra were recorded as explained in the appendix. Methanol, dichloromethane, diethyl ether were supplied as drum grade chemicals. The following chemicals were used as supplied from BDH: phenacyl chloride, 2,4-dinitrophenyl hydrazine, guanidine carbonate, NH_4PF_6; M & B: Hydroxylamine hydrochloride; Aldrich: isocyanate thiomorpholine, chloroacetone, 2-bromo-4'-phenylacetophenone, semicarbazide hydrochloride, thiosemicarbazide and isonicotinic acid hydrazide, and tosylhydrazide.

2.4.1 Synthesis of the Alkylating Agents

The alkylating agents were either synthesised following the literature procedure or for the first time as a new compound. $ClCH_2C(=NNHC(O)NH_2)Ph$[17] **2.1a**, $ClCH_2C(=NNHC(O)NH_2)CH_3$[17] **2.2a**, $ClCH_2C(=NOH)Ph$[18] **2.3a**, $ClCH_2C(=NNHC(S)NH_2)CH_3$[19] **2.5a**, $ClCH_2CH_2NHC(O)NHPy$[20] **2.6a**, $ClCH_2C(O)NHC(O)NHCH_2CH_3$[21] **2.8a** $ClCH_2C(=NNHTs)Ph$[22] **2.9a**, $ClCH_2C(=NNHTs)CH_3$[22] 2.**10a**, $BrCH_2C(NNHAr)C_6H_4Ph$[23] **2.13a** and $ClCH_2C\{=NNHC(=NH)NH_2\}Ph$[24] **2.4a** were synthesised following the literature procedures. $PhC(=NHNC(O)Py)CH_2Br$[25] **2.11a** and $BrCH_2C(=NNHC(O)NH_2)C_6H_4Ph$[26] **2.12a** were synthesised by modification of the literature procedures. $ClCH_2CH_2NHC(O)N(CH_2CH_2)_2S$ **2.7a** was originally synthesised and has not been reported previously.

Preparation of $ClCH_2CH_2NHC(O)N(CH_2CH_2)_2S$ 2.7a

$HN(CH_2CH_2)_2S$ (200 mg, 2 mmol) was added to a solution of $ClCH_2CH_2$-NCO (200 mg, 2 mmol) in diethyl ether (30 mL) in a 100 mL round bottomed flask and the mixture stirred for 5 min. A quantitative precipitate of the product formed immediately. The product was filtered and washed with ether (20 mL) and dried under vacuum to give $ClCH_2CH_2NHC(O)N(CH_2CH_2)_2S$ (370 mg, 93%).
ESI-MS: *m/z*: 230 ($[M + Na]^+$, 100%)
^1H NMR ($CDCl_3$, 400MHz): δ_H = 3.65 (2H, *t*, CH_2), 3.57 (2H, *m*, CH_2), 3.67 (4H, *m*, CH_2), 2.20 (4H, *m*, CH_2), 7.26 (1H, *s*, NH).
Elemental analysis: calcd (%) for $C_7H_{13}ClN_2OS$, C 40.28, H 6.28. N 13.42; found: C 40.34, H 6.29, N 13.41.

2.4.2 Synthesis of the Alkylated Derivatives of $Pt_2(\mu\text{-}S)_2(PPh_3)_4]$

Preparation of $[Pt_2(\mu\text{-}S)\{\mu\text{-}SCH_2C(=NNHC(O)NH_2)Ph\}(PPh_3)_4](PF_6)$ $(2.1b\cdot PF_6)$

$PhC(=NNHC(O)NH_2)CH_2Cl$ (16.9 mg, 0.0798 mmol, 1.2 mol equiv.) was added to an orange suspension of $[Pt_2(\mu\text{-}S)_2(PPh_3)_4]$ (100 mg, 0.0665 mmol) in methanol (30 mL). The mixture was stirred at room temperature for 1 hour to give a pale yellow solution. ESI-MS of the mixture indicated complete reaction. The solution was filtered to remove traces of solid matter and excess NH_4PF_6 (150 mg, 0.92 mmol) was added, followed by distilled water (60 mL) to induce

precipitation. A pale yellow powder of **21.1b·PF_6** (109 mg, 90%) was obtained after washing with water (20 mL) and diethyl ether (20 mL) using vacuum suction filtration and drying under vacuum.

m.p.: 192-194 ^oC

$^{31}P\{^1H\}$ NMR: δ_P = 22.7 ppm (*br* s, ^1J(Pt-P_A) 2634 Hz, ^1J(Pt-P_B) 3379 Hz).

^1H NMR (400 MHz, $CDCl_3$): δ_H = 7.41-6.80 ppm (65H, *m*, 13 Ph), 3.95 (2H, br, SCH_2), 8.54 (1H, *s*, NH)

IR (KBr): ν(C=O) 1695 cm^{-1}, ν(NH) 3464 cm^{-1}

ESI-MS: *m/z*: 1679 ($[M]^+$, 100%).

Elemental analysis: calcd (%) for $C_{81}H_{70}F_6N_3OP_5Pt_2S_2$ (1824.59): C 53.32, H 3.87, N 2.30; found: C 52.48, H 3.90, N 2.48.

Pale yellow crystals of $[Pt_2(\mu\text{-}S)\{\mu\text{-}SCH_2C(=NNHC(O)NH_2)Ph\}(PPh_3)_4](PF_6)$ suitable for X-ray crystallographic analysis were obtained by vapour diffusion of diethyl ether into a dichloromethane solution.

Preparation of $[Pt_2(\mu\text{-}S)\{\mu\text{-}SCH_2C(=NNHC(O)NH_2)CH_3\}(PPh_3)_4](PF_6)$ (2.2b·PF_6)

$CH_3C(=NNHC(O)NH_2)CH_2Cl$ (11.9 mg, 0.0798 mmol, 1.2 mol equiv) was added to an orange suspension of $Pt_2(\mu\text{-}S)_2(PPh_3)_4$ (100 mg, 0.0665 mmol) in methanol (30 mL). The mixture was stirred at room temperature for 1 hour to give a pale yellow solution. ESI-MS of the mixture indicated complete reaction. The solution was filtered to remove traces of solid matter and excess NH_4PF_6 (150 mg, 0.92 mmol) was added, followed by distilled water (60 mL) to induce precipitation. A pale yellow powder of **2.2b·PF_6** (96 mg, 82 %) was obtained after washing with water (20 mL) and diethyl ether (20 mL) using vacuum suction filtration and drying under vacuum.

m.p.: 188-190 ^oC

$^{31}P\{^1H\}$ NMR: δ_P = 23.60 ppm [*br s*, ^1J(Pt-P_A) 2607 Hz, ^1J(Pt-P_B) 3332 Hz]

^1H NMR (400 MHz, $CDCl_3$): δ_H = 7.43-6.50 (60H, *m*, 12 Ph), 3.39 (2H, *br*, SCH_2), 8 (1H, *s*, NH), 0.49 (3H, s, CH_3)

IR (KBr): ν(C=O) 1710 cm^{-1}, ν(NH) 3464 cm^{-1}

ESI-MS: *m/z*: 1616 ($[M]^+$, 100%),

Elemental analysis: calcd (%) for $C_{76}H_{68}F_6N_3OP_5Pt_2S_2$ (1762.52): C 52.79, H 3.89, N 2.38; found: C 51.42, H 3.87, N 2.32.

Preparation of $[Pt_2(\mu\text{-}S)\{\mu\text{-}SCH_2C(=NOH)Ph\}(PPh_3)_4](PF_6)$ (2.3b·PF_6)

$PhC(=NOH)CH_2Cl$ (13.5 mg, 0.0798 mmol, 1.2 mol equiv.) was added to an orange suspension of $Pt_2(\mu\text{-}S)_2(PPh_3)_4$ (100 mg, 0.0665 mmol) in methanol (30 mL). The mixture was stirred at room temperature for 1 hour to give a pale yellow solution. ESI-MS of the mixture indicated complete reaction. The solution was filtered to remove traces of solid matter and excess NH_4PF_6 (150 mg, 0.92 mmol) was added to the filtrate followed by distilled water (60 mL) to complete precipitation. A pale yellow powder of **2.3b·PF_6** (94 mg, 79 %) was obtained after washing with water (20 mL) and diethyl ether (20 mL) using vacuum suction filtration and drying under vacuum.

m.p.: 164-166 ^oC

$^{31}P\{^1H\}$ NMR : δ_P = 22.7 ppm [*br, s,* ^1J(Pt-P_A) 2635 Hz, ^1J(Pt-P_B) 3332 Hz]

^1H NMR (300 MHz, $CDCl_3$): δ_H = 7.52-6.80 (65H, 13Ph), 3.89 (2H, *br*, SCH_2).

ESI-MS: *m/z*: 1636 ($[M]^+$, 100%).

IR (KBr): ν 1629 cm^{-1}

Elemental analysis: calcd (%) for $C_{80}H_{68}F_6NOP_5Pt_2S_2$ (1782.55): C 53.90, H 3.85, N 0.79; found: C 53.17, H 3.86, N 0.79.

Preparation of $[Pt_2(\mu\text{-}S)\{\mu\text{-}SCH_2C(=NNHC(=NH_2)NH_2)Ph\}(PPh_3)_4]$ $(PF_6)_2$ (2.4b·$(PF_6)_2$)

$PhC(=NNHC(NH)NH_2)CH_2Cl$ (16.8 mg, 0.0798 mmol, 1.2 mol equiv.) was added to an orange suspension of $Pt_2(\mu\text{-}S)_2(PPh_3)_4$ (100 mg, 0.0665 mmol) in methanol (30 mL). The mixture was stirred at room temperature for 15 min to give a pale yellow solution. ESI-MS of the mixture indicated complete reaction. The solution was filtered to remove traces of solid matter and excess NH_4PF_6 (150 mg, 0.92 mmol) was added, followed by distilled water (60 mL) to complete precipitation. A pale yellow powder of **2.4b·$(PF_6)_2$** (68 mg, 61%) was obtained after washing with water (20 mL) and diethyl ether (20 mL) using vacuum suction filtration and drying under vacuum.

m.p.: 167-170 ^oC

$^{31}P\{^1H\}$ NMR: δ_P = 22.40 ppm (*br, s,* ^1J(Pt-P_B) 2738Hz) and 21.20 ppm (*br, s,* ^1J(Pt-P_A) 3287Hz)

^1H NMR (300 MHz, $CDCl_3$): δ_H = 7.62-6.95 (65H, *m*, 13Ph), 3.35 (2H, *br*, SCH_2), 12.20 (1H, br, NH).

IR (KBr): ν(NH) 3465 cm^{-1}

ESI-MS: *m/z*: 838 ($[M]^{2+}$, 100%).

Elemental analysis: calcd (%) for $C_{81}H_{73}F_{12}N_4P_6Pt_2S_2$ (1970.59): C 49.37, H 3.64, N 2.84; found: C 49.41, H 3.75, N 2.80.

Light yellow crystals of $[Pt_2(\mu\text{-}S)\{\mu\text{-}SCH_2C(=NNHC(NH_2)NH_2)Ph\}(PPh_3)_4](PF_6)_2$ suitable for X-ray crystallographic analysis were obtained by vapour diffusion of pentane into a dichloromethane solution.

Preparation of $[Pt_2(\mu\text{-}S)\{\mu\text{-}SCH_2C(=NNHC(S)NH_2)CH_3\}(PPh_3)_4](PF_6)$ (2.5b·PF_6)

$CH_3C(=NNHC(S)NH_2)CH_2Cl$ (10.6 mg, 0.0639 mmol, 1.2 mol equiv) was added to an orange suspension of $Pt_2(\mu\text{-}S)_2(PPh_3)_4$ (80 mg, 0.053 mmol) in methanol (30 mL). The mixture was stirred at room temperature for 1 hour to give a pale yellow solution. ESI-MS of the mixture indicated complete reaction. The solution was filtered to remove traces of solid matter and excess NH_4PF_6 (100 mg, 0.61 mmol) was added, followed by distilled water (60 mL) to complete precipitation. A pale yellow powder of **2.5b·PF_6** (48 mg, 56%) was obtained after washing with water (40 mL) and diethyl ether (40 mL) using vacuum suction filtration and drying under vacuum.

m.p.: 188-191 ^oC

$^{31}P\{^1H\}$ NMR: δ_P = 22.50 ppm (*br s,* ^1J(Pt-P_A) 2602Hz and, ^1J(Pt-P_B) 3322Hz)

^1H NMR (400 MHz, $CDCl_3$): δ_H = 6.80-7.53 (60H, *m*, 12Ph), 3.34 (2H, *br*, SCH_2), 0.97 (NH), 0.64 (3H, s, CH_3).

IR (KBr): ν(NH) 3462 cm^{-1}

ESI-MS : *m/z*: 1632 ($[M]^+$, 100%).

Elemental analysis: calcd (%) for $C_{78}H_{68}F_6N_3P_5Pt_2S_3$ (1778.58): C 51.32, H 3.85, N 2.36; found: C 50.93, H 3.97, N 2.75.

Preparation of $[Pt_2(\mu\text{-}S)\{\mu\text{-}SCH_2CH_2NHC(O)NHPy\}(PPh_3)_4](PF_6)$ (2.6b·PF_6)

$ClCH_2CH_2NHC(O)NHPy$ (12.8 mg, 0.0639 mmol, 1.2 mol equiv) was added to an orange suspension of $[Pt_2(\mu\text{-}S)_2(PPh_3)_4]$ (80 mg, 0.053 mmol) in methanol (20 mL). The mixture was stirred at room temperature for 24 hours and refluxed at 65 ^oC for another 24 hours to give a pale yellow solution. ESI-MS of the mixture indicated complete reaction. The solution was filtered to remove traces of solid matter and excess NH_4PF_6 (100 mg, 0.61 mmol) was added, followed by distilled water (40 mL) to complete precipitation. A pale yellow powder of **2.6b·PF_6** (55 mg, 57 %) was obtained after washing with water (40 mL) and diethyl ether (40 mL) using vacuum suction filtration and drying under vacuum.

m.p.: 150-153 ^oC

$^{31}P\{^1H\}$ NMR: δ_P = 25.0 ppm (br, *s*, ^1J(Pt-P_A) 2597Hz, ^1J(Pt-P_B) 3281Hz)

^1H NMR (300 MHz, $CDCl_3$): δ_H = 7.07-7.40 (60H, *m*, 12Ph), 2.72 (2H, *br*, SCH_2).

IR (KBr): ν(NH) 3422 cm^{-1}

ESI-MS: *m/z*: 1667 ($[M]^+$, 100 %).

Elemental analysis: calcd (%) for $C_{80}H_{71}F_6N_3OP_5Pt_2S_2$ (1813.59): C 52.98, H 3.95, N 2.32; found: C 52.37, H 4.6, N 2.75.

Preparation of $[Pt_2(\mu\text{-}S)\{\mu\text{-}SCH_2CH_2NHC(O)N(CH_2CH_2)_2S\}(PPh_3)_4](PF_6)$ (2.7b·PF_6)

$ClCH_2CH_2NHC(O)N(CH_2CH_2)_2S$ (13.3 mg, 0.0639 mmol, 1.2 mol equiv.) was added to an orange suspension of $[Pt_2(\mu\text{-}S)_2(PPh_3)_4]$ (80 mg, 0.053 mmol) in methanol (20 mL). The mixture was stirred at room temperature for 24 hours to give a pale yellow solution. ESI-MS of the reaction mixture indicated complete reaction. The solution was filtered to remove traces of solid matter and excess NH_4PF_6 (100 mg, 0.61 mmol) was added, followed by distilled water (40 mL) to complete precipitation. A pale yellow powder of **2.7b·PF_6** (75.3 mg, 79 %) was obtained after washing with deionised water (40 mL) and diethyl ether (40 mL) using vacuum suction filtration and drying under vacuum.

m.p.: 249-252 ^oC

$^{31}P\{^1H\}$ NMR: δ_P = 25.4 ppm (*br, s*, ^1J(Pt-P_A) 2670Hz, ^1J(Pt-P_B) 3232Hz),

^{1}H NMR (400 MHz, $CDCl_3$): δ_H =7.41-6.72 (60H, *m*, 12 Ph), 1.36 (2H, *t*, SCH_2), 3.41 (2H, CH_2) 6.76 (1H, *t*, NH), 3.55 (4H, *t*, CH_2), 2.31(4H, *t*, CH_2).

ESI-MS: *m/z*: 1675 ($[M]^+$, 100%).

IR (KBr): ν(C=O) 1638 cm^{-1}, ν(NH) 3218 cm^{-1}

Elemental analysis: calcd (%) for $C_{79}H_{74}F_6N_2OP_5Pt_2S_3$ (1822.66): C 52.06, H 4.09, N 1.54; found: C 51.76, H 4.09, N 1.50.

Pale yellow crystals of $[Pt_2(\mu\text{-}S)\{\mu\text{-}SCH_2CH_2NHC(O)N(CH_2CH_2)_2S\}(PPh_3)_4](PF_6)$ suitable for X –ray crystallographic analysis were obtained by diffusion of pentane into a dichloromethane solution.

Preparation of $[Pt_2(\mu\text{-}S)\{\mu\text{-}SCH_2C(O)NHC(O)NHCH_2CH_3\}(PPh_3)_4](PF_6)$ (2.8b·PF_6)

$ClCH_2C(O)NHC(O)NHCH_2CH_3$ (66 mg, 0.40 mmol, 1.2 mol equiv) was added to an orange suspension of $[Pt_2(\mu\text{-}S)_2(PPh_3)_4]$ (50 mg, 0.033 mmol) in methanol (20 mL) and the mixture stirred for 15 hours. ESI-MS of the mixture indicated complete reaction. The solution was filtered to remove traces of solid matter and excess NH_4PF_6 (80 mg, 0.49 mmol) was added, followed by distilled water (30 mL) to induce precipitation. A pale yellow powder of the product **2.8b·PF_6** (15 mg, 26 %) was obtained after washing with deionised water (40 mL) and diethyl ether (40 mL) using vacuum suction filtration and drying in a vacuum.

m.p.: 166-168^{o}C.

$^{31}P\{^1H\}$ NMR: δ_P = 24 ppm (*br s*, ^1J(Pt-P_A) 2002Hz, ^1J(Pt-P_B) 3379Hz)

^{1}H NMR (400 MHz, $CDCl_3$): δ_H = 7.08 – 7.42 (60H, *m*, 12Ph), 1.03 (3H, tr, CH_3), 2.84 (2H, br, SCH_2), 3.18 (2H, *m*, CH_2), 7.76 (1H, *t*, C(O) NH), 6.67 (1H, s, NH).

IR (KBr): ν(NH) 3453 cm^{-1}

ESI-MS: *m/z*: 1632 ($[M]^+$, 100%),

Elemental analysis: calcd (%) for $C_{77}H_{70}F_6N_2O_2P_5Pt_2S_2$ (1778.54): C 52.00, H 3.97, N 1.58; found (%) C 51.28, H 4.00, N 1.99.

Pale yellow crystals of $[Pt_2(\mu\text{-}S)\{\mu\text{-}SCH_2C(O)NHC(O)NHCH_2CH_3\}(PPh_3)_4](PF_6)$ suitable for X-ray crystallographic analysis were obtained by vapour diffusion of diethyl ether into a dichloromethane solution.

Preparation of $[Pt_2(\mu\text{-}S)\{\mu\text{-}SCH_2C(=NNHTs)Ph\}(PPh_3)_4](PF_6)$ (2.9b·PF_6)

$PhC(=NNHTs)CH_2Cl$ (25.8 mg, 0.0798 mmol) was added to an orange suspension of $[Pt_2(\mu\text{-}S)_2(PPh_3)_4]$ (100 mg, 0.0665 mmol) in methanol (30 mL). The mixture was stirred at room temperature for 20 min to give a pale yellow solution. ESI-MS of the mixture indicated complete reaction. The solution was filtered to remove traces of solid matter and excess NH_4PF_6 (150 mg, 0.92 mmol) was added, followed by distilled water (60 mL) to complete precipitation. A pale yellow powder of **2.9b·PF_6** (84 mg, 66 %) was obtained after washing with water (40 mL) and diethyl ether (40 mL) using vacuum suction filtration and drying under vacuum.

m.p.: 168-170^{o}C

$^{31}P\{^{1}H\}$ NMR: δ_P = 22.6 ppm [*br s*, ^{1}J(Pt-P_A) 2648Hz, ^{1}J(Pt-P_B) 3375Hz]

^{1}H NMR (400 MHz, $CDCl_3$): δ_H = 7.06-7.48 (60H, *m*, 13 Ph), 3.63 (2H, *b*, SCH_2), 9.59 (1H, *s*, NH), 2.46 (3H, s, $-CH_3$), 6.54 (4H, *t*, CH_2) 7.73 (4H, *t*, CH_2).

IR (KBr): ν(NH) 3451 cm^{-1}

ESI-MS: *m/z* : 1787 ($[M]^+$, 100 %).

Elemental analysis: calcd (%) for $C_{87}H_{75}F_6N_2OP_5Pt_2S_3$ (1935.74): C 53.98, H 3.91, N 1.45; found: C 53.68, H 4.04, N 1.66.

Preparation of $[Pt_2(\mu\text{-}S)\{\mu\text{-}SCH_2C(=NNHTs)CH_3\}(PPh_3)_4](PF_6)$ (2.10b·PF_6)

$CH_3C(=NNHTs)CH_2Cl$ (21 mg, 0.0798 mmol) was added to an orange suspension of $[Pt_2(\mu\text{-}S)_2(PPh_3)_4]$ (100 mg, 0.0665 mmol) in methanol (30 mL). The mixture was stirred at room temperature for 25 min to give a pale yellow solution. ESI-MS of the mixture indicated complete reaction. The solution was filtered to remove traces of solid matter and excess NH_4PF_6 (150 mg, 0.92 mmol) was added, followed by distilled water (60 mL) to complete precipitation. A pale yellow powder of **2.10b·PF_6** (86 mg, 69%) was obtained after washing with water (40 mL) and diethyl ether (40 mL) using vacuum suction filtration and drying under vacuum.

m.p.: 170-173 ^{o}C

$^{31}P\{^{1}H\}$ NMR: δ_P = 23.60 ppm (2P, *br s*, ^{1}J(Pt-P_A) 2613 Hz) and 24.55 ppm (2P, *br s*, ^{1}J(Pt-P_B) 3330 Hz)

^{1}H NMR (300 MHz, $CDCl_3$): δ_H = 7.03-7.50 (60H, *m*, 12Ph), 3.22 (2H, *br*, SCH_2), 2.48 (3H, s, CH_3), 3.8 (3H, s, CH_3).

IR (KBr): ν(NH) 3450 cm^{-1}

ESI-MS: *m/z*: 1735 ($[M]^+$, 100%)

Elemental analysis: calcd (%) for $C_{87}H_{73}F_6N_2O_2P_5Pt_2S_3$ (1874.68): C 52.56, H 3.93, N 1.50; found: C 52.18, H 3.96, N 1.60.

Preparation of $[Pt_2(\mu\text{-}S)\{\mu\text{-}SCH_2C(NNHC(O)Py)Ph\}(PPh_3)_4](PF_6)$ (2.11b·PF_6)

$BrCH_2C(NNHC(O)Py)Ph$ (0.13 g, 0.040 mmol, 1.2 mol equiv) was added to an orange suspension of $[Pt_2(\mu\text{-}S)_2(PPh_3)_4]$ (50 mg, 0.033 mmol) in methanol (20 mL) and the mixture stirred for 1 hr. ESI-MS of the mixture indicated complete reaction. The solution was filtered to remove traces of solid matter and excess of NH_4PF_6 (80 mg, 0.49 mmol) was added, followed by distilled water (30 mL) to induce precipitation. A pale yellow powder of the product **2.11b·PF_6** (46 mg, 73%) was obtained after washing with deionised water (40 mL) and diethyl ether (40 mL) using vacuum suction filtration and drying in a vacuum.

m.p.: 165-168 ^oC

$^{31}P\{^1H\}$ NMR: δ_P = 21.8 ppm [*br s*, ^1J(Pt-P_A) 2668Hz , ^1J(Pt-P_B) 3319Hz]

^{1}H NMR (400MHz, $CDCl_3$): δ_H = 3.22 (2H, *br*, SCH_2), 8.12 (1H, *s*, NH)

IR (KBr): ν(C=O) 1698 cm^{-1}, ν(NH) 3455 cm^{-1}

ESI-MS: *m/z*: 1740 ($[M]^+$, 100%).

Elemental analysis: calcd (%) for $C_{86}H_{72}F_6N_3OP_5Pt_2S_2$ (1886.66.): C 54.75, H 3.85, N 2.23; found: C 53.80, H 3.86, N 2.35

Preparation of $[Pt_2(\mu\text{-}S)\{\mu\text{-}SCH_2C(=NNHC(O)NH_2)C_6H_4Ph\}(PPh_3)_4](PF_6)$ (2.12b·PF_6)

$PhC_6H_4C(=NNHC(O)NH_2)CH_2Br$ (13.3 mg, 0.040 mmol, 1.2 mol equiv) was introduced into an orange suspension of $[Pt_2(\mu\text{-}S)_2(PPh_3)_4]$ (50 mg, 0.033 mmol) in methanol (20 mL). The mixture was stirred at room temperature for 25 mins to give a pale yellow solution. ESI-MS of the mixture indicated complete reaction. The solution was filtered to removed traces of solid matter and excess NH_4PF_6 (80 mg, 0.49 mmol) was added, followed by distilled water (30 mL) to complete precipitation. A pale yellow powder of **2.12b·PF_6** (37 mg, 59 %) was

obtained after washing with water (40 mL) and diethyl ether (40 mL) using vacuum suction filtration and drying under vacuum.

m.p. 188-190^oC

$^{31}P\{^1H\}$ NMR: δ_P = 22.7 ppm (*br s*, ^1J(Pt-P_A) 2619 Hz, 2P, ^1J(Pt-P_B) 3381Hz)

^1H NMR (300 MHz, $CDCl_3$): δ_H = 7.07-7.40 (65H, *m*, 13Ph), 3.39 (2H, *br*, SCH_2), 8.68 (1H, s, NH).

IR (KBr): ν(NH) 3455 cm^{-1}

ESI-MS: *m/z*: 1753 ($[M]^+$, 100%).

Elemental analysis: calcd (%) for $C_{87}H_{74}F_6N_3OP_5Pt_2S_2$ (1900.68): C 54.98, H 3.92, N 2.21; found: C 54.56, H 3.95, N 2.61.

Preparation of $[Pt_2(\mu\text{-}S)(\mu\text{-}SCH_2C(NNHAr)C_6H_4Ph)(PPh_3)_4](PF_6)$ 2.13b·PF_6

$[Pt_2(\mu\text{-}S)_2(PPh_3)_4]$ (100 mg, 0.067 mmol) and $BrCH_2C(NNHAr)C_6H_4Ph$ (36.4 mg, 0.080 mmol), 1.2 mol equivalent) in methanol (25 mL) was stirred. The reaction mixture solubilised and became deep yellow orange in colour after 5 minutes. The ESI-MS indicated complete monoalkylation after 45 minutes. The reaction was allowed to stir for 1 hour. The solution was gravity filtered to remove any solid impurity. The product was precipitated as PF_6^- salt by the addition of excess NH_4PF_6 (80 mg, 0.49 mmol) and distilled H_2O (10 mL). The product **2.13·PF_6** after filtration was washed with diethyl ether (40 mL) and air dried to give (92.5 mg, 68 %) which was further purified by vapour diffusion of diethyl ether into a CH_2Cl_2 solution.

m.p.: 178-180^oC

IR (KBr): υ cm^{-1} 692, 838, 1096, 1333, 1501, 1516, 1434, 1613 and 3455

^{31}P NMR (300 MHz, $CDCl_3$): *Z*- isomer δ_p 24.52 (br, *m*, $^1J_{(Pt\text{-}PA)}$, 3344Hz and $^1J_{(Pt\text{-}PB)}$, 2602 Hz); *E*- isomer δp 23.1 (br, *m*, $^1J_{(Pt\text{-}PA)}$, 2639 Hz) and 22.5 (br, *m*, $^1J_{(Pt\text{-}PB)}$, 3411Hz)

^1H NMR (400 MHz): (*Z*-isomer) δ 10.68 (1H, *s*, NH), 8.93 (Hc, *d*, 1H), 8.29 (Hb, *d*, 1H), 7.94 (Ha, *d*, 1H), 4.39 (2H, b, CH_2); *E*-isomer δ 11.19 (1H, *s*, NH), 9.15 (Hc, *d* 1H), 8.42 (Hb, *d*, 1H), 8.15 (Ha, *d*, 1H), 3.65 (2H, *b*, CH_2).

ESI- MS (MeOH) cone voltage 20V: *m/z*, 1876 $[M]^+$ 100%

Elemental analysis: calcd (%) for $C_{92}H_{75}F_6N_4P_5Pt_2S_2$ (2023.76): C 54.60, H 3.70, N 2.77, Found; C 54.15, H 3.71, N 2.74.

2.5 X-ray Crystal Structure Determinations

All data were obtained at the University of Auckland following the method explained in Section A.7 in the appendix. All the structures were solved by direct methods option of SHELXS-97[27] and first the Pt atoms located. All other non-hydrogen atoms were located from a series of difference maps. Full-matrix least-squares refinement (SHELXL-97[28]) was based on F_o^2 with all non-hydrogen atoms anisotropic and hydrogen atoms in calculated positions. All calculations were carried out by the SHELXS-97 suite of programmes. The crystal data and structure refinement parameter details are given in Tables 2.8 and 2.9.

The crystal of **2.1b·PF$_6$** did not diffract very strongly, so the data were weaker than usual. A final peak in the penultimate difference map was assigned as the O of a water molecule, H-bonded to the C=O of the main molecule and to the F atom of the anion. The H atoms of water were not included in the refinement. The crystal was shown to be monoclinic, with the space group P2(1)/n.

The structure of **2.4b·(PF$_6$)$_2$** was solved by direct methods and developed routinely to give the $[Pt_2(\mu\text{-}S)_2(PPh_3)_4]$ core of the 2+ cation. Subsequent difference maps revealed peaks that could be assigned to the side-chain attached to one S atom, but development of this part of the model was complicated by partial disorder arising from overlap of the side-chain in the reverse orientation by attachment to the other S atom. This is shown in Figure 2.13. This could not be

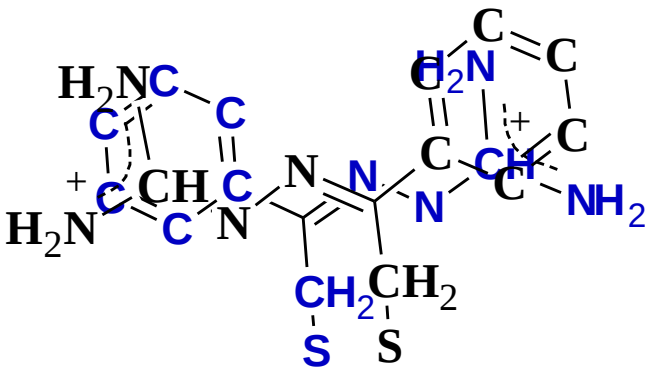

Figure 2.13 A diagram showing how the partial disorder in **2.4b·(PF$_6$)$_2$** arising from overlap of the side-chain in the reverse orientation by attachment to the other S atom to give a similar packing motif.

resolved so the minor disordered fragment was not included in the refinement. Further disorder involved the anions. The cation charge requires 12 anions in the unit cell for neutrality. These were made up from six reasonably ordered PF_6^-

anions in a general position. Two more were rotationally disordered lying on a 3-fold axis coincident with the axial P-F bonds, so the equatorial F atoms were modelled over 9 equivalent sites. Two further PF_6^- anions were located on a 3-bar axis and were translationally disordered over 3 sites but could be modelled sensibly. At this stage a difference map revealed an isolated peak of *ca* 7 e $Å^{-3}$ on a threefold axis, surrounded at a distance of 2.9 Å by C-H bonds. This refined sensibly as an F^- anion, providing the other two negative charges needed. An alternative interpretation of the electron density would be to assign four anions in total to the 3-bar site, and to refine the isolated peak as the O atom of an H_2O of crystallisation, but this was thought to be less likely.

In the final refinement, the side-chain atoms and the disordered PF_6^- anion F atoms were treated isotropically and only the hydrogen atoms associated with the phenyl rings were included. This model led to a satisfactory refinement (R_1 = 0.0569) but there were still residual electron density peaks up to 4 e $Å^{-3}$ (mostly associated with the disordered side-chain) and significant "solvent accessible voids" which indicates that the overall structure determination was not completely resolved. The basic features are unambiguous, but parameters involving the disordered sections will not be reliable.

The pocket formed by the incorporated group in **2.7b·PF$_6$** due to the alkylation of only one sulfide in $[Pt_2(\mu\text{-}S)_2(PPh_3)_4]$ and the phenyl group of PPh_3 was filled by one molecule of CH_2Cl_2 solvent used in isolating the crystals.

The substituent on the sulfide centre in **2.8b·PF$_6$** is disordered so that it is equally distributed across both symmetry related S atoms, generating 2-fold pseudo symmetry. This could be modelled in C2/c, H atoms were not included for the organic fragment, only for the phenyl rings.

Table 2.8 Crystal data and structure refinement details for **2.1b·PF$_6$** and **2.4b·PF$_6$**.

	2.1b·PF$_6$	**2.4b·(PF$_6$)$_2$**
Formula	$C_{81}H_{72}F_6N_3O_2P_5Pt_2S_2$	$C_{81}H_{72}F_{10.33}N_4P_{5.67}Pt_2S_2$
Formula weight	1842.57	1927.56
Temperature (K)	89(2)	89(2)
Wavelength (Å)	0.71073	0.71073
Crystal system	Monoclinic	Triclinic
Space group	P2(1)/n	P-3
a/Å	18.1793(1)	25.8410(2)
b/Å	21.0437(3)	25.8410(2)
c/Å	19.8683(3)	21.5233(3)
β/^{o}	92.995(1)	90
γ/^{o}	90	120
Volume (Å^3)	7590.43(16)	12446.8(2)
Z	4	6
Calculated density (Mgm^{-3})	1.612	1.543
Absorption coefficient (mm^{-1})	3.906	3.595
F(000)	3648	5712
Crystal size (mm)	0.26 x 0.10 x 0.08	0.30 x 0.18 x 0.14
Theta range for data collection	1.41 to 26.30^o	1.82 to 26.39^o
Limiting indices	-21≤h≤22,-25≤k≤26,-14≤l≤24	-32≤h≤32,-31≤k≤32, -14≤l≤26
Reflections collected / unique	43725 / 15323[R(int) = 0.1060]	74050 / 16991[R(int) = 0.0453]
Completeness to theta	99.5 % (26.30^o)	99.8 % (26.39^o)
Absorption correction	Empirical	Semi-empirical from equiv.
Max. and min. transmission	0.7452 and 0.4299	0.7452 and 0.4299
Refinement method	Full-matrix least-squares on F^2	Full-matrix least-squares on F^2
Data / restraints / parameters	15323 / 0 / 900	16991 / 1 / 869
Goodness of fit on F^2	1.083	1.060
Final R indices [I>2σ(I)]	R_1 = 0.0727, wR_2 = 0.1259	R_1 = 0.0569, wR_2 = 0.1495
R indices (all data)	R_1 = 0.1353, wR_2 = 0.1469	R_1 = 0.0786, wR_2 = 0.1659
Largest diff. peak and hole	2.057 and -2.359 e Å^{-3}	4.194 and -1.653 e Å^{-3}

Table 2.9 Crystal data and structure refinement details for **2.7b·PF$_6$** and **2.8b·PF$_6$**

	2.7b·PF$_6$	**2.8b·PF$_6$**
Formula	$C_{80}H_{75}C_{l2}F_6N_2OP_5Pt_2S_3$	$C_{77}H_{69}F_6N_2O_2P_5Pt_2S_2$
Formula weight	1906.53	1777.49
Temperature (K)	89(2)	93(2)
Wavelength (Å)	0.71073	0.71073
Crystal system	Monoclinic	Monoclinic
Space group	P2(1)/c	C2/c
a/Å	12.9507(1)	17.2956(6)
b/Å	22.4127(3)	18.8826(6)
c/Å	28.2565(3)	21.4712(7)
β/^{o}	99.411(1)	90.067(1)
Volume (Å^3)	8091.35(15)	7012.2(4)
Z	4	4
Calculated density (Mg/m^3)	1.565	1.684
Absorption coefficient (mm^{-1})	3.755	4.224
F(000)	3776	3512
Crystal size (mm)	0.28 x 0.24 x 0.20	0.49 x 0.42 x 0.32
Theta range for data collection	1.59 to 26.37^o	2.36 to 31.69^o
Limiting indices	-16≤h≤14, -27≤k≤28,-35≤l≤27	-23≤h≤25,-27≤k≤26, -31≤l≤31
Reflections collected / unique	47739 / 16445[R(int) = 0.0477]	29848 /10648 [R(int) = 0.0237]
Completeness to theta	99.5 % (26.37^o)	66.0 % (31.76^o)
Absorption correction	Semi-empirical	Empirical
Max. and min. transmission	0.5205 and 0.4195	0.3445 and 0.2312
Refinement method	Full-matrix least-squares on F^2	Full-matrix least-squares on F^2
Data / restraints / parameters	16445 / 0 / 937	7810 / 0 / 441
Goodness of fit on F^2	1.156	1.019
Final R indices [I>2σ(I)]	R_1 = 0.0540, wR_2 = 0.1148	R_1= 0.0375, wR_2 = 0.0835
R indices (all data)	R_1 = 0.0665, wR_2 = 0.1206	R_1= 0.0582, wR_2 = 0.0974
Largest diff. peak and hole	2.396 and -1.936 e Å^{-3}	2.84 and -2.24 e Å^{-3}

2.6 References

1. R. Ugo, G. La Monica, S. Cenini, A. Segre and F. Conti, *J. Chem. Soc. A,* 1971, **3**, 522.
2. S. W. A. Fong and T. S. A. Hor, *J. Chem. Soc., Dalton Trans.*, 1999, 639.
3. R. R. Gukathasan, R. H. Morris and A. Walker, *Can. J. Chem.*, 1983, **11**, 2490.
4. J. Chatt and D. M. P. Mingos, *J. Chem. Soc., A.*, 1970, 1243.
5. C. E. Briant, C. J. Gardner, T. S. A. Hor, N. D. Howells and D. M. P. Mingos, *J. Chem. Soc., Dalton Trans.*, 1984, **12** 2645.
6. W. Henderson, S. H. Chong and T. S. A. Hor, *Inorg. Chim. Acta* 2006, 3440.
7. A. P. Novikova, N. M. Perova, L. G. Egorova and E. I. Bragina, *Khimiya Geterotsiklicheskikh Soedinenii*, 1991, **6**, 843.
8. J. Schroder, A. Henke, H. Wenzel, H. Brandstetter, H. G. Stammler, A. Stammler, W. D. Pfeiffer and H. Tschesche, *J. Med. Chem.*, 2001, **44**, 3231.
9. S. M. Devoy, M.Sc. Thesis, The University of Waikato, 2005.
10. S. H. Chong, W. Henderson and T. S. A. Hor, *J. Chem. Soc. Dalton Trans.*, 2007, 4008.
11. S. Uchiyama, M. Ando and S. Aoyagi, *J. of Chromatogr. A*, 2003, **996**, 95.
12. U. Shigehisa, A. Erika, A. Shohei and A. Masanori, *Anal. Chimica Acta*, 2004, **523**, 157.
13. H. Katsuki, C. Tanegashima, M. Tokushige and S. Tanaka, *Bul. Chem. Soc. Japan*, 1971, **45**, 813.
14. W. Henderson, S. Thwaite, B. K. Nickolson and T. S. A. Hor, *Eur. J. Inorg. Chem.*, 2008, 5119.
15. M. Capdevila, W. Clegg, P. González-Duarte, A. Jarid and A. Lledós, *Inorg. Chem.*, 1996, **2**, 490.
16. R. Pryadun, D. Sukumaran, R. Bogadi and D. J. Atwood, *J. Am. Chem. Soc.*, 2004, **126**, 12414.
17. S. G. Cohen, S. Hsiao, E. Saklad and C. H. Wang, *J. Am. Chem. Soc.*, 1957, **79**, 4400.

18. V. Pavlishchuk, F. Birkelbach, T. Weyhermueller, K. Wieghardt and P. Chaudhuri, *Inorg. Chem.*, 2002, **41**, 4405.
19. H. Beyer, W. Lassig and E. Bulka, *Chemische Berichte*, 1954, **87**, 1385.
20. G. Vasilev, P. Ionova, V. Mikhailov and Z. Raikov, *Doklady Bolgarskoi Akademii Nauk* 1984, 811.
21. W. A. Jacobs, M. Heidelberger and I. P. Rolf, *J. Am. Chem. Soc.*, 1919, **41**, 458.
22. C. B. Reese and H. P. Sanders, *J. Chem. Soc., Perkin Trans.* , 1982, 2719.
23. A. I. Vogel, A. R. Tatchell, B. S. Furnis, A. J. Hannaford and P. W. G. Smith, *Vogel's Textbook of Practical Organic Chemistry (5th Edition)*, Logman, London, 1989.
24. H. Beyer and T. Pyl, *Chemische Berrichte*, 1956, **89**, 2556.
25. V. P. Singh, A. Singh and S. Singh, *J. Applied Polymer Sc.*, 2008, **110**, 1336.
26. F. Barba, M. D. Valesco and A. Guarido, *Synthesis*, 1984, 593.
27. G. M. Sheldrick, University of Göttingen, Germany, Editon 1997.
28. G. M. Sheldrick, University of Göttingen, Germany, Editon 1997.

Chapter 3

An Investigation of the Homo- and Heterodialkylation of $[Pt_2(\mu\text{-}S)_2(PPh_3)_4]$

3.1 Introduction

Dinuclear platinum(II) thiolate complexes with $\{Pt_2(\mu\text{-}SR)_2P_4\}$ and $\{Pt_2(\mu\text{-}SR')(\mu\text{-}SR)P_4\}$ cores (P = dppp, PPh_3) have attracted wide interest due to their interesting electronic, structural and conformational properties[1-5]. The incorporated groups R attached to the sulfur atoms range from simple alkyl and aryl[6, 7], ketoaryl[7], urea[4], fluorinated alkyl and aryl[8, 9] and imidazolium and thiazolium[10] groups and organometalllic fragments[11, 12]. Metal thiolate complexes can be made by methods described by Blower and Dilworth[13]. The syntheses of diplatinum thiolate of the type $\{Pt_2(\mu\text{-}SR)_2P_4\}$ can be achieved by the reaction of thiols with triflate complexes e.g. $[Pt(dppp)(CF_3SO_3)_2]$[4] or by direct reaction of appropriate electrophiles with complexes with $\{Pt_2(\mu\text{-}S)_2\}$ core[7]. However, there are only a few reported derivatives of $[Pt_2(\mu\text{-}S)_2(PPh_3)_4]$ **1.1** containing the same or different organic moieties attached to the two sulfide centres [6, 7, 10]. This may be caused by the lack of detailed study of the factors influencing their formation. For instance while it is easy to prepare $[Pt_2(\mu\text{-}SCH_3)_2(PPh_3)_4]^{2+}$ [6] from $[Pt_2(\mu\text{-}S)_2(PPh_3)_4]$ or $[Pt_2(\mu\text{-}S)(\mu\text{-}SCH_3)(PPh_3)_4]$ by reacting **1.1** with excess $(CH_3)_2SO_4$, the reaction of **1.1** with excess alkyl halide like $ClCH_2CH_2CH_2CH_3$ only results in monoalkylation[12]. In addition, stable heterodialkylated derivatives $[Pt_2(\mu\text{-}SCH_3)(\mu\text{-}SR)(PPh_3)_4]^{2+}$ have been reported and can be formed[6] when the resulting leaving group from the second alkylation is not substantially nucleophilic towards

platinum. However, the extent to which the heterogeneity of the bridging groups and the nucleophilic halide leaving groups will affect the stability and the chemistry of a heterodialkylated derivative is not certain. These questions cannot be answered because to date, only the methyl derivatives $[Pt_2(\mu\text{-}SCH_3)(\mu\text{-}SR')(PPh_3)_4]^{2+}$ (R' = organic electrophile) with non-halide leaving group from the second alkylation is known[6, 10].

Results from the investigation in chapter two indicated that any suitable organic group can be incorporated into $[Pt_2(\mu\text{-}S)_2(PPh_3)_4]$ **1.1**[14] due to its exceptional nucleophilicity[15, 16]. However, the reactions of **1.1** with organic halides mainly result in exclusive alkylation of one of the sulfide centres yielding $[Pt_2(\mu\text{-}S)(\mu\text{-}SR)(PPh_3)_4]^+$, except with short chain α,ω-electrophiles e.g. $BrCH_2CH_2Br$ which bridges the two sulfide centres[17]. The transformation of the monoalkylated derivative $[Pt_2(\mu\text{-}S)(\mu\text{-}SR)(PPh_3)_4]^+$ to dialkylated derivative $[Pt_2(\mu\text{-}SR)_2(PPh_3)_4]^{2+}$ or $[Pt_2(SR')(SR)(PPh_3)_4]^{2+}$ (R and R' are organic moieties) has been plagued with problems and is not well understood[6]. The difficulties to further alkylate the second sulfide centre has mainly been attributed to electron delocalisation within the platinum-sulfur ring structure and the formation of a monocation $[Pt_2(\mu\text{-}S)(\mu\text{-}SR)(PPh_3)_4]^+$ which discourages further attack on the second sulfur atom by another electrophile[6]. Nevertheless, recent reports indicated that dialkylation of **1.1** depends on careful choice of alkylating agent and reaction conditions[6, 7]. Latent points in these reports are indicative that, the rate of alkylation, the leaving group and the nature of the residual organic part of an electrophile are likely factors that encourage homodialkylation of $[Pt_2(\mu\text{-}S)_2(PPh_3)_4]$ **1.1** or further alkylation of the unreacted sulfur atom in $[Pt_2(\mu\text{-}S)(\mu\text{-}SR)(PPh_3)_4]^+$. The above factors were considered in selecting the alkylating agents which were employed in the investigation of the dialkylation of **1.1** in this chapter.

3.1.1 Rate of Alkylation

The use of reaction conditions such as prolonged refluxing in methanol to increase the rate of reaction and effect dialkylation of **1.1** may not necessarily lead to complete reaction in all cases. Significant decomposition of the product and

formation of multiple undesired secondary products may occur[6]. However, careful choice of electrophile and manipulation of the reaction conditions were employed to successfully achieve dialkylation of $\{Pt_2S_2\}$[6, 7]. The application of high pressure conditions in the liquid phase have assisted the alkylation of **1.1** and hetero- and homodialkylation of $[Pt_2(\mu\text{-}S)_2(dppp)_2]$ (dppp = $Ph_2P(CH_2)_3PPh_2$ (1,3-bis (diphenylphosphanyl) propane) with less bulky terminal group[18, 19]. Increased concentration of strong alkylating agent has also been used to achieve homodialkylation of **1.1** at normal temperature and pressure[6, 7]. For instance, the reaction with 6 mol equivalent of 2-bromo-4'-phenylacetophenone, an organo-halide resulted in homodialkylation of **1.1** within 1 hour.

3.1.2 Leaving Group Effect

Dimethylation of **1.1** with the powerful methylating agent dimethyl sulfate ($(CH_3)_2SO_4$) to give $[Pt_2(SCH_3)_2(PPh_3)_4](PF_6)_2$[6] was the first example of homodialkylation where identical organic groups are independently attached to the two sulfide centres. Heterodialkylation of **1.1** has also been achieved by interception of the reaction of **1.1** with an electrophile upon complete monoalkylation by introducing $(CH_3)_2SO_4$. This sequential alkylation leads to the isolation of heterodialkylated derivatives e.g. $[Pt_2(\mu\text{-}SCH_2C_6H_5)(\mu\text{-}SCH_3)(PPh_3)_4](PF_6)_2$ and $[Pt_2(\mu\text{-}SC_5H_{10}CO_2CH_2CH_3)(\mu\text{-}SCH_3)(PPh_3)_4](PF_6)_2$[6]. The ability of $(CH_3)_2SO_4$ to dialkylate **1.1** may be attributed to not only the nature of the leaving group but also the high rate at which CH_3^+ is generated from $(CH_3)_2SO_4$. This initial homodialkylation of **1.1** indicates that the rate at which the leaving group departs an electrophile is an important determining factor required in the alkylation of the unalkylated sulfur atom in $[Pt_2(\mu\text{-}S)(\mu\text{-}SR)(PPh_3)_4]^+$.

Alkylation reactions with organohalide electrophiles involves the departure of the leaving groups, halide ions ($X = F^-$, Cl^-, Br^- and I^-) with the pair of electrons from the reacting carbon halogen covalent bond[20]. The relative rate of the departure is dependent on the strength of the C-X bonds and the reaction activation energy. The trend of the strength of C-X bonds is the same as the electronegativity trend; F > Cl > Br > I among the halide group. The energy barrier required to activate the C-X bonds also follows the same trend as that of

the electronegativity in a nucleophilic substitution process[21]. Therefore, the more electronegative a halogen atom, the stronger the covalent carbon-halogen bond it forms and the more the energy it requires for the electrophile to leave. Iodo-organo electrophiles will therefore alkylate **1.1** faster than bromo-organo electrophiles. However, the resulting I^- or Br^- ion may lead to the formation of a secondary product by displacing the coordinated PPh_3 group(s) as has been observed in an ESI-MS survey of the alkylation chemistry of **1.1**[16]. Formation of halide derivatives $[Pt_2(\mu\text{-}SR)_2(PPh_3)_3I]^+$ and $[Pt_2(\mu\text{-}SR)(\mu\text{-}SR')(PPh_3)_3I]^+$ of **1.1** as secondary products results from the displacement of a terminal PPh_3 by an iodide ion, formed as a product from the alkyliodide alkylating agent. Formation of this type of product is much more likely to occur with dialkylated dication than with a monoalkylated monocation. This can be attributed to the generation of dication which is more electrophilic towards anionic iodide ions (I^-). This secondary reaction has mainly been observed in reactions where the platinum atom in the dialkylated product is sterically accessible by the leaving halide ions. Neutral $[Pt_2(\mu\text{-}S)_2(PPh_3)_4]$ **1.1** has low affinity for halide ions because it is neutrally charged. However, the affinity of halide ions towards Pt(II) is enhanced upon formation of alkylated cationic derivative of **1.1** and follows the order; $I^- > Br^- > Cl^- >> F^-$ [22]. I^- ion is therefore a better nucleophile than Br^- and Cl^- ions and more likely to displace PPh_3. Also based on the Pearson's hard soft [Lewis] acid base principle[23, 24], I^- ion is a softer Lewis base than Br^- and Cl^- and will easily react with the soft Lewis acid, Pt(II).

3.1.3 Effect of Residual Organic Part of Electrophile

In addition to good leaving groups, electrophiles with large, electron-rich, conjugated aromatic organic parts with appropriate leaving groups have been suggested to encourage alkylation of the two sulfide centres in **1.1**[7]. However, this is dependent on the structural orientation of the organic part of the electrophile upon monoalkylation. Electrophiles with a non planar structure, upon monoalkylation of **1.1** may occupy more space over the $\{Pt_2(\mu\text{-}S)_2\}$ core and sterically shield the unalkylated S atom from alkylation by another molecule of the electrophile. On the other hand, appropriate planar, large, electron-rich and

conjugated aromatic acetylbromide electrophiles dialkylate **1.1**. This is exemplif ied by the mono alkylated semicarbazone derivative $[Pt_2(\mu\text{-}S)(\mu\text{-}SCH_2C(NNHC(O)CNH_2)(PPh_3)_4]$ (PF_6)[14] and homodialkylated derivatives $[Pt_2(\mu\text{-}SCH_2C(O)C_6H_4Ph)_2(PPh_3)_4](PF_6)_2$ and $[Pt_2(\mu\text{-}SC_{10}H_{10}N)_2(PPh_3)_4](PF_6)_2$ (where $(CH_2C(O)C_6H_4Ph)$ and $(C_{10}H_{10}N)$ are from 2-bromo-4'-phenylacetophenone and 3-(2-bromo ethyl) indole respectively) as reported by Chong *et al*[7].

3.2 Results and Discussion

The following sections outline the results of a study into the factors that encourage an electrophile to dialkylate $[Pt_2(\mu\text{-}S)_2(PPh_3)_4]$. Electrophiles used were selected considering the aforementioned factors. The detailed results of the investigation and the ESI-MS, NMR, IR spectroscopic and some X-ray characterisations of the successfully isolated products are presented and discussed in the following sections.

3.2.1 Homodialkylation of $[Pt_2(\mu\text{-}S)_2(PPh_3)_4]$

The investigations of the homodialkylation reactions of **1.1** were carried out with a number of electrophiles with different functionalities and structures. The initial electrophiles used in the study included $PhC(O)CH_2Cl$ **3.1** and $PhC(O)CH_2Br$ **3.1a**. The reaction of **1.1** with a large excess of $PhC(O)CH_2Cl$ (10 mol equiv.) in MeOH at room temperature for 48 hours and refluxed at 65^oC for an additional 24 hours only yielded the known monoalkylated derivative $[Pt_2(\mu\text{-}S)(\mu\text{-}SCH_2C(O)Ph)(PPh_3)_4]^+$ **2.14**[25].

The ESI-MS monitored reaction of a large excess of $PhC(O)CH_2Br$ with **1.1** at room temperature was fast, indicating complete formation of the monoalkylated derivative $[Pt_2(\mu\text{-}S)(\mu\text{-}SCH_2C(O)Ph)(PPh_3)_4]^+$ (*m/z* 1621) and 3% formation of dialkylated derivative $[Pt_2(\mu\text{-}SCH_2C(O)Ph)_2(PPh_3)_4]^{2+}$ **3.1b** within the first 5 mins. The alkylation reaction proceeded stepwise as shown in Scheme 3.1. The first step involved fast monoalkylation of **1.1** followed by a slower second alkylation of the second sulfur atom. This is evident from the dominant peak of $[Pt_2(\mu\text{-}S)(\mu\text{-}SCH_2C(O)Ph)(PPh_3)_4]^+$ (*m/z* 1621, 100%) in the initial ESI-MS of the reaction (Figure 3.1). The peak for dialkylated derivative $[Pt_2(\mu$-

$SCH_2C(O)Ph)_2(PPh_3)_4]^{2+}$ **3.1b** (*m/z* 870) became the prominent peak after overnight (13 hours) reaction at room temperature. The reaction was completed (with no trace of a PPh_3 exchange by Br) giving the pure homodialkylated derivative after 18 hours. The peaks below 2% intensity at *m/z* 806, 988 and 1560 could not be identified as any reaction intermediate and may be residual impurities in the ESI-MS. The complex was isolated as its PF_6^- salt $[Pt_2(\mu\text{-}SCH_2C(O)Ph)_2(PPh_3)_4](PF_6)_2$ **3.1b·(PF$_6$)$_2$** by the addition of excess NH_4PF_6 and distilled water. The compound was further characterised by IR, NMR and elemental analysis.

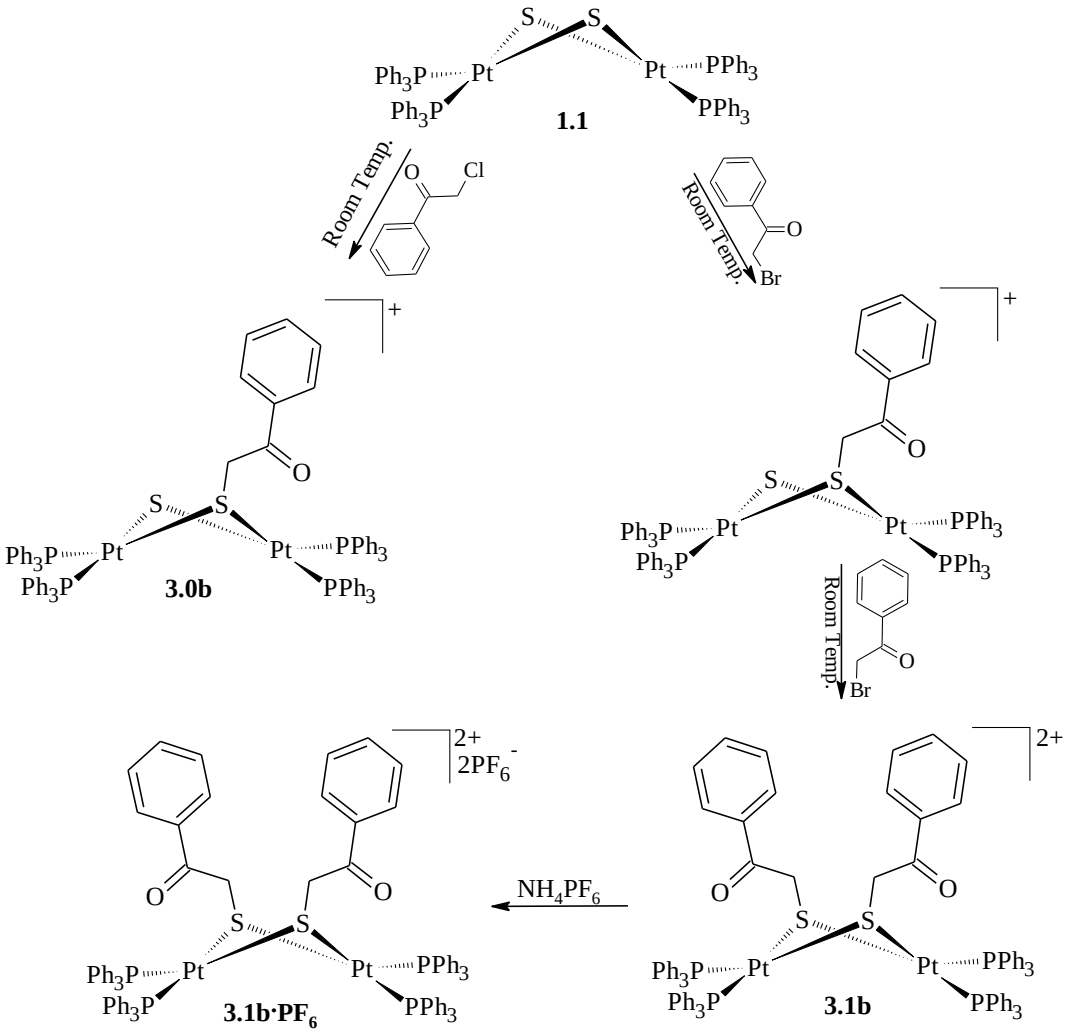

Scheme 3.1 The different products of the reaction of $[Pt_2(\mu\text{-}S)_2(PPh_3)_4]$ with excess $PhC(O)CH_2Cl$ and $PhC(O)CH_2Br$

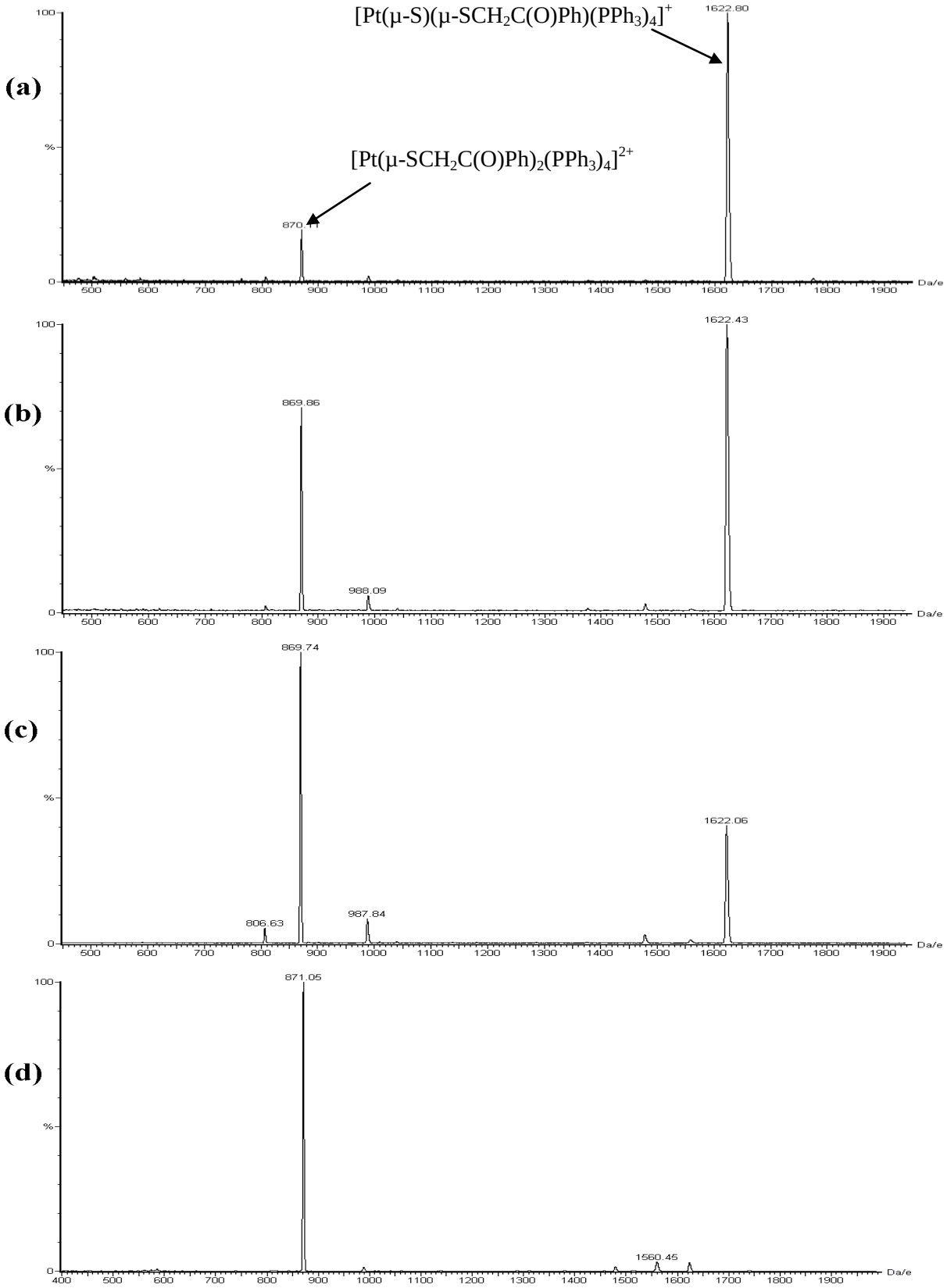

Figure 3.1 Reaction progress of $[Pt_2(\mu\text{-}S)_2(PPh_3)_4]$ with $PhC(O)CH_2Br$ monitored by positive ion ESI-MS after **(a)** 5 mins, **(b)** 30 mins, **(c)** 1hour 30 mins and **(d)** 18 hours.

The alkylation of the second sulfur atom proceeded at a slower rate than the first due to the reduced nucleophilicity of the monoalkylated cation and steric hindrance after the alkylation of the first sulfide centre. The reaction progress monitored at intervals, Figure 3.1, showed the intensity of monoalkylated species gradually diminished to 0% and a gradual increase in the intensity of the peak for the homodialkylated species to 100%.

The formation of the homodialkylated derivative of $[Pt_2(\mu\text{-}S)_2(PPh_3)_4]$ with $PhC(O)CH_2Br$ is obviously due to the difference in the halogen leaving groups. The C-Br bond is weaker than the C-Cl bond and therefore will break faster than C-Cl bond, thus increasing the rate of the nucleophilic attack from the sulfide centres in **1.1**. The increased rate with which Br^- leaves the electrophile helps to activate the reaction in favour of alkylation of the second sulfur atom.

Excess of the oximes $PhC(=NOH)CH_2Cl$ **2.3a** (derived from **3.1**) and $PhC(=NOH)CH_2Br$ **2.3c** (derived from **3.1a**) were also reacted with **1.1**. The results showed the formation of only the corresponding monoalkylated derivative in both reactions. The ESI-MS did not indicate any trace of another product after prolonged reaction time of up to 24 hours and refluxing at 65 ^oC for additional 24 hours. The inability of **2.3a** or **2.3c** to activate the unalkylated sulfur atom in the monoalkylated derivative $[Pt_2(\mu\text{-}S)\{\mu\text{-}SCH_2(=NOH\}Ph)(PPh_3)_4]^+$ for second alkylation can be attributed to the electronic influence of imine >C=N- group on the alkylating strength of the oximes. The electron density around the alkylating carbon due to the introduction of imine >C=N- functional group is higher compare to >C=O, which caused a reduction in the positive charge on the α-halogenocarbon. The imine (>C=N-) group comparatively has a lesser electron withdrawing effect on the α-halogenocarbon atom than the carbonyl group (>C=O).

The ^{13}C and ^1H NMR chemical shifts of the halogeno-carbon and hydrogen atoms in $PhC(O)CH_2Cl$, $PhC(O)CH_2Br$, $PhC(NOH)CH_2Cl$ and $PhC(NOH)CH_2Br$ were obtained to check if it has a direct correlation to the different reactivity of **3.1** and **3.1a** towards **1.1**. The NMR results in Table 3.1 show that the chloro-carbon $-CH_2-Cl$ is more deshielded as a result of the higher electronegativity of chlorine and supposedly should have more electrophilic α-

carbon toward **1.1** than **3.1a**. However, bromide is a better leaving group because the C-Br bond (293.08 kJ mol^{-1}) is weaker compared to the C-Cl bond (351.69 kJ mol^{-1})[26, 27]. A combination of these factors encouraged the successful homodialkylation of **1.1** by **3.1a**.

Table 3.1 ^{13}C and ^{1}H NMR shifts of the halogeno-carbon and hydrogen of **2.3a, 2.3c**, **3.1** and **3.1a**, in $CDCl_3$

No.	Compound	Chemical shifts		
		Carbon	Hydrogen	Ref.
2.3a	$PhC(NOH)CH_2Cl$	32.38	4.63	28
2.3c	$PhC(NOH)CH_2Br$	32.34	4.63	
3.1	$PhC(O)CH_2Cl$	46.07	4.70	
3.1a	$PhC(O)CH_2Br$	31.10	4.42	

The reactions of excess conjugated aromatic semicarbazones $BrCH_2C(=NNHC(O)NH_2)C_6H_4C_6H_5$ **2.12a** (derived from $BrCH_2C(O)C_6H_4C_6H_5$) which itself reportedly dialkylated **1.1**[7] and $BrCH_2(=NNHC(O)NH_2)Ph$ **2.1** (derived from **3.1**) gave similar results as the oximes **2.3a** and **2.3a'**. The ESI-MS of the reaction mixture of **2.12a** with **1.1** showed purely a monoalkylated derivative even after stirring at room temperature for 24 hours and further refluxing at 65^{o}C for another 24 hours. Steric effect may have contributed in preventing the second alkylation as $-C=NNHC(O)NH_2$ is bigger than -C=O and probably solvated in solution, so its effective size is even greater. In addition, upon formation of $[Pt_2(\mu\text{-}S)\{\mu\text{-}SCH_2C(=NNHC(O)NH_2)R\}(PPh_3)_4]^+$ where R = -Ph or $-C_6H_4C_6H_5$, the attached organic moiety $-CH_2C(=NNHC(O)NH_2)Ph$ is not planar as can be seen from the structure of $[Pt_2(\mu\text{-}S)\{\mu\text{-}SCH_2C(=NNHC(O)NH_2)Ph\}(PPh_3)_4](PF_6)$ **2.1b·PF$_6$** in Figure 2.3. The spatial orientation of the attached group is such that it slightly flipped over the unalkylated sulfur atom in $\{Pt_2(\mu\text{-}S_2\}$ core and sterically shielded it from reacting with another electrophile. Thus, steric hindrance could be an important additional factor that hinders the alkylation of the second sulfide centre with such electrophiles.

Organic electrophiles that possess large π-conjugated aromatic systems and an α-bromo-keto group namely, 1-(bromoacetyl)pyrene $CH_2C(O)pyr$ (pyr =

pyrene) **3.2a** and 3-(bromoacetyl)coumarin **3.4a** shown below reacted with **1.1** in a similar way as $PhC(O)CH_2Br$ **3.1a** resulting in dialkylkation of the two sulfur atoms. The reaction of **3.2a** with **1.1** understandably proceeded at a much slower rate due to the bulky nature of the organic part but with significant formation of the dialkylated species within the first 12 hours. The reaction proceeded to completion in about a week of stirring at room temperature, followed by the addition of NH_4PF_6 to give $[Pt_2(\mu\text{-}SCH_2C(O)pyr)_2(PPh_3)_4](PF_6)_2$ **3.2b·(PF$_6$)$_2$**.

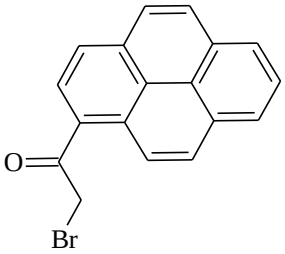

3.2a

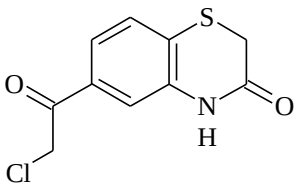

3.3a

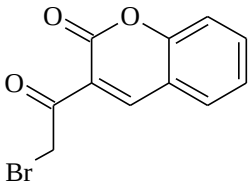

3.4a

This was confirmed by the ESI-MS of the reaction mixture which indicated a major peak for the dicationic species at *m/z* 996 with 100% relative intensity (RI) and a minor monoalkylated monocation peak at *m*/*z* 1748, about 4%. Under the same conditions 3-(bromoacetyl)coumarin, $BrCH_2C(O)cyl$ (cyl = coumaryl) **3.4a** reacted with **1.1** to predominantly form the dialkylated derivative but the reaction was never completed. The ESI-MS of the reaction mixture of **1.1** with **3.4a** indicated a dominant peak at *m*/*z* 939 (100%) due to $[M]^{2+}$ ion $[Pt_2(\mu\text{-}SCH_2C(O)cyl)_2(PPh_3)_4]^{2+}$ **3.4b** and a minor peak at *m*/*z* 1697, about 5% due to the $[M]^+$ ion $[Pt_2(\mu\text{-}S)(\mu\text{-}SCH_2C(O)cyl)(PPh_3)_4]^+$ after stirring for 168 hours at room temperature. Further prolonged stirring to drive the reaction to completion only resulted in the decomposition of a significant amount of the product. The product was isolated as the PF_6^- salt $[Pt_2(\mu\text{-}SCH_2C(O)cyl)_2(PPh_3)_4](PF_6)_2$ **3.4b·(PF$_6$)$_2$**, and purified by crystallisation.

The reaction of excess α-chloro-keto benzothiazine derivative 6-chloro-acetyl-2H-1,4-benzo thiazin-3(4H)-one **3.3a** with **1.1** was also monitored with ESI-MS. Complete formation of the corresponding dialkylated derivative was not achieved after prolonged stirring at room temperature for a week and refluxing at 65 ^oC for another week. The ESI-MS only indicated incomplete reaction with only

two peaks of about equal intensities attributable to the $[M]^{2+}$ ion $[Pt_2(\mu\text{-}SCH_2C(O)C_6H_3SCH_2C(O)NH)_2(PPh_3)_4]^{2+}$ **3.3b** *m/z* 957, 100% and $[M]^+$ ion $[Pt_2(\mu\text{-}S)(\mu\text{-}SCH_2C(O)C_6H_3SCH_2C(O)NH)(PPh_3)_4]^+$ *m/z* 1711, 99% derivatives respectively. The extended reaction time and refluxing of the reaction mixture only resulted in significant decomposition of the compounds which was confirmed by the diminishing of the dialkylated $[M]^{2+}$ ion and the monocation observed peaks in ESI-MS. The slower rate and incomplete reaction observed for **3.3a** is obviously due to the slower rate at which chloride ion Cl^- leaving group departs the electrophile when compared with Br^- ion in **3.1a**, **3.2a** and **3.4a**.

3.2.2 Dialkylation of Cationic Alkylthiolate Complexes $[Pt_2(\mu\text{-}S)(\mu\text{-}SR)(PPh_3)_4]^+$

The reaction of **1.1** with excess alkyl halides n-Bu-Br **3.5a** and Et-Br **3.6a** yielded only the monoalkylated derivatives $[Pt_2(\mu\text{-}S)(\mu\text{-}SBu)(PPh_3)_4]^+$ known to act as cationic ligand towards Ph_3PAu^+ and $R'Hg^+$ [12] (R' = Ph or Fc) and $[Pt_2(\mu\text{-}S)(\mu\text{-}SEt)(PPh_3)_4]^+$ respectively. The reaction was stopped in each case as soon as the ESI-MS indicated complete formation of the monoalkylated derivative $[Pt_2(\mu\text{-}S)(\mu\text{-}SR)(PPh_3)_4]^+$ (R = n-Bu and Et). The solvent and the excess alkyl bromide were removed by evaporation. The residue obtained was redissolved in MeOH, and excess of $PhC(O)CH_2Br$ **3.1a** introduced and the reaction mixture monitored by ESI-MS.

The alkylation of the second sulfide in $[Pt_2(\mu\text{-}S)(\mu\text{-}SBu)(PPh_3)_4]^+$ was fast forming the heterodialkylated derivative $[Pt_2(\mu\text{-}SCH_2C(O)Ph)(\mu\text{-}SBu)(PPh_3)_4]^{2+}$. This was followed by spontaneous displacement of one of the terminal PPh_3 groups by the resulting Br^- ion (Scheme 3.2). The ESI-MS of the reaction mixture indicated four important peaks at *m/z* 839 (19%) for $[Pt_2(\mu\text{-}SCH_2C(O)Ph)(\mu\text{-}SBu)(PPh_3)_4]^{2+}$ **3.5b**, *m/z* 1497 (40%) for $[Pt_2(\mu\text{-}SCH_2C(O)Ph)(\mu\text{-}SBu)(PPh_3)_3Br]^+$ **3.5c**, *m/z* 1560, (100%) for $[Pt_2(\mu\text{-}S)(\mu\text{-}SBu)(PPh_3)_4]^+$ and $[Pt_2\{\mu\text{-}SC(O)Ph\}(\mu\text{-}SBu)(PPh_3)_3\text{-}H]^+$ at *m/z* 1415 (90%), after stirring for 6 hours. On further stirring the reaction mixture up to 48 hours, the ESI-MS indicated an increase in the relative intensity of the peak at *m/z* 1497 to 100% and a reduction in the intensity of the peaks at *m/z* 1415 to 15%. It also showed a very minor negligible peak at *m/z* 839.

The problem of triphenylphosphine group displacement was not effectively controlled initially as the generated bromide ions were very nucleophilic towards platinum and quickly displaced a PPh_3 group. The major product at the end of the reaction was the bromide derivative **3.5c** resulting from the secondary reaction. The product was isolated by precipitation with excess NH_4PF_6. The product was further purified by crystallisation to give brown crystals suitable for X-ray analysis which was further confirmed to be $[Pt_2(\mu\text{-}SCH_2C(O)Ph)(\mu\text{-}SBu)(PPh_3)_3Br](PF_6)$ **3.5c·PF$_6$** by X-ray crystal structure analysis, NMR and elemental analysis.

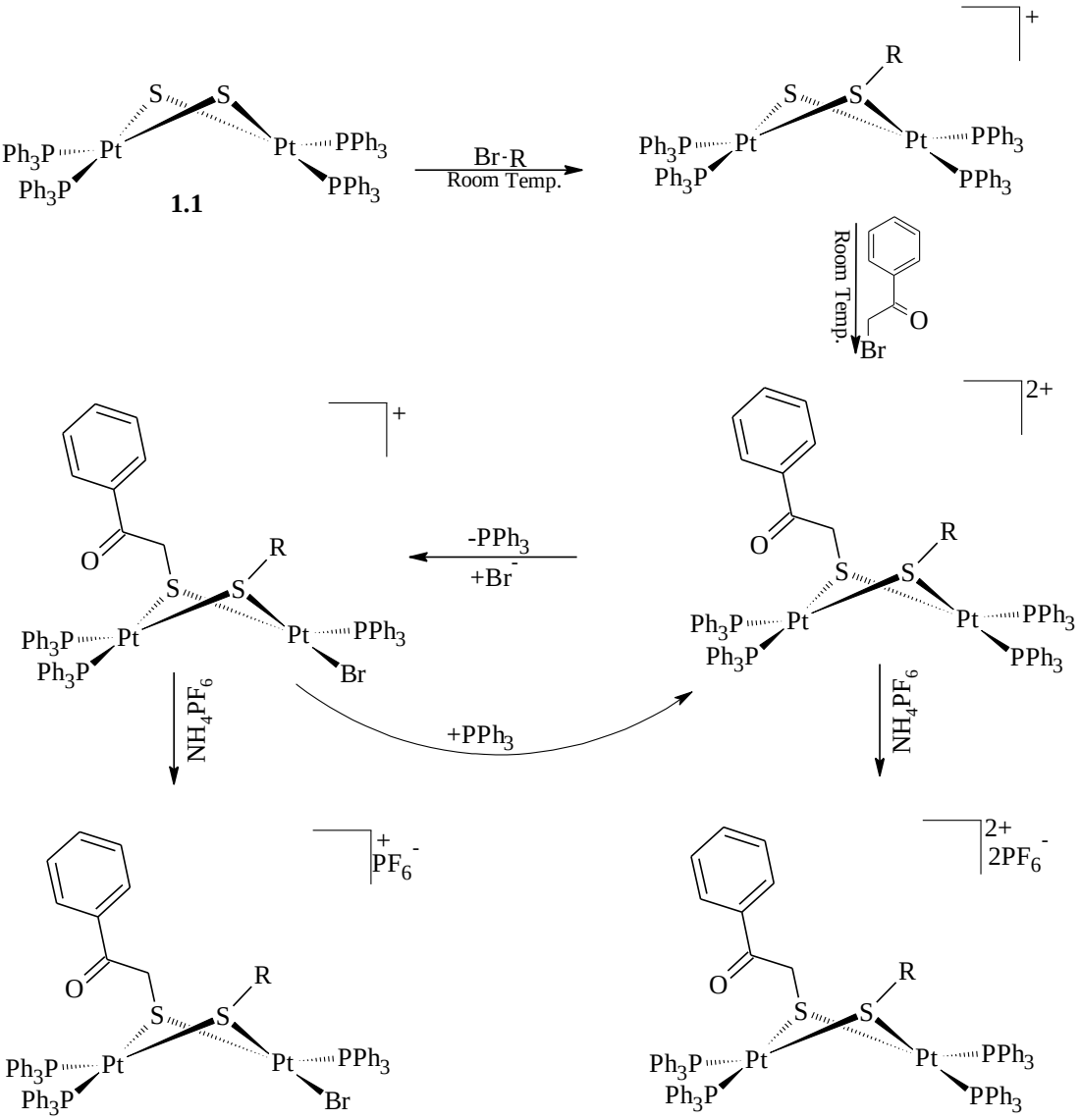

Scheme 3.2 Homo- and Heterodialkylation of **1.1** via the alkylation of $[Pt_2(\mu\text{-}S)(\mu\text{-}SR)(PPh_3)_4]^+$ with $PhC(O)CH_2Br$

The reaction of **1.1** with Br-Bu was repeated with the addition of 1 mol equiv. of PPh_3 to the reaction mixture as soon as the bromide derivative $[Pt_2(\mu\text{-}SCH_2C(O)Ph)(\mu\text{-}SBu)(PPh_3)_3Br]^+$ was formed and the solution stirred for and additional 12 hours. The ESI-MS of the reaction mixture indicated about 99% conversion of the bromide derivative $[Pt_2(\mu\text{-}SCH_2C(O)Ph)(\mu\text{-}SBu)(PPh_3)_3Br]^+$ to the complete heterodialkylated derivative $[Pt_2(\mu\text{-}SCH_2C(O)Ph)(\mu\text{-}SBu)(PPh_3)_4]^{2+}$ **3.5b**. Also indicated are peaks due to disintegration of reactant and/or products at *m/z* 981 for $[\mathbf{1.1} + H - 2(PPh_3)]^+$, 718 for $[Pt(PPh_3)(PPh_2C_6H_4)]^+$ which were previously observed[17] and a minor peak at 1415 for $[Pt_2\{\mu\text{-}SC(O)Ph\}(\mu\text{-}SBu)(PPh_3)_3\text{-}H]^+$ as shown in Figure 3.2. The increase in the concentration of PPh_3 significantly shifted the reaction in favour of heterodialkylated dication $[Pt_2(\mu\text{-}SCH_2C(O)Ph)(\mu\text{-}SBu)(PPh_3)_4]^{2+}$ **3.5b** which was isolated as the PF_6^- salt $[Pt_2(\mu\text{-}SCH_2C(O)Ph)(\mu\text{-}SBu)(PPh_3)_4](PF_6)_2$ **3.5b·(PF$_6$)$_2$**. Recrystallisation of the PF_6^- salt did not give good crystals for X-ray diffraction analysis but the BPh_4^- salt gave good crystals which were used for structure determination.

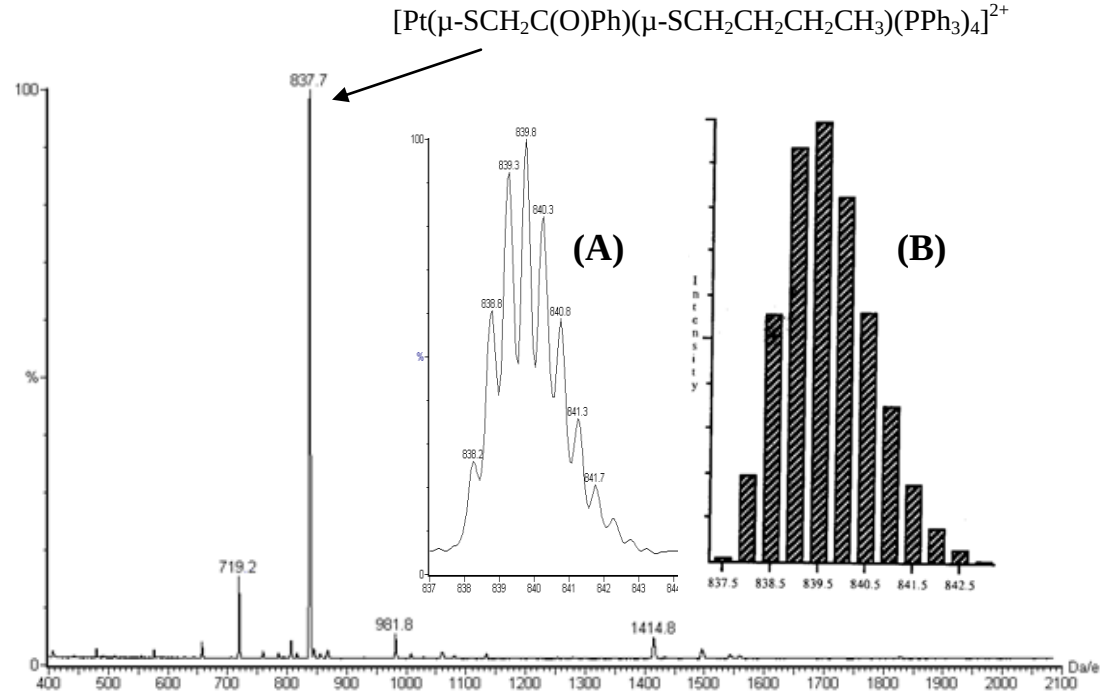

Figure 3.2 ESI-MS of the reaction mixture of heterodiakylation of **1.1** with n-Bu-Br and $PhC(O)CH_2Br$ after the addition of PPh_3. Insert is the practical (**A**) and theoretical (**B**) isotope patterns

Similar results were obtained from ESI-MS monitoring of the reactions of $[Pt_2(\mu\text{-}S)(\mu\text{-}SEt)(PPh_3)_4]^+$ with **3.1a**. The products were also isolated as the PF_6^-

salts $[Pt_2(\mu\text{-}SCH_2C(O)Ph)(\mu\text{-}SEt)(PPh_3)_4](PF_6)_2$ **3.6b·(PF$_6$)$_2$** and $[Pt_2(\mu\text{-}SCH_2C(O)Ph)(\mu\text{-}SEt)(PPh_3)_3Br](PF_6)$ **3.6c·PF$_6$** respectively. Further characterisation by NMR, elemental analysis and X-ray structure analysis further proved them to be **3.6b·(PF$_6$)$_2$** and **3.6c·PF$_6$**. These isolated products **3.5b·(PF$_6$)$_2$** and **3.5c·PF$_6$**, and **3.6b·(PF$_6$)$_2$** and **3.6c·PF$_6$** represent a significant new class of mixed dithiolate derivatives in the development of the alkylation chemistry of **1.1** that has not been reported before.

The formation of the heterodialkylated derivatives $[Pt_2(\mu\text{-}SCH_2C(O)Ph)(\mu\text{-}SBu)(PPh_3)_4]^{2+}$ **3.5b** and $[Pt_2(\mu\text{-}SCH_2C(O)Ph)(\mu\text{-}SEt)(PPh_3)_4]^{2+}$ **3.6b** is particularly dependent on the sequence of the alkylation as shown in Scheme 3.2. Thus, heterodialkylation involving weak electrophile like n-Bu-Br **3.5a** and Et-Br **3.6a** could not be achieved by generating $[Pt_2(\mu\text{-}SCH_2C(O)Ph)(\mu\text{-}S)(PPh_3)_4]^+$ first and further reacting with Bu-Br or Et-Br. This is because the second alkylation is dependent on the strength and ability of an electrophiles to alkylate the second sulfur atom after generation of a monocation $[Pt_2(\mu\text{-}S)(\mu\text{-}SR)(PPh_3)_4]^+$ (R = organic group) by a weaker electrophile.

In contrast to the formation of only the homodialkylated derivative from reaction of $PhC(O)CH_2Br$ **3.1a** with **1.1**, the formation of bromide derivatives $[Pt_2(\mu\text{-}SCH_2C(O)Ph)(\mu\text{-}SBu)(PPh_3)_3Br](PF_6)$ **3.5c·PF$_6$**, and $[Pt_2(\mu\text{-}SCH_2C(O)Ph)(\mu\text{-}SEt)(PPh_3)_3Br](PF_6)$ **3.6c·PF$_6$** was observed only in heterodialkylation reactions involving monoalkylated derivative in which a simple alkyl group (Et or Bu) is attached to one of sulfur atoms.

The $SCH_2C(O)$- group has been observed to have lower *trans*- influence than the SCH_2CH_2- groups[14]. The greater *trans*- influence of the SCH_2CH_2-thiolate group was further observed in the crystal structure analysis of **3.5b·BPh$_4$** (Table 3.2). Therefore, the Pt-P bond *trans* to the butyl group is weaker and thus is more easily broken than the corresponding *cis* Pt-P bond. In addition, the alkyl group attached to one of the sulfur atoms is expected to cause an uneven shielding of the platinum atoms in the heterodialkylated molecule. The two platinum atoms are therefore not equally sterically shielded on both sides of the molecule as in **3.1b·PF$_6$**, thus allowing Br^- ion an easy access to attack the platinum atoms to displace a terminal triphenylphosphine ligand from either phenacylthiolate side or

the alkyl (butyl or ethyl) side of the molecule. The Br^- ion can thus either bond to the platinum atoms on the phenylacylthiolate side or the butyl- or ethylthiolate side. The resulting product of the bromide nucleophilic attack on the platinum atoms will therefore be a mixture of the two possible isomers shown in Scheme 3.3.

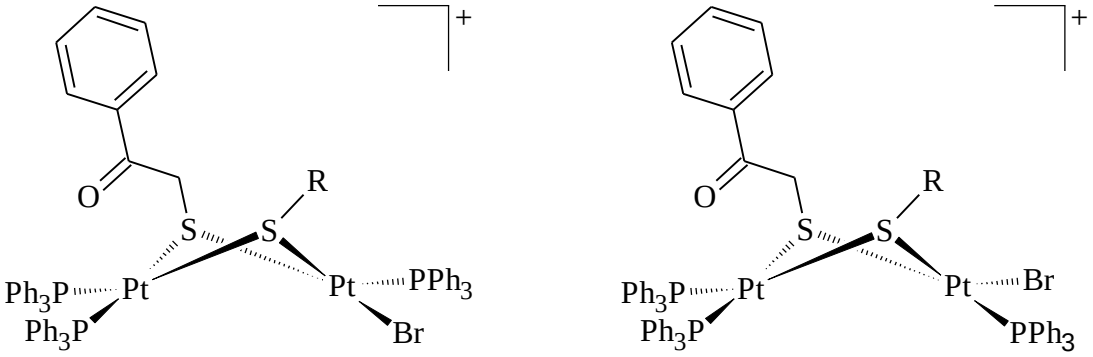

R = CH_2CH_3 **or** $CH_2CH_2CH_2CH_3$

Scheme 3.3 Two possible products of the displacement of a PPh_3 group by bromide ion

3.3 X-ray Crystal Structures

Known derivatives with $\{Pt_2(\mu\text{-}SR)_2P_4\}$ and $\{Pt_2(\mu\text{-}SR)(\mu\text{-}SR')P_4\}$ cores P = PPh_3) usually adopt mainly *syn*- conformation[6, 7] (with the two thiolate bridges on the same side) or an *anti*- (opposite sides) configuration. In general, the different conformational orientations of R groups affects the size of the dihedral angle (θ) between the two PtSS planes of the $\{Pt_2S_2\}$ core in the *syn*- ($\theta < 180°$) and the *anti*- ($\theta = 180°$) conformations[2, 4, 29] as shown in Figure 3.3. As explained in Section 1.4, the factors affecting the relative orientation of the R group in this class of complexes reported by Capdevila *et al*[2] includes the through-ring antibonding interaction. Weak through-ring antibonding interaction gives rise to *anti*- configuration while stronger through ring antibonding interaction gives rise to *syn*- configuration.

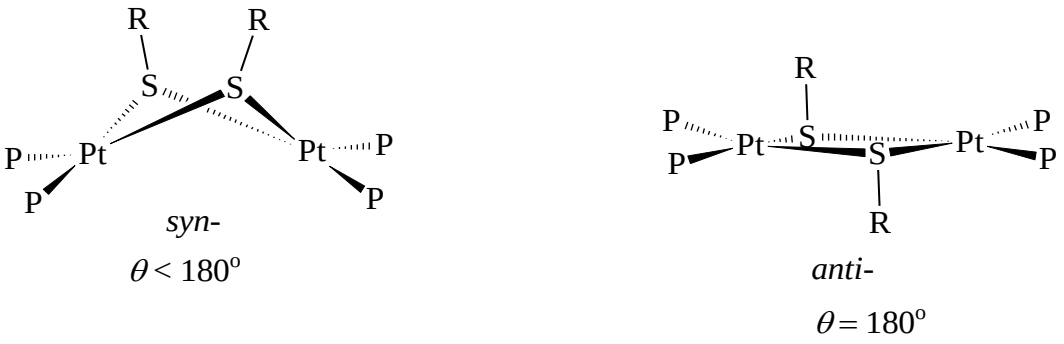

Figure 3.3 The *syn*- and *anti*- conformations of the dialkylated derivatives of $[Pt_2(\mu\text{-}S)_2(PPh_3)_4]$

The *anti*- conformation is not common in the $\{Pt_2(\mu\text{-}S)_2\}$ core with bulkier PPh_3 terminal ligands but has been reported in derivatives with reduced steric hindrance for example with the $Ph_2P(CH_2)_3PPh_2$ terminal ligand in place of PPh_3[4]. However, there are noticeable increases in the dihedral angles (θ) from monoalkylated derivatives $[Pt_2(\mu\text{-}S)(\mu\text{-}SR)(PPh_3)_4]^+$ e.g. $[Pt_2(\mu\text{-}S)(\mu\text{-}SCH_2C(O)Ph)(PPh_3)_4](PF_6)$ (133.8°)[25] to the dialkylated derivatives $[Pt_2(\mu\text{-}SR)_2(PPh_3)_4]^{2+}$ and $[Pt_2(\mu\text{-}SR)(\mu\text{-}SR')(PPh_3)_4]^{2+}$ e.g. $[Pt_2(\mu\text{-}SCH_2C(O)Ph)_2(PPh_3)_4](PF_6)_2$ **3.1b·(PF$_6$)$_2$** (156.36°) and $[Pt_2(\mu\text{-}SCH_2C(O)Ph)(\mu\text{-}SBu)(PPh_3)_4](BPh_4)_2$ **3.5b·(BPh$_4$)$_2$** (145.11°) reported herein. This may be due to intramolecular adjustments to accommodate the additional incorporated organic group[6, 7]. The X-ray crystal structure analysis of these novel complexes is particularly important in confirming the effects of the incorporated groups on the dihedral angular conformation of the $\{Pt_2(\mu\text{-}S)_2\}$ core and to determine which isomer was obtained. The X-ray crystal structure and atom numbering schemes of $[Pt_2(\mu\text{-}SCH_2C(O)Ph)_2(PPh_3)_4](PF_6)_2$ **3.1b·(PF$_6$)$_2$** $[Pt_2(\mu\text{-}SCH_2C(O)Ph)(\mu\text{-}SBu)(PPh_3)_4](BPh_4)_2$ **3.5b·(BPh$_4$)$_2$** and bromide derivatives $[Pt_2(\mu\text{-}SCH_2C(O)Ph)(\mu\text{-}SBu)(PPh_3)_3Br](PF_6)$ **3.5c·PF$_6$** and $[Pt_2(\mu\text{-}SCH_2C(O)Ph)(\mu\text{-}SEt)(PPh_3)_3Br](PF_6)$ **3.6c·PF$_6$** which has not been reported before are as shown in Figures 3.4 and 3.5 respectively. Selected bond lengths and angles are shown in Tables 3.2 and 3.4 respectively.

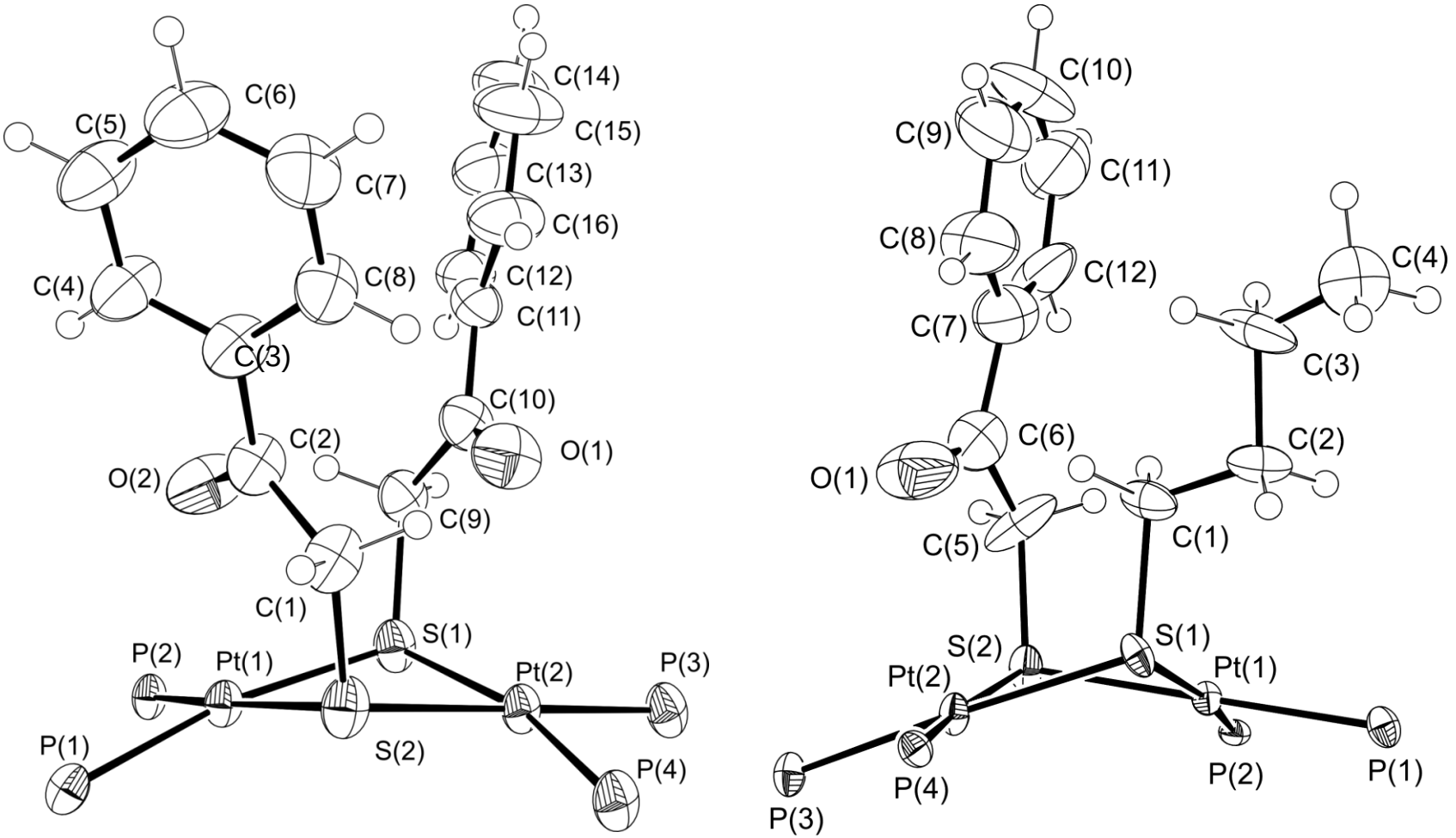

Figure 3.4 Molecular structures of $[Pt_2(\mu\text{-}SCH_2C(O)Ph)_2(PPh_3)_4](PF_6)_2$ **3.1b·(PF$_6$)$_2$** and $[Pt_2(\mu\text{-}SCH_2C(O)Ph)(\mu\text{-}SBu)(PPh_3)_4](BPh_4)_2$ **3.5b·(BPh$_4$)$_2$** showing the atom numbering scheme with thermal ellipsoids at the 50% probability level. The PF_6^- , BPh_4^- counterions and the phenyl rings of PPh_3 were removed for clarity.

Table 3.2 Selected bond lengths and atomic distances (Å) and bond angles (°) for $[Pt_2(\mu\text{-}SCH_2C(O)Ph)_2(PPh_3)_4](PF_6)_2$ **3.1b·(PF$_6$)$_2$** and $[Pt_2(\mu\text{-}SCH_2C(O)Ph)(\mu\text{-}SCH_2CH_2CH_2CH_3)(PPh_3)_4](BPh_4)_2$ **3.5b·(BPh$_4$)$_2$** (Estimated standard deviations are *in* brackets).

Bond lengths and atomic distances (Å)							
$[Pt_2(\mu\text{-}SCH_2C(O)Ph)_2(PPh_3)_4](PF_6)_2$ **3.1b·(PF$_6$)$_2$**				$[Pt_2(\mu\text{-}SCH_2C(O)Ph)(\mu\text{-}SBu)(PPh_3)_4](BPh_4)_2$ **3.5b·(BPh$_4$)$_2$**			
Pt(1)-P(2)	2.2902(14)	Pt(1)-S(1)	2.3917(16)	Pt(1)-P(2)	2.321(3)	Pt(1)-S(1)	2.347(3)
Pt(1)-P(1)	2.2871(16)	Pt(1)-S(2)	2.3681(15)	Pt(1)-P(1)	2.294(3)	Pt(1)-S(2)	2.383(3)
Pt(2)-P(3)	2.2703(19)	Pt(2)-S(1)	2.3562(15)	Pt(2)-P(3)	2.303(3)	Pt(2)-S(1)	2.380(3)
Pt(2)-P(4)	2.2901(16)	Pt(2)-S(2)	2.3843(18)	Pt(2)-P(4)	2.284(3)	Pt(2)-S(2)	2.371(3)
C(2)-O(2)	1.215(8)	C(2)-C(3)	1.486(10)	S(2)-C(5)	1.830(8)	C(6)-O(1)	1.250(12)
S(2)-C(1)	1.808(8)	C(10)-O(1)	1.222(9)	S(1)-C(1)	1.829(10)	C(3)-C(4)	1.434(11)
S(1)-C(9)	1.817(8)	C(9)-C(10)	1.507(10)	C(1)-C(2)	1.533(12)	C(5)-C(6)	1.5144
C(1)-C(2)	1.504(10)	C(10)-C(11)	1.491(11)	C(2)-C(3)	1.533(10)	C(6)-C(7)	1.599(10)
Pt(1)---Pt(2)	3.495	S(1)---S(2)	3.132	Pt(1)---Pt(2)	3.416	S(1)---S(2)	3.107
Bond angles (°)							
S(2)-Pt(1)-S(1)	82.32(6)	Pt(1)-S(1)-Pt(2)	94.81(6)	S(2)-Pt(1)-S(1)	82.14(11)	Pt(1)-S(1)-Pt(2)	92.54(11)
S(2)-Pt(2)-S(1)	82.72(6)	Pt(2)-S(2)-Pt(1)	94.69(6)	S(2)-Pt(2)-S(1)	81.67(11)	Pt(2)-S(2)-Pt(1)	91.86(11)
S(2)-C(1)-C(2)	119.5(5)	O(1)-C(10)-C(9)	123.7(7)	S(1)-C(1)-C(2)	110.8(7)	O(1)-C(6)-C(5)	119.9(5)
S(1)-C(9)-C(10)	119.7(5)	O(2)-C(2)-C(3)	120.2(7)	C(1)-C(2)-C(3)	109.4(8)	C(6)-C(5)-S(2)	125.6(3)
C(1)-S(2)-Pt(1)	107.5(2)	C(9)-S(1)-Pt(2)	110.4(2)	C(2)-C(3)-C(4)	115.7(9)	C(5)-C(6)-C(7)	123.5(5)
C(1)-S(2)-Pt(2)	108.0(3)	C(9)-S(1)-Pt(1)	112.2(3)	C(1)-S(1)-Pt(1)	106.0(3)	C(5)-S(2)-Pt(2)	107.9(3)
				C(1)-S(1)-Pt(2)	112.3(4)	C(5)-S(2)-Pt(1)	102.7(3)

The X-ray structural characterisation of **3.1b·$(PF_6)_2$** confirmed a *syn*-conformation with the two phenacyl groups attached on the same side of the $\{Pt_2(\mu\text{-}S)_2\}$ core. The angular geometry of the $\{Pt_2(\mu\text{-}S)_2\}$ core confirmed a hinge structure with a dihedral angle (θ) of 156.36°. In the case of **3.5b·$(BPh_4)_2$**, the dihedral angle is 145.11° with the two thiolate ligands adopting axial positions. A comparison of dihedral angles and other structural parameters of **3.1b·$(PF_6)_2$** and **3.5b·$(BPh_4)_2$** with reported homodialkylated complexes $[Pt_2(\mu\text{-}SCH_3)_2(PPh_3)](PF_6)_2$[6] **3.7** and $[Pt_2(\mu\text{-}SC_{10}H_{10}N)_2(PPh_3)_4](PF_6)_2$[7] **3.8** and the heterodialkylated derivatives $[Pt_2(\mu\text{-}SCH_2CH{=}CH_2)(\mu\text{-}SCH_3)(PPh_3)_4](PF_6)_2$[6] **3.9** and $[Pt_2(\mu\text{-}SCH_2C_6H_5)(\mu\text{-}SCH_3)(PPh_3)_4](PF_6)_2$[6] **3.10** are shown in Table 3.3.

The calculated mean of Pt-S-Pt, S-Pt-P and S-Pt-S angles of the homo- and heterodialkylated derivatives in Table 3.3 is between 2.2845(16) and 2.304(2) Å. These values are significantly more than those calculated for the monoalkylated derivatives (Table 2.5). For example, the calculated averages Pt-S-Pt [88.4(2)°], S-Pt-P [88.9(3)°] and S-Pt-S [81.9(3) °] angles in the monoalkylated derivative $[Pt_2(\mu\text{-}S)(\mu\text{-}SCH_2C(O)Ph)(PPh_3)_4](BPh_4)$ **2.14·$(BPh_4)_2$** is Pt-S-Pt [94.75(6)°], S-Pt-P [89.01(6)°] and S-Pt-S [82.52(6)°] in the corresponding homodialkylated derivative in **3.1b·$(PF_6)_2$**. The Pt---Pt and S---S distances in the monoalkylated derivatives increased in the dialkylated derivatives. These increases are expected as a consequence of the hinge distortion due to the two thiolate groups. The separation between the two sulfur atoms in **3.1b·$(PF_6)_2$** and **3.5b·$(BPh_4)_2$** are 3.132 Å and 3.107 Å respectively, a little higher than 3.094 Å and 3.100 Å, 3.109 Å and 3.091 Å obtained for **3.7**, **3.8**, **3.9** and **3.10** respectively (See Table 3.3).

The dihedral angles of dialkylated derivatives are generally more than that observed in the monoalkylayted derivatives shown in Table 2.5. The significant increase may be due to structural adjustments to reduce the increased intramolecular repulsion between the attached groups and the bulky terminal PPh_3. The flexibility of the $\{Pt_2(\mu\text{-}S)_2\}$ core along the S(1)---S(2) axis also helped the molecules to maintain a balance of the steric forces to accommodate the second attached group. The angle at which the phenacyl group in **3.5b·$(BPh_4)_2$** attached to the sulfide which has a less bulky butyl group attached to one sulfur

atom is 93.43° (S(1)-S(2)-C(5)) while in **3.1b·$(PF_6)_2$** the phenayl groups are bonded at angles of 109.30° (C(9)-S(1)-S(2)) and 103.64° (C(1)-S(2)-S(1)) to the sulfur atoms. The increase in the angles of attachment is the resultant effect repulsion between the phenyl groups which caused them to tilted away from each other resulting in a final separation distance of 6.649 Å between the tip carbon C(6) and C(14) (the *para* carbons) of the two phenacyl phenyl rings. The phenacyl groups in **3.1b·$(PF_6)_2$** also adopt axial positions and are attached in such a way that the carbonyl groups facing opposite directions thereby reducing crowding and repulsion which may have occurred if they were facing the same direction.

The thiolate ligands in **3.1b·$(PF_6)_2$** are similar and thus the Pt-P bonds lengths in **3.1b·$(PF_6)_2$** have very similar values. Among the Pt-P bonds lengths in **3.5b·$(BPh_4)_2$**, the Pt(2)-P(4) bond (2.284(3) Å) and Pt(1)-P(1) (2.294(3) Å) which are *trans* to the phenacylthiolate (S-CH_2C(O)Ph) are shorter than the associated Pt(2)-P(3) 2.303(3) Å and Pt(1)-P(2) 2.321(3)Å which is *trans* to the butyl thiolate. This suggests that the butylthiolate group has a higher *trans* influence than the phenacyl thiolate group.

Table 3.3 Comparison of the structural parameters of $[Pt_2(\mu\text{-}SCH_2C(O)Ph)_2(PPh_3)_4](PF_6)_2$ **3.1b·$(PF_6)_2$**, $[Pt_2(\mu\text{-}SCH_3)_2(PPh_3)_4](PF_6)_2$ **3.7**, $[Pt_2(\mu\text{-}SC_{10}H_{10}N_2)_2(PPh_3)_4](PF_6)_2$ **3.8**, $[Pt_2(\mu\text{-}SCH_2C(O)Ph)(\mu\text{-}SCH_2\text{-}CH_2CH_2CH_3)(PPh_3)_4](BPh_4)_2$ **3.5b·$(BPh_4)_2$**, $[Pt_2(\mu\text{-}SCH_2CH{=}CH_2)(\mu\text{-}SCH_3)(PPh_3)_4](PF_6)_2$ **3.9** and $[Pt_2(\mu\text{-}SCH_2C_6H_5)(\mu\text{-}SCH_3)(PPh_3)_4](PF_6)_2$ **3.10**. θ = Dihedral angle between Pt_1SS and Pt_2SS planes.

Parameters	**3.1b·$(PF_6)_2$**	**3.7**	**3.8**	**3.5b·$(BPh_4)_2$**	**3.9**	**3.10**
Mean Pt-S	2.3751(16)	2.3578(15)	2.3633(12)	2.370(3)	2.367(2)	2.360(3)
Mean Pt-P Å	2.2845(16)	2.2899(15)	2.3015(13)	2.301(3)	2.304(2)	2.300(3)
Pt---Pt Å	3.495	3.486	3.349	3.416	3.428	3.481
S---S Å	3.132	3.094	3.100	3.107	3.109	3.091
Mean Pt-S-Pt (º)	94.75(6)	95.34(5)	90.23(4)	92.20(11)	92.80(7)	95.06(11)
Mean S-Pt-P (º)	89.01(6)	90.54(5)	90.47(5)	90.09(11)	89.39(8)	90.11(11)
Mean S-Pt-S (º)	82.52(6)	82.03(5)	81.98(4)	81.91(11)	82.11(7)	81.84(10)
Dihedral angle θ	156	157	140	145	148	155

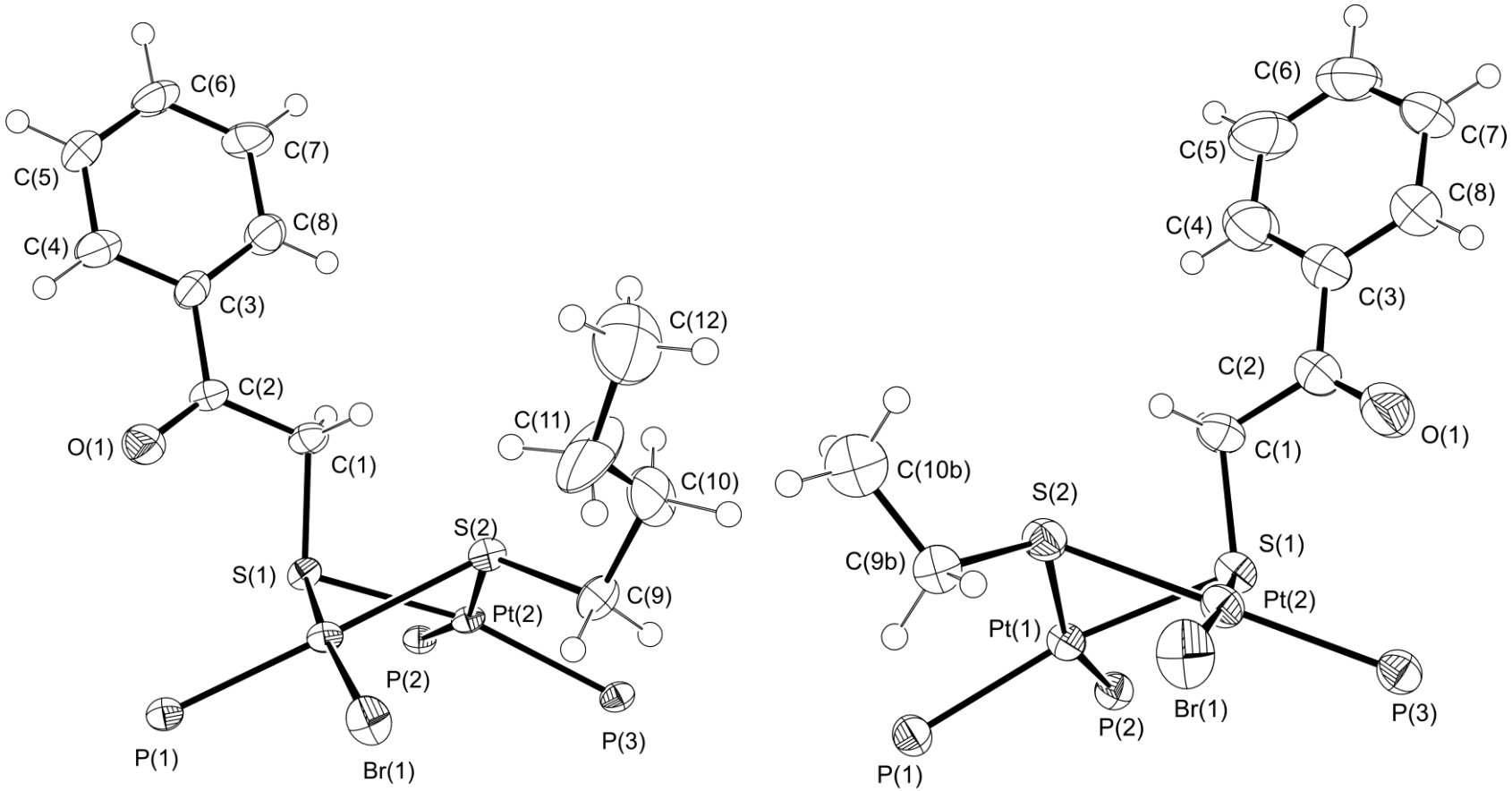

Figure 3.5 Molecular structures of $[Pt_2(\mu\text{-}SCH_2C(O)Ph)(\mu\text{-}SBu)(PPh_3)_3Br](PF_6)$ **3.5c·PF$_6$** and $[Pt_2(\mu\text{-}SCH_2C(O)Ph)(\mu\text{-}SEt)(PPh_3)_3Br](PF_6)$ **3.6c·PF$_6$** showing the atom numbering scheme with thermal ellipsoids at the 50% probability level. The PF_6^- counter ion, H_2O in **3.5c·PF$_6$**, CH_2Cl_2 in **3.6c·PF$_6$** and the phenyl rings of PPh_3 ligands have been omitted for clarity.

Table 3.4 Selected bond lengths and atomic distances (Å) and bond angles (°) for $[Pt_2(\mu\text{-}SCH_2C(O)Ph)(\mu\text{-}SBu)(PPh_3)_3Br](PF_6)$ **3.5c·PF$_6$** and $[Pt_2(\mu\text{-}SCH_2C(O)Ph)(\mu\text{-}SEt)(PPh_3)_3Br](PF_6)$ **3.6c·PF$_6$** Estimated standard deviations are in brackets.

Bond lengths and atomic distances (Å)							
$[Pt_2(\mu\text{-}SCH_2C(O)Ph)(\mu\text{-}SBu)(PPh_3)_3Br](PF_6)$ **3.5c·PF$_6$**				$[Pt_2(\mu\text{-}SCH_2C(O)Ph)(\mu\text{-}SEt)(PPh_3)_3Br](PF_6)$ **3·6c.PF$_6$**			
Pt(2)-P(2)	2.270(2)	Pt(2)-S(1)	2.364(19)	Pt(1)-P(2)	2.2729(11)	Pt(1)-S(1)	2.3655(10)
Pt(1)-P(1)	2.268(2)	Pt(2)-S(2)	2.3823(19)	Pt(1)-P(1)	2.2992(11)	Pt(1)-S(2)	2.3725(11)
Pt(2)-P(3)	2.302(2)	C(2)-C(3)	1.496(11)	Pt(2)-P(3)	2.2669(11)	Pt(2)-S(1)	2.2799(11)
Pt(1)-Br(1)	2.4640(8)	S(1)-C(1)	1.824(8)	Pt(1)-Br(1)	2.4657(5)	Pt(2)-S(2)	2.3702(11)
C(1)-C(2)	1.507(11)	S(2)-C(9)	1.830(8)	C(1)-C(2)	1.508(6)	C(2)-C(3)	1.492(6)
C(2)-O(1)	1.221(9)	C(9)-C(10)	1.563(14)	C(2)-O(1)	1.198(6)	S(1)-C(1)	1.821(4)
Pt(1)-S(1)	2.280(18)	C(10)-C(11)	1.506(19)	Pt(1)---Pt(2)	3.214	S(1)---S(2)	2.961
Pt(1)-S(2)	2.375(2)	C(11)-C(12)	1.480(16)				
Pt(1)---Pt(2)	3.220	S(1)---S(2)	2.979				
Bond angles (°)							
S(2)-Pt(1)-S(1)	47.19(5)	Pt(1)-S(1)-Pt(2)	87.78(6)	S(2)-Pt(1)-S(1)	77.36(4)	S(1)-Pt(2)-P(3)	93.45(4)
S(2)-Pt(2)-S(1)	77.74(7)	Pt(2)-S(2)-Pt(1)	85.19(7)	S(2)-Pt(2)-S(1)	79.08(4)	Pt(1)-S(1)-Pt(2)	87.52(4)
S(1)-C(1)-C(2)	110.8(6)	C(9)-C(10)-C(11)	112.5(10)	S(1)-C(1)-C(2)	111.6(3)	Pt(2)-S(2)-Pt(1)	85.30(3)
S(2)-C(9)-C(10)	109.0(6)	O(1)-C(2)-C(3)	121.6(7)	C(1)-S(1)-Pt(1)	105.2(15)	O(1)-C(2)-C(3)	121.7(4)
C(1)-S(1)-Pt(1)	109.2(3)	C(9)-S(2)-Pt(2)	120.8(3)	C(1)-S(1)-Pt(2)	108.0(16)	S(2)-Pt(2)-Br(1)	96.16(3)
C(1)-S(1)-Pt(2)	104.0(3)	C(9)-S(2)-Pt(1)	114.8(3)				
S(1)-Pt(1)-P(1)	93.63(7)	S(2)-Pt(1)-Br(1)	96.22(5)				

The crystal structures of **3.5c·PF$_6$** and **3.6c·PF$_6$** are in accord with the masses obtained from the ESI-MS for the compounds and confirmed the displacement of the PPh_3 by the resulting Br^- ion. The structural parameters of the $\{Pt_2(\mu\text{-}S)_2\}$ core of **3.5c·PF$_6$** and **3.6c·PF$_6$** contrasts that of the homo- and heterodialkylated derivatives **3.1b·(PF$_6$)$_2$** and **3.5b·(BPh$_4$)$_2$** reported herein in Figure 3.4 and other known dialkylated derivatives. The loss of the terminal PPh_3 ligand is expected to reduce intramolecular repulsion between the PPh_3 in $[Pt_2(\mu\text{-}S)_2(PPh_3)_4]$ moiety. The separation between the incorporated group and the remaining PPh_3 ligands due to repulsion is also enhanced because Br is smaller than PPh_3. This caused a large degree of bending along S---S axis and reduction in the dihedral angles to 124.66° and 123.84° for **3.5c·PF$_6$** and **3.6c·PF$_6$** respectively, which is the lowest so far recorded between the Pt(1) S(1) S(2) and Pt(2) S(1) S(2) planes. There is also a reduction in the S(1)---S(2) separation distances 2.979 Å, **3.5c·PF$_6$** and 2.961 Å, **3.6c·PF$_6$** when compared with the same distance in **3.5b·(BPh$_4$)$_2$**, 3.107 Å and other known heterodialkylated derivatives in Table 3.3. In contrast to **3.5b·(BPh$_4$)$_2$**, the phenacyl moieties in **3.5c·PF$_6$** and **3.6c·PF$_6$** adopted an axial position while the butyl and ethyl groups took the equatorial position. The difference in the position of the ethyl and butyl substituents in **3.5b·(BPh$_4$)$_2$** and **3.5c·PF$_6$** and **3.6c·PF$_6$** is due to the replacement of the bulkier PPh_3 group by smaller Br. The intramolecular repulsion between the terminal PPh_3 groups and the attached alkyl groups is consequently reduced opening up a pocket between the two thiolate groups and allowing the butyl and ethyl groups to adopt an equatorial position. In both **3.5c·PF$_6$** and **3.6c·PF$_6$** the Br is *trans* to phenacyl groups. The Pt(1)-S(1) 2.280(18) Å bond length in **3.5c·PF$_6$** which is *trans* to Pt-Br bond is shorter than the corresponding *cis*-Pt(1)-S(1) 2.364(19) Å bond, an indication that PPh_3 is a higher *trans* influence ligand than Br.

3.4 NMR Characterisation

3.4.1 ^{1}H NMR

^{1}H NMR was used to characterise the alkylated derivatives. Detailed ^{1}H NMR studies were carried out where necessary to completely assign the signals.

For instance, Selective Total Correlated Spectroscopy (SELTOCSY) excitation experiments were performed to distinguish the hydrogen (H) atoms of the butyl group and fully assign the ^{1}H NMR of **3.5b·(PF$_6$)$_2$** shown in Figure 3.6 below. Selective irradiation of the methyl group at 0.28 ppm and the use of shell mixing time of 12 µsec enhanced the signal of the adjacent methylene group (0.47 ppm). When the mixing was extended to 32 µsec, the β-methylene signal also appeared in the spectrum, at -0.51 ppm. A mixing time of 80 µsec enhanced the α, β and γ-methylene groups, the methylene adjacent to sulfur appeared at 1.98 ppm.

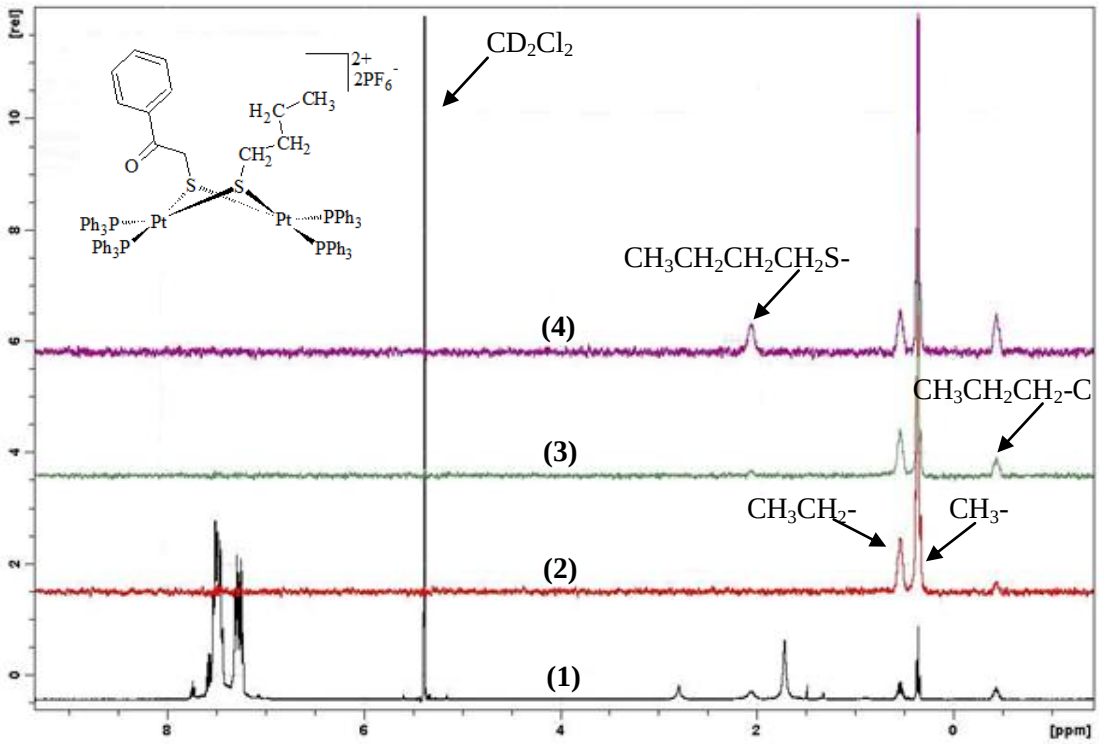

Figure 3.6 ^{1}H NMR spectrum (**1**) and the SELTOCSY (**2**), (**3**), (**4**) experiments to differentiate and assign the NMR signals of $[Pt_2(\mu\text{-}SCH_2C(O)Ph)(\mu\text{-}SBu)(PPh_3)_4](PF_6)_2$ **3.5b·(PF$_6$)$_2$**

The ^{1}H NMR of the isolated crystals of **3.6b·(PF$_6$)$_2$** showed a major peak for $-CH_3$ of ethyl group in the product at -0.40 ppm. It also indicated two minor $-CH_3$ proton signals at -0.24 and 0.09 ppm. The minor signals are attributable to the presence of two possible isomers of the bromide derivatives (see section 3.2.2). Selective irradiation of the methylene $-CH_2$ protons of the ethyl group at 2.13, 2.31 and 2.38 ppm at a shell mixing time of 30 µsec were used to correlate the signals and assign the peaks. The CH_2 (major) of **3.6b·(PF$_6$)$_2$** at 2.13 ppm correlated to the major -CH_3 signal at -0.40 ppm. The CH_2 signals at 2.31 and 2.38

ppm correlated to the CH_3 at -0.24 and -86 ppm. The signals for phenacyl CH_2 was observed at 2.68 ppm and the minor 2.83 ppm.

The ^1H NMR spectrum of **3.5c·PF_6** and **3.6c·PF_6** showed clear proton signals of the PPh_3 rings. The signals for attached alkyl (butyl and ethyl) groups were not clear as in **3.5b·$(PF_6)_2$** and **3.6b·$(PF_6)_2$**. Overlapping signals between 0.078 ppm and 1.60 ppm were observed for **3.5c·PF_6**. This is outside the expected chemical shifts of the methyl and methylene hydrogen atoms. SELTOCSY experiments were used to correlate the protons signal at 0.51, 0.79 and 1.09 ppm. The rest could not be clearly assigned due to the overlap. However, there is a good agreement between the masses of **3.5c·PF_6** and **3.6c·PF_6** obtained from ESI-MS with the X-ray structures obtained.

3.4.2 $^{31}P\{^1H\}$NMR

Complex **3.1b·$(PF_6)_2$** contains chemically equivalent phosphorus atoms and gave a $^{31}P\{^1H\}$ NMR spectrum (Figure 3.7) that supported the structure shown in Figure 3.4.

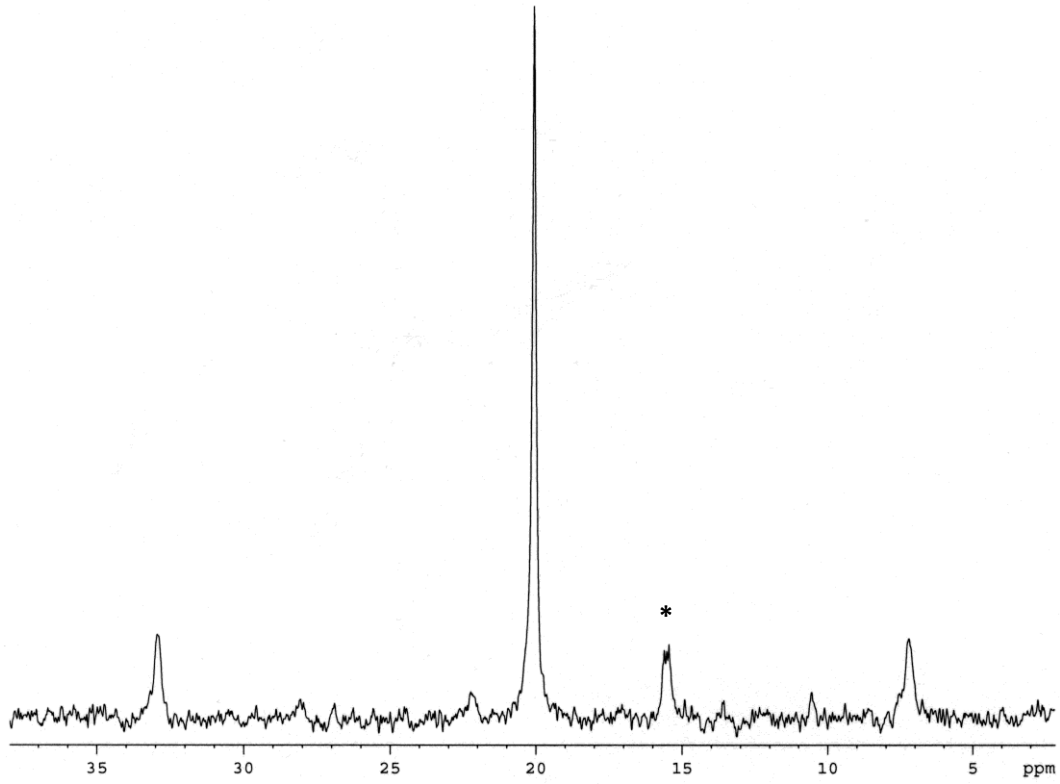

Figure 3.7 $^{31}P\{^1H\}$ NMR spectrum of **3.1b·$(PF_6)_2$** showing the single satellite peaks and an unidentified impurity (*) at 15.5 ppm.

The spectrum showed a single phosphorus environment at 20.07 ppm, with ^{195}Pt coupling, and an unidentified peak at 15.55 ppm. The $^{31}P\{^1H\}$ NMR spectra of the homodialkylated derivatives **3.2b·(PF$_6$)$_2$** and **3.4b·(PF$_6$)$_2$** also showed similar spectra that supported the expected homodialkylated structures.

The $^{31}P\{^1H\}$ NMR of **3.5b·(PF$_6$)$_2$** (Figure 3.8) and **3.6b·(PF$_6$)$_2$** in CD_2Cl_2 gave signals from the two different phosphorus environments, overlapped and appeared at 19.64 ppm and 19.71 ppm respectively. The $^{31}P\{^1H\}$ NMR in DMSO could not separate the overlapping phosphorus signals but gave signals at slightly different chemical shifts between 19.30 to 19.90 ppm. The spectrum of each of the heterodialkylated derivatives showed two satellite peaks on each side of the phosphorus signal. The two sets of satellite peaks on both sides indicated that there are two sets of inequivalent phosphorus environments. This is due to the different groups attached to each sulfur atom in the $\{Pt_2S_2\}$ core as confirmed by the X-ray structure of **3.5b·(BPh$_4$)$_2$** shown in Figure 3.4.

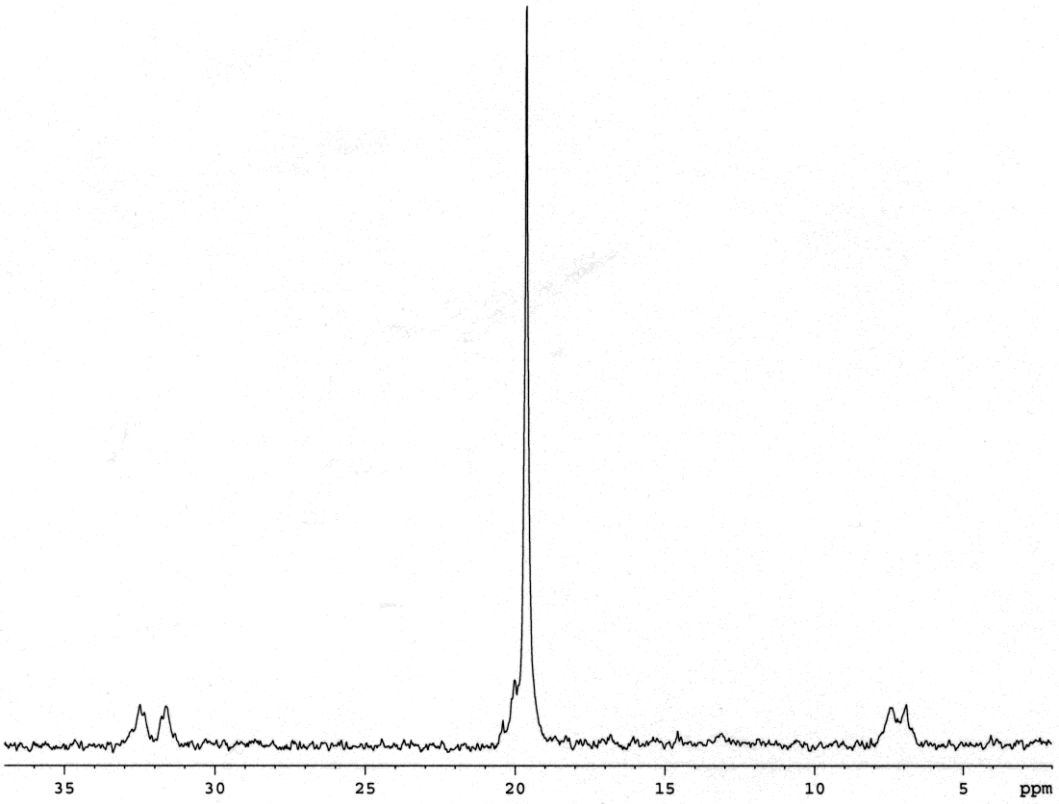

Figure 3.8 $^{31}P\{^1H\}$ NMR spectrum of **3.5b·(PF$_6$)$_2$** showing two close satellite peaks due ^1JPt-P coupling of the two phosphorus environments.

The heterodialkylated bromide derivatives **3.5c·PF$_6$** and **3.6c·PF$_6$** were expected to show three different $^{31}P\{H\}$ NMR signals but showed an unexpected phosphorus spectrum. Because of the presence of two isomers, six distinct different ^{31}P signals were expected from each compound **3.5c·PF$_6$** and **3.6c·PF$_6$** but instead the spectrum showed overlapping signals. The signals were not clearly differentiated to show the six signals due to coincidental overlap. The overlapping signals were at 13.86, 14.71, 15.78 and 16.67 ppm of **3.5c·PF$_6$** (Figure 3.9) and 14.05, 14.77, 15.01 and 16.71 ppm for **3.6c·PF$_6$**. The corresponding satellite peaks were also overlapped. As discussed in section 3.2.2, this is likely due to the different isomers formed by the displacement of a PPh_3 by the leaving Br^- ion in the reaction of $PhC(O)CH_2Br$ with $[Pt_2(\mu\text{-}S)(\mu\text{-}Bu)(PPh_3)_4]^+$ and $[Pt_2(\mu\text{-}S)(\mu\text{-}Et)(PPh_3)_4]^+$ respectively to form the bromide derivatives, **3.5c·PF$_6$** and **3.6c·PF$_6$**.

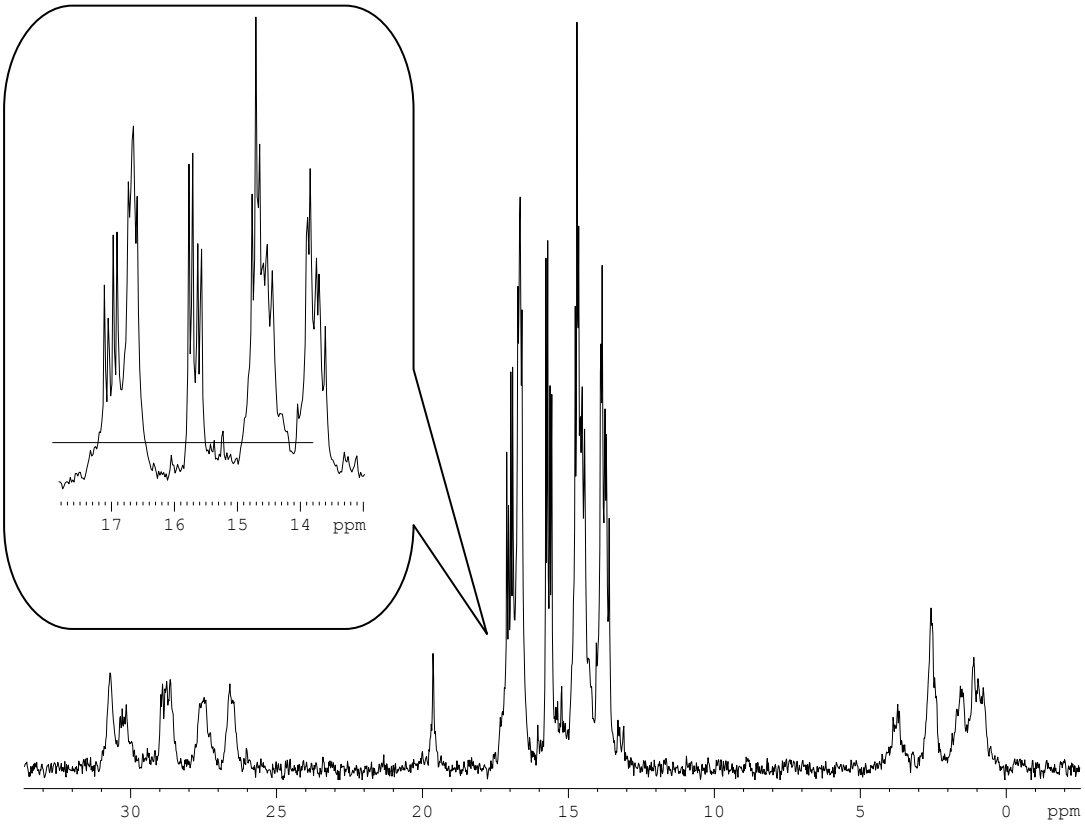

Figure 3.9 $^{31}P\{^1H\}$ NMR spectrum of **3.5c·PF$_6$** showing overlapping satellite peaks due ^1JPt-P coupling.

The presumption that the leaving bromide (Br^-) ion in the alkylation reactions displaced PPh_3 from only the alkyl thiolate side of **3.5c·PF$_6$** and **3.6c·PF$_6$** did not correlate with the results obtained from NMR characterisation. The expectation was that the $^{31}P\{^1H\}$ NMR will show three different signals in accordance with the three phosphorus environments in **3.5c·PF$_6$** and **3.6c·PF$_6$**. The NMR spectrum showed a more complicated overlapping signal presumably because the product is a mixture of the two isomers shown in Scheme 3.3.

3.5 IR Characterisation

The IR spectra of the complexes showed distinct absorption bands characteristic of the functional groups in the incorporated thiolate ligands. The absorption band for >C=O functional group in **3.1b·(PF$_6$)$_2$** (1673 cm^{-1}) , **3.2b·(PF$_6$)$_2$** (1638 cm^{-1}) and **3.4b·(PF$_6$)$_2$** (1725 cm^{-1}) reflects the different electronic environments of the incorporated groups. The >C=O IR absorption band in **3.5b·(BPh$_4$)$_2$**, (1637 cm^{-1}) increased to 1681 cm^{-1} in **3.5c·PF$_6$** due to the displacement of a PPh_3 by Br^-. The difference in absorption band of **3.5b·(PF$_6$)$_2$** and **3.5c·PF$_6$** indicates an increase in vibration frequency of the carbonyl group in the bromide derivative **3.5c·PF$_6$**.

3.6 Conclusion

This study has successfully established the properties of electrophiles that encourage the stepwise homodialkylation and heterodialkylation of sulfide ligands in **1.1**. The results of the investigation show that complete dialkylation of **1.1** can be achieved with appropriate organic electrophiles with good leaving group. In addition to the known effect of increased concentration of the alkylating agent[21], a combination of other factors which include; nature of the electrophile and conjugated aromatic residual organic part of the electrophile and the functional group on the β-carbon augment the ability of an electrophile to dialkylate **1.1**. The successful conversion of the sulfides in **1.1** into mixed thiolates and its halide derivative has also provided another simple route to new class of mixed-thiolato complexes of **1.1** which to date have only one reported synthetic route[6]. The

ability of **1.1** to carry different thiolate groups indicates that the nucleophilicity of the sulfide centres can potentially be utilised in synthesising multifunctional thiolate template cationic ligands for constructing multimetallic coordination compounds.

3.7 Experimental

Solvents used were generally drum grade as supplied. Complex $[Pt_2(\mu\text{-}S)_2(PPh_3)_4]$ **1.1** was synthesised by metathesis of *cis*-$[PtCl_2(PPh_3)_2]$ with $Na_2S.9H_2O$ in benzene[30] and obtained at a yield of 88%. ESI-MS; +20 V distilled MeOH : *m/z* 1503 $[M + H]^+$. Unless otherwise stated, all ^1H NMR ESI-MS mass spectra were recorded as explained in the appendix. Methanol, dichloromethane, diethyl ether were supplied as drum grade chemicals. The following chemicals were used as supplied from BDH: phenacyl chloride, phenacyl bromide, 1-bromobutane, bromoethane and $NaBPh_4$; Aldrich: 1-(bromoacetyl) pyrene, 3-bromoacetyl coumarin, 6-chloroacetyl-2H-1, 4-benzothiazin-3(4H)-one and NH_4PF_6.

Preparation of $[Pt_2(\mu\text{-}SCH_2COPh)_2(PPh_3)_4](PF_6)_2$ (3.1b·$(PF_6)_2$)

To a methanol (30 mL) suspension of $[Pt_2(\mu\text{-}S)_2(PPh_3)_4]$ (100 mg, 0.067 mmol) was added $BrCH_2C(O)Ph$ (132.4 mg, 0.67mmol, 10 mol equiv.) and the mixture stirred at room temperature for 1 hour during which time the solution changed from a cloudy orange solution to a clear pale yellow. The solution was allowed to further stir for 24 hours during which it turned to a near colourless solution. ESI-MS indicated complete formation of $[Pt_2(\mu\text{-}SCH_2COPh)_2(PPh_3)_4]^{2+}$. The solution was filtered to remove traces of solid matter and excess NH_4PF_6 (80 mg, 0.49 mmol) was added, followed by the addition of distilled water (30 mL) to induce precipitation from solution. The solid was filtered and washed successively with water (10 mL), methanol (10 mL), and diethyl ether (10 mL) and dried under vacuum giving a near white powder of the product $[Pt_2(\mu\text{-}SCH_2COPh)_2\text{-}(PPh_3)_4](PF_6)_2$ (90.5 mg, 67 %). Crystals suitable for X-ray diffraction analysis were obtained by vapour diffusion from dichloromethane and diethyl ether.

m.p. 221-223°C

IR (KBr disc) ν cm^{-1}: 839, 1097, 1443, 1673

$^{31}P\{H\}$ NMR (CD_2Cl_2): δp = 20.1 (*s*, $^1J_{Pt\text{-}P}$ = 3128 Hz)

^1H NMR (300MHz, CD_2Cl_2): δ 2.11 (*br*, *s*, 4H, $2SCH_2$), 7.06-7.79 (*m*, 70 H, 14 C_6H_5)

ES-MS (MeOH): *m/z* 870 ($[M]^{2+}$ 100%)

Elemental analysis (%): calcd. for $C_{88}H_{74}F_{12}O_2P_6Pt_2S_2$ (2031.64): C, 52.02; H, 3.67; found: C, 51.77; H, 3.69.

Preparation of $[Pt_2(\mu\text{-}SCH_2C(O)pyr)_2(PPh_3)_4](PF_6)_2$ (3.2b·$(PF_6)_2$)

1-(Bromoacetyl)pyrene (129 mg, 0.399 mmol, 6 mole equiv.) was introduced into an orange suspension of $[Pt_2(\mu\text{-}S)_2(PPh_3)_4]$ (100 mg, 0.067 mmol) in methanol (25 mL). The solution was left to stir for 7 days. Complete reaction was confirmed by ESI-MS. The yellow solution was gravity filtered to remove any solid impurity. Excess NH_4PF_6 (40 mg, 0.25 mmol) was added to the filtrate resulting in the formation of a bright yellow precipitate. Distilled water (10 mL) was added to complete precipitation. A bright yellowish-orange powder of the product $[Pt_2(\mu\text{-}SCH_2C(O)pyr)_2(PPh_3)_4](PF_6)_2$ (98 mg, 65%) was obtained after washing with water (40 mL) and diethyl ether (40 mL) using suction filtration.

m.p.: 222-224°C

IR (KBr disc) ν cm^{-1}: 839, 1097, 1436, 1638

$^{31}P\{H\}$ NMR (300 MHz, CD_2Cl_2): δ_P = 22.4 (*s*, $^1J_{Pt\text{-}P}$ = 3136 Hz)

^1H NMR (300 MHz, CD_2Cl_2): δ = 2.47 (br, *s*, 4H, $2SCH_2$), 6.68-8.45 (*m*, 94 H)

ESI-MS (MeOH) cone voltage 20: *m/z* 996 ($[M]^{2+}$, 100%)

Elemental analysis (%): calcd. for $C_{108}H_{82}F_{12}O_2P_6Pt_2S_2$ (2279.92): C, 56.89; H 3.63; found (%): C, 56.69; H, 3.92.

Preparation of $[Pt_2(\mu\text{-}SCH_2C(O)cum)_2(PPh_3)_4](PF_6)_2$ (3.4b·$(PF_6)_2$)

Methanol (25 mL) was added to 3-(bromoacetyl)coumarin (107 mg, 0.399 mmol 6 equiv.) and $[Pt_2(\mu\text{-}S)_2(PPh_3)_4]$ (100 mg, 0.067 mmol) in a round bottomed flask. The mixture was stirred for 7 days and monitored by ESI-MS. The light red solution was gravity filtered to remove any solid impurity and excess NH_4PF_6 (40 mg, 0.25 mmol) was added, resulting in a white precipitate. Distilled water (10

mL) was added to complete precipitation. A dull white powder of the product $[Pt_2(\mu\text{-}SCH_2C(O)cum)_2(PPh_3)_4](PF_6)_2$ (92 mg, 63.8%) was obtained after washing with water (40 mL) and diethyl ether (40 mL) using suction filtration.

m.p.: 178-180°C

IR (KBr disc) ν cm^{-1}: 840, 1096, 1435, 1481, 1557, 1608, 1725

$^{31}P\{H\}$ NMR (300 MHz, CD_2Cl_2) 18.9 [s, $^1J(PtP)$ 3110].

^1H NMR (400 MHz, CD_2Cl_2): δ = 3.52 (*t*, 4H, SCH_2) and 7.05-7.91 (*m*, aromatic CH)

ESI-MS (MeOH): *m/z* 938 ($[M]^{2+}$, 100%)

Elemental analysis (%): calcd. for $C_{94}H_{74}F_{12}O_6P_6Pt_2S_2$ (2167.7): C, 52.08; H, 3.44; found (%): C, 51.77; H =3.59

Preparation of $[Pt_2(\mu\text{-}SCH_2C(O)Ph)(\mu\text{-}SBu)(PPh_3)_3Br](PF_6)$ (3.5c·PF_6)

1-Bromobutane (1 mL, 9.30 mol equiv.) was introduced into an orange suspension of $[Pt_2(\mu\text{-}S)_2(PPh_3)_4]$ (100 mg, 0.067 mmol) in methanol (25 mL). The solution was stirred and dissolution of $[Pt_2(\mu\text{-}S)_2(PPh_3)_4]$ occurred after about 7 min. yielding a pale yellow solution that was left to stir for 1 hour. ESI-MS indicated complete formation of $[Pt_2(\mu\text{-}S)(\mu\text{-}SBu)(PPh_3)_4]^+$, and the reaction solvent and excess bromobutane were removed by rotary evaporation. The residue was dissolved in methanol (25 mL), and stirred for about 5 min. and excess $BrCH_2C(O)Ph$ (66.2 mg, 0.34 mmol) was added and stirred for 48 hours. ESI-MS indicated complete formation of $[Pt_2(\mu\text{-}SCH_2C(O)Ph)(\mu\text{-}SBu)(PPh_3)_3Br]^+$. The light brown solution was gravity filtered to remove any solid impurity and excess NH_4PF_6 (40 mg, 0.25 mmol) was added, resulting in a brownish suspension. Distilled water (10 mL) was added to complete precipitation. A brownish powder of the product (61 mg, 56 %) was obtained after washing with water (40 mL) and diethyl ether (40 mL) using suction filtration. Crystals suitable for X-ray structure was isolated from vapour diffusion of diethyl ether into a dichloromethane solution.

m.p.: 216-218°C

IR (KBr disc) ν cm^{-1}: 834, 1096, 1435, 1681

ESI-MS (MeOH): *m/z* 1497 ($[M]^+$, 100%)

Elemental analysis (%): calcd. for $C_{66}H_{61}Br_1F_6O_1P_4Pt_2S_2$ (1642.28): C, 48.27; H, 3.44; found: C, 47.35; H, 3.84.

Preparation of $[Pt_2(\mu\text{-}SCH_2C(O)Ph)(\mu\text{-}SBu)(PPh_3)_4](PF_6)_2$ (3.5b·$(PF_6)_2$)

$[Pt_2(\mu\text{-}S)(\mu\text{-}SCH_2CH_2CH_2CH_3)(PPh_3)_4]^+$ was prepared following the procedure for **3.5c·PF_6**. The resulting residue was redissolved in methanol (25 mL) and stirred for 5 mins and excess $BrCH_2C(O)Ph$ (66.2 mg, 0.34 mmol, 5 mol equiv.) was added and stirred overnight. PPh_3 (17.5 mg, 0.067mmol) was added to the reaction mixture and further stirred for another 12 hours to complete the formation of **3.5b**. ESI-MS indicated complete formation of $[Pt_2(\mu\text{-}SCH_2C(O)Ph)(\mu\text{-}SBu)(PPh_3)_4]^{2+}$ and the solution was gravity filtered to remove any solid impurity and excess NH_4PF_6 (40 mg, 0.25 mmol) was added, resulting in an off-white precipitate. Distilled water (10 mL) was added to complete precipitation. A near white powder of the product $[Pt_2(\mu\text{-}SCH_2C(O)Ph)(\mu\text{-}SBu)(PPh_3)_4](PF_6)_2$ (69.5 mg, 53%) was obtained after washing with water (40 mL) and diethyl ether (40 mL) using suction filtration.

m.p.: 188-191°C

IR (KBr disc) ν cm^{-1}: 839, 1097, 1436, 1637

$^{31}P\{^1H\}$ NMR (CD_2Cl_2): δ_p = 19.64 (*br s*, $J_{Pt\text{-}P(1)}$ 3107 Hz, $J_{Pt\text{-}P(2)}$ 2934 Hz)

^1H NMR (400 MHz, CD_2Cl_2): δ = 0.28 (2H, *m*, CH_3), 0.47 (2H, *m*, CH_2), -0.50 (2H, *m*, CH_2), 1.98 (2H, *b*r, S-CH_2), 2.71 (*br*, 2H, S-CH_2), 7.15-7.65 (65H, *m*, $13C_6H_5$)

ESI-MS (MeOH): *m/z* 839 ($[M]^{2+}$, 100%)

Elemental analysis: calcd. (%) for $C_{84}H_{76}F_{12}O_1P_6Pt_2S_2$ (1969.61): C, 51.22; H, 3.89; found: C, 51.08; H, 3.89.

Preparation of $[Pt_2(\mu\text{-}SCH_2C(O)Ph)(\mu\text{-}SCH_2CH_3)(PPh_3)_3Br](PF_6)$ (3.6c.PF_6)

Following the same procedure for **3.5c·PF_6**, $[Pt_2(\mu\text{-}S)_2(PPh_3)_4]$ (100 mg, 0.067 mmol) and CH_3CH_2Br (1 mL, 0.09 mol) reacted to formed the monoalkylated derivative $[Pt_2(\mu\text{-}S)(\mu\text{-}SCH_2CH_3)(PPh_3)_4]^+$. The resulting yellow solution was filtered and the solvent and excess CH_3CH_2Br removed by

evaporation. The residue was dissolved in methanol and $BrCH_2C(O)Ph$ (66.2 mg, 0.34 mmol 5 mol equiv) added. The reaction mixture was stirred for 48 hours, filtered. NH_4PF_6 (40 mg, 0.25 mmol) and 10 mL distilled water was added to the filtrate. The light brown precipitate of the product was filtered using suction filtration and washed with water (2 x 20 mL) and diethyl ether (2x 20 mL) to give (67 mg, 62%).

m.p.: 191-194°C

IR (KBr disc) ν cm^{-1}: 1095, 1436, 1481, 1689

ESI-MS (MeOH): *m/z* 1469 ($[M]^+$, 100%)

Elemental analysis: calcd. (%) for $C_{64}H_{57}F_6O_1P_4Pt_2S_2$ (1614.22): C, 47.62; H, 3.56; found: C, 46.51; H , 3.38.

Preparation of $[Pt_2(\mu\text{-}SCH_2C(O)Ph)(\mu\text{-}SCH_2CH_3)(PPh_3)_4](PF_6)_2$ (3.6b·$(PF_6)_2$)

Following the same procedure for **3.5c·PF_6**, $[Pt_2(\mu\text{-}S)_2(PPh_3)_4]$ (100 mg, 0.067 mmol) with CH_3CH_2Br (1 mL, 0.09 mol) to form the monoalkylated derivative $[Pt_2(\mu\text{-}S)(\mu\text{-}SCH_2CH_3)(PPh_3)_4]^+$. The resulting yellow solution was filtered and the solvent and excess CH_3CH_2Br removed by evaporation. The residue was dissolved in methanol and $BrCH_2C(O)Ph$ (66.2 mg, 0.34 mmol, 5 mol equiv) and stirred overnight. PPh_3 (17.5 mg, 0.067 mmol) was added and futher stirred for 48 hours, filtered and added NH_4PF_6 (40 mg 0.25 mmol) and 10 mL distilled water. The white precipitate of the product $[Pt_2(\mu\text{-}SCH_2C(O)Ph)(\mu\text{-}SEt)(PPh_3)_4](PF_6)_2$ was filtered using suction filtration and washed with water (2 x 20 mL) and diethyl ether (2x 20 mL) to give (74 mg, 57%).

m.p.:211-213 °C

IR (KBr disc) ν cm^{-1}: 836, 1096, 1436, 1481, 1674 cm^{-1}

$^{31}P\{^1H\}$ NMR (300MHz, CD_2Cl_2): 19.71(*br*, *m*, $J_{Pt\text{-}P(1)}$ 3050Hz, $J_{Pt\text{-}P(2)}$ 2942Hz)

^1H NMR (400MHz CD_2Cl_2): δ = -0.40 (*tr*, CH_3), 2.13 (*tr*, CH_2), 2.68 (*br*, CH_2)

ESI-MS (MeOH): *m/z* 826 ($[M]^{2+}$, 100%)

Elemental analysis: calcd. (%) for $C_{82}H_{72}F_{12}O_1P_6Pt_2S_2$ (1941.56): C, 50.73; H, 3.49; found: C, 50.53; H, 3.65

3.8 X-ray Crystal Structure Determinations

All X-ray measurements for **3.1b·$(PF_6)_2$**, **3.5b·$(BPh_4)_2$** and **3.5c·PF_6** were made as explained in the Section A.7 of the appendix. Pt, S and P atoms were located and ll other non-hydrogen atoms were located from a series of difference maps. Full-matrix least-squares refinement of (SHELXL-97[31]) was based on F_o^2 with all non-hydrogen atoms anisotropic and hydrogen atoms in calculated positions. A summary of crystallographic parameters for the data collections and refinements is given in Table 3.5 and 3.6.

Most of the details of the structure of **3.1b·$(BPh_4)_2$** evolved normally on refinement. The asymmetric unit of the refined structure contained the dication $[Pt_2(\mu\text{-}SCH_2C(O)Ph)_2(PPh_3)_4]^{2+}$, $2PF_6^-$ and CH_2Cl_2. When the main details were included in the refinement, there was a significant peak adjacent to Pt(2) which was modeled as a partially disordered occupancy of the Pt(2) site. This refined to 92.8% occupancy. One molecule of CH_2Cl_2 was well-resolved, and residual density suggested a less defined one. This was included in the refinement with

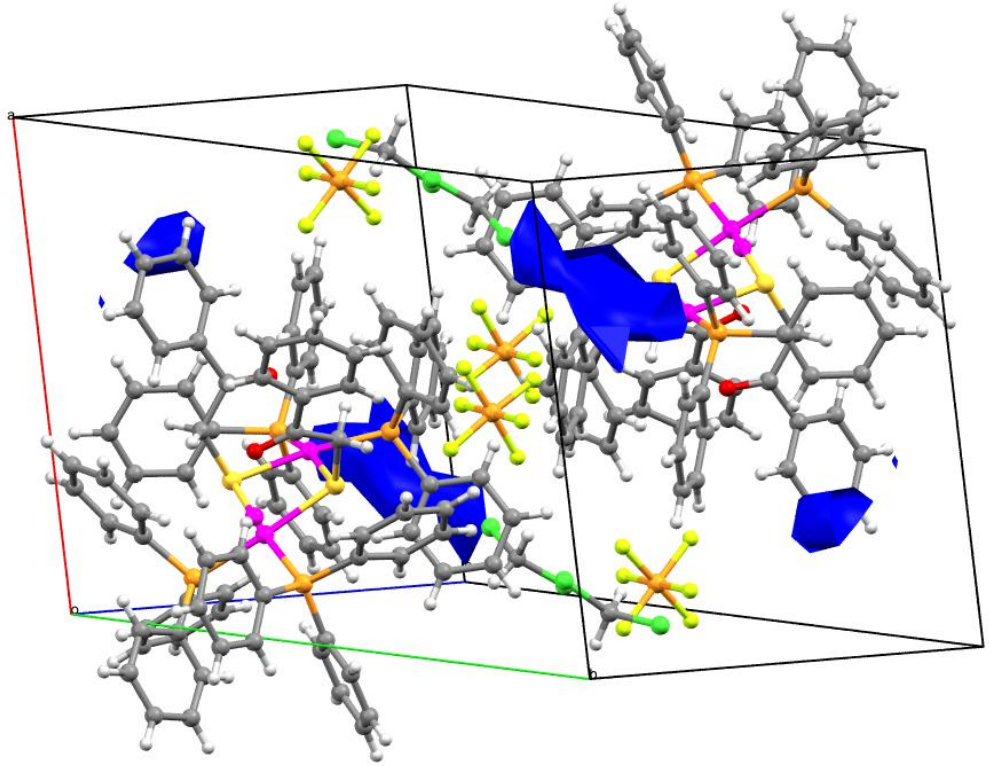

Figure 3.10 The unit cell crystal packing showing the solvent accessible voids in the final crystal structure map for $[Pt_2(\mu\text{-}SCH_2C(O)Ph)_2(PPh_3)_4](PF_6)_2$ **3.1b·$(BPh_4)_2$**

constrained C-Cl bond lengths and refined to 83% occupancy. A final difference map revealed more electron density (*ca* 3-4 eÅ^{-3}) in a region with solvent accessible voids of *ca* 160 Å^3 which was presumably more solvent molecules (possibly an Et_2O) as shown in Figure 3.10. This could not be successfully modelled so was not included in the model. All non-H atoms were refined anisotropically except for the minor Pt(2) component and H atoms were included in calculated positions.

The crystal data of **3.5b·$(BPh_4)_2$** were acquired in C2/c space group but could not be solved in that space group as there are two different subsituents on the sulfur atoms. The crystal was solved by direct methods in space group Cc. The platinum, sulfur and phosphorus atoms evolved followed by all other atoms on refinement. All non hydrogen atoms were refined anisotropically except C(4) which was very floppy. A disordered solvent molecule was treated as a disordered chlorine atom of CH_2Cl_2 and included in the final refinement.

The structure of **3.5c·PF_6** was solved by direct methods and almost all details evolved normally. All the atoms except H were refined anisotropically. At the end of the first refinement, two residual peaks of about 4 e Å^{-3} revealed as solvent accessible spaces. In the final refinement they were treated and refined as the oxygen atoms of partial H_2O molecules taking into account the H – bonding distances.

The X-ray structure data for **3.6c·PF_6** were obtained as explained in the appendix. The structure was refined by full-matrix least squares on F^2 with anisotropic thermal parameters for nonhydrogen atoms. The asymmetric unit contains half a cation $\{Pt_2(\mu\text{-}SCH_2C(O)Ph)(\mu\text{-}SCH_2CH_3)(PPh_3)_3Br\}$, one anion PF_6^- and one solvent CH_2Cl_2. The ethyl group attached to S(2) has a very large thermal motion. In final refinement cycles it was treated as disordered (into two parts) to obtain better bond lengths and thermal parameters.

Table 3.5 Crystal data and structure refinement details for **3.1b·$(PF_6)_2$** and **3.5b·$(BPh_4)_2$**

Complex	**3.1b·$(PF_6)_2$**	**3.5b·$(BPh_4)_2$**
Formula	$C_{90}H_{78}C_{l4}F_{12}O_2P_6Pt_2S_2$	$C_{133}H_{118}B_2Cl_2OP_4Pt_2S_2$
Formula weight	2201.44	2402.97
Temperature (K)	93(2)	89(2)
Wavelength (Å)	0.71073	0.71073
Crystal system	Triclinic	Monoclinic
Space group	P -1	Cc
a/Å	13.9856(5)	31.9776(4)
b/Å	17.5866(6)	14.7512(2)
c/Å	18.9340(6)	27.7611(4)
α/°	91.906(2)	90
β/°	101.551(2)	115.73(1)
γ/°	93.392(2)	90
Volume ($Å^3$)	4549.8(3)	11796.7(3)
Z	2	4
Calculated density (Mg/m^3)	1.607	1.353
Absorption coefficient (mm^{-1})	3.411	2.554
F(000)	2176	4864
Crystal size (mm^3)	0.29 x 0.27 x 0.15	0.25 x 0.22 x 0.20
Theta range for data collection	1.10 to 28.00°	1.41 to 27.97
Limiting indices	$-18 \le h \le 18, -23 \le k \le 25, -25 \le l \le 25$	$-37 \le h \le 42, -19 \le k \le 19, -36 \le l \le 36$
Reflections collected / unique	106616 / 21940 [R(int) = 0.0448]	73575 / 25367 [R(int) = 0.0305]
Completeness to theta	28.00, 99.9 %	27.97, 99.6 %
Absorption correction	Semi-empirical from equivalents	Semi-empirical from equivalents
Max. and min. transmission	0.6286 and 0.4379	0.6292 and 0.5677
Refinement method	Full-matrix least-squares on F^2	Full-matrix least-squares on F^2
Data / restraints / parameters	21940 / 20 / 1069	25367 / 301 / 1306
Goodness of fit on F^2	1.110	1.055
Final R indices [$I>2\sigma(I)$]	$R_1 = 0.0500$, $wR_2 = 0.1252$	R1 = 0.0439, $wR_2 = 0.1362$
R indices (all data)	$R_1 = 0.0709$, $wR_2 = 0.1403$	R1 = 0.0538, $wR_2 = 0.1450$
Largest diff. peak and hole	3.562 and -1.439 e $Å^{-3}$	3.279 and -0.997 e $Å^{-3}$

Table 3.6 Crystal data and structure refinement details for **3.5c·PF_6** and **3.6c·PF_6**

Complex	**3.5c.PF_6**	**3.6c.PF_6**
Formula	$C_{66}H_{63}BrF_6O_2P_4Pt_2S_2$	$C_{65}H_{59}BrCl_2F_6OP_4Pt_2S_2$
Formula weight	1660.25	1699.11
Temperature (K)	89(2)	223(2)
Wavelength (Å)	0.71073	0.71073
Crystal system	Monoclinic	Monoclinic
Space group	P2(1)/c	P2(1)/c
a/Å	13.8278(4)	13.9445(6)
b/Å	22.7551(7)	22.6725(11)
c/Å	19.8603(6)	20.0422(9)
α/°	90	90
β/°	92.221(2)	90.4150(10)
γ/°	90	90
Volume ($Å^3$)	6244.4(3)	6336.3(5)
Z	4	4
Calculated density (Mg/m^3)	1.766	1.781
Absorption coefficient (mm^{-1})	5.347	5.352
F(000)	3248	3312
Crystal size (mm^3)	0.28 x 0.22 x 0.20	0.46 x 0.26 x 0.10
Theta range for data collection	1.36 to 28.09°	1.46 to 27.50°
Limiting indices	$-18 \leq h \leq 18$, $-29 \leq k \leq 30$, $-22 \leq l \leq 25$	$-17 \leq h \leq 18$, $-25 \leq k \leq 29$, $-25 \leq l \leq 26$
Reflections collected / unique	74187/14958 [R(int) = 0.0680]	44741/14543 [R(int) = 0.0435]
Completeness to theta	28.09°, 98.3 %	27.50° 99.9 %
Absorption correction	Semi-empirical from equivalents	None
Max. and min. transmission	0.4144 and 0.3159	0.6166 and 0.1921
Refinement method	Full-matrix least-squares on F^2	Full-matrix least-squares on F^2
Data / restraints / parameters	14958 / 0 / 748	14543 / 2 / 744
Goodness of fit on F^2	1.209	1.004
Final R indices [$I>2\sigma(I)$]	$R_1 = 0.0505$, $wR_2 = 0.0938$	$R_1 = 0.0351$, $wR_2 = 0.0792$
R indices (all data)	$R_1 = 0.0914$, $wR_2 = 0.1063$	$R_1 = 0.0474$, $wR_2 = 0.0835$
Largest diff. peak and hole	1.813 and -2.631 e. $Å^{-3}$	1.575 and -0.583 e.$Å^{-3}$

3.9 References

1. M. Capdevila, P. González-Duarte, C. Foces-Foces, F. Cano and M. Martinez-Ripoll, *J. Chem. Soc. Dalton Trans.*, 1990, 143.
2. M. Capdevila, W. Clegg, P. González-Duarte, A. Jarid and A. Lledós, *Inorg. Chem.*, 1996, **35**, 490.
3. G. Aullón, G. Ujaque, A. Lledos and S. Alvarez, *Chem. Eur. J.*, 1999, **5**, 1391.
4. C. Mentoza, J. Benet-Buchholz, M. A. Pericas and R. Vilar, *Dalton Trans.*, 2009, 2974.
5. G. Aullón, G. Ujaque, A. Lledós, S. Alvarez and P. Alemany, *Inorg. Chem*, 1998, **37**, 804.
6. S. H. Chong, L. L. Koh, W. Henderson and T. S. A. Hor, *Chem. Asian J.*, 2006, 264.
7. S. H. Chong, W. Henderson and T. S. A. Hor, *J. Chem. Soc. Dalton Trans.*, 2007, 4008.
8. K. R. Dixon, K. C. Moss and M. A. R. Smith, *J. Chem. Soc. Dalton Trans.*, 1974, 971.
9. L. Villanueva, M. Arroyo, S. Bernès and H. Torrens, *Chem. Comm.*, 2004, 1942.
10. J. Li, F. Li, L. L. Koh and T. S. A. Hor, *Dalton Trans.*, 2010, **39**, 2441.
11. Z. Li, Z. Loh, K. F. Mok and T. S. A. Hor, *Inorg. Chem.*, 2000, **39**, 5299.
12. W. Henderson, B. K. Nicholson, S. M. Devoy and T. S. A. Hor, *Inorg. Chim. Acta*, 2008, **361**, 1908.
13. P. J. Blower and J. R. Dilworth, *Coord. Chem. Rev.*, 1987, **76**, 121.
14. O. T. Ujam, S. M. Devoy, W. Henderson, B. K. Nicholson and T. S. A. Hor, *Inorg. Chim. Acta*, 2010, **363**, 3558.
15. S. W. A. Fong and T. S. A. Hor, *J. Chem. Soc., Dalton Trans.*, 1999, **5**, 639.
16. W. Henderson, S. H. Chong and T. S. A. Hor, *Inorg. Chim. Acta*, 2006, **359**, 3440.

17. S. H. Chong, A. Tjindrawan and T. S. A. Hor, *J. Mol. Cat, A: Chemical*, 2003, **204-205**, 267.
18. S. H. Chong, D. J. Young and T. S. A. Hor, *J. Organomet. Chem.*, 2006, **691**, 349.
19. S. H. Chong, D. J. Young and T. S. A. Hor, *Chem. Asian J.* , 2007, **2**, 1356.
20. F. A. Carey and R. J. Sundberg, *Advanced Organic Chemistry PART A: Structure and Mechanisms*, Fifth edn., Springer science + Business Media, New York, 2007.
21. A. Nova, P. González-Duarte, A. Lledós, R. Mas-Ballesté and G. Ujaque, *Inorg. Chim. Acta*, 2006, **359**, 3736
22. S. Ahrland, J. Chatt and N. R. Davies, *Quart. Rev. Chem. Soc.*, 1958, **12**, 265.
23. R. G. Pearson, *J. Am. Chem. Soc.*, 1963, **85**, 3533.
24. R. G. Pearson, *J. Chem. Educ.*, 1968, **45**, 581.
25. S. M. Devoy, M.Sc. Thesis, University of Waikato, 2005.
26. S. W. Benson, *J. Chem. Educ.*, 1965, **42**, 502.
27. J. A. Kerr, *Chem. Rev.*, 1966, **66**, 465.
28. V. Pavlishchuk, F. Birkelbach, T. Weyhermueller, K. Wieghardt and P. Chaudhuri, *Inorg. Chem.* , 2002, **41**, 4405.
29. H. Liu, A. L. Tan, C. R. Cheng, K. F. Mok and T. S. A. Hor, *Inorg. Chem*, 1997, **36**, 2916.
30. R. Ugo, G. La Monica, S. Cenini, A. Segre and F. Conti, *J. Chem. Soc. A*, 1971, 522.
31. G. M. Sheldrick, in *SHELXL-97 Programs for the Refinement of Crystal Structures*, University of Göttingen, Germany, Editon, 1997.

Chapter 4

Multifunctional Bridging Dialkylation of $[Pt_2(\mu\text{-}S)_2(PPh_3)_4]$

4.1 Introduction

The investigations in chapters two and three involved studies on the alkylation reactions of the sulfide centres in $[Pt_2(\mu\text{-}S)_2(PPh_3)_4]$ **1.1** with suitable monohalide electrophiles. Multifunctional organic groups have been successfully, incorporated into **1.1** through monoalkylation[1] and dialkylation of the two sulfide groups. This progressed from earlier reports of limited alkyl and aryl moieties incorporated into **1.1**[2-7]. Suitable dihalides have been reacted with **1.1** to form bridged derivatives[2, 4, 8-11]. However, studies on the reactivity of **1.1** with multifunctional dihalide alkylating agents have not been reported. Thus, this chapter include the alkylation chemistry studies of the reactivity of **1.1** towards multifunctional dihalide electrophiles. This is aimed at the syntheses of intra- and intermolecular bridged derivatives of the two sulfide groups in **1.1**. This was informed by the interest to further develop the use of the alkylated derivatives as precursor for constructing multimetallic molecules[12, 13] in which the metal centre(s) are attached to the donor atoms of the incorporated group.

The nucleophilic sulfides in **1.1** have been extensively utilised in constructing mono- and multimetallic sulfide bridged aggregates[2, 13-17]. An example of the typical metallic aggregate formed by **1.1** is shown in Scheme 4.1. It involves the bridging of the two sulfur atoms in a molecule of **1.1** by a metal fragment.

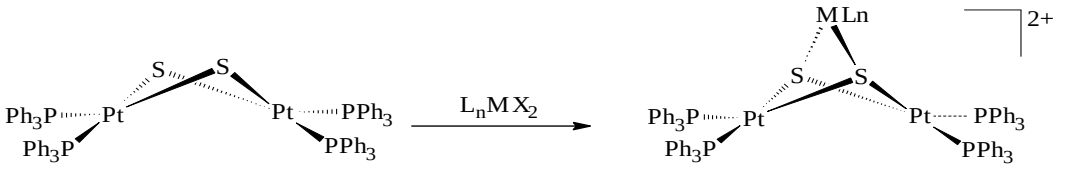

Scheme 4.1 Typical reaction $[Pt_2(\mu\text{-}S)_2(PPh_3)_4]$ with metal-halide complex L_nMX_2 where L is a neutral ancillary ligand such as a phosphine etc and X = halide or pseudohalide[18].

In reactions with organic electrophiles, monoalkylation of the sulfide centres dominates unless with an electrophile strong enough to dialkylate the two sulfides. An exception to the above common reactivity of **1.1** towards organic electrophiles has been observed with the use of appropriate α,ω-dialkylating electrophiles as shown in Scheme 4.2. Flexible monofunctional alkyl and aryl α,ω-dialkylating agents with up to five spacer atoms between the alkylating halogeno-carbon atoms react to form intramolecular bridged derivatives $[Pt_2(SCH_2RCH_2S)(PPh_3)_4]^{2+}$ [4, 8-10] (R = alkyl or aryl group). α,ω-Dialkylating agents with R more than four spacer atoms or a more rigid group between the alkylating halogeno-carbon atoms either form monoalkylated species $[Pt_2(\mu\text{-}S)(\mu\text{-}SCH_2R\text{-}CH_2X)(PPh_3)_4]^{+}$ or intermolecular dithiolate bridged Pt_4 aggregate $[(PPh_3)_4\,Pt_2(\mu\text{-}S)(\mu\text{-}SCH_2RCH_2S\text{-}\mu)(\mu\text{-}S)Pt_2\,(PPh_3)_4]^{2+}$ [2, 11]. The latter involve the alkylation

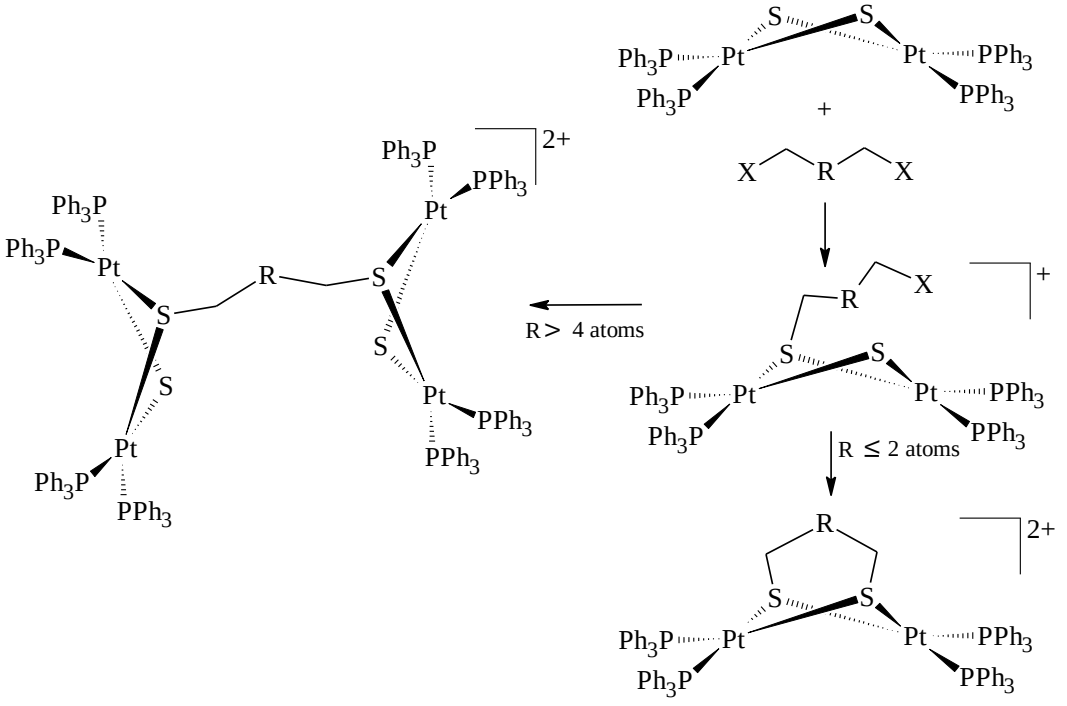

Scheme 4.2 The formation of different bridged dithiolate ($-SCH_2RCH_2S-$) ligands via bridging dialkylation of one or two molecules of $[Pt_2(\mu\text{-}S)_2(PPh_3)_4]$ **1.1**

of one molecule of **1.1** at each end of the α,ω-electrophile[2]. Recently this reaction mode of **1.1** has proved constructive in the synthesis of hexametallic assemblies $[(PPh_3)_4Pt_2(\mu\text{-}S)(\mu\text{-}S\text{-}M\text{-}R\text{-}M\text{-}S\text{-}\mu)(\mu\text{-}S)Pt_2(PPh_3)_4]^{2+}$ (M = Hg) involving two $\{Pt_2(\mu\text{-}S)_2\}$ units spanned by dimercurated arene moiety $[HgC_6Me_4Hg]^{2+}$ [13].

The length and flexibility of the spacer atoms or groups in an α,ω-dialkylating organic electrophile determines the nature of the product of bridging alkylation reaction of **1.1**. However, the alkylation chemistry of **1.1** with multifunctional α,ω-dialkylating agents has not been investigated. Considering that alkylated derivatives of **1.1** can act as cationic metalloligands[19], multifunctional alkylation of **1.1** offers potential advantages not only in the extension of the reactivity of the alkylated cationic derivatives but also in enhancing the coordinating ability of the resulting cationic ligand through the additional organic functionalities. Developing this area of alkylation chemistry of **1.1** will therefore be a productive approach to construct multimetallic frameworks using the coordinating ability of the incorporated functionalised organic moieties.

4.2 Results and Discussion

The following sections outline the study of the reactions of multifunctional α,ω-dialkylating agents with different number spacer atoms and functionalities with **1.1**. Further studies were carried out where unexpected chemistry was observed especially on derivatives expected to lose a proton from the α-carbon atom upon alkylation or on addition of a base. The ESI-MS of the compounds in dilute acidic and basic solution are studied and applied in the isolation and further characterisation of resulting products. NMR, IR, elemental analysis and where possible, X-ray crystallographic results are discussed and compared.

4.2.1 Intramolecular Insertion of Carbon Atom into the $\{Pt_2S_2\}$ core Ring System

α,ω-Dialkylating agents exhibit different alkylation chemistry depending on their functionality. The presence of low acidic hydrogen atoms on bridging carbon atoms gives a stable dithiolate product. On the other hand, presence of very acidic hydrogen atoms results in secondary reactions. In a reported study it was observed that $ClCH_2CH{=}CHCH_2Cl$ reacted with **1.1** to form $[Pt_2(\mu\text{-}SCH_2CH{=}C$

$HCH_2S)(PPh_3)_4]^{2+}$[8]. However, in a preliminary study different chemistry was observed with electrophiles having more acidic hydrogen atoms on the alkylating carbon[4] e.g. $ClCH_2C(O)CH_2Cl$ **4.1a** and $ClCH_2C(=NNH\text{-}Ar)CH_2Cl$ (Ar = 2,4-dinitrophenyl). The hydrogen atoms on the alkylating carbon atoms are thus very reactive due to the electron-withdrawing effect of the carbonyl (>C=O) in **4.1a** and the S^+ group in the alkylated complex. In the case of the 2,4-dinitrophenyl hydrazone the electron-withdrawing effect of the azomethine (>C=N) is further enhanced by the presence of two NO_2 groups attached to the phenyl ring. One of the hydrogen atoms on the alkylating carbon can therefore be easily lost leading to other secondary reactions. A reported preliminary study on the reaction of $ClCH_2C(=NNHAr)CH_2Cl$ with **1.1** led to isolation of the first five-membered ring product $[Pt_2(\mu\text{-}SCH_2C(=NNHAr)CHS(PPh_3)_3Cl]$[4] which was only characterised by an X-ray crystal structure analysis. The proposed mechanism of the ring opening reaction[4] suggested the deprotonation of one of the sulphide ($-CH_2$-S-) groups upon dialkylation, generating a nucleophile (carbanion) which led to intramolecular rearrangement and subsequent displacement of a PPh_3 group by Cl^- and opening of the normally robust four-membered $\{Pt_2(\mu\text{-}S)_2\}$ ring to a five-membered ring. However, it is not known if other electrophiles of similar structure and different functionality exhibit similar non-standard alkylation chemistry. The loss of a $-CH_2$ proton was also earlier observed in the reaction of $ClCH_2C(O)CH_2Cl$ with **1.1**[4]. Upon formation of bridged dialkylated derivative $[Pt_2(\mu\text{-}SCH_2C(O)CH_2S)(PPh_3)_4]^{2+}$, a proton ($H^+$) is lost from one of the (CH_2-S-) carbon atoms to form the monocation $[Pt_2(\mu\text{-}SCH_2C(O)CHS)(PPh_3)_4]^+$. The reaction $[M]^{2+} \rightarrow [M\text{-}H]^+$ leading to the formation of $[Pt_2(\mu\text{-}SCH_2C(O)CHS)(PPh_3)_4]^+$ was only observed in the ESI-MS and the product has never been isolated for further characterisation to ascertain the structure. Bridged dialkylated dicationic derivatives that have acidic hydrogen atoms undergo incomplete spontaneous loss of a proton to form $[M - H]^+$. Complete inter-conversion to either dialkylated $[M - H]^+$ or $[M]^{2+}$ dialkylated derivative is achieved by the addition of dilute base or acid respectively[4]. This is illustrated by the interconversion of the dialkylated $[M]^{2+}$ ion and dialkylated $[M- H]^+$ in acidic and basic media shown in Scheme 4.3. This initial observation provided the incentive for further study of the protonation/deprotonation chemistry of this system.

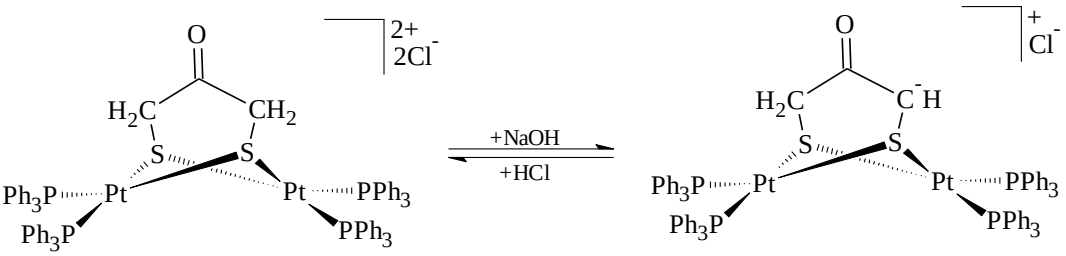

(colourless) (yellow)

Scheme 4.3 Interconversion of the dialkylated $[M]^{2+}$ ion and dialkylated $[M]^{+}$ in acidic and basic media

The reaction of $ClCH_2C(O)CH_2Cl$ **4.1a** with **1.1** in methanol indicated the formation of three identifiable products after 1 hour. The ESI-MS of the reaction mixture (Figure 4.1(**A**)) showed three product peaks, *m*/*z* 778, 30% assignable to the dialkylated dication M^{2+} ion $[Pt_4(\mu\text{-}SCH_2C(O)CH_2S)(PPh_3)_4]^{2+}$. A methanol adduct of the $[M]^{2+}$ ion proposed to be $[Pt_2(\mu\text{-}SCH_2COH(OCH_3)CH_2S)(PPh_3)_4]^{2+}$ **4.1c** at *m*/*z* 796, 10% was also observed. The structure of the adduct that was earlier proposed[4] is shown below. A peak for the dialkylated monocation $[M\text{-}H]^{+}$ ion at *m*/*z* 1568, 100 % formed from the spontaneous deprotonation of one of the methylene ($-CH_2-$) groups was also observed. These observations were in agreement with the previous ESI-MS study[4].

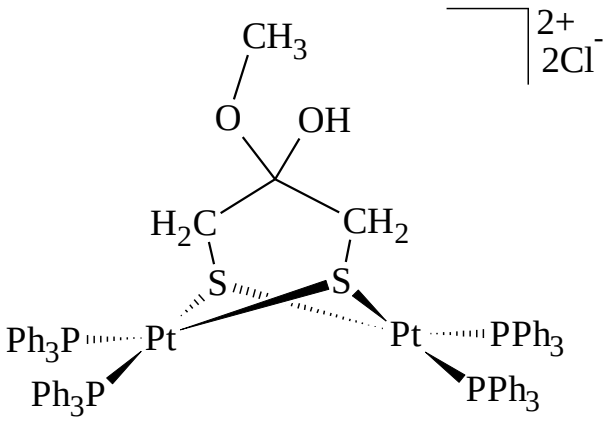

4.1c

After an additional 30 minutes of stirring the peak for the M^{2+} ion became 100% intensity with a slight increase of 3% in the peak attributed to the methanol adduct. The $[M\text{-}H]^{+}$ ion reduced to about 60 % relative intensity with the emergence of a small peak attributable to the chloride derivative $[Pt_2(\mu\text{-}SCH_2C$

$(O)CH_2S)(PPh_3)_3Cl]^+$ at *m*/*z* 1427. The peak attributable to the chloride derivative was not observed when the reaction was repeated. This indicates that its formation may not be a stable secondary reaction. The reaction did not go to completion to form either the $[M]^{2+}$ or $[M\text{-}H]^+$ after further stirring for 90 minutes but maintained the same stable equilibrium position between the $[M]^{2+}$ and $[M\text{-}H]^+$ ions as shown in Figure 4.1(**B**).

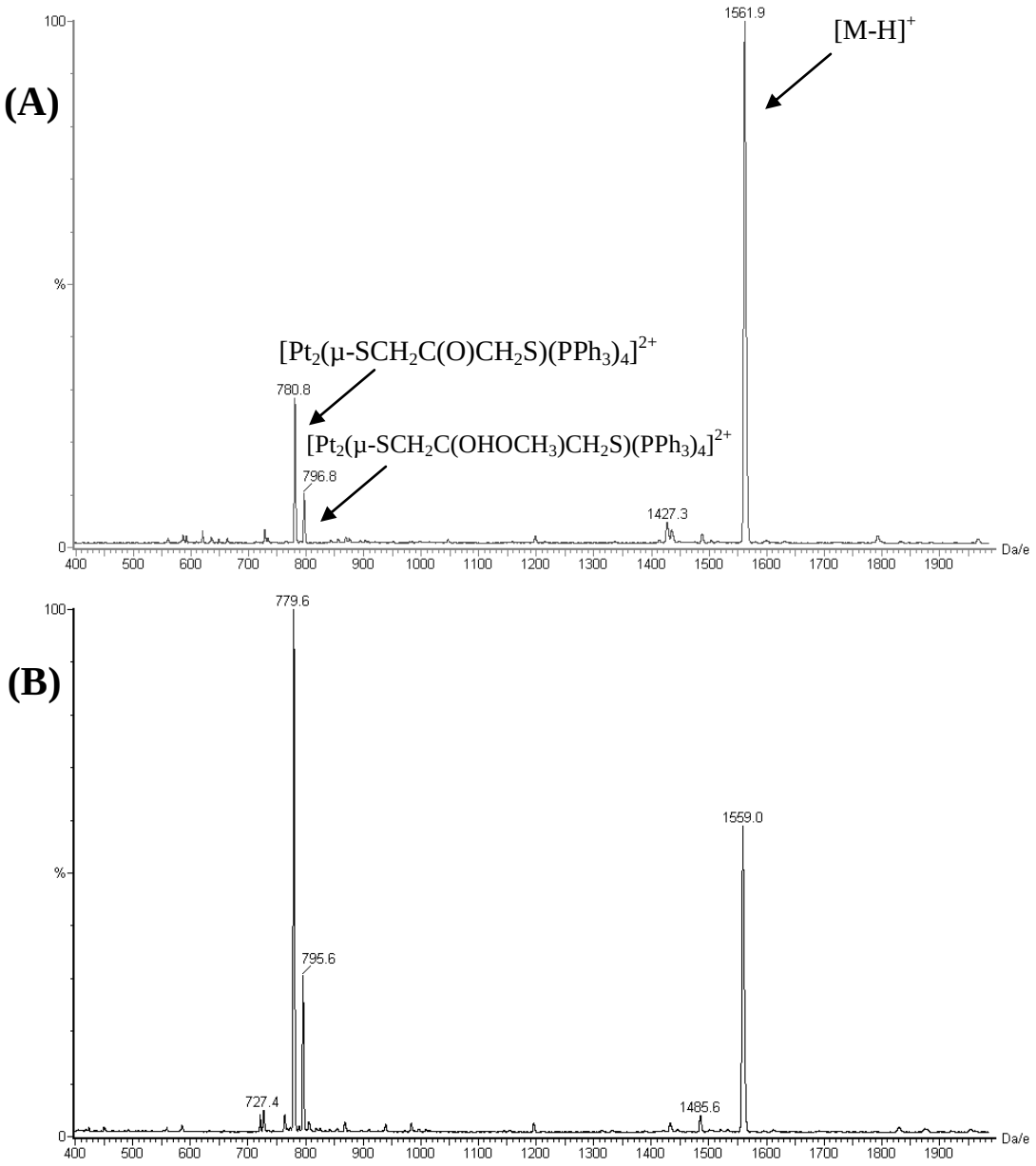

Figure 4.1 ESI-MS of the reaction mixture of $ClCH_2C(O)CH_2Cl$ **4.1a** and **1.1** (**A**) after stirring for 1 hour and (**B**) after stirring for 90 minutes in MeOH.

A shift in the equilibrium position on addition of dilute aqueous HCl favouring the complete formation of the M^{2+} ion was reportedly observed and

employed to successfully isolate the dialkylated derivative as a BPh_4^- salt[4]. However, the corresponding dialkylated $[M\text{-}H]^+$ ion $[Pt_2(\mu\text{-}SCH_2C(O)CHS)(PPh_3)_4]^+$ (which could be either S, S or S, C bonded) has never been isolated, thus the actual structure is not known. Controlled addition of a basic solution to the reaction mixture was employed to shift the equilibrium to the opposite direction i.e. favouring the formation of the deprotonated derivative. Initial addition of 0.006 mL (1 mol equiv.) of pyridine had no effect on the intensity of the ESI-MS peak of $[M - H]^+$ and thus did not effect any conversion of the $[M]^{2+}$ ion to $[M - H]^+$. The addition of 0.5 mL of 0.1 mol L^{-1} NaOH solution to reaction mixture containing 0.067 mmol $[Pt_2(\mu\text{-}S)_2(PPh_3)_4]$ in 25 mL methanol, effected substantial reduction in the intensity of peak of the M^{2+} ion and methanol adduct $[Pt_2(\mu\text{-}SCH_2C(OHOCH_3)CH_2S)(PPh_3)_4]^{2+}$. Complete conversion of $[M]^{2+}$ (Colourless) to $[M - H]^+$ (yellow) was achieved with further addition 0.5 mL of 0.1 mol L^{-1} NaOH. No trace of the M^{2+} ion and methanol adduct peaks was observed within three minutes as indicated in the ESI-mass spectrum shown Figure 4.2.

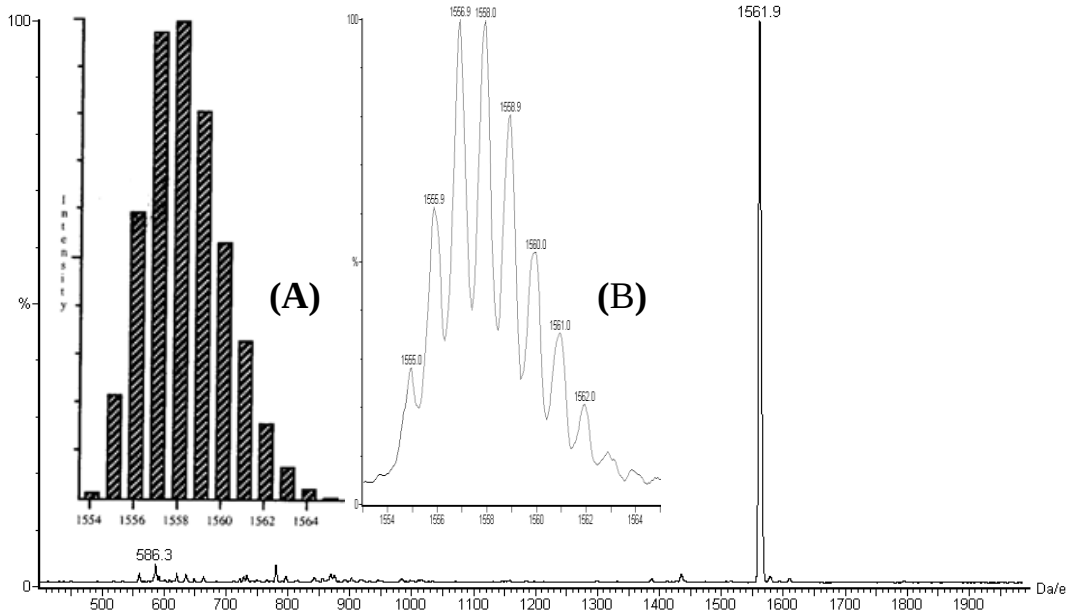

Figure 4.2 ESI-MS of the reaction mixture of $ClCH_2C(O)CH_2Cl$ **4.1a** and **1.1** after the addition of 1 mL 0.1 mol L^{-1} NaOH solution. The inset shows the theoretical (**A**) and practical (**B**) isotope patterns of $[Pt_2(\mu\text{-}SCH_2C(O)CHS)(PPh_3)_4]^+$.

The product was isolated as the BPh_4^- salt by the addition of excess $NaBPh_4$. The ESI-MS of the isolated product gave only two peaks, a major 100% $[M – H]^+$ ion peak for the deprotonated species and a minor 10% $[M]^{2+}$ ion of the

protonated dialkylated derivative. The minor conversion to the $[M]^{2+}$ may have been because the product was dissolved in methanol (ESI-MS solvent) which is a protic solvent. Further purification of the isolated product by vapour diffusion of diethyl ether into a CH_2Cl_2 solution did not yield any crystals but when isolated as the PF_6^- salt gave orange block crystals suitable for X-ray analysis. However, the crystal structure discussed in Section 4.2.1.1 revealed an S, C bonded compound which coincidentally has exactly the same *m*/*z* 1569 value and isotope pattern as the expected deprotonated S, S bonded four membered ring structure. The X-ray structural analysis revealed the opening of the normally robust four-membered ring structure of $\{Pt_2S_2\}$ to a stable five-membered ring and formation of a platinum-carbon bond incorporated in the ring system.

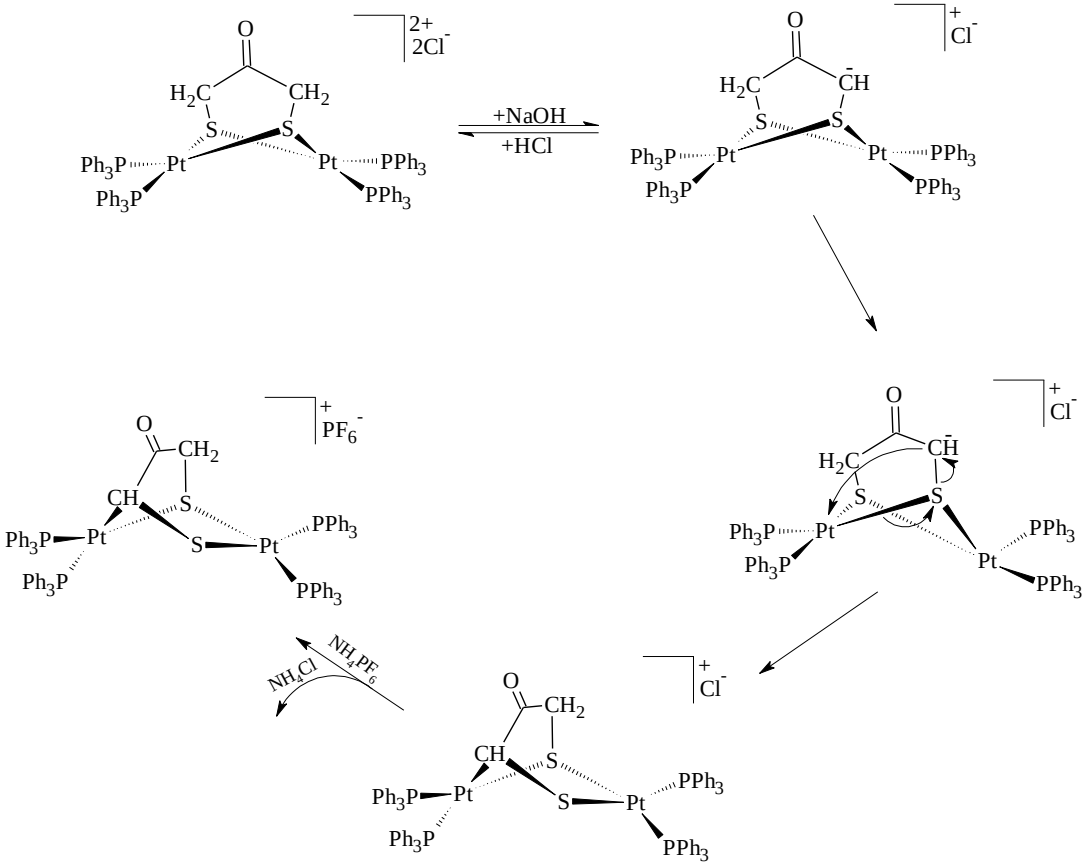

Scheme 4.4 Plausible reaction mechanism for the opening of the $\{Pt_2(\mu\text{-}S)_2\}$ ring after formation of the deprotonated species $[Pt_2(\mu\text{-}SCH_2C(O)CHS)(PPh_3)_4]^+$ **4.1b**. Adopted and modified from Ref 4

A plausible reaction mechanism of the ring opening reaction is shown in Scheme 4.4. It involves the formation of a carbanion after deprotonation of one of the two -CH_2S groups. This is followed by the bonding of the methyne carbon to

one of the platinum atoms, followed by the breaking of the Pt-S bond, leading to opening of the four membered $\{Pt_2(\mu\text{-}S)_2\}$ to a stable five-membered ring containing C-Pt bond.

The displacement of PPh_3 in alkylated derivatives of **1.1** by the resulting chloride ion (Cl^-) is not a common occurrence compared to bromide (Br^-) and iodide (I^-) ions[3, 7]. This is because Cl^- is less nucleophilic than Br^- and I^-. However, Cl^- was observed to displace PPh_3 in the 2,4-dinitrophenylhydrazone derivative containing five-membered $\{Pt_2(\mu\text{-}S)_2\}$ ring[4]. This is probably due to the very high *trans*- influence of carbon in addition to the strong electron withdrawing groups in the incorporated hydrazone. Deprotonation of one of the alkylating methylene carbons in the incorporated electrophile, subsequent displacement of a PPh_3 group by the resulting chloride ion (Cl^-) and the subsequent expansion of the four-membered $\{Pt_2(\mu\text{-}S)_2\}$ ring to a five-membered ring derivative $[Pt_2(\mu\text{-}SCH_2C(=NNHAr)CHS)(PPh_3)_3Cl]$ (Ar = 2,4-dinitrophenyl) has been reported[4].

The displacement of a PPh_3 group was not observed in the present studies involving $ClCH_2C(NNHC(O)NH_2)CH_2Cl$ **4.2a** (section 4.3) and $ClCH_2C(O)CH_2Cl$ **4.1a**. The differences in the reactivities the alkylating agents with **1.1** are obviously due to the relative differences in the strength of inductive effect of the different groups (>C=N and >C=O) in the ligands. The electronegativity of nitrogen and oxygen are 3.04 and 3.44 respectively. It is therefore expected that C=O in **4.1b·PF$_6$** will have a stronger electron withdrawing effect than C=N group on the $-CH_2-$ group. But, the presence of the 2,4-dinitrophenyl group is expected to augment the electron withdrawing ability of the azomethine (>C=N) group in $[Pt_2(\mu\text{-}SCH_2C(=NNHAr)CH_2S)(PPh_3)_4]^{2+}$ more than $-NHC(O)NH_2$ in **4.2b** and the carbonyl (C=O) group in **4.1b·PF$_6$**. NO_2 group is known to have high inductive (*-I*) effect and a small electron-withdrawing resonance effect[20]. Therefore, the combined high inductive effect of the two NO_2 (*ortho*- and *para*-) groups in addition to the small *-I* resonance effect is expected to increase the net positive charge on the azomethine nitrogen and subsequently on the CH_2-S groups as shown in Scheme 4.5 below. The increase in the positive charge subsequently increased the spontaneity of the proton loss from one of the alkylating carbons ($-CH_2-$). This is followed by the ring opening reaction, the formation of Pt-C bond and the displacement of a PPh_3 ligand by Cl^-.

The electronic effect of NO_2 groups in addition to the structure of the 2,4-dinitrophenyl moiety on $\{Pt_2(\mu\text{-}S)_2\}$ and the higher *trans*- influence of carbon[21-24] than the thiolate -SR (R = 2,4-dinitrophenyl hydrazone) is expected to weaken the corresponding *trans*-Pt-P bonds making the platinum atom more susceptible to attack by the less nucleophilic Cl^- ion. In the case of **4.1b** the displacement of PPh_3 did not occur. The greater stability of **4.1b** is probably due to a lesser bulky attached group, *trans*- influence and electron-withdrawing effect upon insertion of one of the methyne carbon atom in the $\{Pt_2(\mu\text{-}S)_2\}$ ring than the 2,4-dinitro phenylhydrazone analogue.

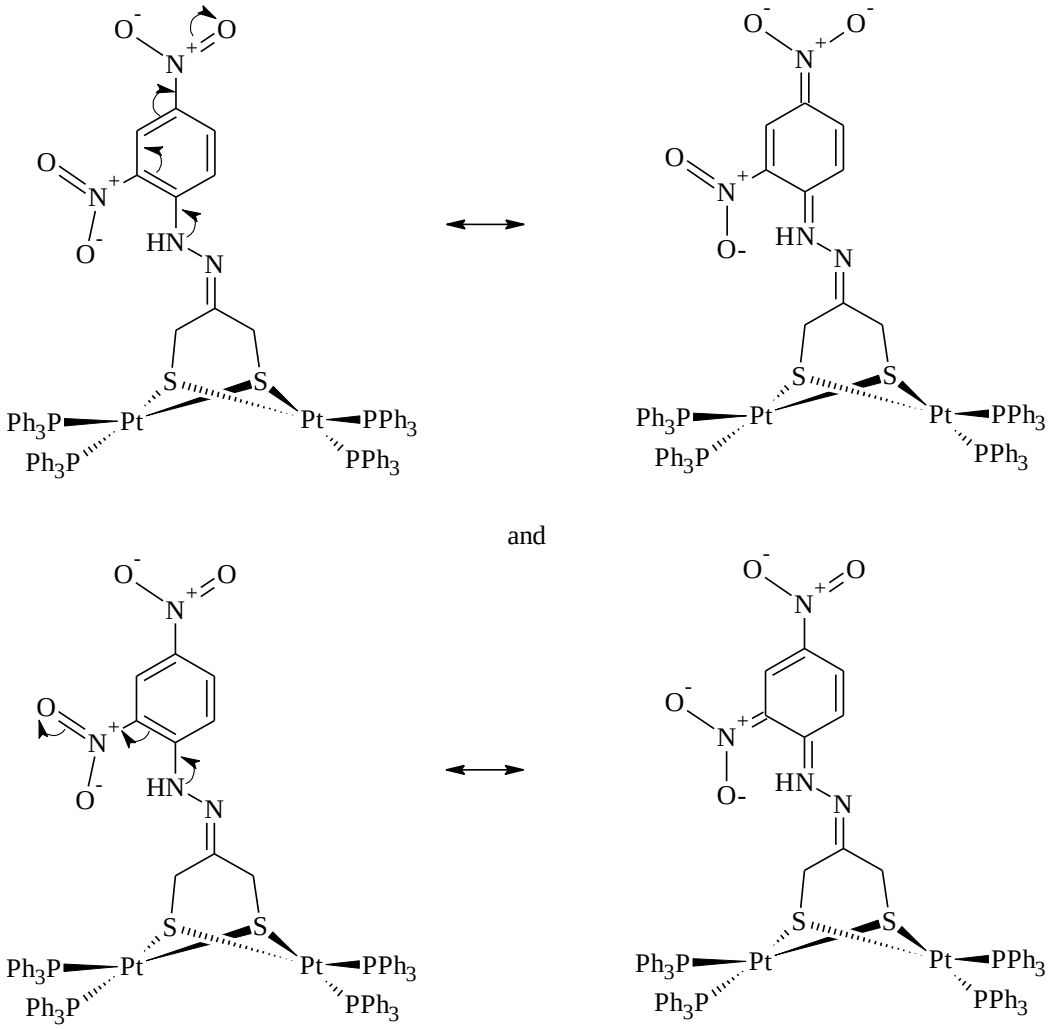

Scheme 4.5 Combined electron withdrawing effect of the *para*- and *ortho*- NO_2 groups

4.2.1.1 X-ray Crystal Structure of 4.1b·PF_6

The X-ray crystal structure and the atom numbering scheme of $[Pt_2\{\mu\text{-}SCH_2C(O)CHS\}(PPh_3)_4](PF_6)$ **4.1b·PF_6** is as shown in Figure 4.3 and bond lengths and angles in Table 4.1. The ESI-MS and NMR data did not give clear structural information of **4.1b·PF_6**. It is also not clear if the compound was isolated as a stable carbanion or rearranged structure, hence the crystal structure analysis which confirmed the structure.

Table 4.1 Selected bond lengths and atomic distances (Å) and bond angles (°) for $[Pt_2\{\mu\text{-}SCH_2C(O)CHS\}(PPh_3)_4](PF_6)$ **4.1b·PF_6** (Estimated standard deviations are in brackets).

Bond lengths and atomic distances (Å)					
Pt(2)-C(1)	2.090(3)	Pt(2)-S(1)	2.3684(16)	Pt(1)-S(2)	2.3323(13)
Pt(2)-P(4)	2.2902(16)	Pt(1)-P(1)	2.3034(13)	Pt(1)-S(1)	2.3589(14)
Pt(2)-P(3)	2.3510(13)	Pt(1)-P(2)	2.3051(15)	S(1)-C(2)	1.823(3)
O(1)-C(3)	1.207(4)	C(2)-C(3)	1.511(4)	C(1)-C(3)	1.483(4)
S(2)-C(1)	1.823(3)				

Bond angles (°)			
C(1)-Pt(2)-P(4)	90.64(8)	P(4)-Pt(2)-S(1)	168.96(3)
C(1)-Pt(2)-P(3)	170.41(8)	P(3)-Pt(2)-S(1)	91.80(3)
P(4)-Pt(2)-P(3)	98.58(3)	P(1)-Pt(1)-P(2)	99.23(4)
C(1)-Pt(2)-S(1)	79.20(8)	P(1)-Pt(1)-S(2)	89.54(5)
P(2)-Pt(1)-S(2)	159.39(3)	P(1)-Pt(1)-S(1)	167.80(3)
P(2)-Pt(1)-S(1)	87.44(4)	S(2)-Pt(1)-S(1)	87.57(5)
C(2)-S(1)-Pt(1)	101.28(11)	C(1)-S(2)-Pt(1)	107.51(10)
C(2)-S(1)-Pt(2)	98.95(10)	C(3)-C(1)-S(2)	113.4(2)
Pt(1)-S(1)-Pt(2)	97.58(3)	C(3)-C(1)-Pt(2)	107.12(19)
S(2)-C(1)-Pt(2)	105.40(14)	C(3)-C(2)-S(1)	109.2(2)
O(1)-C(3)-C(1)	123.0(3)	O(1)-C(3)-C(2)	120.3(3)
C(1)-C(3)-C(2)	116.7(2)		

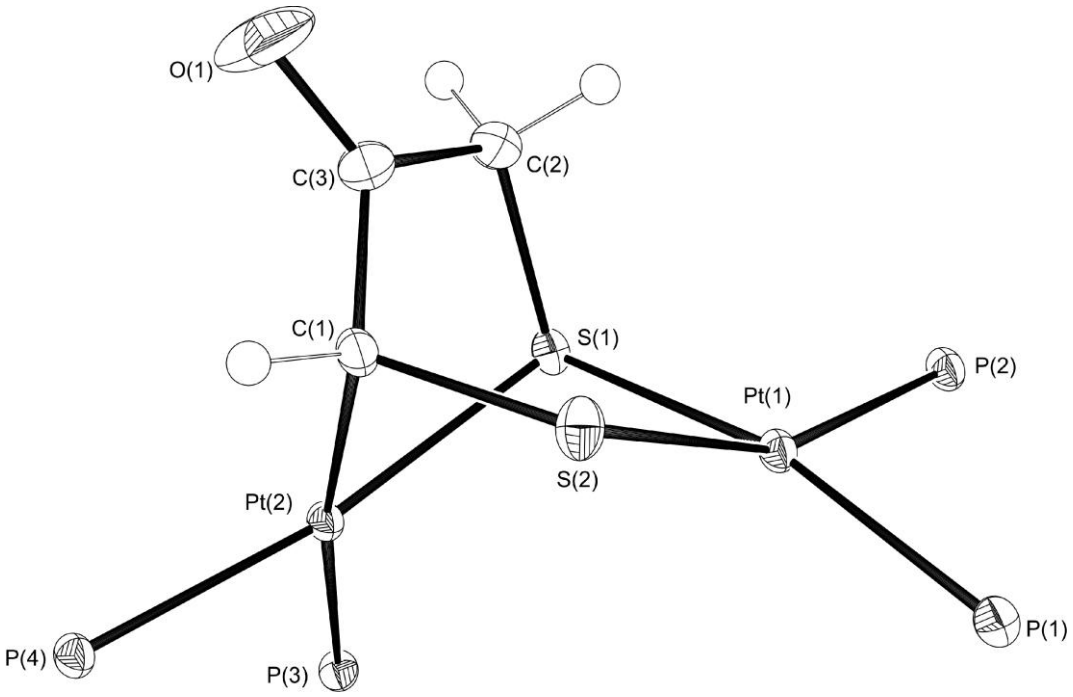

Figure 4.3 Molecular structure of $[Pt_2\{\mu\text{-}SCH_2C(O)CHS\}(PPh_3)_4]$ (PF_6) **4.1b·PF_6** showing the atom numbering scheme with thermal ellipsoids at the 50% probability level. The PF_6^- ion and the phenyl ring of PPh_3 were omitted for clarity

The structure reveals an interesting disfigured structure of the usual "butterfly structure" shape of alkylated derivatives of $[Pt_2(\mu\text{-}S)_2(PPh_3)_4]$. The structure also confirmed the deprotonation of one of the alkylating carbon atoms which has lead to an intramolecular rearrangement and opening of the $\{Pt_2(\mu\text{-}S)_2\}$ ring structure to a five-membered ring allowing the formation of a C-Pt bond in the ring system. The *trans*-influence of a ligand is known to predominate over other factors such as crystal packing and *cis*-influence in predetermining the structural conformation of a compound[25, 26]. Carbon has a stronger *trans*-influence ligand than the thiolate SR[23] and the bond distances showed that the *trans*-influence follow the order C > S > SR. Consequently, the Pt-P bond *trans*- to the C-Pt bond, Pt(2)-P(3) 2.3510(13) Å is the longest P-Pt bond. Thus, the corresponding *cis*- Pt(2)-P(4) 2.2902(16) Å is the shortest Pt-P bond in **4.1b·PF_6**. The Pt(1)-P(2) 2.3051(15) Å is longer than the Pt(1)-P(1) 2.3034(13) Å bond due to the greater *trans* influence of S^{2-} than the thiolate SR. In addition, the S-Pt bond distances are different because of the rearrangement caused by the insertion of the

carbon ligand into the ring system. The S(1)-Pt(2) 2.3684(16) Å bond is the longest followed by Pt(1)-S(1) 2.3589(14) Å and Pt(1)-S(2), 2.3323(13) Å.

4.2.1.2 $^{31}P\{H\}$ NMR of $[Pt_2(\mu\text{-}SCH_2C(O)CHS)(PPh_3)_4]$ 4.1b·PF_6

The four phosphorus atoms in **4.1b·PF_6** all have different electronic environments due to the formation of the Pt-C-S bonds in the normally symmetrical $\{Pt_2(\mu\text{-}S)_2\}$ ring system. The ^{31}P NMR spectrum (Figure 4.4) shows the schematic numbering of the four phosphorus atoms.

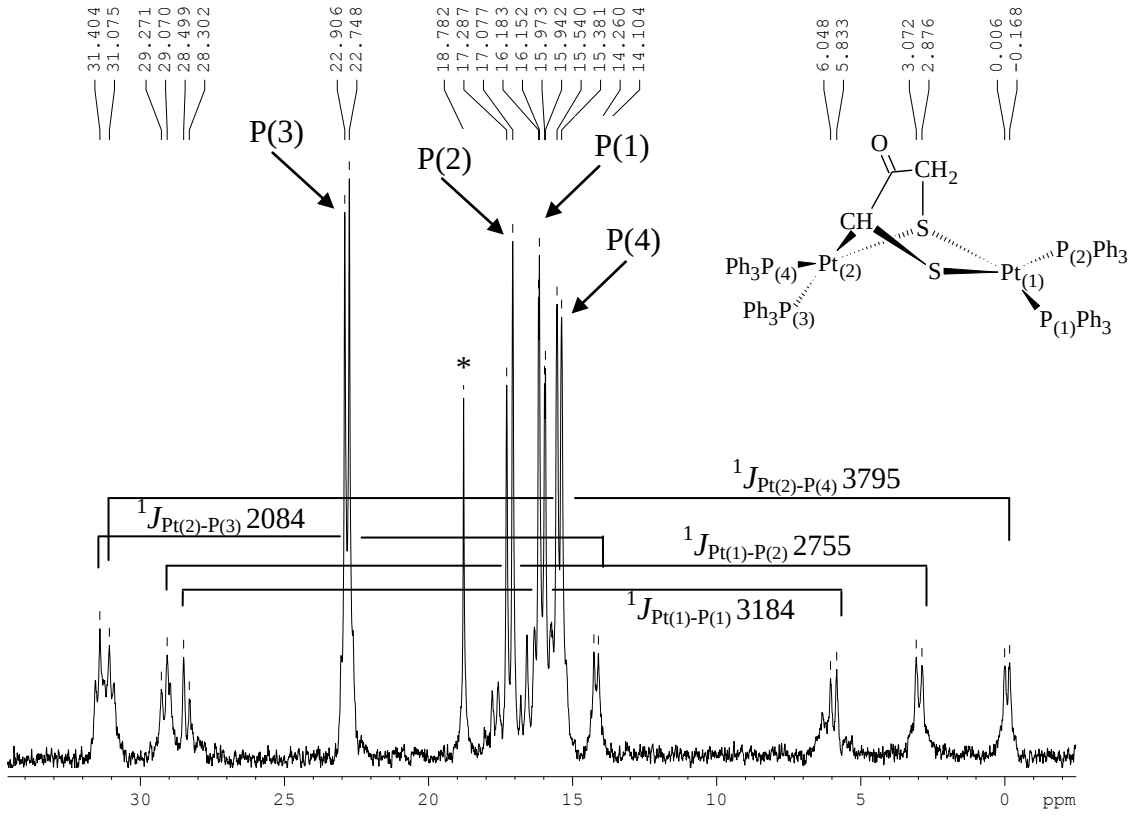

Figure 4.4 $^{31}P\{H\}$ NMR spectrum of **4.1b·PF_6** showing the four different phosphorus signals. * is an unidentified signal.

Four different phosphorus signals at δ_p 15.5 ppm, 16.2 ppm, 17.1 ppm, and 22.8 ppm with four corresponding satellite signals due to $^1J_{Pt\text{-}P}$ coupling, 3795 Hz, 3184 Hz, 2755 Hz and 2084 Hz respectively were observed. The phosphorus atoms were assigned based on the expected coupling constants related to the X-ray structure bond lengths. Alkyl group bonded through carbon has a very high *trans*-influence[21-24] and this is evident from the X-ray structure analysis of **4.1b·PF_6**. The longest Pt-P bond, Pt(2)-P(3) [2.3510(13) Å] is *trans* to the Pt-C

bond thus is expected to have the smallest $^1J_{Pt(2)\text{-}P(3)}$ coupling, 2084 Hz. Consequently the associated Pt(2)-P(4) bond [2.2902(16) Å] is the shortest and accordingly is assigned to the phosphine with the largest $^1J_{Pt(2)\text{-}P(4)}$, coupling, 3795 Hz. The bond lengths of Pt(1)-P(2) and Pt(1)-P(1) are 2.3051(15) Å and 2.3034(13) Å respectively, and gave the $^1J_{Pt(1)\text{-}P(2)}$ couplings of 2755 Hz and $^1J_{Pt(1)\text{-}P(1)}$, 3184 Hz. The $^2J_{(P\text{-}P)}$ coupling between P(3) and P(4) is *ca* 19 Hz and P(1) and P(2) *ca* 25.7 Hz.

4.2.1.3 IR Characterisation

There is a variation between the IR absorption of carbonyl group >C=O in the α,ω-electrophile $ClCH_2C(O)CH_2Cl$ **4.1a (**1745 cm^{-1}), the dialkylated dication $[Pt_2(\mu\text{-}SCH_2C(O)CH_2S(PPh_3)_4](PF_6)_2$, **4.1c·(PF$_6$)$_2$** (1697 cm^{-1}) and the dialkylated monocation $[Pt_2(\mu\text{-}SCH_2C(O)CHS(PPh_3)_4](PF_6)$, **4.1b·PF$_6$** (1676 cm^{-1}). The IR absorption values indicates that there is substantial reduction in the vibration frequency of the carbonyl (>C=O) bond after dialkylation ($[M]^{+2}$] and further upon deprotonation and insertion of carbon atom into the $\{Pt_2(\mu\text{-}S)_2\}$ ring.

4.3 Intramolecular Bridging Alkylation

Hydrazine-based compounds and their derivatives find extensive industrial applications in medicine as drugs e.g. isoniazide[27] and hydralazine[28], or in agriculture as herbicides or fungicides. Derivatives like semicarbazones have been widely studied due to their good ligating properties and structural features[29], biochemical properties[30] and applications as synthetic precursors[30, 31]. Carbonyl compounds are well known templates for the synthesis of many compounds including hydrazones. The reactivity of the bridging multifunctional α,ω-dialkylating semicarbazone and amide electrophiles **4.2a** and **4.3a** towards **1.1** were also investigated by ESI-MS.

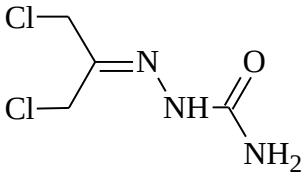

4.2a

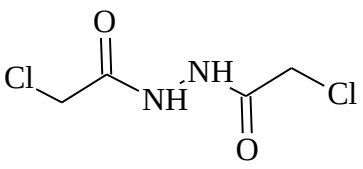

4.3a

The reaction of α,ω-dialkylating semicarbazone **4.2a** with **1.1** occurred in a fast, two step alkylation. The orange suspension of **1.1** solubilised to yield a colourless solution within 5 minutes of stirring in MeOH (Scheme 4.6). The short reaction time is because **4.2a** has only three spacer atoms with an high electronegative atom on the β-carbon atom and therefore is a strong bridging α,ω-dialkylating agent.

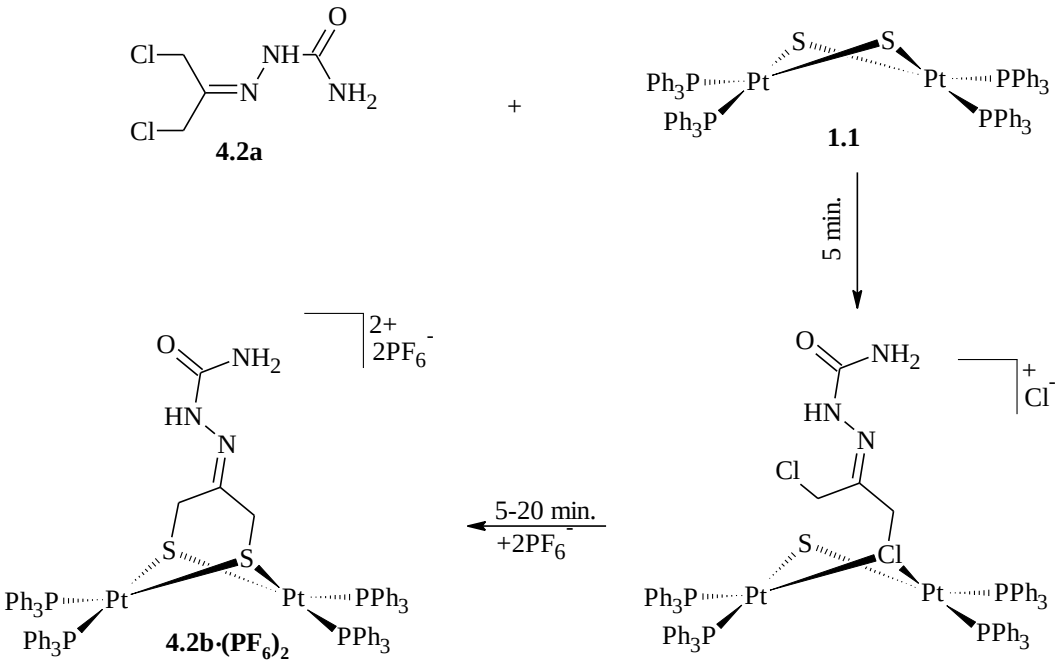

Scheme 4.6 Fast two stage reaction of **4.2a** and **1.1** to give **4.2b·$(PF_6)_2$**

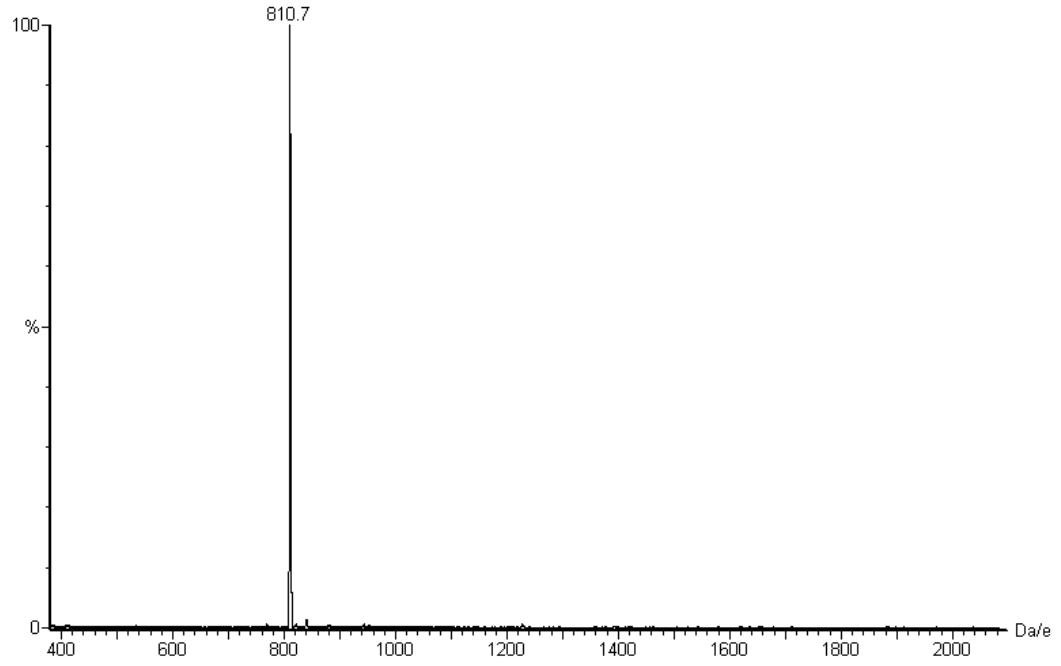

Figure 4.5 The ESI-MS of the reaction mixture of **4.2a** and **1.1** showing a single peak for **4.2b** at m/z 810.7.

After 20 minutes, ESI-MS (Figure 4.5) of the reaction solution indicated a single peak attributable to only the dialkylated dicationic species at *m/z* 810.7 $[Pt_2\{SCH_2C(NNHC(O)NH_2)CH_2S\}(PPh_3)_4]^{2+}$. Recrystallisation of the product, isolated as a PF_6^- salt did not give any suitable crystals for X-ray analysis but the product isolated as the BPh_4^- salt $[Pt_2\{SCH_2C(NNHC(O)NH_2)CH_2S\}(PPh_3)_4](BPh_4)_2$ **4.2b·(BPh$_4$)$_2$** gave suitable crystals for X-ray analysis discussed in Section 4.3.1

Spontaneous deprotonation of one of the CH_2 groups of **[**$Pt_2\{SCH_2C(NNHC(O)NH_2)CH_2S\}(PPh_3)_4]^{2+}$ to give the corresponding $[M\text{-}H]^+$ ion was anticipated, but not observed in the ESI-MS of the reaction mixture of **4.2a** and **1.1**. This is most probably because the (>C=N) group has lower electron withdrawing effect than the (C=O) group. However, the deprotonation of $[Pt_2\{SCH_2C(NNHC(O)NH_2)CH_2S\}(PPh_3)_4]^{2+}$ in basic medium was also observed. It is noteworthy of the possibility that the deprotonation may have been from other groups (NH or NH_2) in the molecule. On addition of 1 mL of 0.1 $molL^{-1}$ NaOH solution to a reaction mixture of 100 mg of **1.1** and 15 mg (1.2 mol equivalent) of **4.2a** in 25 mL methanol after the formation of $[M]^{2+}$ ion, the colour of the reaction mixture immediately changed to bright clear yellow, the commonly observed colour of a monoalkylated derivative. The ESI-MS of the mixture indicated a substantial but incomplete conversion to the $[M - H]^+$ ion at *m/z* 1616 with 100% intensity. Other smaller unidentified peaks due to secondary reactions were also observed.

4.3.1 X-ray Crystal Structure of 4.2b·(BPh$_4$)$_2$

The X-ray crystal structure and the atom numbering scheme of $[Pt_2\{\mu\text{-}SCH_2C(=NNHC(O)NH_2)NH_2)CH_2S\}(PPh_3)_4](BPh_4)_2$ **4.2b·(BPh$_4$)$_2$** is shown in Figure 4.6. The selected bond lengths, angles and atomic distances are shown in Table 4.2. The crystal structure determination was carried out to confirm the structure of the complex and to provide comparison with other intramolecular bridged derivatives previously reported.

The X-ray structure analyses reveals an asymmetric attachment of the semicarbazone moiety to the sulfide centres due to the spatial conformation of (>C=N) group. The ^1H and ^{13}C NMR of semicarbazone $ClCH_2C(NNHC(O)$-

$NH_2)CH_2Cl$ **4.2a** had shown different signals for the two -CH_2 carbon and hydrogen atoms. Electron repulsion due to the lone pair of electron on the azomethine nitrogen (>C=N) in the semicarbazone and the adjacent N-C bond caused the semicarbazide moiety of the electrophile to bend to one side. This difference is maintained upon its incorporation onto the $\{Pt_2(\mu\text{-}S)_2\}$ core. Consequently, the conformation is reflected in the X-ray structure of **4.2b·$(BPh_4)_2$**.

Table 4.2 Selected bond lengths and atomic distances (Å) and bond angles (°) for $[Pt_2\{\mu\text{-}SCH_2C(=NNHC(O)NH_2)CH_2S\}(PPh_3)_4](BPh_4)_2$ **4.2b·$(BPh_4)_2$** (Estimated standard deviations are in brackets).

Bond lengths and atomic distances (Å)					
Pt(1)-P(2)	2.275(19)	Pt(2)-S(1)	2.366(18)	C(3)-N(1)	1.291(10)
Pt(1)-P(1)	2.294(1)	Pt(2)-S(2)	2.343(19)	N(1)-N(2)	1.375(9)
Pt(2)-P(3)	2.302(2)	S(2)-C(1)	1.835(8)	N(2)-C(4)	1.385(12)
Pt(2)-P(4)	2.287(19)	S(1)-C(2)	1.824(8)	C(4)-O(1)	1.371(12)
Pt(1)-S(1)	2.353(18)	C(1)-C(3)	1.510(11)	C(4)-N(3)	1.209(11)
Pt(1)-S(2)	2.376(19)	C(2)-C(3)	1.491(11)		
Pt(1)---Pt(2)	3.363	S(1)---S(2)	3.027		

Bond angles (°)			
S(2)-Pt(1)-S(1)	79.58(6)	S(1)-Pt(1)-P(2)	94.00(7)
S(2)-Pt(2)-S(1)	80.00(7)	S(1)-Pt(2)-P(3)	86.62(7)
S(1)-C(2)-C(3)	114.12(5)	S(2)-Pt(2)-P(4)	94.65(7)
S(2)-C(1)-C(3)	117.91(6)	Pt(1)-S(1)-Pt(2)	90.91(6)
C(2)-C(3)-N(1)	124.53(7)	Pt(2)-S(2)-Pt(1)	90.90(6)
C(1)-C(3)-N(1)	114.86 (7)	N(2)-C(4)-O(1)	115.90(9)
S(2)-Pt(1)-P(1)	88.87(7)	N(3)-C(4)-O(1)	125.2(10)

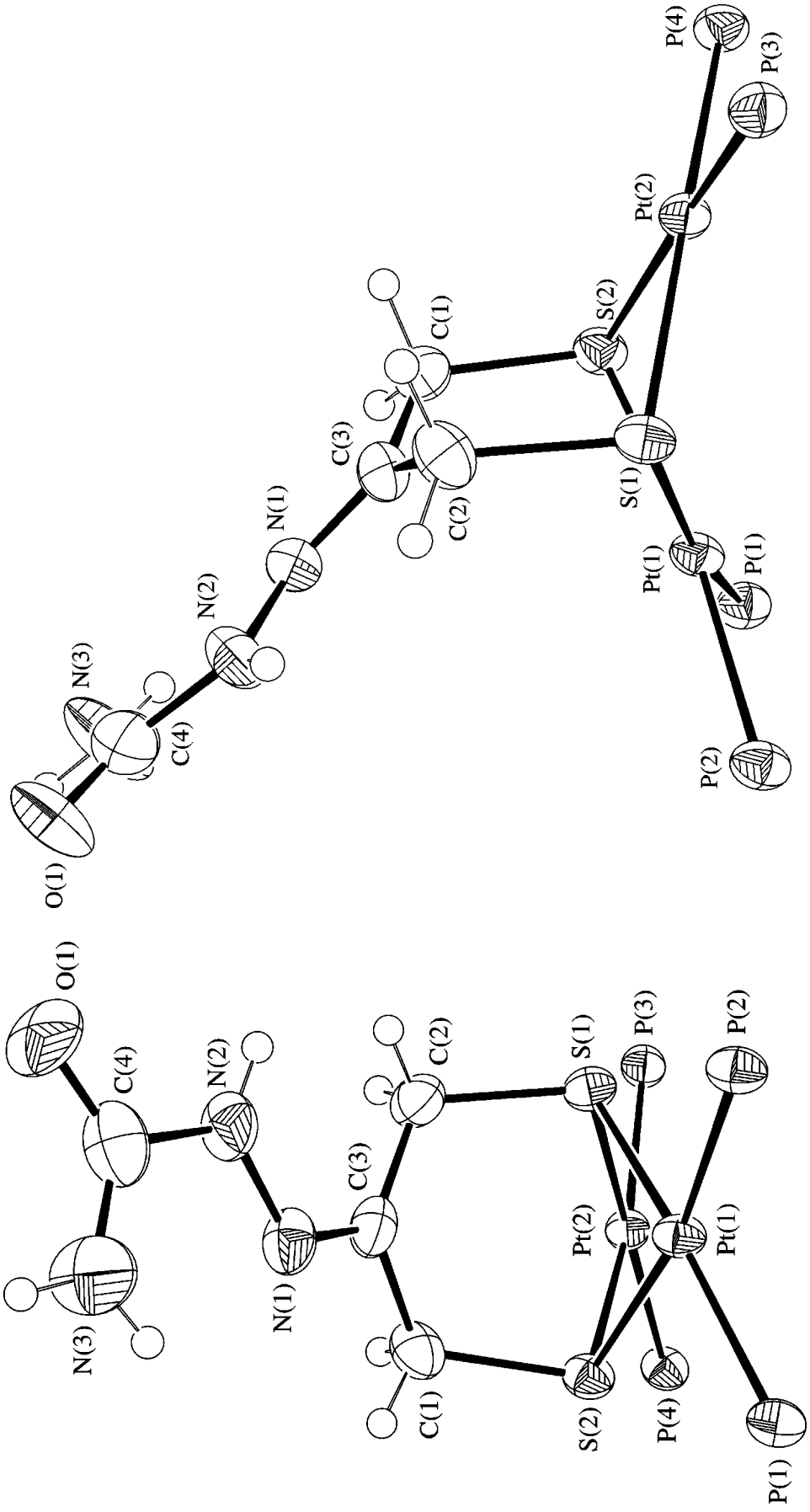

Figure 4.6 Two views of the molecular structure of the core $[Pt_2\{\mu\text{-}SCH_2C(NNHC(O)NH_2)CH_2S\text{-}\mu\}(PPh_3)_3](BPh_4)_2$ **4.2b·(BPh$_4$)$_2$** showing the atom numbering scheme with thermal ellipsoids at the 50% probability level.

The bond distances between C(1)-C(3) 1.510 (11) Å and C(2)-C(3) 1.491 (11) Å are slightly different. The semicarbazone group $=NNHC(O)NH_2$ is directed to one side of the vertical axis of the S(1) C(3) S(2) plane. The S(1) C(1) S(2) and S(1) C(2) S(2) planes make angles of 47º and 45.9º respectively to the C(1) C(3) C(2) plane. The crystal structure of **4.2b·(BPh$_4$)$_2$** also confirmed the expected hinge structure of the $\{Pt_2S_2\}$ core with the two PtSS planes making a dihedral angle (θ) of 136.5º. It is known that the backbone $>C=NNHC(O)NH_2$ of unsubstituted semicarbazones in solid state is usually almost planar, with the oxygen atom *trans* to the azomethine N[32]. However, several other factors which may cause a distortion of the expected planarity include crystal packing and electronic factors. In **4.2b·(BPh$_4$)$_2$** the oxygen atom and the azomethine nitrogen are *cis* to each other. Intramolecular repulsion forces may have contributed to the distortion of the usual plane conformation of semicarbazone. The semicarbazone moiety of **4.2b·(BPh$_4$)$_2$** is not on the same plane with the ketone moiety plane as observed earlier in the monoalkylated semicarbazone derivative **2.1b·PF$_6$** (Figure 2.3). The angle between the C(3) N(1) N(2) and N(2) C(4) O(1) N(2) planes is about 9.71º, an indication of substantial intramolecular repulsion between the $-NHC(O)NH_2$ atoms of the semicarbazone moiety and the phenyl groups of PPh_3.

The two PtSS planes in $\{Pt_2(\mu\text{-}S)_2\}$ core are flexible along the S---S vectors. Unlike in the homodialkylated derivatives, e.g. **3.1b·(PF$_6$)$_2$** discussed in Chapter 3, increased repulsion between the newly incorporated electrophile and terminal triphenylphosphine (PPh_3) may not be the only contributing factor that determines the size of the dihedral angles in bridged dialkylated derivatives of **1.1**. An interesting trend is observed on comparing the dihedral angles and the Pt---Pt and S---S distances of **4.2b·(BPh$_4$)$_2$** with those of known bridged dialkylated derivatives **4.2c·(PF$_6$)$_2$**, **4.2d·(PF$_6$)$_2$**, **4.2e·(PF$_6$)$_2$**, **4.2f·(BPh$_4$)$_2$**, **4.2g·(PF$_6$)$_2$** and **4.2h·(PF$_6$)$_2$** in Table 4.3 below. A plot of the number of atoms in the bridged vs the S---S distances in Figure 4.7 showed a trend. The relationship is not perfectly linear but shows that the S---S and Pt---Pt distances increase with the number of spacer atoms. The deviations of **4.2d·(PF$_6$)$_2$** and **4.2f·(BPh$_4$)$_2$** from the line joining the points may be due to the electronic effect of the different functional groups in the ligands.

Table 4.3 Comparison of the dihedral angles (°) and the Pt---Pt and S---S distances (Å) of **4.2b·$(BPh_4)_2$**, **4.2c·$(PF_6)_2$**, **4.2d·$(PF_6)_2$**, **4.2e·$(PF_6)_2$**, **4.2f·$(BPh_4)_2$**, **4.2g·$(PF_6)_2$** and **4.2h·$(PF_6)_2$** (NA = number of spacer atoms)

	Compound	(*θ*)	Pt--Pt	S--S	NA	Ref
4.2c·$(PF_6)_2$	$[Pt_2(\mu\text{-}SCH_2CH_2S)(PPh_3)_4](PF_6)_2$	123.8	3.265	2.944	2	11
4.2b·$(BPh_4)_2$	$[Pt_2(\mu\text{-}SCH_2C(NNHC(O)NH_2)CH_2S)(PPh_3)_4](BPh_4)_2$	136.5	3.363	3.027	3	
4.2d·$(PF_6)_2$	$[Pt_2(\mu\text{-}SCH_2C(O)CH_2S)(PPh_3)_4](PF_6)_2$	137.8	3.340	3.033	3	4
4.2e·$(PF_6)_2$	$[Pt_2(\mu\text{-}SCH_2C_6H_4CH_2S)(PPh_3)_4](PF_6)_2$	139.7	3.383	3.055	4	9
4.2f·$(BPh_4)_2$	$[Pt_2(\mu\text{-}SCH_2CH{=}CHCH_2S)(PPh_3)_4](BPh_4)_2$	135.5	3.317	3.078	4	8
4.2g·$(PF_6)_2$	$[Pt_2(\mu\text{-}SCH_2CH_2CH_2CH_2CH_2S)(PPh_3)_4](PF_6)_2$	147.2	3.431	3.075	5	10
4.2h·$(PF_6)_2$	$[Pt_2(\mu\text{-}S_2CH_2C_6H_4\text{-}C_6H_4CH_2)(PPh_3)_4](PF_6)_2$	146.6	3.425	3.103	6	2

The dihedral angles increase with the number of spacer atoms. The dihedral angle of **4.2h·$(PF_6)_2$** (with bridging alkyl group with five spacer atoms) has the highest dihedral angle (θ = 147.20°) and **4.2c·$(PF_6)_2$**, with just two spacer atoms, has θ = 123.8°. The difference between **4.2b·$(BPh_4)_2$** and **4.2d·$(PF_6)_2$** is not very significant but could be attributed to the different substituents on the sp^2 carbon atom bonded to N in **4.2b·$(BPh_4)_2$** and O in **4.2d·$(PF_6)_2$** respectively. The C=C bond length (1.34 Å) is shorter than the C-C bond lengths in a benzene ring (1.39 Å) due to complete π bonding in the former. Thus, the difference in the dihedral angles of **4.2e** and **4.2f·$(BPh_4)_2$** is due to the shorter carbon-carbon distance in **4.2f·$(BPh_4)_2$** and the conjugated π bonding system of the linking benzene ring in **4.2f·$(BPh_4)_2$**.

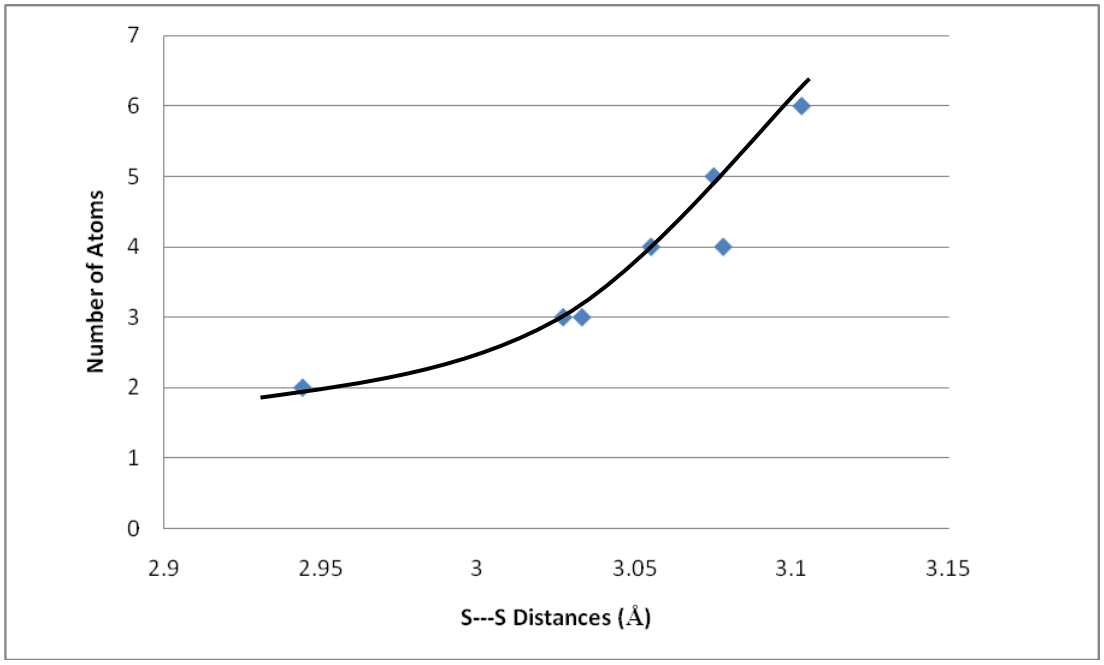

Figure 4.7 A plot of the number of spacer atoms (excluding sulfur atoms) vs the S---S distances in **4.2b·$(BPh_4)_2$**, **4.2c·$(PF_6)_2$**, **4.2d·$(PF_6)_2$**, **4.2e·$(PF_6)_2$**, **4.2f·$(BPh_4)_2$**, **4.2g·$(PF_6)_2$** and **4.2h·$(PF_6)_2$**

4.3.2 $^{31}P\{H\}$ NMR of $[Pt_2(\mu\text{-}SCH_2C(NNHC(O)NH_2)CH_2S)(PPh_3)_4](BPh_4)_2$ 4.2b·$(BPh_4)_2$

The structure of **4.2b·$(BPh_4)_2$** as discussed in Section 4.3.1 revealed that the semicarbazone moiety is bent to one side of the C(1) and C(2) axis making it closer to the two phosphorus atoms P(2) and P(3) on either side of the molecule.

In addition, the conformation of the semicarbazone due to the lone pair of electrons on the azomethine (>C=N) nitrogen makes the carbonyl oxygen [O(1)] closer to the phosphorus P(2) atom as shown in Figure 4.9.

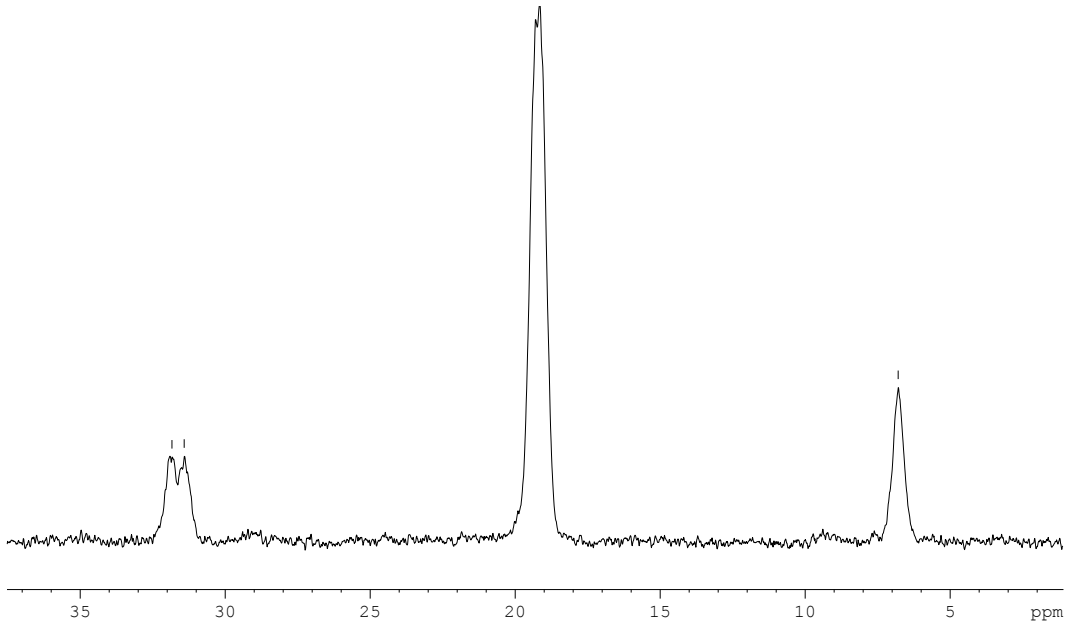

Figure 4.8 $^{31}P\{^1H\}$ NMR of $[Pt_2\{\mu\text{-}SCH_2C(NNHC(O)NH_2)CH_2S\text{-}\mu\}(PPh_3)_4](BPh_4)_2$ **4.2b·$(BPh_4)_2$** showing uneven overlap of the satellite peaks

The C(1)-C(3), C(2)-C(3), S(1)-C(2) and S(1)-C(1) etc bonds will not be rigid in solution unlike in the solid state. Therefore the semicarbazone moiety will be flexible and will flip to either side of the molecule. Thus, P(2) and P(3) are therefore expected to have slightly different electronic environment from P(1) and P(4). However, the signal for the two sets phosphorus are overlapped at 19.1 ppm but the satellite peak due to the $^1J_{P\text{-}Pt}$ coupling are slightly different, 3043 Hz and 2992 Hz as in Figure 4.8. The bond length of Pt(1)-P(2) 2.275(19) Å is shorter than Pt(1)-P(1) 2.294(1) Å as in Table 4.2 and correspondingly if the semicarbazone moiety is bent to the other side, Pt(2)-P(4) (2.288(19) Å) bond length will be shorter than Pt(2)-Pt(3) (2.302(2) Å) bond. Consequently P(2) and P(4) atoms are therefore expected to have larger $^1J_{P\text{-}Pt}$ coupling constant (3043 Hz).

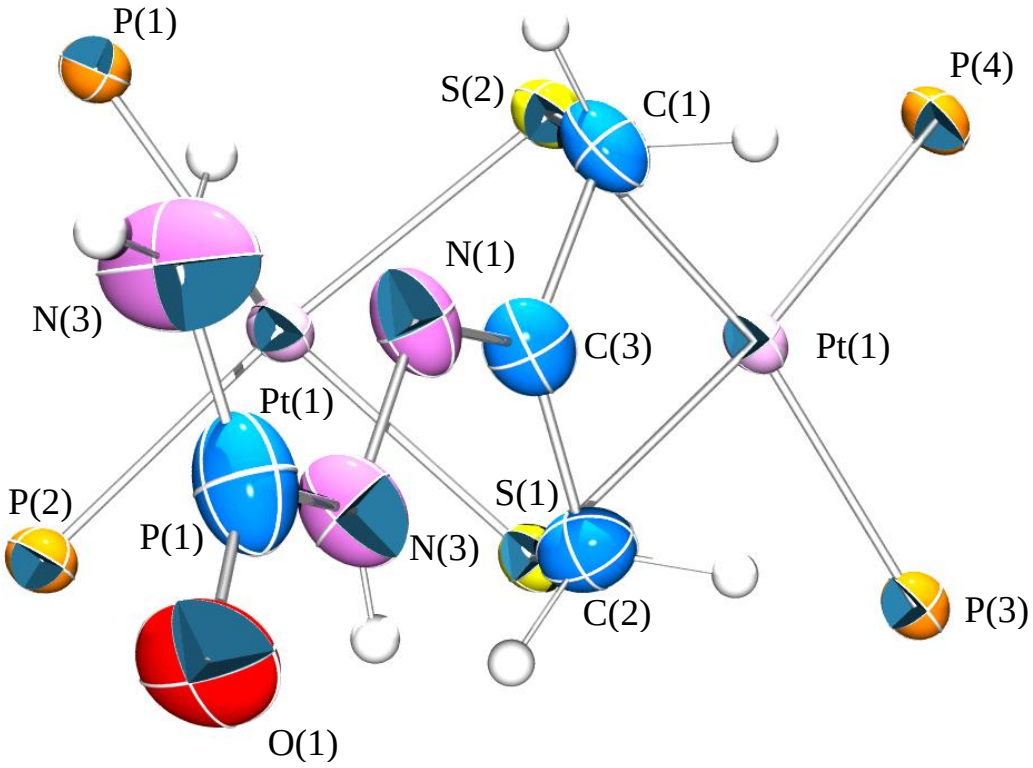

Figure 4.9 Two sets of phosphorus {P(2), P(3)} and {P(1), P(4)} in complex **4.2b·$(BPh_4)_2$** due to the conformation of the semicarbazone moiety over $\{Pt_2(\mu\text{-}S_2\}$ core.

The reaction of 1 mol equiv. of $ClCH_2C(O)NHNHC(O)CH_2Cl$ **4.3a** with **1.1** involved a two step reaction as shown in Scheme 4.7. The first step is a fast monoalkylation of **1.1** in 45 mins. The second step is a much slower reaction to form the dialkylated product $[Pt_2\{SCH_2C(O)NHNHC(O)CH_2S\}(PPh_3)_4]^{2+}$. The ESI-MS of the reaction mixture showed a peak at *m/z* 808 with 100% intensity due to the $[M]^{2+}$ and a peak of about 38% intensity for $[Pt_2\{(\mu\text{-}S)(SCH_2C(O)NHNHC(O)CH_2Cl\}(PPh_3)_4]^{+}$ ion after 24 hours of stirring in MeOH as shown in Figure 4.10 (**A**).

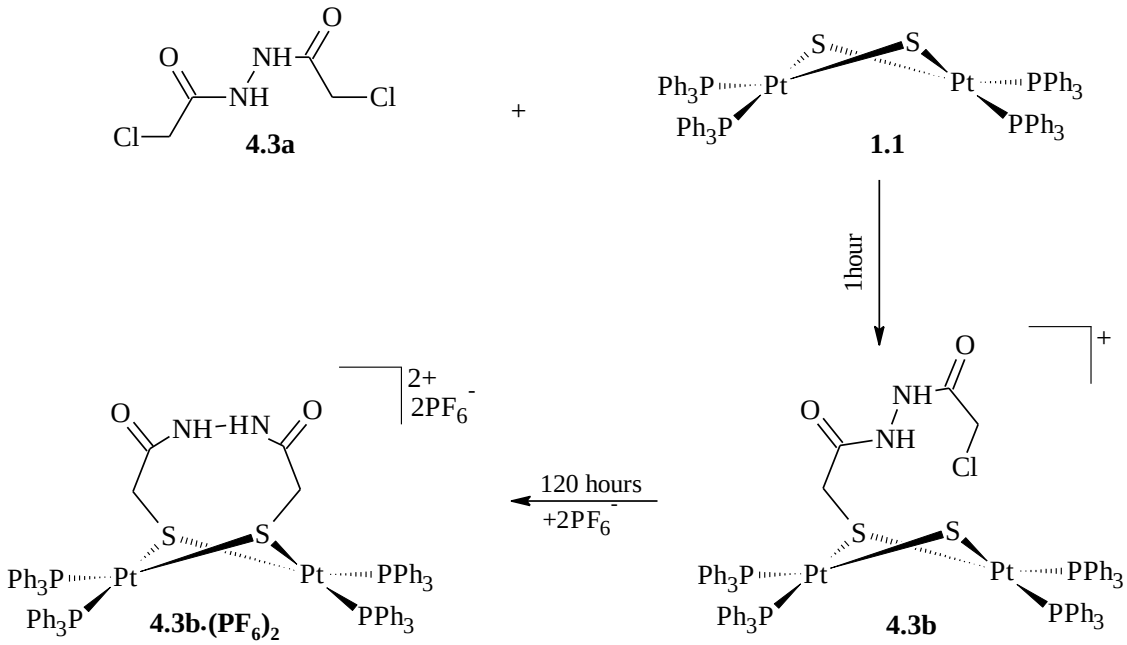

Scheme 4.7 Formation of multifunctional intramolecular bridged dithiolate derivative **4.3b·$(PF_6)_2$** with amide electrophile **4.3a** with six spacer atoms

The reaction after 48 hours indicated a reduction in the peak attributable to $[Pt_2\{(\mu\text{-}S)(SCH_2C(O)NHNHC(O)CH_2Cl\}(PPh_3)_4]^+$ to 20%. Complete formation of the dialkylated product was achieved after 120 hours without any trace of monoalkylated ion in the ESI-MS as shown in Figure 4.10 (**B**). The longer time it took to complete this reaction could be attributed to the expected *trans* conformation commonly adopted by acetyl hydrazine compounds[33-35] and the relatively long spacer length of six atoms. The product was isolated as a PF_6^- salt following addition of excess NH_4PF_6. Further ESI-MS and IR, NMR and elemental analysis confirmed the product to be the bridged dialkylated product $[Pt_2\{SCH_2C(O)NHNHC(O)CH_2S\}(PPh_3)_4]$ $(PF_6)_2$ **4.3b·$(PF_6)_2$**.

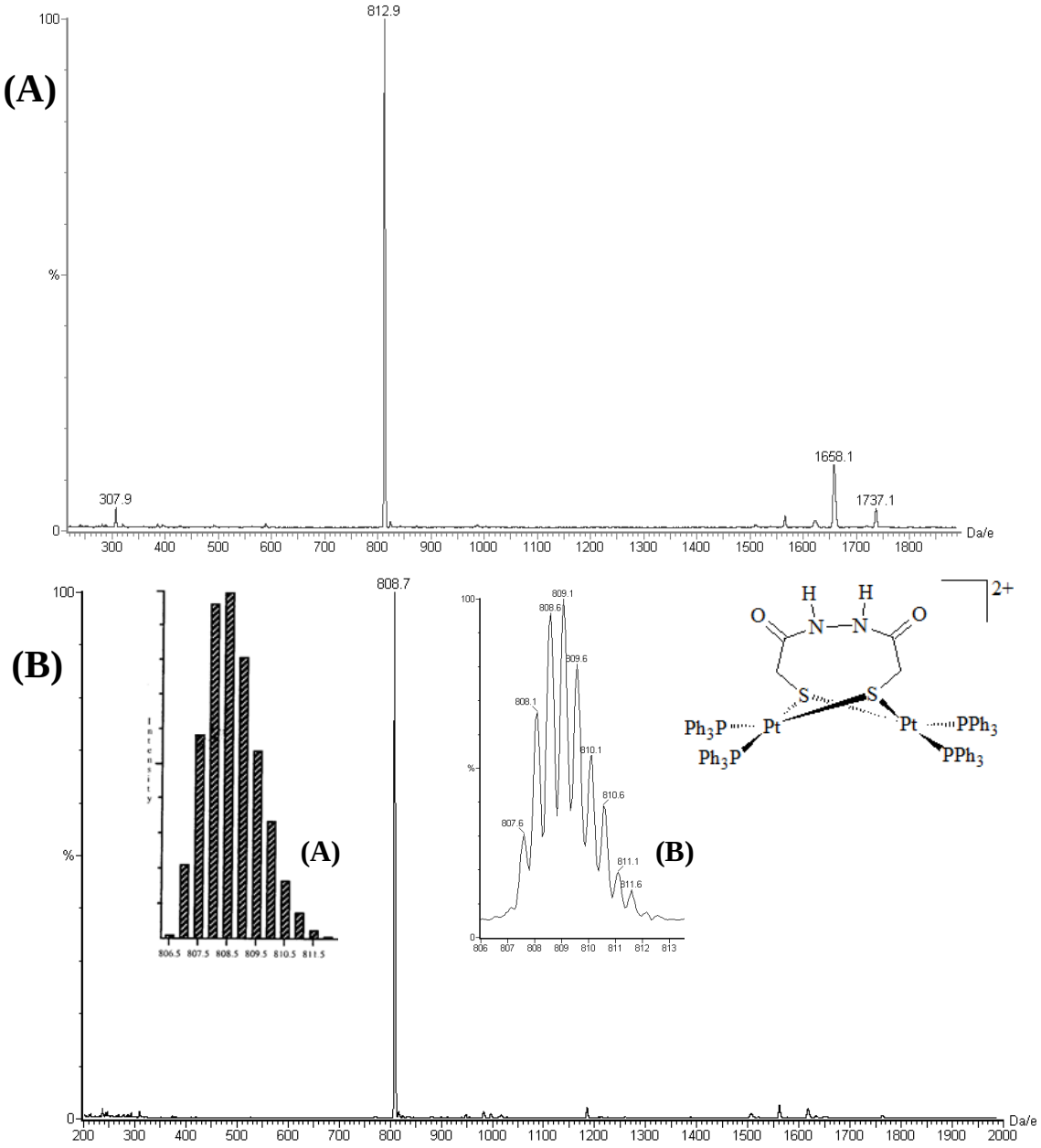

Figure 4.10 ESI-MS spectra of the reaction mixture of $[Pt_2(\mu\text{-}S)_2(PPh_3)_4]$ **1.1** with $ClCH_2C(O)NHNHC(O)CH_2Cl$ **4.3a** after (**A**) 48 and (**B**) 120 hours of stirring in methanol at room temperature. Insert is (**A**) theoretical and (**B**) practical isotope patterns of $[Pt_2\{SCH_2C(O)NHNHC(O)CH_2S\}(PPh_3)_4]^{2+}$ **4.3b**.

4.4 Intermolecular Bridging Alkylation

As mentioned in Section 4.1 the α,ω-dialkylating dihalides with more than six spacer atoms encourage the formation of intermolecular bridged derivatives. Furthermore, the ability of the resulting monoalkylated alkylhalide derivative of **1.1** to act as an electrophile makes it possible to incorporate another molecule of **1.1** through the C-X bond of $[Pt_2\{(\mu\text{-}S)(\mu\text{-}SCH_2RCH_2X)(PPh_3)_4]^+$ (where R =

alkyl, aryl group or combination of both, X = halide) resulting from the initial monoalkylation.

Amide and diamides are important building blocks in chemical synthesis and can be used for the production of a variety of functionalised α-chloroamides and diamides[36]. The multifunctional dialkylating agents *p*-$ClCH_2C(O)NH\text{-}C_6H_4NHC(O)CH_2Cl$ **4.4a** and *o*-$ClCH_2C(O)NHC_6H_4NHC(O)CH_2Cl$ **4.5a** derived from *ortho*- and *para*- phenylenediamines reacted with **1.1** in two stages. The first stage is the monoalkylation of **1.1** to give the monocation $[Pt_2\{(\mu\text{-}S)(\mu\text{-}SCH_2C(O)NHC_6H_4NHC(O)CH_2Cl)(PPh_3)_4]^+$. The monoalkylated derivative provided the enabling condition for a second intermolecular nucleophilic attack by another molecule of **1.1** yielding the bridged Pt_4 aggregates **4.4b** and **4.5b** spanned by *o*- or *p*-$CH_2C(O)NHC_6H_4NHC(O)CH_2$- respectively (Scheme 4.8). The reaction of **4.4a** and **1.1** in a 1:2 mole ratio indicated only the formation of $[Pt_2\{(\mu\text{-}S)(\mu\text{-}S\text{-}p\text{-}CH_2C(O)NHC_6H_4NHC(O)CH_2Cl)(PPh_3)_4]^+$ **4.4b** after stirring for 1 hour. After 72 hours of reaction at room temperature there was a dominant peak *m*/*z* 1598, (100%), attributable to the corresponding Pt_4 aggregate with similar ESI-MS to the reaction mixture of **4.5a** and **1.1** (Scheme 4.8). The product was isolated as a BPh_4^- salt and purified by vapour diffusion of CH_2Cl_2 and diethyl ether to give crystals which ESI-MS showed to be purely **4.4b·(BPh$_4$)$_2$**. The reaction of a 1:2 mole ratio of *o*-$ClCH_2C(O)NHC_6H_4NHC(O)CH_2Cl$ **4.5a** with **1.1** was complete after 24 hours, as confirmed from ESI-MS (Figure 4.11), yielding purely Pt_4 overhead bridged aggregates of two $[Pt_2(\mu\text{-}S)_2(PPh_3)_4]$ molecules. The product was isolated as $[(PPh_3)_4Pt_2\{(\mu\text{-}S)(\mu\text{-}S\text{-}o\text{-}CH_2C(O)NHC_6H_4NHC(O)CH_2S)(\mu\text{-}S)\}Pt_2(PPh_3)_4](BPh_4)_2$ **4.5b·(BPh$_4$)$_2$**, (Scheme 4.8) with the addition of excess $NaBPh_4$. Crystals suitable for X-ray structure analysis were isolated by vapour diffusion of ether into the CH_2Cl_2 solution.

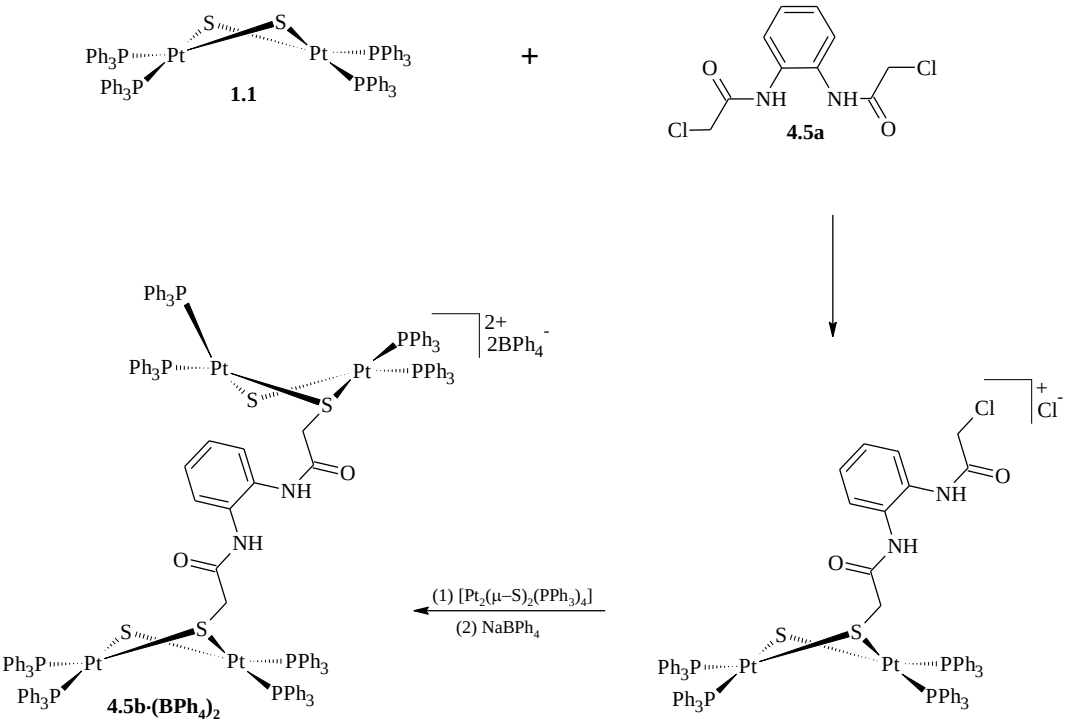

Scheme 4.8 Two stage reaction for the formation of Pt_4 aggregates **4.5b·(BPh$_4$)$_2$** from the reaction of **4.5a** with **1.1**

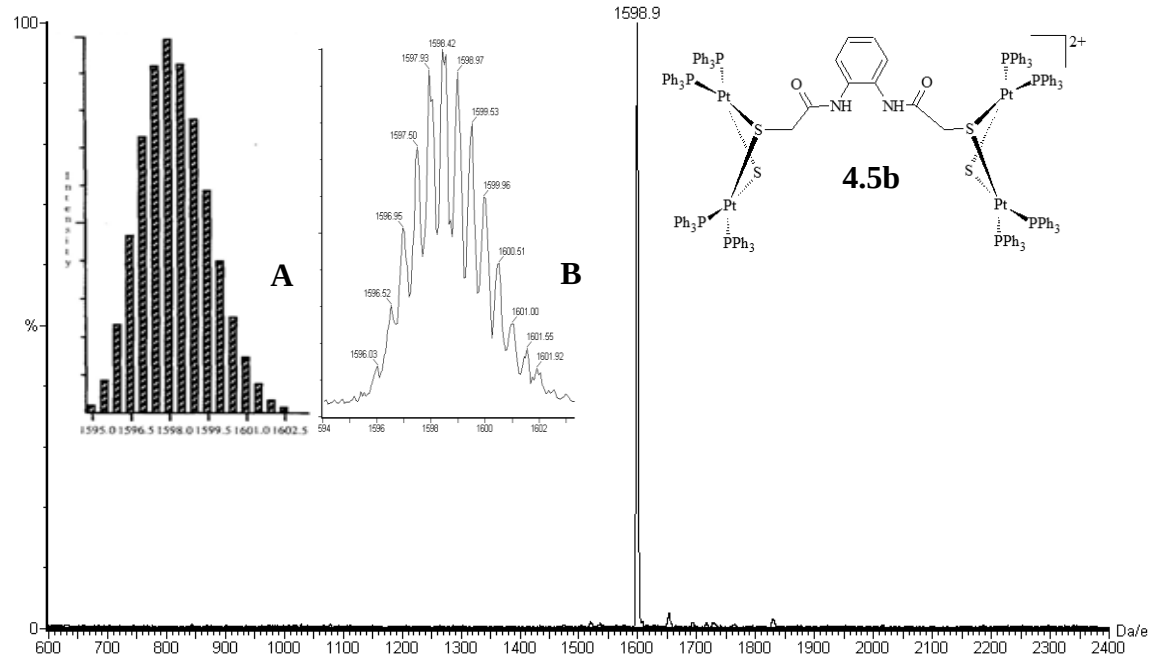

Figure 4.11 ESI-MS of the reaction of o-$ClCH_2C(O)NHC_6H_4NHC(O)CH_2Cl$ and $[Pt_2(\mu\text{-}S)_2(PPh_3)_4]$ in a 1:2 mole ratio. Inset shows the theoretical (**A**) and practical (**B**) isotope patterns of $[(PPh_3)_4Pt_2\{(\mu\text{-}S)(\mu\text{-}S\text{-}o\text{-}CH_2C(O)NHC_6H_4NHC(O)CH_2S)(\mu\text{-}S)\}Pt_2(PPh_3)_4]^{2+}$.

The use of low temperature and a larger reaction solvent volume was applied to investigate the formation of intramolecular bridged dialkylated derivative by the reaction of **4.5a** with **1.1**. These conditions were used to slow down the rate of formation of the Pt_4 aggregate *via* reduced concentration of reactants per volume of the reaction solvent and the likely formation of the Pt_4 aggregate alongside the target intramolecular dialkylated product. The ESI-MS of a 1:1 mole ratio of **4.5a** and **1.1** in a large volume of MeOH at 0 ^oC indicated two M^{2+} peaks. The major peak at *m/z* 1598 correspond to the intermolecular dialkylated Pt_4 aggregate **4.5b** and the minor peaks of about 30 % intensity at *m/z* 849 which agreed with the computer based isotope pattern of intramolecular bridged dialkylated derivative $[Pt_2(\mu\text{-}SCH_2C(O)NHC_6H_4NHC(O)H_2CS)(PPh_3)_4]^{2+}$ **4.5c**. Intramolecular bridging of **1.1** by α,ω-dialkylating agents mainly depend on the number of spacer atoms.[10] The above result is an indication that the conformation of α,ω-dialkylating electrophile may influence the formation of intermolecular bridged derivative.

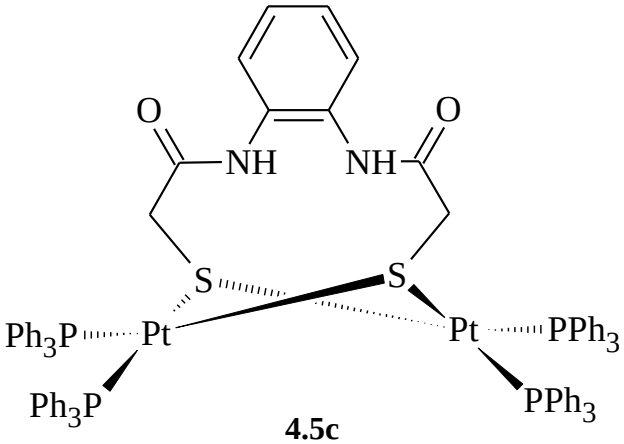

4.5c

The base peak at *m/z* 1598 for **4.5b** indicates that the major product of the reaction is the Pt_4 aggregate **4.5b**. Additional factors which may have favoured the predominant formation of the Pt_4 aggregate from the two different stoichiometric combinations of the reactants is the number of spacer atoms and length and nature of the electrophile.

4.4.1 X-ray Crystal Structures of 4.4b·$(BPh_4)_2$ and 4.5b·$(BPh_4)_2$

The X-ray crystal structures and atom numbering schemes of $[(PPh_3)_4Pt_2(\mu\text{-}S)\{\mu\text{-}S\text{-}o\text{-}CH_2C(O)NHC_6H_4NHC(O)CH_2S\}(\mu\text{-}S)Pt_2(PPh_3)_4](BPh_4)_2$ **4.4b·$(BPh_4)_2$** and $[(PPh_3)_4Pt_2(\mu\text{-}S)\{\mu\text{-}S\text{-}p\text{-}CH_2C(O)NHC_6H_4NHC(O)CH_2S\}(\mu\text{-}S)Pt_2(PPh_3)_4](BPh_4)_2$ **4.5b·$(BPh_4)_2$** are as shown in Figures 4.12 and 4.13 respectively. Selected bond lengths and angles are shown in Tables 4.4 and 4.5 respectively. These compounds are novel and the crystal structures were carried out to confirm the true nature of the compounds and the spatial conformations. The spatial orientations of the functional group will be important in designing synthesis for the extension of functionalities of the incorporated groups or incorporating metallic fragments.

Table 4.4 Selected bond lengths and interatomic distances (Å) and bond angles (°) for $[(PPh_3)_4Pt_2(\mu\text{-}S)\{\mu\text{-}p\text{-}SCH_2C(O)NHC_6H_4NHC(O)CH_2S\}(\mu\text{-}S)Pt_2(PPh_3)_4](BPh_4)_2$ **4.4b·$(BPh_4)_2$** (Estimated standard deviations are in brackets).

Bond lengths and interatomic distances (Å)					
Pt(1)-P(4)	2.259(3)	Pt(1)-S(1)	2.374(3)	S(1)-C(1)	1.825(11)
Pt(1)-P(3)	2.305(3)	Pt(1)-S(2)	2.313(3)	C(2)-N(1)	1.341(15)
Pt(2)-P(1)	2.279(3)	Pt(2)-S(1)	2.361(2)	N(1)-C(3)	1.394(14)
Pt(2)-P(2)	2.296(3)	Pt(2)-S(2)	2.323(3)	C(2)-O(1)	1.203(13)
S(1)---S(2)	3.055	Pt(1)---Pt(2)	3.262		
Bond angles (°)					
P(4)-Pt(1)-P(3)	100.66(12)		P(1)-Pt(2)-P(2)	101.84(10)	
P(4)-Pt(1)-S(2)	89.62(11)		P(1)-Pt(2)-S(2)	84.74(10)	
P(3)-Pt(1)-S(2)	169.63(10)		P(4)-Pt(1)-S(1)	170.62(11)	
P(3)-Pt(1)-S(1)	88.45(10)		P(2)-Pt(2)-S(1)	91.86(10)	
S(2)-Pt(1)-S(1)	81.34(10)		S(2)-Pt(2)-S(1)	81.42(9)	
Pt(1)-S(2)-Pt(2)	89.44(10)		Pt(2)-S(1)-Pt(1)	87.10(9)	
C(2)-C(1)-S(1)	111.8(7)		O(1)-C(2)-C(1)	120.6(11)	
C(2)-N(1)-C(3)	129.3(9)		N(1)-C(2)-C(1)	115.0(10)	
O(1)-C(2)-N(1)	124.4(12)				

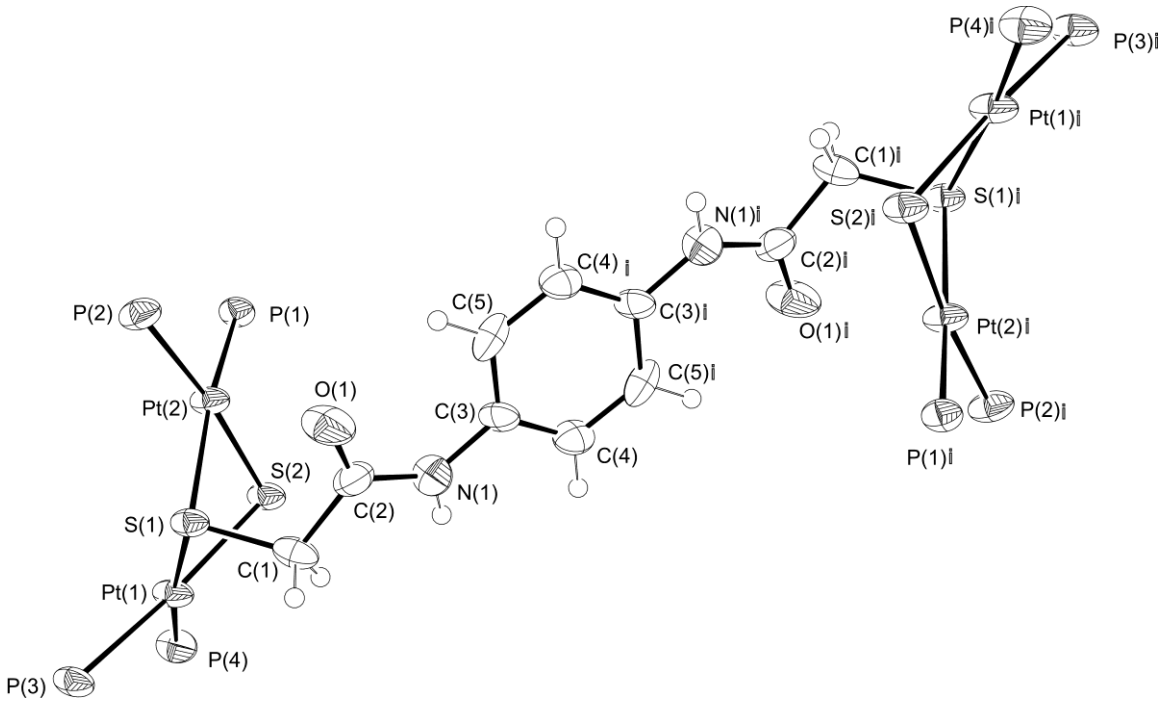

Figure 4.12 Molecular structure of the core of $[(PPh_3)_4Pt_2(\mu\text{-}S)\{\mu\text{-}S\text{-}p\text{-}CH_2C(O)NHC_6H_4NH\text{-}C(O)CH_2S\text{-}\mu\}(\mu\text{-}S)Pt_2(PPh_3)_4](BPh_4)_2$ **4.4b·(BPh$_4$)$_2$** showing the atom numbering scheme with thermal ellipsoids at the 50% probability level. The BPh_4^- counter ione were omitted for clarity.

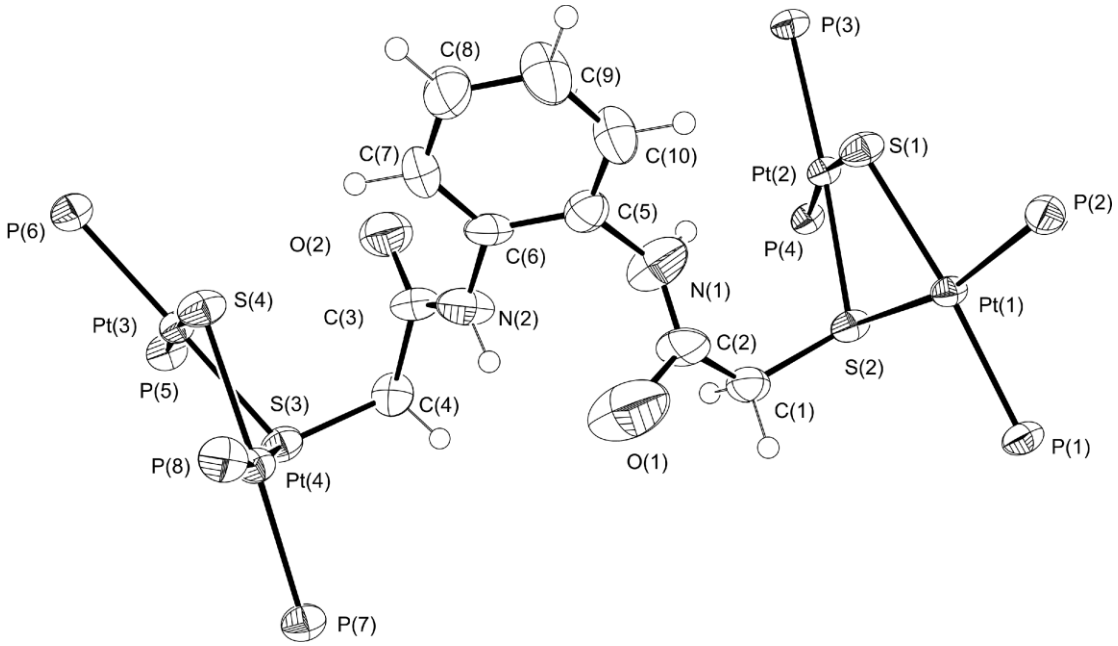

Figure 4.13 Molecular structure of the core of $[(PPh_3)_4Pt_2(\mu\text{-}S)\{\mu\text{-}S\text{-}o\text{-}CH_2C(O)NHC_6H_4NHC(O)\text{-}CH_2S\text{-}\mu\}(\mu\text{-}S)Pt_2(PPh_3)_4](BPh_4)_2$ **4.5b·(BPh$_4$)$_2$** showing the atom numbering scheme with thermal ellipsoids at the 50% probability level. The BPh_4^- counter ions were omitted for clarity.

Table 4. 5 Selected bond lengths and atomic distances (Å) and bond angles (°) for $[(PPh_3)_4Pt_2(\mu\text{-}S)\{\mu\text{-}o\text{-}SCH_2C(O)NHC_6H_4NHC(O)CH_2S\}(\mu\text{-}S)Pt_2(PPh_3)_4](BPh_4)_2$ **4.5b·(BPh$_4$)$_2$** (Estimated standard deviations are in brackets).

Bond lengths and atomic distances (Å)					
Pt(1)-P(1)	2.282(3)	Pt(3)-P(5)	2.268(3)	S(2)-C(1)	1.821(13)
Pt(1)-P(2)	2.285(3)	Pt(3)-P(6)	2.284(3)	S(3)-C(4)	1.829(13)
Pt(2)-P(3)	2.273(3)	Pt(4)-P(7)	2.308(3)	C(1)-C(2)	1.526(18)
Pt(2)-P(4)	2.298(3)	Pt(4)-P(8)	2.273(3)	C(4)-C(3)	1.524(16)
Pt(1)-S(1)	2.330(3)	Pt(3)-S(3)	2.342(3)	C(2)-N(1)	1.232(16)
Pt(1)-S(2)	2.337(3)	Pt(3)-S(4)	2.325(2)	C(3)-N(2)	1.293(16)
Pt(2)-S(1)	2.311(3)	Pt(4)-S(3)	2.355(3)	N(1)-C(5)	1.430(16)
Pt(2)-S(2)	2.373(3)	Pt(4)-S(4)	2.321(3)	N(2)-C(6)	1.411(15)
S(1)---S(2)	3.070	S(3)---S(4)	3.058	C(2)-O(1)	1.265(17)
Pt(1)---Pt(2)	3.391	Pt(3)---Pt(4)	3.412	C(3)-O(2)	1.233(14)

Bond angles (°)			
P(1)-Pt(1)-P(2)	99.98(11)	S(4)-Pt(4)-S(3)	81.67(10)
P(3)-Pt(2)-P(4)	100.83(10)	P(7)-Pt(4)-S(3)	86.71(10)
P(1)-Pt(1)-S(2)	93.21(10)	P(8)-Pt(4)-S(4)	89.19(11)
P(2)-Pt(1)-S(1)	84.73(10)	C(2)-C(1)-S(2)	123.5(9)
S(1)-Pt(1)-S(2)	82.28(10)	C(3)-C(4)-S(3)	117.2(9)
S(1)-Pt(2)-S(2)	81.89(9)	O(1)-C(2)-C(1)	113.3(12)
P(3)-Pt(2)-S(1)	91.36(10)	O(2)-C(3)-C(4)	120.2(12)
P(4)-Pt(2)-S(2)	86.29(10)	N(1)-C(2)-O(1)	119.7(14)
P(5)-Pt(3)-P(6)	100.03(11)	O(2)-C(3)-N(2)	123.6(12)
P(8)-Pt(4)-P(7)	102.56(11)	N(1)-C(2)-C(1)	120.4(11)
P(5)-Pt(3)-S(3)	92.56(11)	N(2)-C(3)-C(4)	116.3(11)
P(6)-Pt(3)-S(4)	85.61(11)	C(2)-N(1)-C(5)	131.7(12)
S(4)-Pt(3)-S(3)	81.86(10)	C(3)-N(2)-C(6)	127.3(11)

The X-ray structure of **4.4b·(BPh$_4$)$_2$** shown in Figure 4.12 has an inversion centre and is thus centrosymmetric, with only one half of the cation being unique. The structure features of the $\{Pt_2(\mu\text{-}S)_2\}$ core are typical for the monoalkylated derivative of this type[1]. The $\{Pt_2(\mu\text{-}S)_2\}$ core is puckered in the

usual way with a dihedral angle (between the two PtS_2 planes) of 133.4°. The structure has a centre of symmetry in the linking aromatic group with the two sides are *anti* to each other. The Pt-S distances to the sulfide ligand Pt(1)-S(2) [2.313(3) Å] and Pt(2)-S(2) [2.323 Å] are shorter than to the thiolate ligand [Pt(1)-S(1) 2.374(3) Å and Pt(2)-S(1) [2.361(2)Å] Due to the higher *trans* influence[37] of sulfide (S^{2-}), the Pt(1)-P(3), [2.305(3) Å] and Pt(2)-P(2) [2.296(3) Å] bonds are longer than the associated Pt(1)-P(4) [2.259(3) Å] and Pt(2)-P(1) [2.279(3) Å] *trans* to thiolate (SR^-) ligand. The amide groups are slightly twisted out of the plane of the bridging phenyl ring, with a C(5)- C(3)-N(1)-C(2) torsion angle of 14.3º. The packing of the cations does not appear to result in any intermolecular hydrogen-bonding interactions, which are kept separated by the considerable steric bulk of the eight PPh_3 ligands.

The X-ray structure of **4.5b·$(BPh_4)_2$** shown in Figure 4.13 also confirmed the Pt_4 aggregate comprise of two molecules of $[Pt_2(\mu\text{-}S)_2(PPh_3)_4]$ **1.1** spanned by the ortho isomer of -$CH_2C(O)NHC_6H_4NHC(O)CH_2$-. The carbonyl group oxygen atoms are *anti* to each other across the aromatic ring. Such an arrangement is also seen in the simple *ortho*-phenylene diamide derivative $C_6H_4(NHC(O)CH_3)_2$[38]. The carbonyl carbon atoms C(2) and C(3) lie respectively 0.750 and 0.777 Å from the least-square planes of the $C_6H_4N_2$ group of **4.5b·$(BPh_4)_2$**. Although the amide hydrogens were not able to be located in the penultimate refinement (all the hydrogen atoms are in calculated positions), there appears to be intramolecular hydrogen bond involving the two amide groups, from the hydrogen on nitrogen N(2) to the oxygen atom of the other carbonyl group O(1) [N(2)···O(1) 2.868 Å]. The hydrogen-bonded carbonyl C(2)-O(1) is longer [1.265(17) Å] compared to the free carbonyl [C(3)-O(2) 1.233(14) Å].

The other amide NH group [N(1)-H(1)] is in relatively close proximity to the sulfide S(1) [N(1)···S(1) 3.297 Å], which on the basis of N···S distances in other system known to show N-H···S hydrogen bonding may represent a modest interaction[39]. For example, in a ferredoxin model complex, containing an $[Fe_4S_4(SBu^t)_4]^{2-}$ core, N-H···S hydrogen bonding interaction involving N-H bond of $Me_3NCH_2C(O)NH_2^+$ counterion have an N···S bond distances of 3.356(3) Å to thiolate sulfur, and 3.625(3) Å to the triply-bridging sulfide[40]. The compounds $[Tm^{Ph}]ZnSCH_2C(O)NHPh$ (Tm^{Ph} = tris(2-mercapto-1-phenyllimidazolyl hydro-borato ligand) and its ethanol adduct $[Tm^{Ph}]ZnSCH_2C(O)NHPh\cdots O(H)Et$ have

considerably shorter N···S separations of 3.06 and 2.99 Å respectively[41]. It is also worth noting that the di-ethanol adduct of $[Pt_2(\mu\text{-}S)_2(PPh_3)_4]$, containing an O-H···S hydrogen bond to a μ_2-sulfide ligand, has an O···S distance of 3.42 Å[42].

The two $[Pt_2(\mu\text{-}S)_2(PPh_3)_4]$ molecules and their attendant thiolate ligands in **4.5b·$(BPh_4)_2$** were expected to have the same geometry. However, the dihedral angle of 148° between PtSS planes in one $[Pt_2(\mu\text{-}S)_2(PPh_3)_4]$ moiety is slightly different from 150º for the other $[Pt_2(\mu\text{-}S)_2(PPh_3)_4]$ moiety. This is no doubt caused by crystal packing forces, the effect of which also gave rise to the differences in the atomic distances of the $\{Pt_2(\mu\text{-}S)_2\}$ core at both ends of the molecule. For example the Pt(3)---Pt(4) (3.412 Å) is longer than Pt(1)---Pt(2) (3.391 Å). From the selected bond length, atomic distances and bond angles in Table 4.5, there are also small differences in the angles and bond distances on both sides of the aromatic ring of the amide spanning the two $[Pt_2(\mu\text{-}S)_2(PPh_3)_4]$ moieties. For instance the angle between N(1)-C(2)-C(1) is 120.4° while N(2)-C(3)-C(4) is 116.3º. Also bond distances C(2)-O(1) 1.265(17) Å is longer compared to similar bond distance C(3)-O(2) 1.233(14) Å on the other side. However, the ^{1}H and ^{31}P NMR of **4.5b·$(BPh_4)_2$** is in perfect agreement with the symmetric nature of the molecule in solution and indicated no difference in the two sides of the molecule as discussed in Section 4.5.

The effect of *trans*- influence of the sulfide (S^{2-}) and the thiolate ligand cannot be compared because of the aforementioned differences in bond lengths and angles in the two $\{Pt_2(\mu\text{-}S)_2\}$ sides of the molecule. The *trans* influence of S^{2-} {S(1)} is well defined on one side of the $\{Pt_2(\mu\text{-}S)_2\}$ rings but became inverse on the other side. For instance on one side of the molecule P(2)-P(4) 2.298(3) Å bonds which are *trans* to S^{2-} is longer than Pt(2)-P(3) 2.273(3) Å. On the other side of the molecule the corresponding Pt(1)-P(1) 2.283(3) Å bond *trans* to the S^{2-} is comparable same to Pt(1)-P(2) 2.285(3) Å. The two Pt-S bond distances are not also equal. The S(1)-Pt(1) 2.330(3) Å is longer than S(1)-Pt(2) 2.311(3) Å and the S(2)-Pt(1) 2.337(3) Å is shorter than S(2)-Pt(2) 2.373(3) Å.

4.4.2 ^{31}P{H} NMR of 4.3b·$(PF_6)_2$, 4.4b·$(BPh_4)_2$ and 4.5b·$(BPh_4)_2$

^{31}P{H} NMR spectra of **4.3b·$(PF_6)_2$**, **4.4b·$(BPh_4)_2$** and **4.5b·$(BPh_4)_2$**, were in good agreement with the corresponding ^{1}H NMR spectra as expected**.** Due to the structural diversity of these derivatives, the ^{31}P NMR gave different but unique ^{31}P NMR spectra which were in accordance with the characteristic phosphorus environments in the respective compounds.

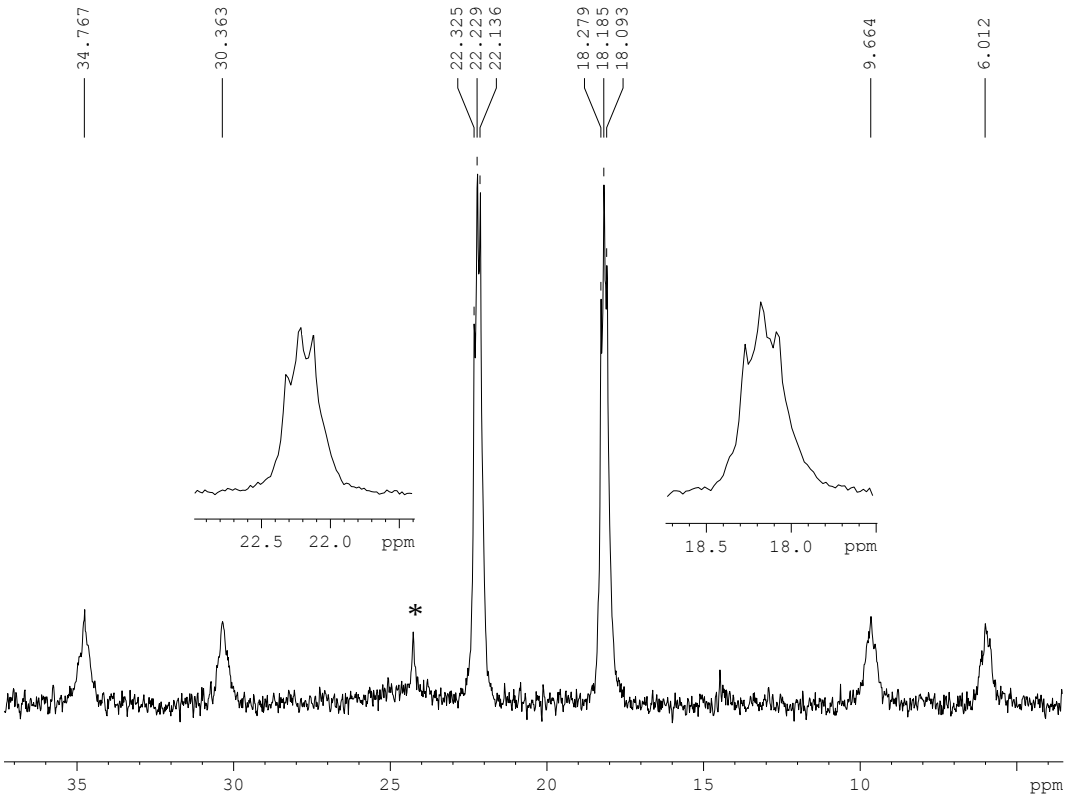

Figure 4.14 ^{31}P{^{1}H} NMR of $Pt_2\{\mu\text{-}SCH_2C(O)NHNHC(O)CH_2S\}(PPh_3)_4(PF_6)_2$ **4.3b·$(PF_6)_2$** and the $^{2}J_{(p\text{-}p)}$ coupling and unidentified impurity (*).

The ^{31}P{H} NMR of **4.3b·$(PF_6)_2$** shown in Figure 4.14 corroborated the unusual ^{1}H NMR result discussed earlier. Similar ^{31}P NMR spectra was observed for the monofunctional bridged compound $[Pt_2SCH_2C_6H_4\text{-}C_6H_4CH_2S\ (PPh_3)_4](PF_6)_2]$[2]. The *trans*- conformation of the incorporated amide groups explain the difference in the CH_2- signals and consequently the ^{31}P NMR showed two distinct resonances at δp 18.2 ppm (*tr*, $J_{(Pt\text{-}P)}$, 2978, $^{2}J_{(p\text{-}p)}$) and 22.2 ppm (*tr*, $J_{(Pt\text{-}P)}$, 3053, $^{2}J_{(p\text{-}p)}$) that correspond to the two different set of phosphorus environments. At room temperature there is no fluxional process operating to average out the phosphine

environments. When a $(CD_3)_2SO$ solution of **4.3·$(PF_6)_2$** was heated to 360 K, there was effectively no change to the $^{31}P\{^1H\}$ NMR spectrum, suggesting a high energy barrier to equilibration of the phosphine ligands.

4.4b·$(BPh_4)_2$ and **4.5b·$(BPh_4)_2$** are symmetrical (as shown in Scheme 4.9) and thus each side of the molecule is expected to show the same NMR signals. The ^{31}P NMR spectra of **4.4b·$(BPh_4)_2$** and **4.5b·$(BPh_4)_2$** (Figure 4.15) are therefore expected to be similar to ^{31}P NMR of the $[M]^+$ monoalkylated derivative shown in Figure 2.7 which is characteristic of one side of the symmetric structures. The ^{31}P NMR spectra of the $[M]^{2+}$ overhead bridged dialkylated complexes, **4.4b·$(BPh_4)_2$** and **4.5b·$(BPh_4)_2$** expectedly is an AA'BB'X spin system due to the mixed thiolate-sulfide nature of the complexes at each end of the molecule. There are two sets of similar inequivalent phosphorus environments (in blue and black) at each end of the symmetrical molecule as shown in Scheme 4.9. One set is *trans* to the unsubstituted

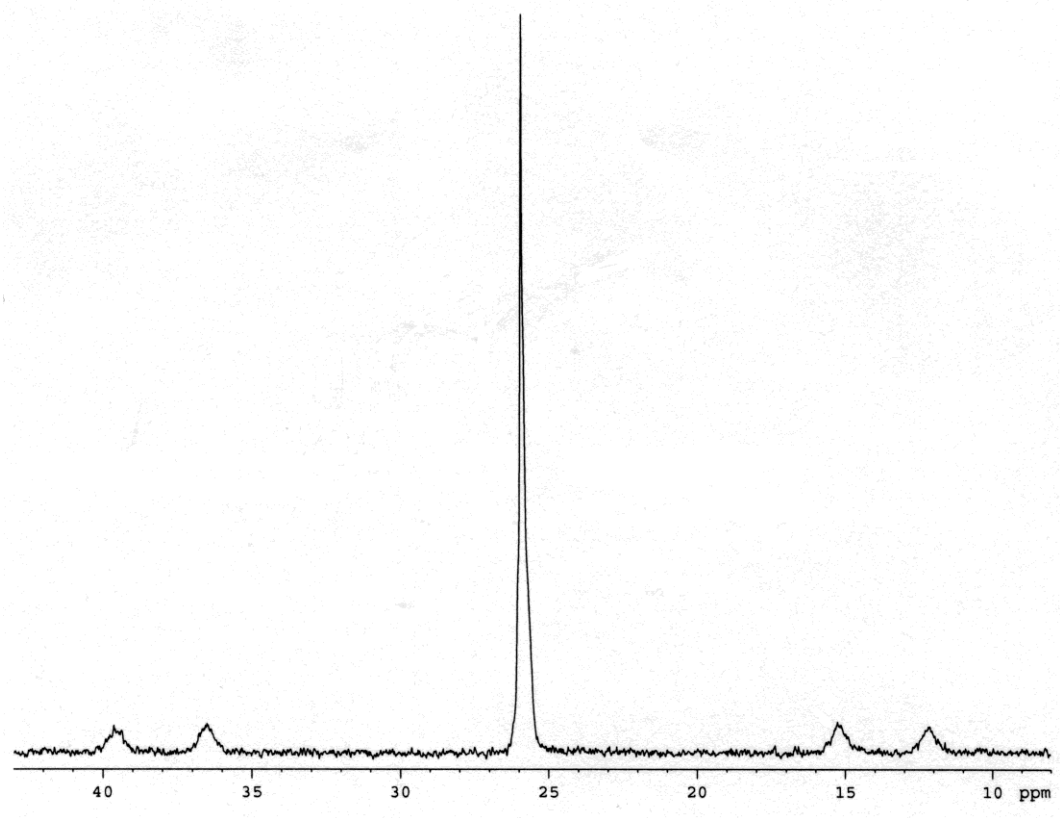

Figure 4.15 $^{31}P\{^1H\}$ NMR of $[(PPh_3)_4Pt_2(\mu\text{-}S)\{\mu\text{-}o\text{-}SCH_2C(O)NHC_6H_4NHC(O)CH_2S\text{-}\mu\}(\mu\text{-}S)Pt_2(PPh_3)_4](BPh_4)_2$ **4.5b·$(BPh_4)_2$** showing the overlapping phosphorus signals and the satellite peaks

sulfide, S^{2-} and thiolate ligand, and the other trans to the SR, respectively, each giving rise to a doublet in the ^{31}P NMR spectrum. The doublet appears to be superimposed on one another because the two sets of phosphorus atoms have similar chemical shifts and are only distinguishable by their different coupling constant to ^{195}Pt as shown in the ^{31}P $\{^1H\}$ NMR spectrum of **4.5b·(BPh$_4$)$_2$** in Figure 4.15.

The two sets of phosphines *trans* to the thiolate (SR) ligand, P_B, should show a higher Pt-P coupling ($^1J_{Pt\text{-}P}$ 3341 Hz) because the alkylation of the sulfide (to SR) lengthens the two Pt-SR bonds, and results in the corresponding shortening of the Pt-P_B bond. Thereby, phosphines *trans* to the S^{2-} ligand, P_A, are expected to give rise to the smaller Pt-P coupling constant ($^1J_{Pt\text{-}P}$ 2579 Hz) because of the higher *trans* influence of S^{2-}, relative to SR, which weakens the Pt-P_A bond, resulting in the smaller $^1J_{Pt\text{-}P}$ value.

4.5 ^{1}H NMR Spectroscopic Characterisation

^1H NMR studies were used to further characterise the dialkylated compounds reported in this chapter. Clearly defined signals of the incorporated groups were identified and assigned. The NMR signals of PPh_3 ligands and the counter ions BPh_4^- **4.1b·PF$_6$**, **4.2b·(BPh$_4$)$_2$**, **4.3b·(PF$_6$)$_2$**, **4.4b·(BPh$_4$)$_2$** and **4.5b·(BPh$_4$)$_2$**, and were observed as overlapping and complicated signals between ≈ 6-8 ppm .

The ^1H NMR of the incorporated hydrazine derivative in **4.3b·(PF$_6$)$_2$** was not as expected. The two S-CH_2 hydrogen atoms were expected to be identical and appear as overlapping signals. The chemical shifts for the two hydrogen atoms were different. Hydrazine compounds of the type R-NH-NH-R similar to **4.3a** are known to exhibit *cis*- and *trans*- conformations. From the reported crystal structures of acetylhydrazine compounds[33-35, 43], the *trans*-conformation is more preferred when not in a ring system. Thus, the amide derivative upon alkylation is expected to maintain a *trans* conformation which placed the two NH groups as close as possible to the preferred *trans* arrangement. This gave rise to two different signal which appeared to suggest two different -CH_2 ^1H signals. However, the Heteronuclear Single Quantum Correlation (HSQC) NMR and superimposed ^1H NMR signal in Figure 4.16 revealed that the alkylating carbon

atoms in **4.3b·$(PF_6)_2$** are electronically similar. Due to the conformation of the complex the two hydrogen atoms attached to each carbon atom are different but same as the corresponding hydrogen atoms on the other similar alkylating carbon atom S-CH_2.

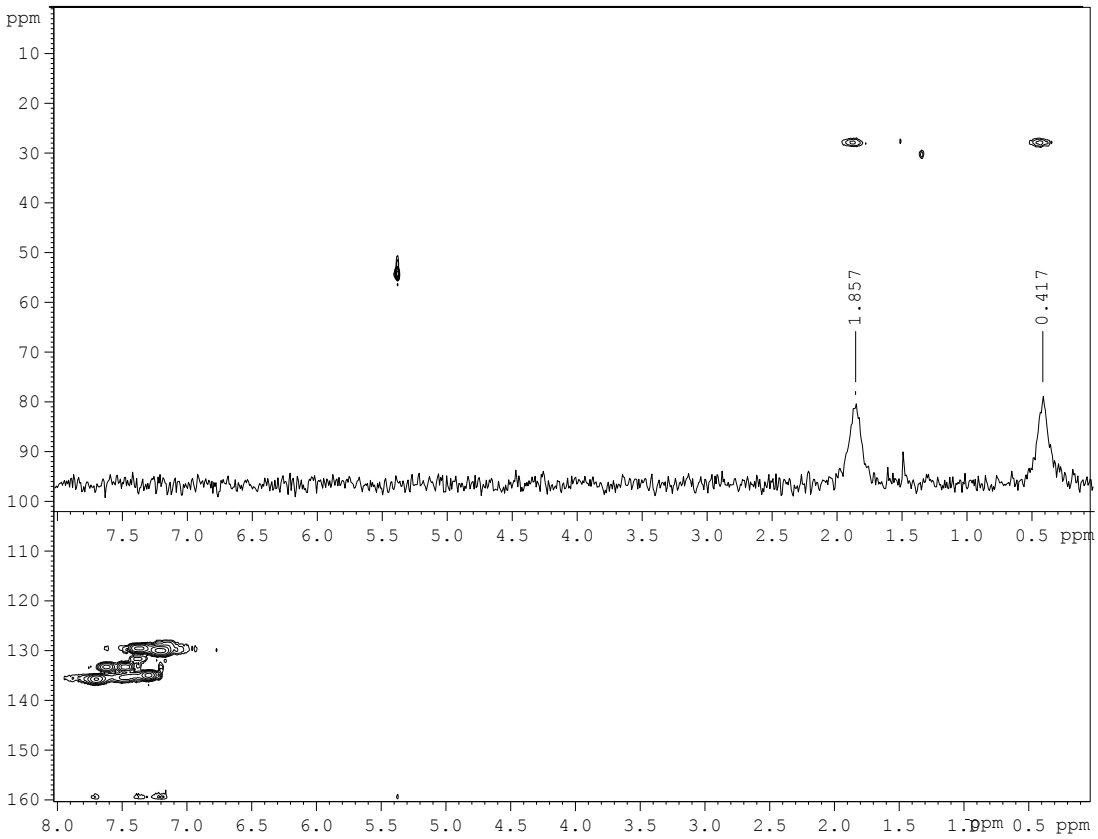

Figure 4.16 The HSQC and the superimposed ^{1}H NMR of **4.3b·$(PF_6)_2$** showing two sets of different ^{1}H signals from two inequivalent carbon atoms.

In the case of **4.4b·$(BPh_4)_2$** and **4.5b·$(BPh_4)_2$**, the structures are C_2 symmetric and have the same atomic environments on the two sides of the symmetry A and B as represented in Scheme 4.9. As expected the NMR signals due to the (-SCH_2) and the amine (–NH) groups in **4.5b·$(BPh_4)_2$** gave single overlapping peaks as shown in the ^{1}H NMR spectrum in Figure 4.17. Similar NMR signal was observed for –SCH_2 group in **4.4b·$(BPh_4)_2$.**

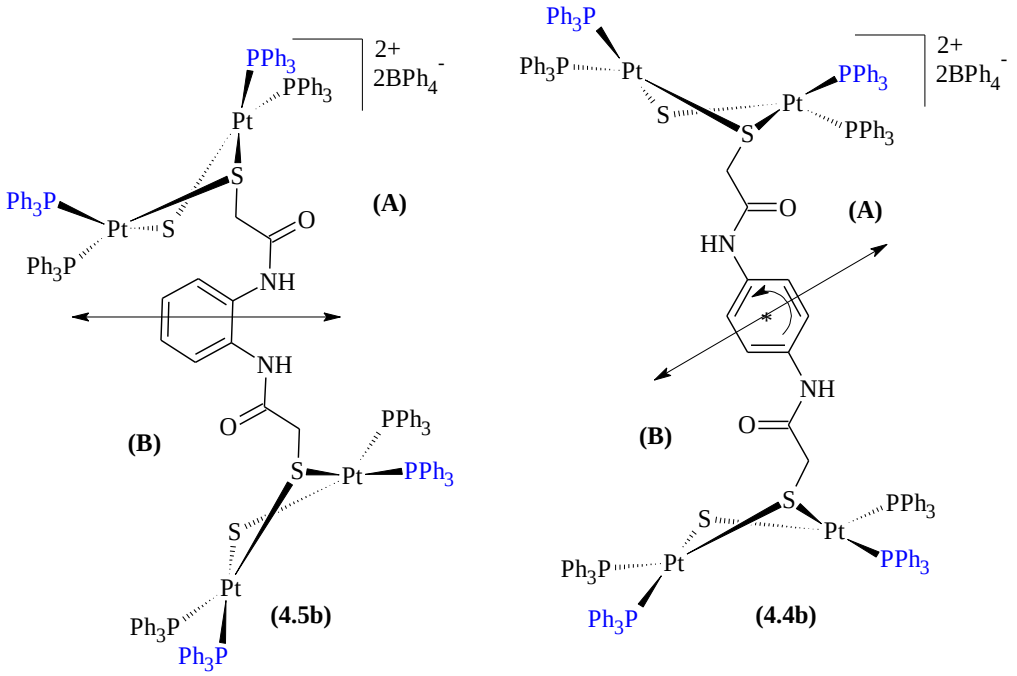

Scheme 4.9 Schematic representations of the symmetries in **4.4b·(BPh$_4$)$_2$** and **4.5b·(BPh$_4$)$_2$**. (*) indicates the inversion center of **4.4b·(BPh$_4$)$_2$**

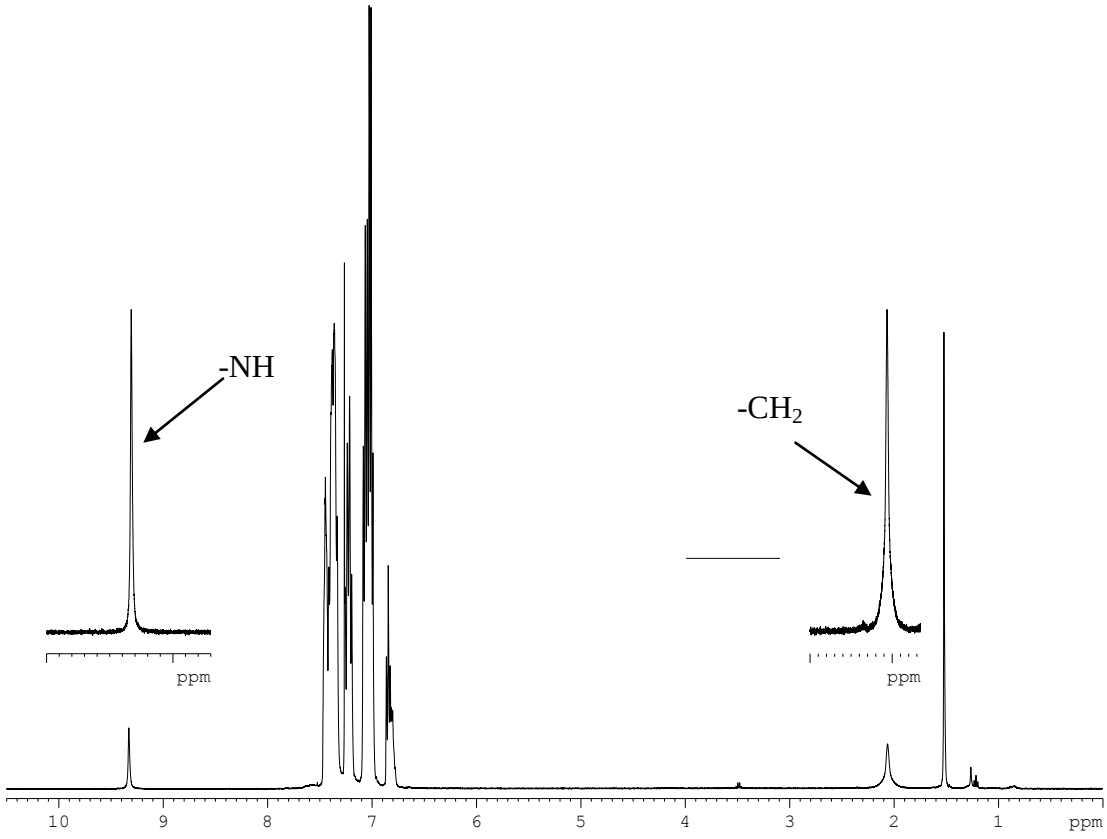

Figure 4.17 ^{1}H NMR spectrum of $[(PPh_3)_4Pt_2(\mu\text{-}S)\{\mu\text{-}SCH_2C(O)NHC_6H_4NHC(O)CH_2S\text{-}\mu\}(\mu\text{-}S)Pt_2(PPh_3)_4](BPh_4)_2$ **4.5b·(BPh$_4$)$_2$**. Insert is the enlarged -NH protons and -CH_2 protons signals

The two -CH_3 groups in the semicarbazone $CH_3C(NNHC(O)NH_2)CH_3$ derived from acetone reportedly gave different ^1H and ^{13}C NMR signals[31]. As expected, the two methylene hydrogen and carbon (–CH_2) atoms in the α,ω-dichloro-semicarbazone ligand **4.2a** gave different ^1H NMR signals as reported in Section 4.5 and same for the ^1H NMR of **4.2b·$(BPh_4)_2$** shown in Figure 4.18. This is because of the different electronic environments of the two –CH_2 groups due to the lone pair of electrons on azomethine (C=N) nitrogen atom of the semicarbazone ligand. The intra-atomic repulsion and symmetry effect made the >C=NNHC(O)NH_2 asymmetrical between the two sets of hydrogen atoms and thus gave rise to different ^1H NMR signals. This difference was maintained upon alkylation to give different the two -S–CH_2 groups in the bridged alkylated derivative **4.2b·$(BPh_4)_2$**. The difference in the electronic environments and the structure of the semicarbazone also caused a difference in the electronic environment of one set of the phosphorus atoms on one side of **4.2b·$(BPh_4)_2$** as discussed in Section 4.3.2.

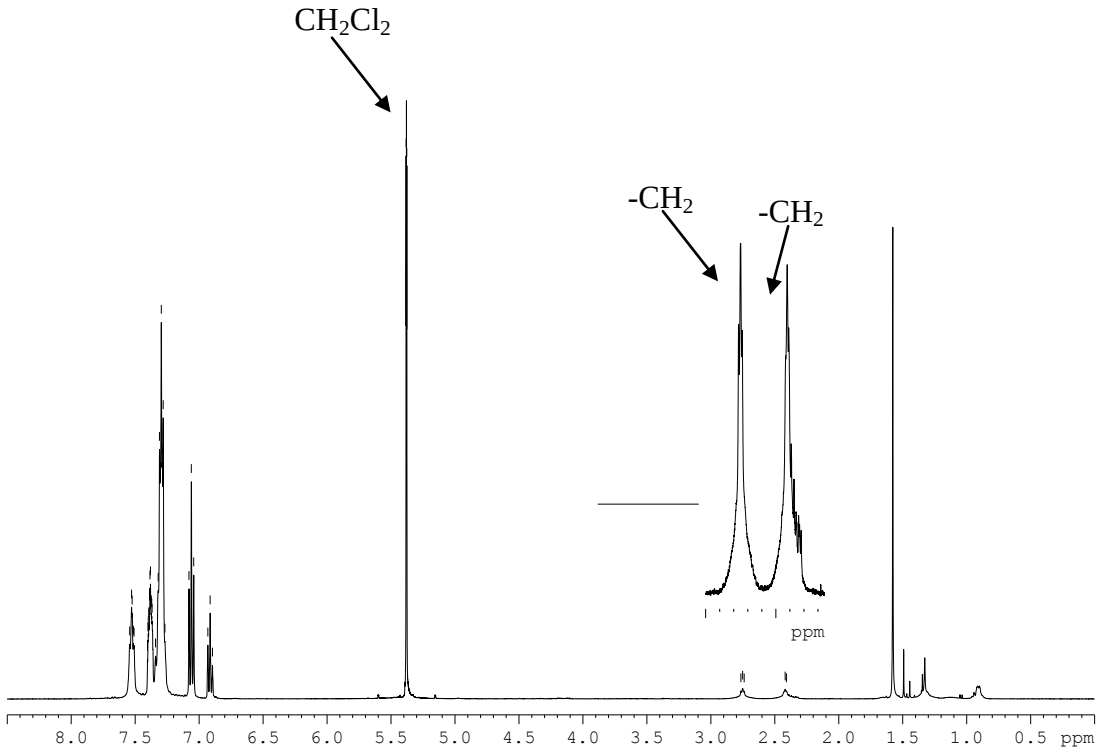

Figure 4.18 ^1H NMR of $[Pt_2\{\mu\text{-}SCH_2C(NNHC(O)NH_2)NH_2)CH_2S\text{-}\mu\}(PPh_3)_3](BPh_4)_2$ **4.2b·$(BPh_4)_2$** showing the two different -CH_2 groups.

4.6 IR Characterisation

The infrared (IR) spectra of the complexes were obtained in most cases for completeness in the characterisation of the alkylated complexes and to show the presence of the functional groups due to incorporated electrophiles. The IR absorption band of the >C=N in **4.2b·(BPh$_4$)$_2$** and carbonyl (>C=O) groups in the complexes **4.2b·(BPh$_4$)$_2$** (1694 cm^{-1}) , **4.3b·(PF$_6$)$_2$** (1683 cm^{-1}), **4.4b·(BPh$_4$)$_2$** (1678 cm^{-1}) and **4.5b·(BPh$_4$)$_2$** (1644 cm^{-1}) were distinct as recorded in experimental section.

4.7 Conclusion

Synthesis and characterisation of a new set of novel functionalised dialkylated products of **1.1**, **4.1b·PF$_6$**, **4.2b·(BPh$_4$)$_2$**, **4.3b·(PF$_6$)$_2$**, **4.4b·(BPh$_4$)$_2$** and **4.5b·(BPh$_4$)$_2$** were achieved. ESI-MS clearly showed the deprotonation and conversion of $[Pt_2(\mu\text{-}SCH_2C(O)CH_2S)(PPh_3)_4]^{2+}$ **4.5c** to $[Pt_2(\mu\text{-}SCH_2C(O)CHS)(PPh_3)_4]^{+}$**4.1b**. However, the insertion of carbon atom into the four membered $\{Pt_2(\mu\text{-}S)_2\}$ ring and the formation of a Pt-C bond was confirmed by X-ray structure analysis and NMR. The trend in the X-ray crystal structural parameters of **4.2b·(BPh$_4$)$_2$** and other similar reported bridged dialkylated derivatives revealed that dihedral angles within the $\{Pt_2(\mu\text{-}S)_2\}$ is effected by the number atoms and functionalities of the group. The X-ray structure analysis of **4.5b·(BPh$_4$)$_2$** derivative shows that the formation of such multinuclear aggregate is controlled by number of the spacer atoms and conformation of α,ω-electrophile. One of the reasons for the multifunctional alkylation of **1.1** is to extend the reactive sites of the incorporated organic moieties with good ligating functional groups. The incorporation of amides which are known important building blocks in chemical synthesis[44, 45] therefore offers a good incentive to extending the length and functionality of the incorporated group. In addition, multimetallic assembly using **1.1** has been achieved through direct bonding of metal fragments with the nucleophilic sulfide centres. These results thus, offer a new opportunity for designing supramultimetallic frameworks by incorporating metal fragments through the additional incorporated ligands.

4.8 Experimental

The alkylating agents $ClCH_2C(O)NHNHC(O)CH_2Cl$[46], *o*-$ClCH_2C(O)NHC_6H_4NHC(O)CH_2Cl$[36], *p*-$ClCH_2C(O)NHC_6H_4NHC(O)CH_2Cl$[36] employed in the studies were synthesised according to the literature methods. $[Pt_2(\mu\text{-}S)_2(PPh_3)_4]$ **1.1** was synthesised by the metathesis reaction of *cis*-$PtCl_2(PPh_3)_2$ with $Na_2S.H_2O$ in benzene[5]. $ClCH_2C(=NNHC(O)NH_2)CH_2Cl$ is a new compound synthesised according to the general method described by Vogel[47]. The analytical grade chemicals, $ClCH_2C(O)Cl$, $ClCH_2C(O)CH_2Cl$ (Sigma-Aldrich), $NH_2NHC(O)NH_2{\cdot}HCl$ (Sigma), *o*- and *p*-phenylene diamine (BDH) were used as supplied for the synthesis. Methanol, dichloromethane, diethyl ether were supplied as drum grade chemicals. The NMR spectra were run on Bruker 400MHz or 300MHz spectrometers, IR were obtained with a Perkin Elmer Spectrum 100, FT-IR Spectrometer, Melting points of the compounds were determined with a Reichert melting point machine.

Preparation of $ClCH_2C(=NNHC(O)NH_2)CH_2Cl$ (4.2a)

A solution of $NH_2NHC(O)NH_2.HCl$ (88 mg, 0.79 mmol) in water (2 mL) at 40^oC was added to a solution of $ClCH_2C(O)CH_2Cl$ (100 mg, 0.79 mmol) in ethanol (9 mL) in a round bottomed flask. The resulting solution was stirred for 5 minutes with gradual addition of $NaHCO_3$ (66 mg, 0.79 mmol). The mixture was boiled for 4 minutes and cooled to room temperature and kept in the freezer for two days. The resulting needle crystals were filtered under suction, washed with ethanol (2 x 10 mL) and dried to give the product (105 mg, 72%).

Melting Point: 117-119^oC

IR (KBr): υ 3462, 3314, 3223, 1720 cm^{-1}

^1H NMR (400 MHz, $CDCl_3$): δ 4.2 (*s*, 2H, CH_2) 4.3 (*s*, 2H, CH_2), 9.8 (*s*, 2H, NH_2).

^{13}C NMR (400 MHz, $CDCl_3$) δ 158.8, (*s*, C=O), 141.4, (*s*, C=N), 45.98, (*s*, CH_2), 34.1, (*s*, CH_2).

ESI-MS (MeOH): $[M + H]^+$ *m/z* 184

Elemental analysis: calcd (%) for $C_4H_7Cl_2N_3O$ (184.02): C, 26.11; H, 3.83; N, 22.83, found: C, 26.39; H, 4.10; N, 22.98.

Preparation of $[Pt_2\{(\mu\text{-}SCH_2C(O)CHS\}(PPh_3)_4](PF_6)$ (4.1b·PF_6)

Methanol (25 mL) was added to $ClCH_2C(O)CH_2Cl$ (10.1 mg, 0.080 mmol) and $[Pt_2(\mu\text{-}S)_2(PPh_3)_4]$ (100 mg, 0.067 mmol) and the solution stirred. The solution changed from an orange suspension to bright yellow clear solution after an hour. As soon as the ESI-MS indicated a parallel formation of $[M]^{2+}$ ion $[Pt_2(\mu\text{-}SCH_2C(O)CH_2S)(PPh_3)_4]^{2+}$ and $[M - H]^+$ ion, $[Pt_2(\mu\text{-}SCH_2C(O)CHS)(PPh_3)_4]^+$, 1 mL of aqueous 0.1 mol L^{-1} NaOH solution was added to convert the $[M]^{2+}$ to $[M - H]^+$ ion. The reaction was stopped as soon as ESI-MS indicated complete conversion to $[M - H]^+$ ion (about 1 minute). The solution was gravity filtered to remove any solid impurity and the product isolated by the addition of NH_4PF_6 (43 mg) and distilled water (10 mL). The yellow precipitate was filtered and washed with distilled water (2 x 10 mL) and diethyl ether (20 mL) to give $[Pt_2\{(\mu\text{-}SCH_2C(O)CHS\}(PPh_3)_4](PF_6)$ $.2CH_2Cl_2$ (83 mg, 73%). Crystals suitable for X-ray analysis were isolated by vapour diffusion of diethyl ether into a CH_2Cl_2 solution of the product.

Melting Point: 180-182 ^oC

IR (KBr): υ cm^{-1} 1676, 1481 1436, 1096 and 838

$^{31}P\{^1H\}$ NMR (300 MHz, $CDCl_3$): δ_p 15.5 ppm (br, *d*, $J_{Pt(1)\text{-}P(4)}$ 3795 Hz) 16.2 ppm (br, *d*, $J_{Pt(1)\text{-}P(1)}$ 3184) 17.07 ppm (br, *d*, $J_{Pt(1)\text{-}P(2)}$ 2755 Hz) and 22.8 ppm (br, *d*, $J_{Pt(2)\text{-}P(3)}$ 2084 Hz),

^1H NMR (400 MHz, $CDCl_3$): δ 2.23 (1H, *m*, -CH), 2.9 (2H, *br* $-CH_2$), 6.94 -7.50 (63H, *m* 12Ph).

ESI-MS (MeOH) cone voltage 20: *m/z* 1562 ($[M]^+$ 100%)

Elemental analysis: calcd (%) for $[Pt_2(\mu\text{-}SCH_2C(O)CHS)(PPh_4)_4](PF_6).2CH_2Cl_2$, $C_{77}H_{67}Cl_4F_6OP_5Pt_2S_2$ (1873.33): C, 49.37; H, 3.60, found: C, 50.08; H, 3.95.

Preparation of $[Pt_2\{SCH_2C(NNHC(O)NH_2)CH_2S\}(PPh_3)_4](BPh_4)_2$ (4.2b·$(BPh_4)_2$)

$ClCH_2C(NNHC(O)NH_2)CH_2Cl$ (15 mg, 0.080 mmol) was added to a suspension of $[Pt_2(\mu\text{-}S)_2(PPh_3)_4]$ (100 mg, 0.067 mmol) in MeOH (25 mL). The mixture was stirred at room temperature for 1 hr during which solubilisation occurred. After confirming the formation of expected product $[Pt_2\{SCH_2C(NNHC(O)NH_2)CH_2S\}(PPh_3)_4]^{2+}$ by ESI-MS, the colourless solution was filtered. The white product was precipitated out of the solution by the addition of $NaBPh_4$

(40 mg). The precipitate was filtered, washed with water (50 mL) and ether (40 mL) and dried to give $[Pt_2\{SCH_2C(NNHC(O)NH_2)CH_2S\}(PPh_3)_4](BPh_4)_2$ (111 mg, 74%). Crystals suitable for X-ray analysis were isolated by vapour diffusion of diethyl ether into a dichloromethane solution.

Melting Point: 175-177^oC

IR (KBr): υ 1096, 1436, 1480, 1694, 3054, 3479 cm^{-1}

$^{31}P\{^1H\}$ NMR (300 MHz, CD_2Cl_2): δ_p 19.2 (br, *s*, $J_{Pt\text{-}P(1)}$ 3043 Hz, br, *s*, $J_{Pt\text{-}P(2)}$ 2992Hz)

^1H NMR (400 MHz, CD_2Cl_2): δ 2.4 (2H, *tr*, CH_2), 2.8 (2H, *tr*, CH_2), 6.9-7.5 (160H, *m*, 32Ph).

ESI-MS (MeOH): *m/z* 808 ($[M]^{2+}$ 100%]

Elemental analysis: calcd (%) for $C_{124}H_{107}B_2N_3OP_4Pt_2S_2$ (2255.01): C, 66.05; H, 4.78; N, 1.86, found: C, 65.05; H, 4.97; N, 1.81.

Preparation of $[Pt_2\{\mu\text{-}SCH_2C(O)NHNHC(O)CHS\}(PPh_3)_4](PF_6)_2$ (4.3b·$(PF_6)_2$)

$[Pt_2(\mu\text{-}S)_2(PPh_3)_4]$ (100 mg, 0.067 mmol) and $ClCH_2C(O)NHNHC(O)CH_2Cl$ (14.8 mg, 0.080 mmol) in methanol (25 mL) in a 100 mL round bottomed flask was stirred for 120 hours at room temperature. Complete formation of the bridged product was confirmed by ESI-MS which showed the $[Pt_2\mu\text{-}SCH_2C(O)NHNHC(O)CH_2S\text{-}\mu)(PPh_3)_4]^{2+}$ ion. The solution was filtered and NH_4PF_6 (43 mg) added to the clear, colourless filtrate. The white solid precipitate of $[Pt_2(\mu\text{-}SCH_2C(O)NHNHC(O)CH_2S\text{-}\mu)(PPh_3)_4](PF_6)_2$ was washed with water (40 mL) and diethyl ether (2 x 20 mL) yielding **4.3b·$(PF_6)_2$** (69.3 mg, 55%).

Melting Point: 184-186 ^oC

IR (KBr): υ 1097, 1436, 1481, 1683, 3437 cm^{-1}

$^{31}P\ \{^1H\}$ NMR (300 MHz, CD_2Cl_2): δ_p 18.2 (br, *s*, $J_{Pt\text{-}P}$, 2978) 22.2 (br, *s*, $J_{Pt\text{-}P}$, 3053)

^1H NMR (400 MHz, CD_2Cl_2): δ 0.42 (*tr*, 2H, CH_2), 1.86 (*tr*, 2H,CH_2).

ESI- MS (MeOH): *m/z* 808, ($[M]^{2+}$ 100%]

Elemental analysis: calcd (%) for $C_{76}H_{66}F_{12}N_2O_2P_6Pt_2S_2$: C, 47.85; H, 3.49; N, 1.47, found; C, 47.69; H, 3.39; N, 2.03.

Preparation of $[(PPh_3)_4Pt_2(\mu\text{-}S)(\mu\text{-}S\text{-}p\text{-}CH_2C(O)NHC_6H_4NHC(O)CH_2S)(\mu\text{-}S)Pt_2(PPh_3)_4](BPh_4)_2$ (4.4b·$(BPh_4)_2$)

$[Pt_2(\mu\text{-}S)_2(PPh_3)_4]$ (100 mg, 0.067 mmol) and *p*-$ClCH_2C(O)NHC_6H_4NHC(O)CH_2Cl$ (8.7 mg, 0.033 mmol) in methanol (25 mL) in a 50 mL round bottomed flask was stirred for 24 hours at room temperature. Complete formation of the compound was observed by ESI-MS. The solution was filtered and $NaBPh_4$ (45 mg) added to the clear golden yellow-orange filtrate. The light orange precipitate, Pt_4 aggregate $[(PPh_3)_4Pt_4(\mu\text{-}S)(\mu\text{-}S\text{-}p\text{-}CH_2C(O)NHC_6H_4NHC(O)CH_2S)(\mu\text{-}S)Pt_2(PPh_3)_4](BPh_4)_2$ was washed with water (40 mL) and diethyl ether (2 x 20 mL) yielding (117 mg, 46%) of **4.4b·$(BPh_4)_2$**.

Melting Point: 179-181 ^oC

IR (KBr): υ 1095, 1435, 1479, 1678, 3467 cm^{-1}

$^{31}P\{^1H\}$ NMR (300 MHz, $CDCl_3$): δ_P = 24.8 (br, *s*, $J_{Pt\text{-}P(1)}$ 3358.85 Hz, $J_{Pt\text{-}P(2)}$ 2613.16 Hz)

^1H NMR (400 MHz, $CDCl_3$): δ 3.00 (4H, br, $2CH_2$), 6.84-7.5 (167H, *m*, 32Ph).

ESI- MS (MeOH): *m/z* 1598 ($[M]^{2+}$ 100%]

Elemental analysis: calcd (%) for $C_{202}H_{170}B_2N_2O_2P_8Pt_4S_4$ (3835.53): C, 63.25; H, 4.47; N, 0.73, found; C, 63.37; H, 4.35; N, 0.67.

Preparation of $[(PPh_3)_4Pt_2(\mu\text{-}S)(\mu\text{-}S\text{-}o\text{-}CH_2C(O)NHC_6H_4NHC(O)CH_2S)(\mu\text{-}S)Pt_2(PPh_3)_4](BPh_4)_2$ (4.5b·$(BPh_4)_2$)

$[Pt_2(\mu\text{-}S)_2(PPh_3)_4]$ (100 mg, 0.067 mmol) and *o*-$ClCH_2C(O)NHC_6H_4NHC(O)CH_2Cl$ (8.7 mg, 0.033 mmol) in methanol (25 mL) in a 50 mL round bottomed flask was stirred for 24 hours at room temperature. Complete formation of the compound was confirmed by ESI-MS. The solution was filtered and $NaBPh_4$ (45 mg) added to the clear golden yellow orange filtrate. The precipitated product $[(PPh_3)_4Pt_4(\mu\text{-}S)(\mu\text{-}S\text{-}o\text{-}CH_2C(O)NHC_6H_4NHC(O)CH_2S)(\mu\text{-}S)Pt_2(PPh_3)_4](BPh_4)_2$ was filtered, washed with water (40 mL) and diethyl ether (2 x 20 mL) yielding (199 mg, 78 %) of **4.5b·$(BPh_4)_2$**.

Melting Point: 258-260 ^oC

IR (KBr): υ 1094, 1434, 1479, 1644, 3052 cm^{-1}

$^{31}P\{^1H\}$ NMR (300 MHz, $CDCl_3$): δ_P = 26.0 (br, *s*, $J_{Pt\text{-}P(1)}$ 3340.6 Hz, $J_{Pt\text{-}P(2)}$ 2578.9 Hz)

^{1}H NMR (400 MHz, $CDCl_3$): δ 9.3 (2H, *s*, 2NH), 6.8-7.5 (167H, *m*, 32Ph), 2.06 (4H, br, $2CH_2$).

ESI- MS (MeOH): *m/z* 1598 ($[M]^+$ 100%)

Elemental analysis: calcd (%) for $C_{202}H_{170}B_2N_2O_2P_8Pt_4S_4$ (3835.53) C, 63.25; H, 4.47; N, 0.73, found: C, 63.17; H, 4.63; N, 0.71.

4.9 X- ray Crystal Structure Determinations

All data were obtained at the University of Canterbury following the method explained in Section A.7 in the appendix. The structures were solved using SHELXS-97[48] and SHELXL-97[49] was used for structure refinements and reporting. The structures were refined by full-matrix least-squares based on F_o^2 (SHELXL-97[49]) with anisotropic thermal parameters for non-hydrogen atoms. A summary of crystallographic parameters for the data collections and refinements is given in Table 4.6 and 4.7.

The crystal structure of **4.1b·$(PF_6)_2$** was solved by direct methods. The platinum, sulfur and phosphorus atoms were first located. The carbon atom bonded to platinum and all the atoms were located in subsequent refinements. All non hydrogen atoms were refined as anisotropic. The refined structure contains $[Pt_2\{\mu\text{-}SCH_2C(O)CHS\}(PPh_3)_4]^+$, a PF_6^- ion and two molecules of CH_2Cl_2. The R values were $R_1 = 0.0244$, $wR_2 = 0.0539$ with the largest residual peak and hole of 1.245 and -1.539 e $Å^{-3}$ in the final difference map.

The crystal structure **4.2b·$(BPh_4)_2$** was solved by direct methods. The platinum, sulfur and phosphorus atoms were located followed by other atoms. All non hydrogen atoms were refined as anisotropic. The refined structure contained $[Pt_2\{\mu\text{-}SCH_2C(NNHC(O)NH_2)CH_2S\text{-}\mu\}(PPh_3)_4]^{2+}$, two BPh_4^- ions and a molecule of disordered CH_2Cl_2. The remaining residual peaks in the final difference map could not be resolved and were treated as disordered with solvent accessible voids of about 536 $Å^3$ shown in Figure 4.19.

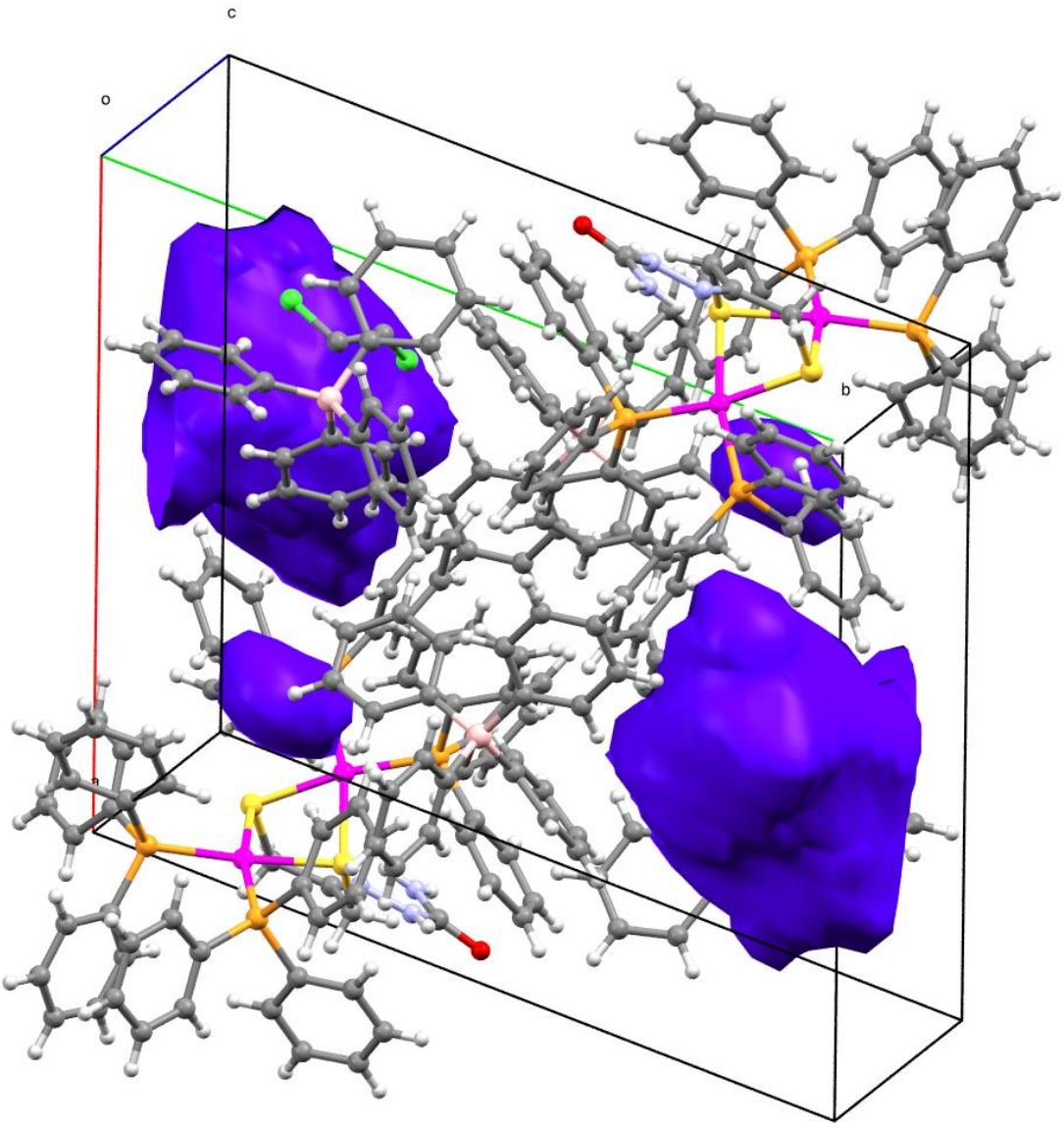

Figure 4.19 The unit cell crystal packing showing the solvent accessible voids in the final crystal structure map for $[Pt_2\{\mu\text{-}SCH_2C(NNHC(O)NH_2)CH_2S\}(PPh_3)_4](BPh_4)_2$ **4.2b·(BPh$_4$)$_2$**

The crystal structure of **4.4b·(BPh$_4$)$_2$** was solved by direct methods. The cation has a centre of symmetry so half of the molecule makes up the asymmetric unit. The other part was automatically generated. All non hydrogen atoms were refined as anistropic. The refined structure contains $[(PPh_3)_4Pt_2(\mu\text{-}S)\{\mu\text{-}o\text{-}S\text{-}CH_2C(O)NHC_6H_4NHC(O)CH_2S\}(\mu\text{-}S)Pt_2(PPh_3)_4]^{2+}$ **4.4b**, and two ions of BPh_4^-. Refinement with the main cation and anion included converged with R_1= 0.11. There were extra residual peaks that were associated with solvent but this could not be modelled sensibly. PLATON indicated a total 1327.0 Å^3 solvent accessible void. The SQUEEZE routine of PLATON was used to generate a modified data set which was used in the final refinement cycle. A higher residual peak (5.34 Å^{-3})

than usual was in the final difference map. This was adjacent to the Pt atom so it is ripple peaks from data that may have been caused by poor crystal quality.

The crystal structure of **4.5b·$(BPh_4)_2$** was solved by Patterson methods. The refined structure contains $[(PPh_3)_4Pt_2(\mu\text{-}S)\{\mu\text{-}o\text{-}SCH_2C(O)NHC_6H_4NHC(O)CH_2S\}(\mu\text{-}S)Pt_2(PPh_3)_4]^{2+}$, two BPh_4^- ions and partially disordered CH_2Cl_2 solvent molecules. The residual peaks in the final difference map could not be refined and were treated as disordered solvent molecules, occupying a volume of 810 $Å^3$, which explains the high R values of $R_1 = 0.0627$ and $R_2 = 0.1529$.

Table 4.6 Crystal data and structure refinement details for **4.1b·PF_6** and **4.2b·$(BPh_4)_2$**

Identification Code	**4.1b·PF_6·$(2CH_2Cl_2)$**	**4.2b·$(BPh_4)_2$**
Formula	$C_{77}H_{67}Cl_4F_6OP_5Pt_2S_2$	$C_{125}H_{109}B_2Cl_2N_3OP_4Pt_2S_2$
Formula weight	1873.26	2339.85
Temperature (K)	90(2)	90(2)
Wavelength (Å)	0.71073	0.71073
Crystal system	Monoclinic	Triclinic
Space group	P 2(1)/n	P -1
a/Å	19.577(13)	17.8478(5)
b/Å	14.693(10)	18.5906(5)
c/Å	26.924(18)	18.8511(5)
α/°	90	83.448(2)
β/°	110.392(7)	70.165(2)
γ/°	90	71.444(2)
Volume ($Å^3$)	7259(8)	5577.7(3)
Z	4	2
Calculated density (Mg/m^3)	1.714	1.393
Absorption coefficient (mm^{-1})	4.226	2.699
F(000)	3688	2360
Crystal size (mm^3)	0.34 x 0.18 x 0.10	0.35 x 0.10 x 0.02
Theta range for data collection	1.60 to 27.89°	2.34 to 29.13°.
Limiting indices	$-25 \le h \le 24$, $-19 \le k \le 19$, $-35 \le l \le 35$	$-24 \le h \le 24$,$-25 \le k \le 25$,$-25 \le l \le 25$
Reflections collected / unique	91680/17315 [R(int) = 0.0403]	139910/29703 [R(int) = 0.1233]
Completeness to theta	27.89°, 99.8 %	27.50°, 99.9 %
Absorption correction	Semi-empirical from equivalents	Multi-scan
Max. and min. transmission	1.000 and 0.652	0.7458 and 0.5675
Refinement method	Full-matrix least-squares on F^2	Full-matrix least-squares on F^2
Data / restraints / parameters	17315 / 0 / 874	29703 / 0 / 1279
Goodness of fit on F^2	1.019	1.022
Final R indices [$I>2\sigma(I)$]	$R_1 = 0.0244$, $wR_2 = 0.0539$	$R_1 = 0.0579$, $wR_2 = 0.1426$
R indices (all data)	$R_1 = 0.0314$, $wR_2 = 0.0565$	$R_1 = 0.1303$, $wR_2 = 0.1732$
Largest diff. peak and hole	1.245 and -1.539 $eÅ^{-3}$	2.091 and -1.165 e $Å^{-3}$

Table 4.7 Crystal data and structure refinement details for **4.4b·$(BPh_4)_2$** and **4.5b·$(BPh_4)_2$**

Identification Code	**4.4b·$(BPh_4)_2$**	**4.5b·$(BPh_4)_2$**
Formula	$C_{202}H_{170}B_2N_2O_2P_8Pt_4S_4$	$C_{204}H_{170}B_2Cl_6O_2P_8N_2Pt_4S_4$
Formula weight	3835.38	4072.10
Temperature (K)	123(2)	90(2)
Wavelength (Å)	0.71073	0.71073
Crystal system	Triclinic	Triclinic
Space group	P -1	P -1
a/Å	13.9301(7) Å	13.633(3) Å
b/Å	16.2595(9) Å	24.228(6) Å
c/Å	23.2219(13) Å	29.422(6) Å
α/°	99.096(3)°	80.864(8)
β/°	101.835(3)°	80.823(8)°
γ/°	90.720(4)°	81.647(8)
Volume ($Å^3$)	5077.6(5)	9400(3)
Z	1	2
Calculated density (Mg/m^3)	1.254	1.439
Absorption coefficient (mm^{-1})	2.898	3.218
F(000)	1918	4064
Crystal size (mm^3)	0.51 x 0.47 x 0.14	0.36 x 0.29 x 0.08
Theta range for data collection	1.92 to 26.90°	0.86 to 25.50°
Limiting indices	$-17\leq h\leq 17$, $-20\leq k\leq 20$, $-29\leq l\leq 29$	$-16h\leq h\leq 16$, $-29\leq k\leq 29$, $-35\leq l\leq 35$
Reflections collected / unique	105166/21753 [R(int) = 0.0948]	180628/34993 [R(int) = 0.1026]
Completeness to theta	26.90°, 99.1 %	25.50°, 99.9%
Absorption correction	Semi-empirical from equivalents	Semi-empirical from equivalents
Max. and min. transmission	0.6871 and 0.3196	0.746 and 0.562
Refinement method	Full-matrix least-squares on F^2	Full-matrix least-squares on F^2
Data / restraints / parameters	21753 / 0 / 1009	34993 / 0 / 2098
Goodness of fit on F^2	1.018	1.050
Final R indices [$I>2\sigma(I)$]	$R_1 = 0.0787$, $wR_2 = 0.1954$	$R_1 = 0.0627$, $wR_2 = 0.1529$
R indices (all data)	$R_1 = 0.1486$, $wR_2 = 0.2252$	$R_1 = 0.1183$, $wR_2 = 0.1860$
Largest diff. peak and hole	5.340 and -3.235 e $Å^{-3}$	3.596 and -1.961 e$Å^{-3}$

4.10 Reference

1. O. T. Ujam, S. M. Devoy, W. Henderson, B. K. Nicholson and T. S. A. Hor, *Inorg.Chim. Acta*, 2010, **363**, 3558.
2. S. H. Chong, W. Henderson and T. S. A. Hor, *Eur. J. Inorg. Chem.*, 2007, 4958.
3. W. Henderson, S. H. Chong and T. S. A. Hor, *Inorg. Chim. Acta* 2006, **359**, 3440.
4. S. M. Devoy, M.Sc. Thesis, University of Waikato, 2005.
5. R. Ugo, G. La Monica, S. Cenini, A. Segre and F. Conti, *J. Chem. Soc. A* 1971, 522.
6. S. H. Chong, W. Henderson and T. S. A. Hor, *Dalton Trans.*, 2007, 4008.
7. S. H. Chong, L. L. Koh, W. Henderson and T. S. A. Hor, *Chem. Asain J.*, 2006, 264.
8. S. M. Devoy, W. Henderson, B. K. Nicholson and T. S. A. Hor, *Inorg. Chim. Acta*, 2009, **362**, 1194.
9. S. H. Chong, D. J. Young and T. S. A. Hor, *J. Organomet. Chem.*, 2006, **691**, 349.
10. S. M. Devoy, W. Henderson, B. K. Nicholson and T. S. A. Hor, *Inorg. Chimica Acta.*, 2009, **363**.
11. S. H. Chong, A. Tjindrawan and T. S. A. Hor, *J. Mol. Cat, A: Chemical*, 2003, **204-205**, 267.
12. W. Henderson, B. K. Nicholson, S. M. Devoy and T. S. A. Hor, *Inorg. Chim. Acta*, 2007, **361**, 1908.
13. N. E. Cameron, R. A. Linklater, W. Henderson, B. K. Nicholson and T. S. A. Hor, *J. Organomet. Chem.*, 2008, **693**, 3711.
14. S.-W. A. Fong, W. T. Yap, J. J. Vittal, T. S. A. Hor, W. Henderson, A. G. Oliver and C. E. F. Richard, *J. Chem. Soc., Dalton Trans.*, 2001, 1986.
15. S.-W. A. Fong, W. T. Yap, J. J. Vittal, W. Henderson and T. S. A. Hor, *J. Chem. Soc., Dalton Trans.*, 2002, 1826.

16. Z. Li, S.-W. A. Fong, J. S. L. Yeo, W. Henderson, K. F. Mok and T. S. A. Hor, in *Modern Cordination Chemistry: the contribition of Joseph Chatt, Royal Society of Chemistry*, Cambrige, Editon edn., 2002, p. 355.
17. S.-W. A. Fong and T. S. A. Hor, *J. Chem. Soc., Dalton Trans.*, 1999, 639.
18. W. Henderson and J. S. Mclndoe, *Mass Spectrometry of Inorganic, Coordination and Organometallic Compounds*, John Wiley & Sons, Ltd, 2005.
19. W. Henderson, B. K. Nicholson, S. M. Devoy and T. S. A. Hor, *Inorg. Chim. Acta*, 2007, **361**, 1908.
20. Y. Takahata, *International Journal of Quantum Chemistry*, 2008, **108**, 2326.
21. H. C. Clark and L. E. Manzer, *Inorg. Chem.*, 1974, **13**, 1996.
22. L. Manojlović-Muir, K. W. Muir and T. Solomun, *J. Organomet. Chem.*, 1977, **142**, 265.
23. P. N. Kapoor and R. Kakkar, *J. Mol. Str: THEOCHEM*, 2003, **679**, 149.
24. P. Kapoor, V.-Y. Kukushkin, K. Lövqvist and Å. Oskarsson, *J. Organomet. Chem.*, 1996, **517**, 71.
25. Å. Oskarsson, B. Norén, C. Svensson and L. I. Elding, *Acta Cryst. Sec. B*, 1990, **B46** 748.
26. V. Ericson, K. Lövqvist, B. Norén and Å. Oskarsson, *Acta Chemica Scandinavica* 1992, **46**, 854.
27. I. A. Blair, R. M. Tinoco, M. J. Brodie, R. A. Clare, C. T. Dollery, J. A. Timbrell and I. A. Beever, *Hum. Expt. Toxicol.*, 1985, **2**, 195.
28. J. A. Timbrell and S. J. Harland, *Clin. Pharmacol. Ther.* , 1979, **26**, 81.
29. J. S. Casas, M. S. García-Tasende and J. Sordo, *Coord. Chem. Rev.*, 2009, **209**, 197.
30. V. N. Korotchenko, A. V. Shastin, V. G. Nenajdenko and E. S. Balenkovaa, *Org. Biomol. Chem*, 2003, 1906.
31. J. B. Fulton and J. Warken, *Can. J. Chem.*, 1987, **65**, 1177.
32. J. S. Casas, M. S. García-Tasende and J. Sordo, *Coord. Chem. Rev.*, 2000, **209**, 197.
33. R. Sintani, *Acta Cryst. C*, 1960, **13**, 609.

34. Z.-B. Zheng, R.-T. Wu, J.-K. Li and Y.-F. Sun, *Acta Cryst. Sec. E: Struct. Rep.*, 2007, **63**, o4658.

35. M. D. Soutullo, C. I. Odom, E. A. Salter, A. C. Stenson, R. E. Sykora, A. Wierzbicki and J. H. Davis Junior, *J. Comb.Chem.*, 2007, **9**, 571.

36. A. J. Harte and T. Gunnlaugsson, *Tetrahedron Letters*, 2006, **47**, 6321.

37. T. G. Appleton, H. C. Clark and L. E. Manzer, *Coord. Chem. Rev.*, 1973, **10**, 335.

38. A. Shivanyuk, K. Rissanen, S. K. Körner, D. M. Rudkevich and J. Rebek Jr., *Helv. Chim. Acta*, 2000, **83**, 1778.

39. C. S. Mullins, C. A. Grapperhaus and P. M. Kozlowski, *J. Biol. Inorg. Chem.*, 2006, **11**, 617.

40. M. A. Walters, C. L. Roche, A. L. Rheingold and S. W. Kassel, *Inorg. Chem.*, 2005, **44**, 3777.

41. M. Morlok, K. E. Janak, G. Zhu, D. A. Quarless and G. Parkin, *J. Am. Chem. Soc.*, 2008, **127**, 14039.

42. W. Henderson, S. Thwaite, B. K. Nicholson and T. S. A. Hor, *Eur. J. Inorg. Chem.*, 2008, 5119.

43. T. Ottersen and J. Almolf, *Acta Chem. Scand. A*, 1978, **32**, 219.

44. J. M. Humphrey and A. R. Chamberlin, *Chem. Rev.*, 2006, **97**, 2243.

45. P. D. Beer, N. G. Berry, A. R. Cowley, E. J. Hayes, E. C. Oates and W. W. H. Wong, *Chem. Commun.*, 2003, 2408.

46. S. Heng, K. A. Stieglitz, J. Eldo, J. Xia, J. P. Cardia and E. R. Kantrowitz, *Biochem.*, 2006, **45**, 10062.

47. A. I. Vogel, A. R. Tatchell, B. S. Furnis, A. J. Hannaford and P. W. G. Smith, *Vogel's Textbook of Practical Organic Chemistry (5th Edition)*, Longman, London, 1989.

48. G. M. Sheldrick, in *SHELXS-97 Programs for the Solution and Refinement of Crystal Structures*, University of Göttingen, Germany, Editon 1997.

49. G. M. Sheldrick, in *SHELXL-97 Programs for the Solution and Refinement of Crystal Structures*, University of Göttingen, Germany, Editon 1997.

Chapter 5

Immobilisation of $[Pt_2(\mu\text{-}S)_2(PPh_3)_4]$ on Polymer Supports

5.1 Introduction

The use of polymeric supports in chemistry enjoys significant interests especially for reagents in solid phase synthesis[1-4] and application of metal complexes in catalysis[5, 6]. Transition metal coordination compounds supported on stable solid polymeric matrices are used in homogenous[7-9] or heterogeneous[5, 10] catalysis. The advantages of supported metal catalysts used for heterogeneous catalysis include the ease of handling and physical separation of the target product(s) from the catalyst and the solid support, thus recycling of the catalyst (especially those containing expensive precious metals)[11] is easier. In addition, they have high thermal stability and solvent tolerance and can be applied in catalysis of high temperature reactions.

Immobilisation of metal fragments on polymer supports can be achieved in two different ways. Polymer materials that have been functionalised with a good ligating organic group can be coordinated/linked to a metal fragment. An example is the palladium supported compound (Scheme 5.1) prepared by the reaction of PS-PPh_2 with $PdCl_2(Cod)$[12] (where PS = polystyrene framework).

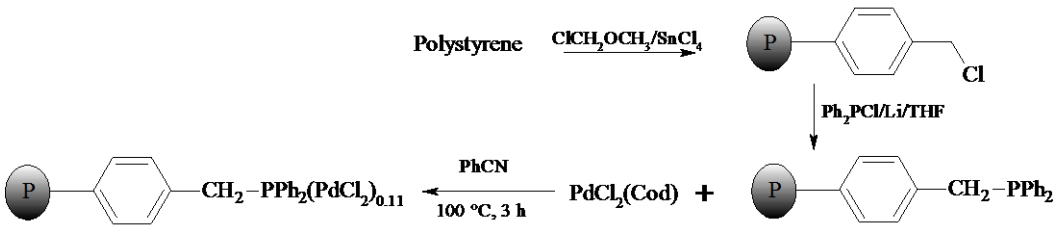

Scheme 5.1 Synthesis of polymer-bound $PdCl_2$ (adopted from ref [13, 14])

Secondly, a metal complex containing an appropriate reactive site can be coupled to a support[15]. An example is the immobilisation of an NCN-palladium pincer complex on functionalised silica[16] (Scheme 5.2). In both cases the polymer surface is modified or functionalised to achieve a desired target in catalysis or synthesis. Common materials used as supports for metal complexes and reagents include silica, polysiloxane, controlled pore glass, polystyrene etc. For instance, silica can easily be modified with desired organic and inorganic functionalities[6, 17].

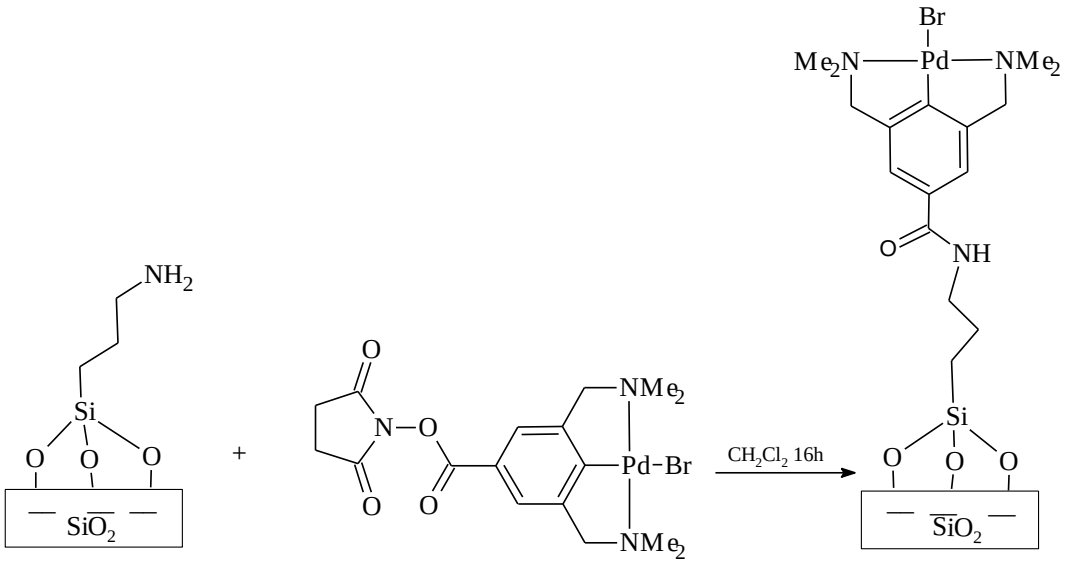

Scheme 5.2 Immobilised NCN-Pd halide complex via an amine functionalised silica (adopted from ref [16].

Results from the investigations in the previous chapters 2-4 showed that any suitable functionalised organic moiety can be incorporated into $[Pt_2(\mu\text{-}S)_2(PPh_3)_4]$ **1.1** through alkylation[18] of one or both of the sulfide centres. The mono or dialkylation of **1.1** by organo-electrophiles can be extended to electrophilic groups, e.g alkyl halides bound to a solid polymer support. Thus, through alkylation, nucleophilic metalloligand $[Pt_2(\mu\text{-}S)_2(PPh_3)_4]$ **1.1** can be immobilised on solid supports. Alternatively, $[Pt_2(\mu\text{-}S)_2(PPh_3)_4]$ can be immobilised through exchange of one or more of the terminal phosphine (PPh_3) ligands with phosphine bound to a polymer support. Both synthetic routes to immobilised **1.1** are expected to lead to synthesis of novel immobilised platinum-sulfide complexes but immobilisation of **1.1** on solid support has never been investigated to date. These productive extensions of the diverging chemistry of **1.1** informed the interest to investigate the immobilisation chemistry of **1.1** on a range of electrophilic solid supports.

The resulting products, which may retain unreacted sulfide centre(s) in **1.1** bound to solid supports, will offer potential advantages as polymeric synthetic templates. In addition, it offers an incentive to a possible application of the stabilised alkylated products in catalysis and solid phase synthesis. Apart from catalytic and synthetic uses of supported metal complexes, polymer surface modifications have been used to create a variance in polymer properties for specific applications. Thus, this investigation will also provide a good incentive to other associated inorganic polymer surface modification chemistry with related system. It is therefore valuable to explore the reactivity of suitable electrophilic solid polymers with **1.1**.

5.2 Results and Discussion

The immobilisation of $[Pt_2(\mu\text{-}S)_2(PPh_3)_4]$ **1.1** on a polymeric support was achieved in two ways. First, is by alkylation of one the sulfide centres with an electrophilic group bound to a polymer support (Scheme 5.3). The resulting product has one unalkylated sulfide centre which is much less reactive than in unreacted **1.1.**

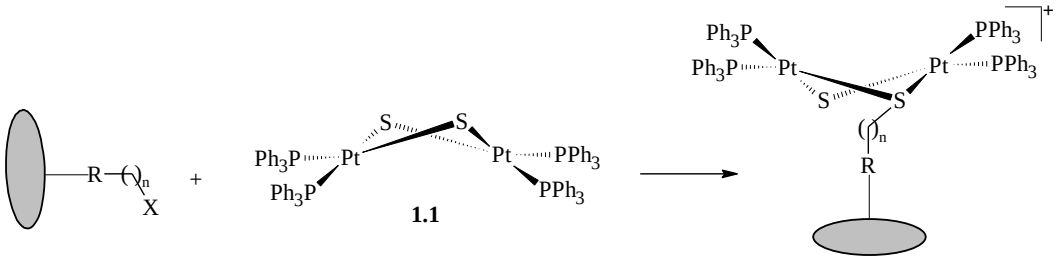

Where $n \geq 1$

Scheme 5.3 Immobilisation of **1.1** by alkylation with electrophilic polymer support.

The second method is by exchange of one or more of the triphenylphosphine (PPh_3) ligands in **1.1** with phosphine ligands bound to a polymer support; an example is shown in Scheme 5.4. The resulting product in this case has two unreacted sulfide centres on the $\{Pt_2(\mu\text{-}S)_2\}$ moiety. Investigations of the immobilisation chemistry of **1.1** through both methods are discussed in the following sections.

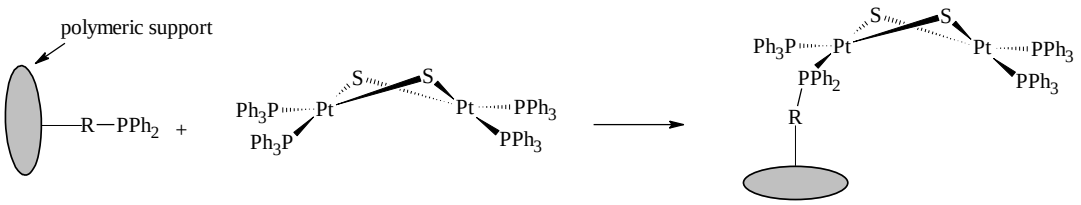

Scheme 5.4 Immobilisation of **1.1** by phosphine exchange reaction

5.2.1 Immobilisation of $[Pt_2(\mu\text{-}S)_2(PPh_3)_4]$ by Alkylation

Alkyl bromides and alkyl chlorides inevitably only give monoalkylated products with **1.1**. An example is the reaction of excess n-butyl bromide or benzyl chloride ($PhCH_2Cl$) to give derivative $[Pt_2(\mu\text{-}S)(\mu\text{-}SBu)(PPh_3)_4]$[19] and $[Pt_2(\mu\text{-}S)(\mu\text{-}SCH_2Ph)(PPh_3)_4]$[20] respectively. Therefore, it is expected that the immobilisation of **1.1** on polymer electrophiles will involve monoalkylation. Following the method outlined in Chapter two, the reaction of a model compound of 3-chloropropyltriethoxysilane **5.1a** (an electrophilic siloxane monomer) with **1.1** (Scheme 5.5) was monitored by ESI-MS. The reaction was completed after 5 hours of refluxing in 100% ethanol with the addition of NaBr. The ESI-MS indicated a simple spectrum with *m/z* 1708, 100% and a very minor unidentified peak at *m/z* 1875, 2%. The stable compound was isolated as the BPh_4^- salt $[Pt_2(\mu\text{-}S)(\mu\text{-}SCH_2(CH_2)_2Si(OEt)_3(PPh_3)_4](BPh_4)$ **5.1b·BPh$_4$** by the addition of excess $NaBPh_4$. Further characterisation of the product by NMR and ESI-MS was in agreement with the structure in Scheme 5.5.

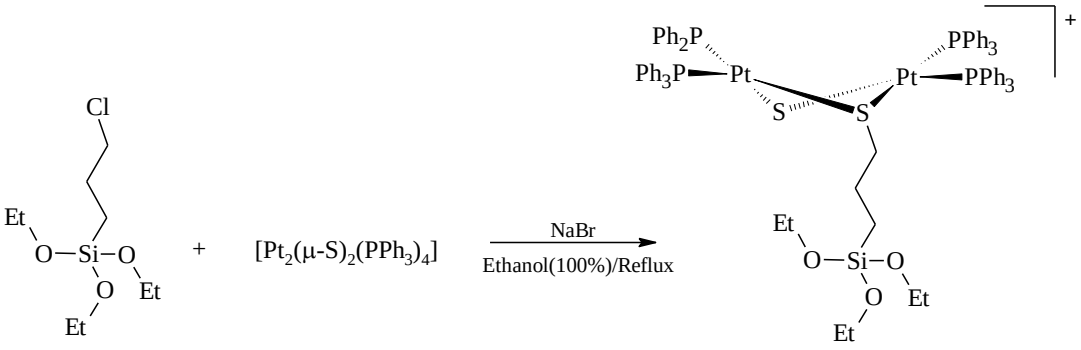

Scheme 5.5 Synthesis of silane thiolate $[Pt_2(\mu\text{-}S)(\mu\text{-}SCH_2(CH_2)_2Si(OEt)_3)(PPh_3)_4]^+$ **5.1b**

The investigations of immobilisation reactions of $[Pt_2(\mu\text{-}S)_2(PPh_3)_4]$ with polymer solid support bound electrophilies used; Merrifield's resin (chloromethylated polystyrene) **5.2a**, bromopropylpolysiloxane **5.3a,** chloropropylsilica **5.4a,**

and chloropropyl functionalised controlled pore glass **5.5a**. $[Pt_2(\mu\text{-}S)_2(PPh_3)_4]$ is insoluble in most hydrocarbon solvents but sparingly soluble in methanol. Merrifield's resin is reported to have maximum swelling in toluene[3]. Thus a combination of methanol and toluene was used for the reaction of $[Pt_2(\mu\text{-}S)_2(PPh_3)_4]$ **1.1** and Merrifield's resin **5.2a**. Merrifield's resin was first swollen in toluene for 4 hours and stirred with **1.1** in an equal volume of methanol. The quantities of the product isolated from three experiments using the same quantity of reactants showed the reaction gave optimum yield of the yellow alkylated product $[Pt_2(\mu\text{-}S)(\mu\text{-}SCH_2C_6H_4\text{–MR})(PPh_3)_4]^+$ **5.2b** (where –MR represents the polymer framework) after 48 hours. Scheme 5.5 shows a simplified alkylated product of the reaction of Merrifield's resin with a sulfide centre in **1.1**.

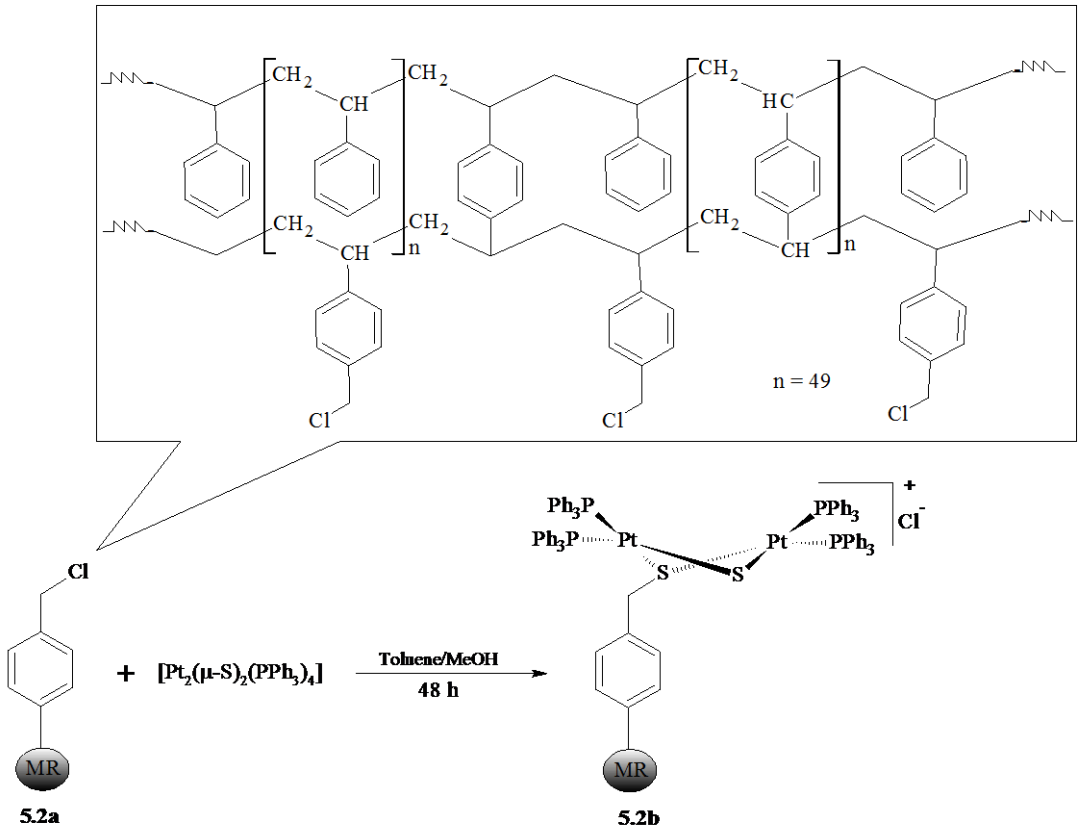

Scheme 5.6 Immobilisation of $[Pt_2(\mu\text{-}S)_2(PPh_3)_4]$ on Merrifield's Resin by alkylation reaction

$[Pt_2(\mu\text{-}S)_2(PPh_3)_4]$ appeared not to show reaction with chloropropyl polysiloxane **5.3** in methanol. The reaction mixture remained a mainly orange suspension after 48 hours. It turned white when washed with CH_2Cl_2 because $[Pt_2(\mu\text{-}S)_2(PPh_3)_4]$ was readily soluble in and reacts with CH_2Cl_2[21]. However, the bromide analogue (bromopropylpolysiloxane) **5.3a** (see Figure 5.1) synthesised by alteration of the literature procedure[22] reacted with **1.1** to give a yellow solid of

the immobilised product **5.3b** (see Table 5.1) and was isolated after 48 hours. A synthetic route to immobilising **1.1** on chloropropylpolysiloxane is by intercepting the reaction of excess **5.1a** with **1.1** upon complete formation of **5.1b** followed by the addition of appropriate quantities of tetraethylammonium hydroxide solution, water, tetraethyl orthosilicate and dimethyl amine. This gave a pale yellow $[Pt_2(\mu\text{-}S)_2(PPh_3)_4]$ immobilised product **5.3c**. This method could be used to moderate the quantity and dispersion of **1.1** in the polymer. While **5.3b** is a polysiloxane polymer surface functionalised with $[Pt_2(\mu\text{-}S)_2(PPh_3)_4]$, **5.3c** is random copolymer with dispersed $[Pt_2(\mu\text{-}S)(\mu\text{-}SCH_2(CH_2)_2Si(OEt)_3)(PPh_3)_4]^+$ **5.1b** monomers in the polymer framework. Chloropropylsilica **5.4a** (Figure 5.1) reacted with **1.1** showing the same colour change as in the case of **5.2a**. The reaction was completed to give a maximum quantity of the corresponding immobilised product **5.4b** after 48 hours. Using the same reaction conditions chloropropyl-functionalised controlled pore glass (CPG) **5.5a** reacted with **1.1** and yielded a bright yellow powdery product **5.5b** after 48 hours of stirring. In each synthesis, the product was isolated by filtering the solid product in a No. 3 sintered glass under suction. The residue was washed repeatedly with CH_2Cl_2 because any excess $[Pt_2(\mu\text{-}S)_2(PPh_3)_4]$ in the alkylation reaction can easily be removed because it is highly soluble in CH_2Cl_2 and $CHCl_3$[21]. The isolated products are left under vacuum to dry to a constant mass. In each case, different reaction time was used to determine optimum yield. The reactions showed a maximum yield of the products after 48 hours.

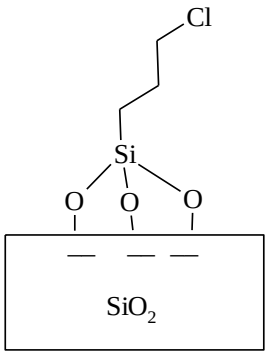

5.4a

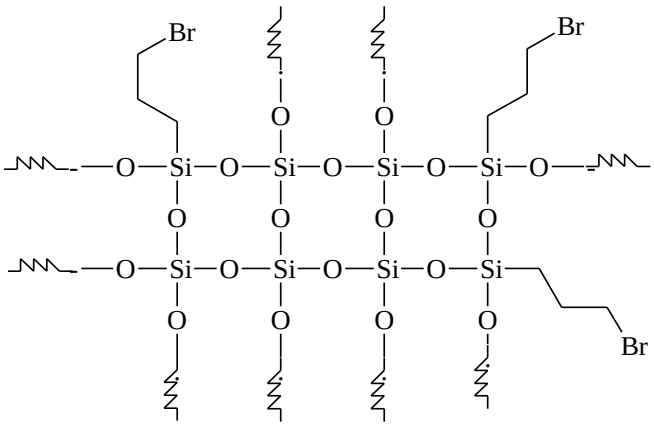

5.3a

Figure 5.1 Simplified structures of **(5.4a)** chloropropyl silica and **(5.3a)** bromopropyl polysiloxane

Table 5.1 Colours of the polymers and the corresponding products with $[Pt_2(\mu\text{-}S)_2(PPh_3)_4]$ after washing with CH_2Cl_2

Polymer	**Colour**	**Colour of Product after washing with CH_2Cl_2**
Merrifield's Resin	white	yellow
3-Bromopropyl polysiloxane	white	yellow
3-Chloropropylsilica	white	yellow
3-Chloropropyl controlled-pore glass	white	bright yellow
Polystyrene	white	white
Silica gel	white	white
Controlled pore glass	white	white

The reaction of **1.1** with polystyrene, silica, and controlled pore glass was done as a control experiment for the reactions of the chloropropyl functionalised derivatives. The formation of the alkylated polymers products of **1.1** was indicated by the colour change of the reaction mixture of the polymeric electrophiles and **1.1** from orange to yellow and the yellow colour of the isolated product after washing with CH_2Cl_2. The absence of colour in the control after washing with CH_2Cl_2 indicates no adsorption of $\{Pt_2(\mu\text{-}S)_2\}$. Further characterisation of the products was done by Scanning Electron Microscopy (SEM), elemental analysis (Pt) by Inductively Coupled Plasma Mass Spectrometry (ICP-MS), $^{31}P\{H\}$ Cross Polarisation Magic Angle Spinning Nuclear Magnetic Resonance (CP-MAS) NMR and X-ray photoelectron spectroscopy (XPS). These provided further evidence that $[Pt_2(\mu\text{-}S)_2(PPh_3)_4]$ was bound to the solid polymer supports.

The Scanning Electron Microscope (SEM) images of the polymer electrophiles and the isolated compounds were examined. In all cases it appears there are only minor differences in the images between the pure polymer and its immobilised products. An example is the images of the pure Merrifield's resin (A) and the corresponding immobilised product (B) shown in Figure 5.2. There is a difference in the texture of the particles of polymeric electrophile and the **1.1** immobilised products. While Merrifield's resin **5.2a** particles are spherical, very sticky and tends to adhere to any surface, the image of the particles taking with Electron Microscope appears loose and non-sticky. The product **5.2b** which is also spherically shaped particles is brittle and non sticky but appears to be sticking together in the SEM image.

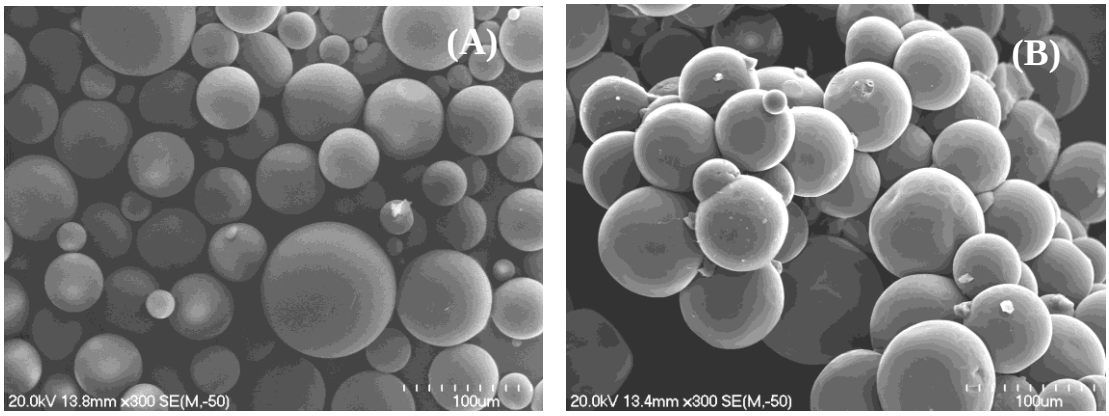

Figure 5.2 Scanning Electron Microscope micrograph image (scale bar 100 μm in each case) of Merrifield's resin **5.2a** (**A**) and $[Pt_2(\mu\text{-}S)_2(PPh_3)_4]$ immobilised on Merrifield's resin **5.2b** (**B**).

5.2.2 Immobilisation of $[Pt_2(\mu\text{-}S)_2(PPh_3)_4]$ by Phosphine Exchange Reactions

One method of immobilising a metal complex containing an exchangeable ligand is by ligand exchange reaction. An example of such ligand is PPh_3. Complexes containing a terminal phosphine ligand can undergo phosphine exchange reaction with phosphine bound on a solid support. For instance the chloride on Merrifield's resin (chloromethylated polystyrene) can be replaced by phosphorus nucleophile e.g. Ph_2P^-. The resulting phosphine group can be exchanged with a PPh_3 of another compound/complex. This reaction was applied to immobilise $[Pt_2(\mu\text{-}S)_2(PPh_3)_4]$ **1.1**. This involves the exchange of the terminal phosphine ligand(s) (PPh_3) in **1.1** with phosphine ligand bound to a polymer support. Scheme 5.7 shows the stepwise reaction through precursors leading to grafting **1.1** onto solid polymer support through its triphenylphosphine ligands.

First, the amine-functionalised polymer **5.6a** was prepared by refluxing polyethertriamine (Jeffamine-T403) with Merrifield's resin **5.2a** in THF for two hours. **5.6a** in THF reacted with excess $[Ph_2P(CH_2OH)_2]Cl$ and aqueous trimethylamine (Me_3N) to incorporate the PPh_2CH_2- linker groups on the amine nitrogen atoms through a Mannich type condensation[23-30] with amine groups (see below) to give the stable diphenylphosphine derivative **5.7a**.

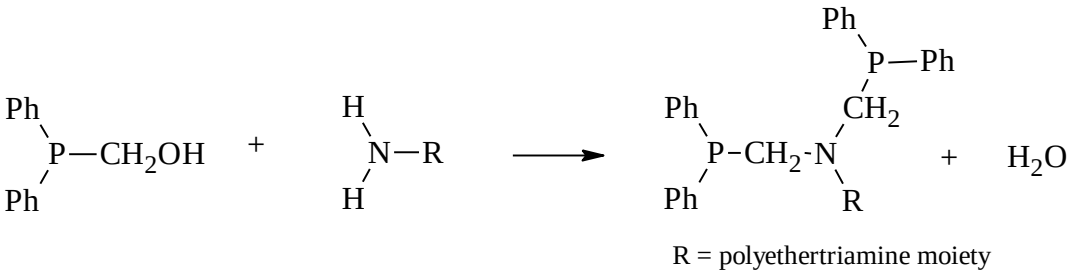

R = polyethertriamine moiety

The reaction of **5.7a** suspended in methanol/benzene (1:1) with excess **1.1** under reflux for 3 hours followed by filtration while hot and a washing with benzene and methanol yielded the immobilised $[Pt_2(\mu\text{-}S)_2(PPh_3)_4]$ product **5.7b**.

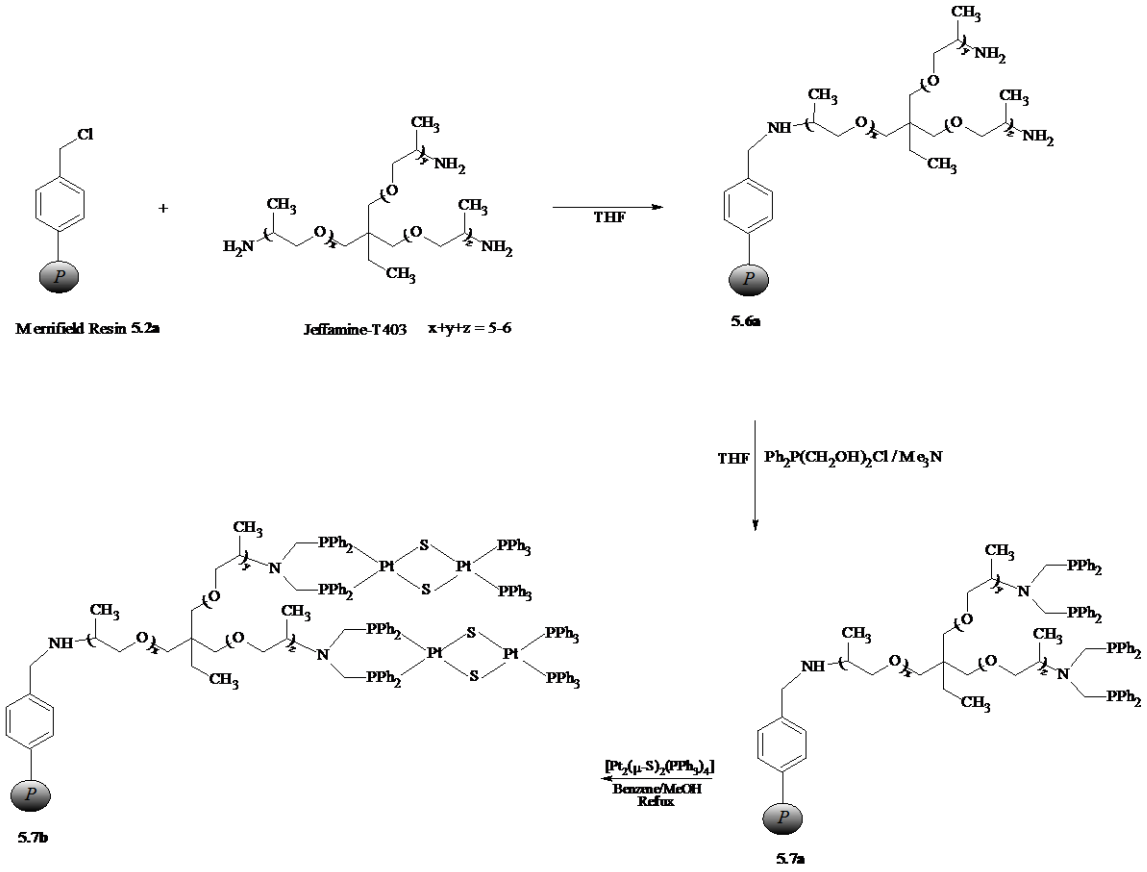

Scheme 5.7 Immobilisation of $[Pt_2(\mu\text{-}S)_2(PPh_3)_4]$ by phosphine exchange reaction

The commercially available diphenylphosphine polystyrene **5.8a** was also reacted with excess **1.1** in methanol/benzene (1:1) under reflux for 24 hours. The reaction mixture was filtered and washed thoroughly with benzene and methanol, dried and resuspended in a large volume of methanol and stirred for 1 hour and filtered to give the product **5.8b** (Scheme 5.8). It is likely that **1.1** may have more than one PPh_3 substituted by DPP. Dichloromethane cannot be used for washing

the phosphine immobilised $[Pt_2(\mu\text{-}S)_2(PPh_3)_4]$ products because the sulfide centers still retained its high nucleophilicity and will react with CH_2Cl_2[21]

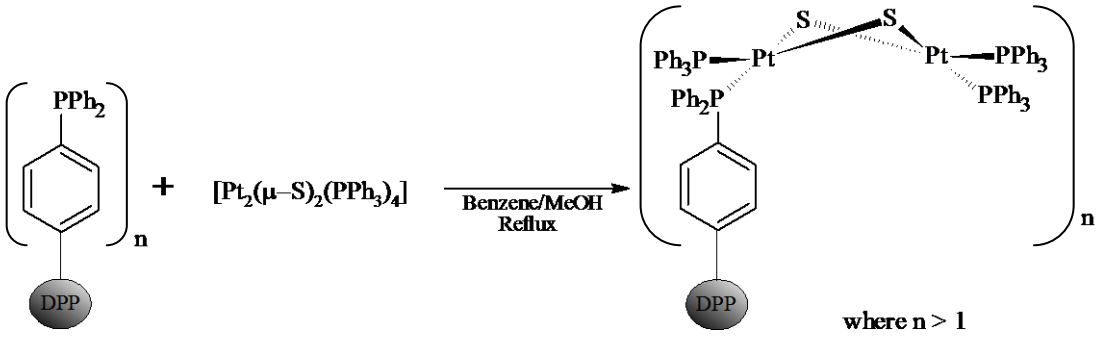

5.8a **5.8b**

Scheme 5.8 Immobilisation of $[Pt_2(\mu\text{-}S)_2(PPh_3)_4]$ on diphenylphosphine polystyrene (DPP) by phosphine exchange reaction.

5.3 Solid State ^{31}P NMR Spectroscopic Characterisation of Immobilised $[Pt_2(\mu\text{-}S)_2(PPh_3)_4]$ Products

The NMR characterisation of $[Pt_2(\mu\text{-}S)_2(PPh_3)_4]$ immobilised on polymer supports was done by $^{31}P\{H\}$ Cross Polarisation Magic Angle Spinning Nuclear Magnetic Resonance (CP-MAS) NMR. The choice of only solid state NMR analysis is due to the limitation imposed by the insolubility of the polymer products in NMR solvents. The NMR of the dried solid products was referenced to $NH_4H_2PO_4$ at 0.81 ppm[31]. The signals from the products were broad and not well resolved compared to liquid state $^{31}P\{H\}$NMR signals of alkylated products of $[Pt_2(\mu\text{-}S)_2(PPh_3)_4]$ **1.1** reported in previous chapters. Consequently, correlation between spectral and structural details is more difficult compared to the simple alkylated products. In addition, a better description of the $^{31}P\{H\}$ (CP-MAS) NMR of the products would have been achieved by comparing the data with literature reports but for the fact that no immobilised compounds of **1.1** have been made or reported. As a result, the $^{31}P\{H\}$ (CP-MAS) NMR spectrum of the solid compounds has therefore been discussed with comparison to the $^{31}P\{H\}$ (CP-MAS) NMR spectrum of $[Pt_2(\mu\text{-}S)_2(PPh_3)_4]$ **1.1** shown in Figure 5.3 and reported solid state ^{31}P NMR of some related phosphorus compounds and $[Pt_2(\mu\text{-}S)(\mu\text{-}SCH_2Ph)(PPh_3)_4](PF_6)$ **5.0·PF$_6$** (Figure 5.4).

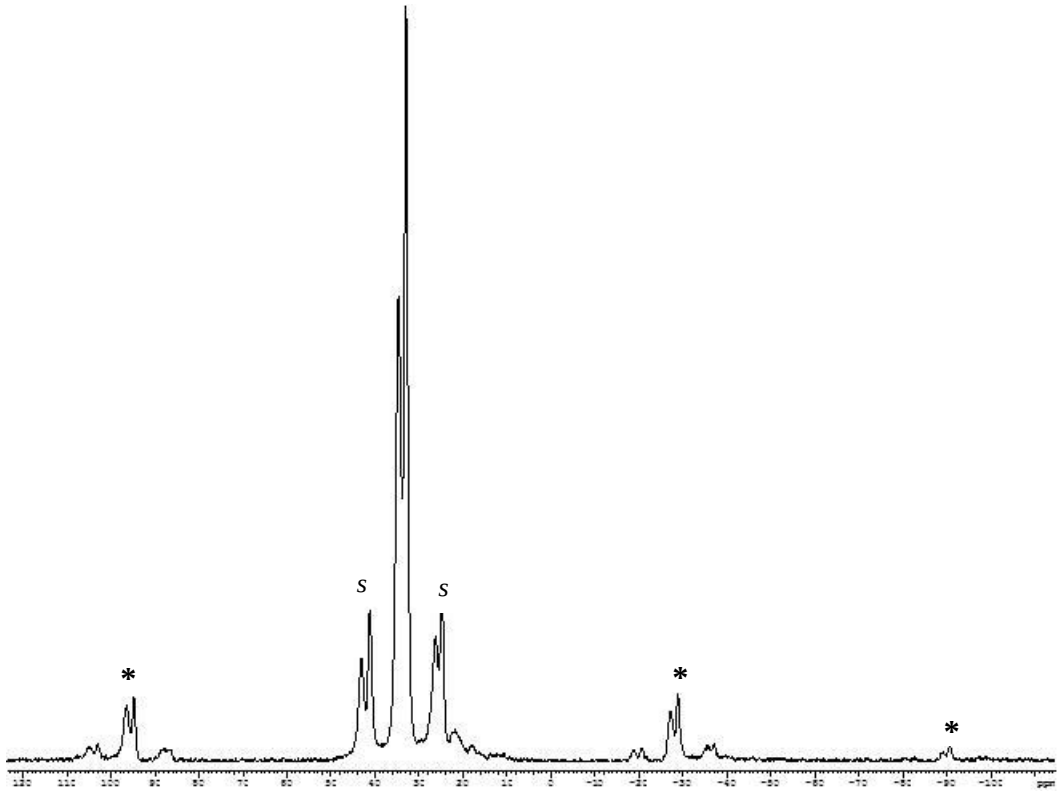

Figure 5.3 The ^{31}P (CP-MAS) NMR spectrum of $[Pt_2(\mu\text{-}S)_2(PPh_3)_4]$ **1.1** with (***s***) the two satellite peaks and (*) the spinning side bands

The four phosphorus atoms in **1.1** are theoretically electronically identical and were expected to show a single resonance. However, the solid state $^{31}P\{H\}$ (CP-MAS) NMR spectrum showed two resonances due to two different PPh_3. The chemical shifts appeared at 33 ppm (major) and 35 ppm (minor) (Figure 5.3). The spectrum also showed two associated satellite peaks (one on each side) of the two signals due to coupling with ^{195}Pt with coupling constants ^1J (Pt-P_A), 2655 and ^1J (Pt-P_B), 2735 Hz respectively. Similar observations were reported in the solid state ^{31}P (CP-MAS) NMR spectrum of cis-$[PtCl_2(PPh_2C_6H_5CH{=}CH_2)_2]$[13]. The existence of two sets of inequivalent phosphorus nuclei may be due the adoption of a fixed conformation in the solid state that reduces the steric effect of the bulky terminal PPh_3 ligands. This explanation is in good agreement with the reported crystal structure of cis-$[PtCl_2(PPh_3)_2]$[32].

$[Pt_2(\mu\text{-}S)(\mu\text{-}SCH_2Ph)(PPh_3)_4](PF_6)$ **5.0·PF$_6$**, of **1.1** has two different sets of phosphorus resonances with the corresponding satellite peaks. The $^{31}P\{H\}$ NMR of the monoalkylated derivative of **1.1** has been discussed in section 2.2.3.2. The liquid state $^{31}P\{H\}$ NMR spectrum of **5.0·PF$_6$** (Figure 5.4(**B**)) showed two

phosphorus resonances at 22.98 and 23.67 ppm with [^1J (Pt-P_A) 2630 Hz and ^1J (Pt-P_B) 3286 Hz] and $^1J_{(P\text{-}F)}$ coupling of PF_6^- of 712 Hz.

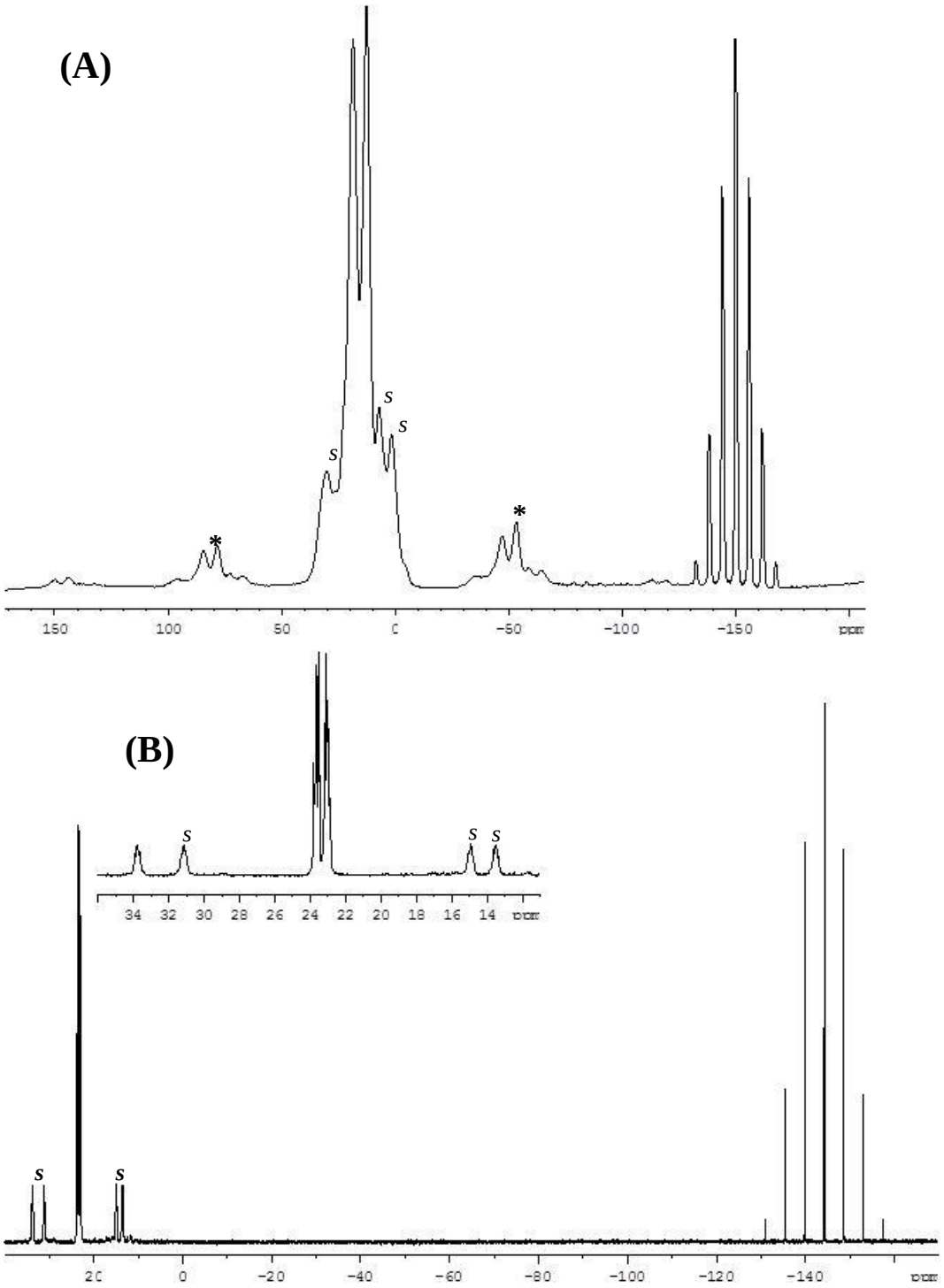

Figure 5.4 The ^{31}P (CP-MAS) NMR (**A**) with (***s***) the two satellite peaks and (*) the spinning side bands and solution phase ^{31}P NMR (**B**) spectrum of $[Pt_2(\mu\text{-}S)(\mu\text{-}SCH_2Ph)(PPh_3)_4](PF_6)$**5.0·PF$_6$**

The $^{31}P\{H\}$ (CP-MAS) NMR (Figure 5.4 (A) also showed two distinct ^{31}P resonance signals at 12.54 and 18.53 ppm for the two different set of phosphorus

environment with corresponding coupling constants [^1J (Pt-P_A) 2655 Hz and ^1J (Pt-P_B) 2798 Hz]. Also observed in the spectrum is the 7-lines around -150 ppm due to PF_6^- anion with $^1J_{(P\text{-}F)}$ 717 Hz. The ^{31}P NMR signals from the compounds **5.2b-5.8b** were broad compared to the signals from **1.1**, thus making it impossible to observe the satellite peaks in the ^{31}P NMR spectra.

All the ^{31}P{H} (CP-MAS) NMR experiments were ran at a spin rate 8 KHz except for **5.0·PF$_6$** and **5.3c** which was at 10 KHz. It was expected that a suitable Spin Rate (SR) and Magic Angle Spinning (MAS) will remove the effect of chemical shift anisotropy and heteronuclear dipolar coupling effect[33, 34]. However, because the spin rate is relatively not high enough, these effects were not entirely eliminated in the ^{31}P{H} (CP-MAS) NMR experiments resulting in poorly resolved signals. Consequently, a set of spinning sidebands were observed in the spectra of the compounds. An example is shown in the spectrum of **1.1** (Figure 5.3) with a set of spinning sidebands signal at -29 ppm and 95 ppm, It also shows a further spinning sideband signal at -91 ppm.

The signals from $[Pt_2(\mu\text{-}S)_2(PPh_3)_4]$ **1.1** immobilised on the polymers showed ^{31}P{H} (CP- MAS) NMR signals expected of the products. Merrifield's resin **5.2a** is a branched random copolymer, thus the "benzyl chloride" branches are repeating irregularly on the polymer backbone. The alkylation reaction of **5.2a** with **1.1** will therefore be expected to give a product in which **1.1** molecules are immobilised on the electrophilic branch/tails in **5.2a** in an irregular pattern. The phosphorus atoms will therefore have different chemical environments and thus the chemical shift of each unit of **1.1** bound to the polymer, $[Pt_2(\mu\text{-}S)(\mu\text{-}SCH_2C_4H_4\text{–}$  $)(PPh_3)_4]$ **5.2b** will be different. The ^{31}P NMR signals of **5.2b** gave broad signals between 0.5 ppm-45 ppm with the corresponding signals due to spinning sidebands. Bromopropylpolysiloxane **5.3a** is a polymer with three-dimensional polysiloxane network-matrix. The ^{31}P{H} (CP-MAS) NMR signals of the immobilised product **5.3b** is thus a reflection of this structure and gave broad overlapping peaks between 5.7 ppm and 34.5 ppm. For the immobilisation product formed with chloropropyl silica **5.4a**, the broad ^{31}P signals came between 8.3 to 34.5 ppm with the signals of spinning sidebands between -45 to -30 ppm and 80 to 92 ppm. The product **5.5b** from the reaction of **1.1** with chloropropyl controlled pore glass gave signals between 1.8 and 38.6 ppm with spinning

sidebands between -45 to -35 ppm and 80- 90 ppm. Table 5.3 is a summary of the range of the broad $^{31}P\{H\}$ (CP-MAS) NMR chemical shifts signals.

Table 5.2 The ^{31}P NMR chemical shifts of **1.1** and **5.0·PF$_6$**, **5.2b-5.5b** and **5.7b** and **5.8b**.

Code	Compounds	Chemical Shift (ppm)
1.1	$[Pt_2(\mu\text{-}S)_2(PPh_3)_4]$	33.0 and 35.0
5.0·PF$_6$	$[Pt_2(\mu\text{-}S)(\mu\text{-}SCH_2Ph)(PPh_3)_4](PF_6)$	12.5 and 18.5
5.2b	$[Pt_2(\mu\text{-}S)(\mu\text{-}SCH_2C_6H_4$—MR$)(PPh_3)_4]^+$	11.1-36.5
5.3b	$[Pt_2(\mu\text{-}S)(\mu\text{-}SCH_2CH_2CH_2$—PPS$)(PPh_3)_4]^+$	5.7-34.5
5.3c	$[Pt_2(\mu\text{-}S)(\mu\text{-}SCH_2CH_2CH_2$—PPS$)(PPh_3)_4]^+$	8.4-36.3
5.4b	$[Pt_2(\mu\text{-}S)(\mu\text{-}SCH_2CH_2CH_2$—PS$)(PPh_3)_4]^+$	8.3-34.5
5.5b	$[Pt_2(\mu\text{-}S)(\mu\text{-}SCH_2CH_2CH_2$—CPG$)(PPh_3)_4]^+$	1.8-38.6
5.7b	$[Pt_2(\mu\text{-}S)_2($*P*$\text{-}PPh_2)_2(PPh_3)_2]$	5.7-45.3
5.8b	$[Pt_2(\mu\text{-}S)_2($DPP$\text{-}PPh_3)_4]$	10.7-51.7

MR, PPS, PS, CPG, *P* and DPP are Merrifield's resin, polypropylsiloxane, propylsilica controlled pore glass, polyether triamine-Merrifield's resin and diphenylpolystyrene polymer frameworks respectively.

In the case of immobilised compounds **5.7b** and **5.8b** (Scheme 5.6 and 5.7 respectively) **1.1** was immobilised on the polymers **5.7a** and **5.8a** respectively by phosphine exchange reaction. In **5.7b** there are two sets of chemically inequivalent phosphorus atoms. The two attached to **5.7a** and two phosphorus atoms of two PPh_3 groups of **1.1**. However, Jeffamine T403 moiety is a polymer with three amine branches with different of lengths of $-CH_3CHCH_2O-$ monomers ranging between 5 and 6 units. The chemical shifts of the two sets of phosphorus atoms will therefore not be the same. Thus, the $^{31}P\{H\}$ (CP-MAS) NMR spectrum showed multiple signals of different intensities between 5.7 to 45.3 ppm as shown in Figure 5.5. Apart from the effect of the $^1J_{Pt\text{-}P}$ coupling observed in the **1.1** moiety, another factor that may have contributed to the multiplicity of the peaks is the relatively lower spin rate of the $^{31}P\{H\}$ (CP-MAS)NMR acquisition which have been observed in the report of Bemi *et al* [35]. The spinning sideband was observed between -41 to -25 ppm and 82 and 99 ppm. The signals for **5.8b** were observed between 10.7-51.7 ppm.

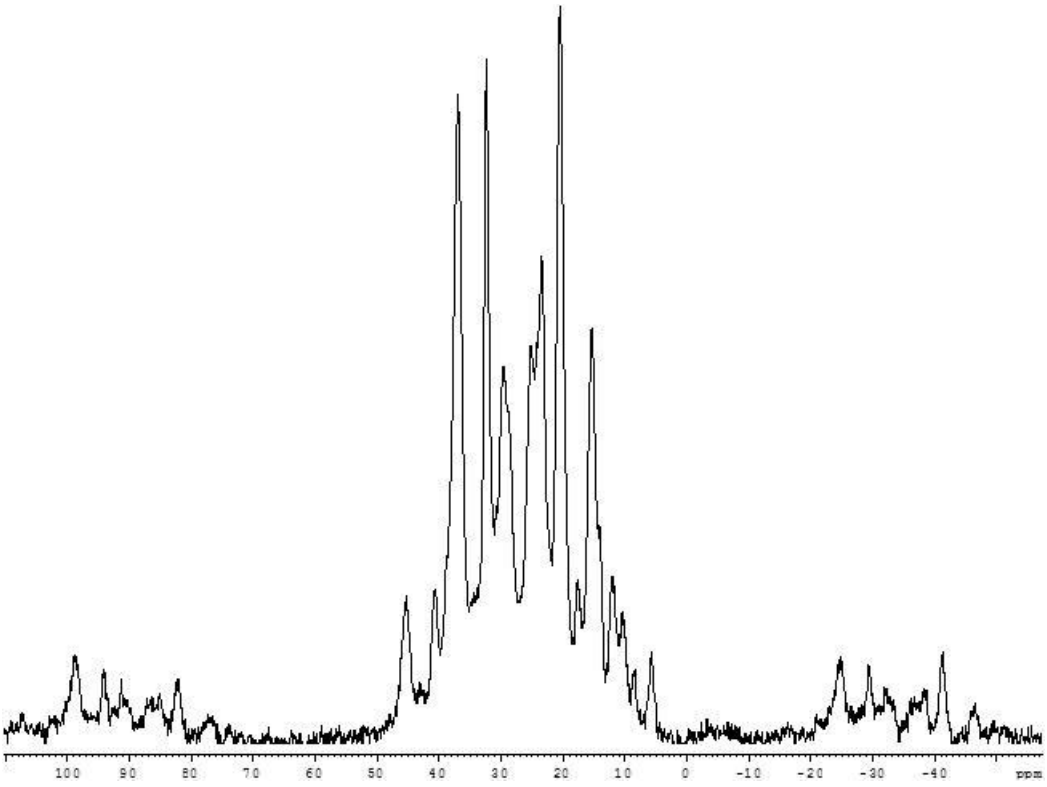

Figure 5.5 The ^{31}P (CP-MAS) NMR spectrum of $[Pt_2(\mu\text{-}S)_2(P(OPh)_2)_2(PPh_3)_2]$ **5.7b**

5.4 Platinum Elemental Analyses by ICP-MS

Elemental (platinum) analyses were done by ICP-MS after ashing and digesting the platinum samples in aqua regia to remove the polymer framework and inorganic contents. The samples were diluted by a factor of 10,000 in type 1 water (details in appendix I). The results from platinum analyses by ICP-MS of **1.1**, $[Pt_2(\mu\text{-}S)(\mu\text{-}SCH_2Ph)(PPh_3)_4](PF_6)$ **5.0b·PF$_6$**, and the immobilised materials **5.2b-5.8b** are shown in Table 5.3. This was done to determine relative content of platinum in the immobilised product of **1.1**. As can be seen from the table, **1.1** and **5.0·PF$_6$** have the highest weight % of platinum at 19.5% and 21% respectively. $[Pt_2(\mu\text{-}S)_2(PPh_3)_4]$ was expected to have the highest quantity of platinum (theoretically, 26%). The lower quantity of platinum recorded may be due to impurities resulting from its synthesis. Understandably, the concentrations of platinum in the immobilised compounds were reduced due to the incorporated polymers. Amongst the polymer compounds **5.2b** has the highest concentration of platinum. This is because it was well swollen in the reaction solvent (THF/ methanol) which increased the sites accessible for alkylation with **1.1**.

Table 5.3 Platinum elemental analyses of **1.1**, **5.0·PF$_6$**, **5.2b**, **5.3b**, **5.4b**, **5.5b**, **5.7b** and **5.8b**

Sample	Weight % Pt
1.1	19.50
5.0b·PF$_6$	21.00
5.2b	12.00
5.3b	6.25
5.4b	7.34
5.5b	3.96
5.7b	10.75
5.8b	10.26

5.5 X-Ray Photoelectron Spectroscopy (XPS)

XPS is a suitable elements sensitive analytical technique for characterising the surface layer of polymers[36], homogenous[37] and heterogeneous catalysts[38, 39] and supported metal complex catalysts[6, 40, 41] and colloidal nanoparticles[42]. XPS studies on the isolated immobilised $[Pt_2(\mu\text{-}S)_2(PPh_3)_4]$ **1.1** complexes were undertaken to show that **1.1** molecules are actually bonded to the accessible electrophilic groups in the polymer supports. XPS characterisation studies on simple monoalkylated and metallated derivatives of **1.1** have been reported by Batisttoni *et al*[43] and Aw *et al*[44]. Extension of this XPS study to the immobilised derivatives will offer an understanding of the chemical nature of atomic layers of the surfaces and its potential applicability in catalysis.

$[Pt_2(\mu\text{-}S)_2(PPh_3)_4]$ **1.1** and the monalkylated compounds $[Pt_2(\mu\text{-}S)(\mu\text{-}SCH_2Ph)(PPh_3)_4](PF_6)$ **5.0·PF$_6$** and $[Pt_2(\mu\text{-}S)(\mu\text{-}SCH_2(CH_2)_2Si(OEt)_3(PPh_3)_4]\text{-}(BPh_4)$ **5.1·BPh$_4$** were considered suitable models for the XPS studies owing to the similarities of the different elemental sites in the compounds with the isolated immobilised compounds thus allowing reasonable correlation to literature reports. The two sulfur atoms, thiolate and the sulfide environments are expected to have slightly different S2p binding energies (B.E). In XPS the B.E. energy increases with oxidation state[37]. Thus, the higher B. E. could be attributed to the higher oxidation states of the thiolate and reduced electron density due to alkylation. This observation is consistent with previous reports[43, 44].

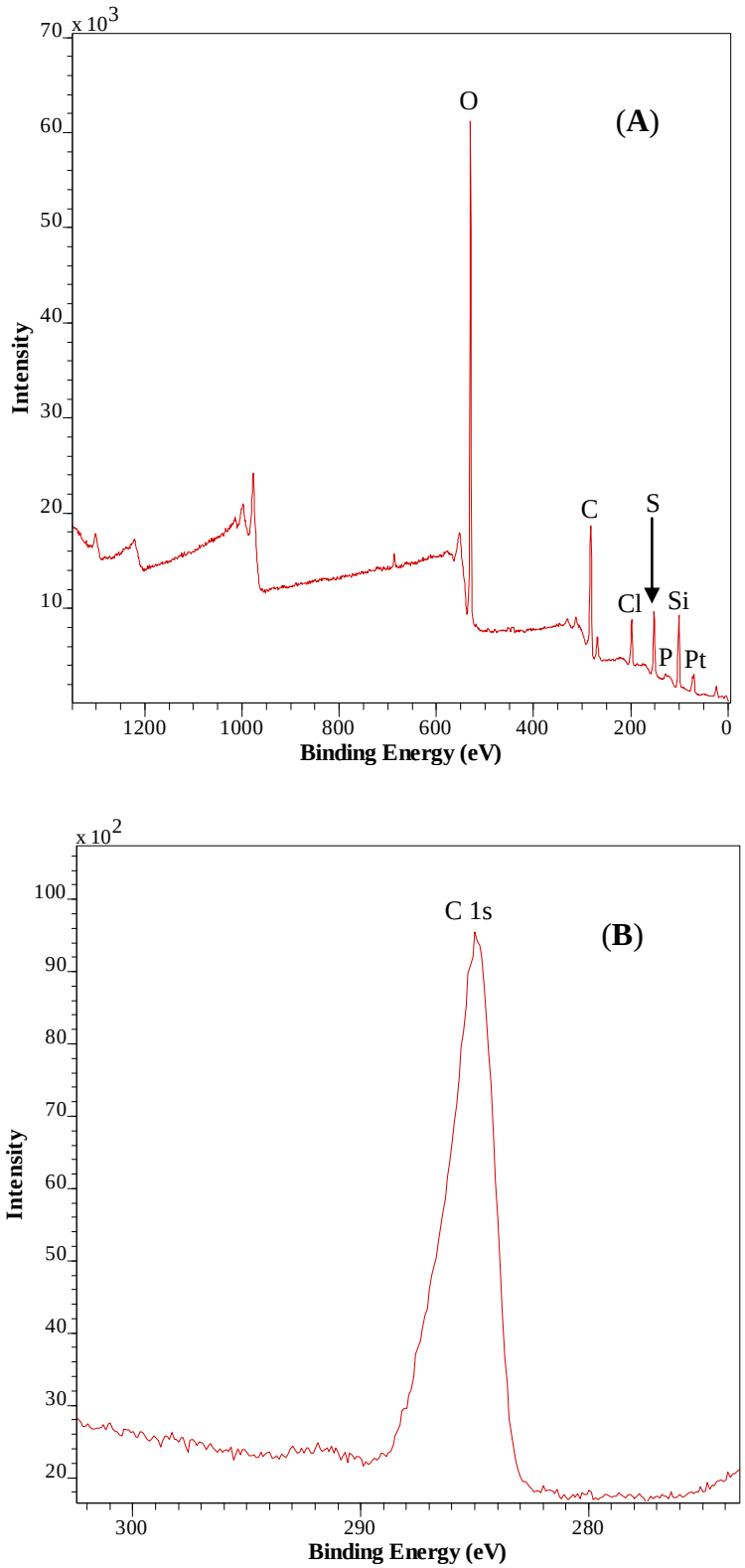

Figure 5.6 Full XPS spectrum **(A)** and the enlarged hydrocarbon peak **(B)** of **5.3b**

The XPS spectra of the immobilised compounds and the model compounds showed a clean hydrocarbon peaks but some other minor peak appeared near the sulfur regions. All the spectra were calibrated and referenced to

the hydrocarbon peak at 285 eV to account for the charging effect[24, 45]. Peaks from phosphorus, platinum, silicon, oxygen etc regions were clearly present, e.g. XPS spectrum and narrow scan of hydrocarbon region of **5.3b** in Figure 5.6.

The $[Pt_2(\mu\text{-}S)_2(PPh_3)_4]$ immobilised compounds XPS studies of the sulfur environment were of particular interest. Analysis of the thiolate and sulfide narrow scan XPS data was done using CasaXPS software. The sulfur environment regions (160 – 164 eV) were created on each spectrum within standard range of sulfide and thiolate regions[46]. $[Pt_2(\mu\text{-}S)_2(PPh_3)_4]$ has two equivalent sulfurs, thus the deconvolution of the S2p peaks gave only two components (see Table 5.4). The sulfur peaks for **5.0·PF$_6$** (see Figure 5.7) and **5.1·BPh$_4$** allowed the extraction of two components ($2p\frac{3}{2}$ and $2p\frac{1}{2}$) in the areas ratio of 2:1 for the two chemical inequivalent sulfur (sulfide and the thiolate) environments.

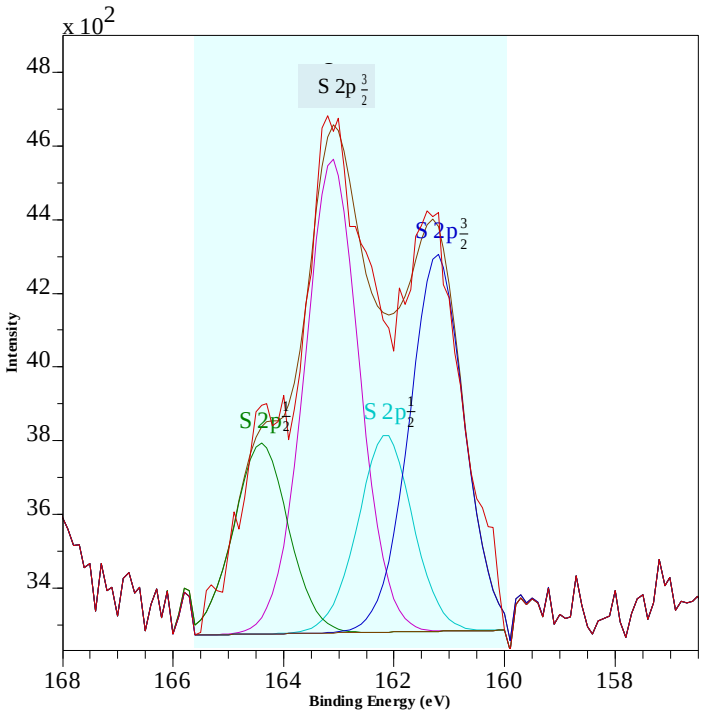

Figure 5.7 Experimental (red), deconvoluted and simulated (green, purple, light blue and blue) S(2p) XPS spectra of $[Pt_2(\mu\text{-}S)(\mu\text{-}SCH_2Ph)(PPh_3)_4]$ (PF_6) **5.0·PF$_6$** showing 1:1 doublet for each 2:1 spin doublet ($2p\frac{3}{2}$ and $2p\frac{1}{2}$) .

The energy difference between the two sulfurs is about 1.67 eV with the higher B.E. attributed to the thiolate. The binding energies of the two sulfurs in the compounds were higher than in **1.1** due to alkylation. A similar observation was reported by Aw *et al*[44] and Battistoni *et al*[43]. There is also considerable

broadening of the sulfur peaks in **5.2b** which allowed only two components to be found with B.E. of 164.35 eV and 162.89 eV. In the compounds with silicon based supports viz **5.3b**, **5.4b** and **5.5b** the two S2p energy levels were also broad and not clearly resolved in the spectrum. The regions created within the sulfide region for these compounds gave only two components each with lower binding energies for both the thiolate and the sulfide environments than in **5.0·PF$_6$** and **5.1·BPh$_4$**. This is not in agreement with the expected result and the reason for this is not known. **5.7b** and **5.8b** has unalkylated sulfide centres similar to the parent compound **1.1** and thus they also gave two components for the S2p spin orbits (2p $\frac{3}{2}$ and 2p $\frac{1}{2}$) with binding energies of [161.23(1.9)and 162.77(1.9) eV] and [160.52(2.4) and 161.17(2.4) eV] respectively.

Table 5. 4 Core-level binding energies (eV) referenced to hydrocarbon peaks 285eV with FWHM values in brackets. MR, PPS, PS, CPG, *P* and DPP are Merrifield's resin, polypropylsiloxane, propylsilica, controlled pore glass, polyethertriamine-Merrifield's resin and diphenylpolystyrene polymer frameworks respectively.

Compound	**S2p**	
	2p $\frac{3}{2}$	2p $\frac{1}{2}$
$[Pt_2(\mu\text{-}S)_2(PPh_3)_4]$	160.75(1.1)	162.16(1.1)
$[Pt_2(\mu\text{-}S)(\mu\text{-}SCH_2Ph)(PPh_3)_4](PF_6)$	163.09(1.3) 161.31(1.3)	164.34(1.3) 162.28(1.3)
$[Pt_2(\mu\text{-}S)(\mu\text{-}SCH_2(CH_2)_2Si(OEt)_3(PPh_3)_4](BPh_4)$	162.89(1.5)	164.35(1.5)
	161.26(1.5)	162.84(1.5)
$[Pt_2(\mu\text{-}S)(\mu\text{-}SCH_2C_6H_4$—(MR))$(PPh_3)_4]^+$	164.21(1.7) 162.88(1.7)	
$[Pt_2(\mu\text{-}S_)(\mu\text{-}SCH_2CH_2CH_2$—(PPS))$(PPh_3)_4]^+$	156.07(1.6) 154.84(1.6)	
$[Pt_2(\mu\text{-}S_)(\mu\text{-}SCH_2CH_2CH_2$—(PPS))$(PPh_3)_4]^+$(**5.3c**)	157.36(2.2) 154.82(2.2)	
$[Pt_2(\mu\text{-}S)(\mu\text{-}SCH_2CH_2CH_2$—(PS))$(PPh_3)_4]^+$	156.62(1.5) 155.49(1.5)	
$[Pt_2(\mu\text{-}S)(\mu\text{-}SCH_2CH_2CH_2$—(CPG))$(PPh_3)_4]^+$	156.63(1.2) 155.47(1.2)	
$[Pt_2(\mu\text{-}S)_2($(*P*)$—PPh_2)_2(PPh_3)_2]$	161.23(1.9)	162.77(1.9)
$[Pt_2(\mu\text{-}S)_2($(DPP)$—(PPh_3)_4]$	160.52(2.4)	161.17(2.4)

5.6 Conclusion

$[Pt_2(\mu\text{-}S)_2(PPh_3)_4]$ **1.1** has been successfully immobilised on polymeric supports either through alkylation of one of the sulfide centres or through a phosphine exchange reaction. Because no such studies have been carried out before, the immobilisation of **1.1** on polymeric supports is a novel development in the chemistry of this system. Transition metal complexes with sulfur ligands are known to act as good catalysts[7]. Thus the isolated products offer a potential application as valuable catalyst or synthetic templates for related products. The advantage of the possible heterogeneous catalytic application of immobilised $[Pt_2(\mu\text{-}S)_2(PPh_3)_4]$ is the ease of recovering the expensive catalyst which will make it economical. However, the challenges that may be faced by the use of the **1.1** on polymer support compounds is that it has reactive sulfide sites which may limit the choice of reaction and solvents for its applications.

5.7 Experimental

3-Chloropropyl polysiloxane was synthesised by modification of the literature procedure[22] with the addition of water to promote hydrolysis and condensation. The polymer supports, 3-chloropropyl silica, chloropropyl-functionalised controlled pore glass and silica and controlled pore glass, were synthesised in the Chemistry Department, University of Waikato by William Henderson following the procedures in section 5.7.1. 3-Bromopropyl polysiloxane was made by stirring 3-chloropropyl polysiloxane with excess NaBr for six hours in methanol. $Ph_2P(CH_2OH)_2Cl$ was synthesised according to literature procedures[47]. Merrifield's Resin, (2% crosslinked chloromethylated polystyrene, Sigma-Aldrich), triphenylphosphine polymer bound (Sigma-Aldrich), trimethylamine (BDH) and polystyrene (Sigma-Aldrich) and Jeffamine-T403 (polyethertriamine) (Texaco) was used as supplied. Solvents; benzene and THF are supplied by BDH. Dichloromethane, toluene, methanol were drum grade solvents and were used as supplied. The SEM images were acquired from a Hitachi S-4700 Field Emission Electron Microscope and the $^{31}P\{H\}$ (CP-MAS) NMR data of the compounds; **1.1**, **5.0b·PF$_6$**, **5.2b**, **5.3b**, **5.4b**, **5.5b**, **5.7b** and **5.8b** were acquired on Bruker DRX 400 at the National University of Singapore. The $^{31}P\{H\}$(CP-MAS) NMR data of **5.0·PF$_6$** and **5.3c** were acquired on Bruker DRX 300 at the University of

Waikato. The XPS spectra of the dried powder samples of the immobilised compounds were obtained from the University of Auckland. The spectra were obtained using Al K_α source (energy 1486.7 eV) Kratos Axis Ultra spectrometer. All the spectra were calibrated to the hydrocarbon C 1s peak at 285 eV to account for charging effects. For the analysis of the sulphide and thiolate, narrow-scan XPS data were recorded using casa XPS software by fitting spectral splitting curves. All deconvolution of the narrow scans was carried out using linear baselines.

5.7.1 Synthesis of the Solid Supports

Activation of silica gel

Silica gel (BDH, 100-200 mesh, ca 100g) was activated by refluxing in 100 mL of 10% nitric acid for 2 hours. After cooling, the silica was filtered, washed with copious quantities of distilled water and dried in an oven at 100 °C for 24 hours.

Preparation of 3-chloropropyl silica (5.4a)

Activated silica gel (10.0 g) was suspended in AR xylene (65 mL) and 3-chloropropyl triethoxysilane (Aldrich, 3.5 mL) added. The suspension was refluxed under nitrogen for 7 hours. The solid was filtered, washed successively with xylene (2 x 30 mL), water (2 x 50 mL), isopropanol (30 mL) and hexane (30 mL) and dried for 12 at 100 °C to give the product (11.8 g)

Activation of glass beads

Glass beads (BDH, 100 mesh, ca 100g) were activated by refluxing in 150 mL of 10% nitric acid for 3 hours. After cooling, the beads were filtered, washed with copious quantities of distilled water and dried in an oven at 100 °C for 24 hours.

Preparation of 3-chloropropyl glass

Following the general method for the preparation of 3-chloropropyl silica, activated glass beads (26.0 g) in xylene (40 mL) and 3-chloropropyl triethoxysilane (7 mL) gave the product (26.0 g).

Activation of controlled pore glass beads

Controlled-pore glass beads (Sigma-Aldrich, 80-120 mesh, mean pore diameter 1049 Å, surface area 22.7 m^2 g^{-1}, 10 mL) were activated by refluxing in 100 mL of 10% nitric acid for 3 hours. After cooling, the beads were filtered, washed with copious quantities of distilled water and dried in an oven at 100 °C for 24 hours.

Preparation of 3-chloropropyl controlled pore glass (5.5a)

Following the general method for the preparation of 3-chloropropyl silica, activated controlled pore glass beads (4.60 g) in xylene (30 mL) and 3-chloro-propyl triethoxysilane (4 mL) on refluxing for 11 hours gave the product (4.84 g).

Preparation of 3-chloropropyl polysiloxane (5.3a)

To methanol (75 mL) was added tetraethoxysilane (Aldrich, 21.4 mL), 3-chloropropyl triethoxysilane (11.6 mL) and water (10 mL) and the mixture stirred to give a clear solution. To the stirred mixture was added 4 drops of 20% tetraethylammonium hydroxide solution (Aldrich), and the mixture allowed to stand overnight. To the resulting turbid solution was added 3 drops of dimethylamine (40% solution in water, BDH) and water (30 mL), rapidly forming a white gel. The mixture was allowed to stand for 24 hours, giving a thick gel. The solid was broken up and allowed to air dry, followed by drying in an oven at 100 °C for 24 hours. The white polymer was ground to a fine powder in a pestle and mortar, and then stirred for 1 hour in a mixture of water (50 mL) and isopropanol (25 mL). The solid was filtered, washed with copious amounts of distilled water and isopropanol and then dried at 100 °C to give 10.20 g of product.

5.7.1.1 Synthesis of $[Pt_2(\mu\text{-}S)(\mu\text{-}SCH_2(CH_2)_2Si(OEt)_3(PPh_3)_4](BPh_4)$ 5.1·BPh_4

To an orange suspension of $[Pt_2(\mu\text{-}S)_2(PPh_3)_4]$ (0.1 g) in ethanol (25 mL) was added NaBr (0.05 g) and excess $ClCH_2CH_2CH_2Si(OEt)_3$ (12 drops). The mixture was stirred and refluxed for 5 hours to give a clear pale yellow solution. ESI-MS of the solution indicated a complete formation of the product. The solution was gravity filtered to remove any solid particles and excess $NaBPh_4$ (43 mg) was

added to precipitate the product. The product was filtered and air dried to give a pale yellow powder of the product **5.1·BPh_4** (0.0678 g, 50% yield)

m.p. 127-129 ºC

$^{31}P\{^1H\}$ NMR: δ_P = 24.1 ppm [*br m*, ^1J(Pt-P_A) 2611 Hz, ^1J(Pt-P_B) 3241Hz]

^1H NMR (400 MHz, $CDCl_3$): δ_H = 0.78 (2H, *m* CH_2), 0.16 (2H, *tr*, $SiCH_2$), 2.19 (2H, *br/m*, SCH_2), 3.73 (6H, *q*, O-CH_2), 1.20 (*tr*, 9H, -CH_3), 6.87-7.40 (65H, *m*, 12Ph),

IR (KBr): υ 524, 693, 1096, 1435, 1632 and 3446 cm^{-1}

ESI-MS: *m/z*: 1708 ($[M]^+$, 100%).

5.7.2 Synthesis of $[Pt_2(\mu\text{-}S)_2(PPh_3)_4]$ Immobilised Products

Immobilisation of $[Pt_2(\mu\text{-}S)_2(PPh_3)_4]$ on Merrifield's Resin

Merrifield's resin (0.1 g) was added to mixture of toluene (7.5 mL) and methanol (7.5 mL) and left to swell for 4 hours. $[Pt_2(\mu\text{-}S)_2(PPh_3)_4]$ (0.1503 g) was added to the mixture and stirred for 48 hours. The yellow product was filtered under suction with No 3 sintered glass, washed repeatedly with chloroform (3 x 20 mL) and methanol (3 x 20 mL) and dried under vacuum to give 0.1912 g of the product **5.2b**.

Immobilisation of $[Pt_2(\mu\text{-}S)_2(PPh_3)_4]$ on 3-bromopropyl polysiloxane

3-Bromopropylpolysiloxane (0.1 g) and $[Pt_2(\mu\text{-}S)_2(PPh_3)_4]$ (0.1 g) in methanol (20 mL) were stirred for 48 hours. The yellow product was filtered under suction with No 3 sintered glass, washed with CH_2Cl_2 (2 x 20 mL) and dried under vacuum to give 0.1698 g of the product **5.3b**.

Synthesis of 5.3c

To an orange suspension of $[Pt_2(\mu\text{-}S)_2(PPh_3)_4]$ (0.2 g) in ethanol (25 mL) was added NaBr (0.05 g) and excess $ClCH_2CH_2CH_2Si(OEt)_3$ (20 drops). The mixture was stirred and refluxed for 5 hours to give a clear pale yellow solution. ESI-MS was used to confirm the complete formation of $[Pt_2(\mu\text{-}S)(\mu\text{-}SCH_2(CH_2)_2Si\text{-}(OEt)_3(PPh_3)_4]^+$. To the resulting solution was added 3 mL of tetraethyl orthosilicate, 3 mL of water and the mixture stirred to a clear solution. To the

stirred mixture was added 2 drops of 20% tetraethylammonium hydroxide solution (Aldrich), and the mixture allowed to stand overnight. To the resulting turbid solution was added 3 drops of dimethylamine (40% solution in water, BDH). The mixture was allowed to stand for 24 hours, giving a light yellow solid which was filtered and crushed, washed with water and dried in oven at 100 ºC for 24 hours to give 0.9711 g of **5.3b**

Immobilisation of $[Pt_2(\mu\text{-}S)_2(PPh_3)_4]$ on 3-chloropropyl silica

Chloropropylsilica (0.1 g) and $[Pt_2(\mu\text{-}S)_2(PPh_3)_4]$ (0.1 g) in methanol (20 mL) was stirred for 48 hours. The yellow product was filtered under suction with No 3 sintered glass, washed with CH_2Cl_2 (2 x 20 mL) and dried under vacuum to give 0.1345 g of the product **5.4b**.

Immobilisation of $[Pt_2(\mu\text{-}S)_2(PPh_3)_4]$ on chloropropyl-functioanlised controlled pore glass

Chloropropyl-functionalised controlled pore glass (0.1 g) and $[Pt_2(\mu\text{-}S)_2(PPh_3)_4]$ (0.1 g) in methanol (20 mL) was stirred for 48 hours. The resulting bright yellow product was filtered under suction with No. 3 sintered and was washed with CH_2Cl_2 (60 mL) and dried under suction to give 0.1450 g of the product **5.5b**.

Immobilisation of $[Pt_2(\mu\text{-}S)_2(PPh_3)_4]$ on polyethertriamine (Jeffamine-T403) functionalised Merrifield's resin by phosphine exchange

Merrifield's Resin (3 g) was added to THF (60 mL) and left to swell for four hours. polyethertriamine (Jeffamine-T403) (8 mL) was added to the suspension and the mixture stirred under reflux for 2 hours. The resulting product was filtered off and washed repeatedly with THF (3 x 20 mL). The resulting product was resuspended in THF (10 mL) and excess $Ph_2P(CH_2OH)_2Cl$ (3 g) and Me_3N(3 g) added and the mixture stirred for 45 minutes. A drop of the solution when tested with $NiCl_2$(aq) to give an orange colour confirming the presence of excess Ph_2PCH_2OH. The product was filtered and washed with THF (2 x 20 mL) and MeOH (2 x 20 mL). 0.50 g of the product and 0.51g of $[Pt_2(\mu\text{-}S)_2(PPh_3)_4]$ in

1:1 benzene/methanol was refluxed for 4 hours. The final product was filtered and washed with benzene and methanol (2 x 30 mL each) and dried under vacuum. The product was resuspended in methanol (40 mL) and stirred for 4 hours at room temperature, filtered, washed with methanol (2 x 30 mL) and dried under vacuum to give 0.4340 g of the final product **5.7b**.

Immobilisation of $[Pt_2(\mu\text{-}S)_2(PPh_3)_4]$ on diphenylphosphine polystyrene

$[Pt_2(\mu\text{-}S)_2(PPh_3)_4]$ (1.0 g) and diphenylphosphine polystyrene (0.1 g) in 1:1 methanol/benzene was stirred under reflux for 24 hours. The yellow product was filtered under suction with No 3 sintered glass, washed with methanol (2 x 30 mL), and dried by suction. The product was resuspended in methanol (40 mL) and stirred for 1 hour, filtered and dried under vacuum for 24 hours and gave 0.1714 g of the immobilised product **5.8b**.

5.8 References

1. M. A. Youngman and S. L. Dax, *J. Comb. Chem.*, 2001, **3**, 469.
2. M. Hori, D. J. Gravert, P. Wentworth Jr and K. D. Janda, *Bioorg. and Med. Chem. Letters*, 1998, **8**, 2363.
3. A. R. Vaino, D. B. Goodin and K. D. Janda, *J. Comb. Chem.*, 2000, **2**, 330.
4. P. Li, L. Wang, M. Wang and Y. Zhang, *Eur. J. Org. Chem.*, 2008, **2008**, 1157.
5. E. Błaż and J. Pielichowski, *Molecule*, 2006, **11**, 115.
6. F. R. Hartley and P. N. Vezey, in *Adv. Organomet. Chem.*, Academic Press N. Y., Editon edn., 1977, p. 189.
7. J. C. Bayón, C. Claver and A. M. Masdeu-Bultó, *Coord. Chem.Rev.*, 1999, **193-195**, 73.
8. D. C. Sherrington, *Pure and Appl. Chem*, 1998, **60**, 401.
9. A. L. Robinson, *Science* 1976, 1261.
10. M. J. Alcón, A. Corma, M. Iglesias and F. Sánchez, *J. Organomet. Chem.*, 2002, **655**, 134.
11. C. A. McNamara, M. J. Dixon and M. Bradley, *Chem Rev.*, 2002, **102**, 3275.
12. K. Inada and N. Miyaura, *Tetrahedron*, 2000, **56**, 8661.

13. C. A. Fyfe, J. A. Davies, H. C. Clark, P. J. Hayes and R. E. Wasylishen, *J. Am. Chem. Soc.*, 1983, **105**, 6577.
14. K. Inada and N. Miyaura, *Tetrahedron*, 2000, **56**, 8661.
15. A. Choplin and F. Quignard, *Coord. Chem. Rev.*, 1998, **178-180**, 1679.
16. N. C. Mehendale, C. Bezemer, C. A. van Walree, R. J. M. Klein Gebbink and G. van Koten, *J. Mol. Cat. A: Chem.*, 2006, **257**, 167.
17. P. M. Price, H. C. Clark and D. J. Macquarrie, *J, Chem Soc., Dalton Trans*, 2000, 101.
18. O. T. Ujam, S. M. Devoy, W. Henderson, B. K. Nicholson and T. S. A. Hor, *Inorg. Chim. Acta*, 2010, **363**, 3558.
19. W. Henderson, B. K. Nicholson, S. M. Devoy and T. S. A. Hor, *Inorg. Chim. Acta*, 2008, **361**, 1908.
20. S. H. Chong, W. Henderson and T. S. A. Hor, *J. Chem. Soc., Dalton Trans.*, 2007, 4008.
21. S.-W. A. Fong and T. S. A. Hor, *J. Chem. Soc., Dalton Trans.*, 1999, 639.
22. I. Ahmed and R. V. Parish, *J. Organomet. Chem.*, 1993, **452**, 23.
23. P. R. Oswald, R. A. Evans, W. Henderson, R. M. Daniel and C. J. Fee, *Enzyme Microb. Technol.*, 1998, **23**, 14.
24. C. Laslau, W. Henderson, Z. D. Zujovic and J. Travas-Sejdic, *Synthetic Metals*, 2010, **160**, 1173.
25. L. S. Bonnington, W. Henderson and H. H. Petach, *Enzyme Microb. Technol.*, 1995, **17**, 746.
26. W. Henderson, H. H. Petach and L. S. Bonnington, *Eur Polym. J.*, **31**, 981.
27. W. Henderson, H. H. Petach and K. Sarfo, *J. Chem.Soc., Chem. Commun.*, 1994, 245.
28. H. H. Petach, W. Henderson and G. M. Olsen, *J, Chem Soc., Chem. Commun.*, 1994, 2181.
29. K. Sarfo, H. H. Petach and W. Henderson, *Enzyme. Microb. Technol.*, 1995, **17**, 804.
30. W. Henderson, G. M. Olsen and L. S. Bonnington, *J. Chem. Soc. Chem. Commun.*, 1994, 1863.
31. B. Beele, J. Guenther, M. Perera, M. Stach, T. Oeser and J. Blümel, *New J. Chem.*, 2010, **34**, 2729.

32. G. K. Anderson, H. C. Clark, J. A. Davies, G. Ferguson and M. Parvez, *J. Crystallogr. Spectrosc. Res.*, 1982, **12**, 449.
33. M. J. Duer, *Introduction to Solid-State NMR Spectroscopy* Blackwell Publishing, Oxford, 2004.
34. G. Wu, B. Sun, R. E. Wasylishen and R. G. Griffin, *J. Magn. Reson.*, 1997, **124**, 366.
35. L. Bemi, H. C. Clark, J. A. Davies, C. A. Fyfe and R. E. Wasylishen, *J. Am. Chem. Soc.*, 1982, **104**, 483.
36. C. Perruchot, M. A. Khan, A. Kamitsi, S. P. Armes, J. F. Watts, T. von Werne and T. E. Patten, *Eur. Polym. J.*, 2004, **40**, 2129.
37. J. C. Muijsers, J. W. Niemantsverdriet, I. C. M. Wehman, D. M. Grove and G. van Koten, *Inorg. Chem.*, 1995, **31**, 2655.
38. R. A. P. Smith, *Platinum Metals Rev.*, 2009, **53**, 55.
39. R. A. P. Smith, *Platinum Metals Rev.*, 2009, **53**, 109.
40. C. J. Vedrine, *J. Phy. chem*, 1978, **82**, 1515.
41. A. R. Silva, V. Budarin, J. H. Clark, B. de Castro and C. Freire, *Carbon*, 2005, **43**, 2096.
42. M. R. Mucalo and C. R. Bullen, *J. Mater. Science. Lett.*, 2001, **20**, 1853.
43. C. Battistoni, G. Mattogno and D. M. P. Mingos, *Inorg. Chim. Acta*, 1984, **86**, L39.
44. B. H. Aw, K. K. Looh, H. S. O. Chan, K. L. Tan and T. S. A. Hor, *J, Chem Soc., Dalton Trans*, 1994, 3177.
45. R. Cook, E. A. Crathorne, A. J. Monhemius and D. L. Perry, *Hydrometallurgy*, 1989, **22**, 171.
46. J. F. Mouder, W. F. Stickle, P. E. Sobol and K. D. Bomben, *Handbook of X-ray photoelectron Spectroscopy: A Reference Book of Standard Spectra for Identification and Intepretation and Identification of XPS data*, Physical Electronics, Eden Prairie, Minnesota, U. S. A, 1995.
47. J. Fawcett, P. A. T. Hoye, R. D. W. Kemmitt, D. J. Law and D. R. Russell, *J. Chem. Soc., Dalton Trans.*, 1993, 2563.

Appendix I

General Experimental Procedures

A.1 General Experimental Techniques

All the compounds used or prepared in this study are not oxygen or moisture sensitive and do not require reactions to be carried out under an inert atmosphere. All the reactions were carried out under normal laboratory conditions. Reactions involving suspected carcinogenic and corrosive compounds like benzene, and chloroactylchloride were handled in a fume hood and accordance with MSDS safety instructions.

A.2 Melting Point and Elemental Analysis

Melting point determinations were undertaken on a Reichert Thermopan Melting Point Machine and are uncorrected. Carbon, Hydrogen and Nitrogen microelemental analyses were undertaken on vacuum dried samples at Campbell Microanalytical Laboratory, University of Otago.

A.3 Mass Spectroscopy

Electrospray ionization mass spectra were obtained on a Fisons Instruments VG Platform II using Mass Lynx V. 2.0 software. The screening and monitoring of promising reactions and characterisation of isolated products were carried out at cone voltages 20 in positive -ion mode. In all cases the practical isotope patterns generated on the ESI-MS platform was compared with theoretical isotope patterns generated using the **Isotope** pattern calculator[1]. Methanol was used as the solvents and no ionisation agents were necessary. Using methanol as

the mobile phase, approximately 1 mg of the solid or 1 drop of reaction solution was dissolved in 1 mL of the mobile phase in an Eppendorf vial, and after centrifuging to isolate any suspended solid matter is then immediately injected into the ESI-MS. In instances where compounds were insoluble in the mobile phase, the compound was dissolved in a few drops of CH_2Cl_2 before addition of the mobile phase.

A.4 ICP-MS

Elemental (platinum) analyses were done by ICP-MS after ashing and digesting the platinum samples to remove the polymer framework and inorganic contents. The samples were diluted by a factor of 10,000 in type 1 water. The ICP-MS analysis was carried out on a Perkin Elmer Elan DRCII instrument using a Cetac ASX 520 auto sampler. The software used was the Elan 3.4 version. The samples were run against a 1ppm calibration standard made up in 1% HCl and 1% HNO3. Platinum being a 'sticky' element it requires the presence of HCl to completely wash it out of polyprop tubes and to avoid carry-over errors between samples. Thus flush blanks containing HCl were used after each sample. The platinum signals were drift corrected by the use of 20 ppb Lutetium as an internal standard. The calibration standard was cross-checked by using a separate commercial 1 ppm platinum standard. The instrument was running in peak hopping scan mode with 50 ms dwell time for each mass.

A.5 Infrared Spectroscopy

Infrared spectra were recorded out on a Perkin Elmer Spectrum 100, FT - IR spectrometer. The spectra were obtained on a disc of 1:10 ratio of the compound and KBr. Observations were made of the carbonyl stretching region carbonyl group (>C=O), (1800-1600 cm^{-1}) , azomethine (>C=N) and amine (>NH) in appropriate compounds.

A.6 Nuclear Magnetic Resonance (NMR) Spectroscopy

NMR spectroscopy was performed using either a Bruker DRX 300 (^1H 300.13 MHz, ^{13}C 75.47 MHz, ^{31}P 121.49 MHz) or Bruker Avance DRX 400 (^1H

400.13 MHz, ^{13}C 100.61 MHz) spectrometer at 30 °C and processed with Topspin-NMR software. Deuterated solvents used for the NMR include $CDCl_3$, CD_2Cl_2 $(CD_3)_2SO$ and D_2O, with ^1H and ^{13}C spectra referenced to TMS (Me_4Si) and ^{31}P spectra referenced to 85% H_3PO_4. In some instances where the 10 mL probe was used, the compounds were dissolved in $CDCl_3$, CD_2Cl_2 or $(CD_3)_2SO$ in a 5 mL NMR tube and inserted in D_2O (as external lock) in a 10 mL tube. In addition to the basic NMR experiments, 1-D and 2-D experiments were performed to fully assign the NMR signals of some compounds.

1D-SELTOCSY experiments were performed to distinguish the ^1H NMR signals in derivative containing many *J* coupled protons. In the experiment one proton signal was irradiated at different mixing time (e.g. 30 ms, 40 ms, 60 ms and 80 ms) and the signal is transferred from it to all the other *J*-coupled protons in a stepwise process. That is, the signals are correlated to the irradiated signal in a peak intensity progression. This was used to assign the NMR signals, e.g. is the ^1H NMR of **3.5b·$(PF_6)_2$** in Section 3.4.1. HSQC (Heteronuclear Single Quantum Coherence) experiments indicates $^1J_{CH}$ and shows which protons are coupled to which carbons, e.g. HSQC of **4.3b·$(PF_6)_2$** shown in Section 4.5.

^1H-^1H COSY (COrrelation SpectroscopY) spectrum was used to determine and correlate the signal arising from neighbouring protons. A correlation (cross peak) appears if the signals are coupled to each other. The standard ^1H-^1H COSY was used was optimised for $^1J_{HH}$ coupling, an example is shown in Figure A.1 which shows ^1H-^1H COSY of **2.7b**. The $^1J_{HH}$ and $^2J_{HH}$ coupling can clearly be seen and from this the order of the protons in the attached group can be determined. The proton at 6.76 ppm (Hc) shows a correlation (a cross peak) to the proton at 3.40 ppm (Hb); the protons at 3.40 ppm (Hb) correlating to the protons at 1.26 ppm (Ha); the protons at 3.52 ppm (He) correlate to the protons at 2.31 ppm (Hd).

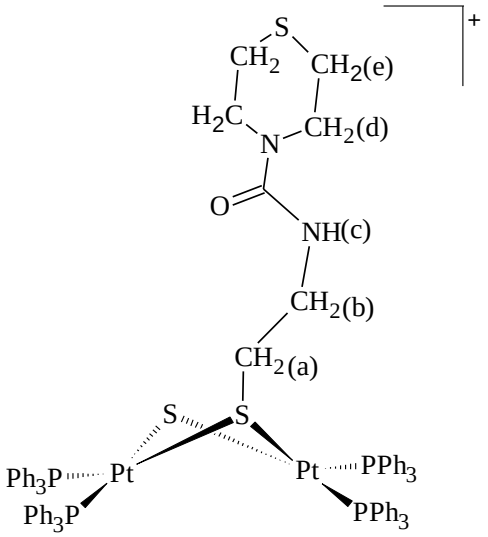

2.7b

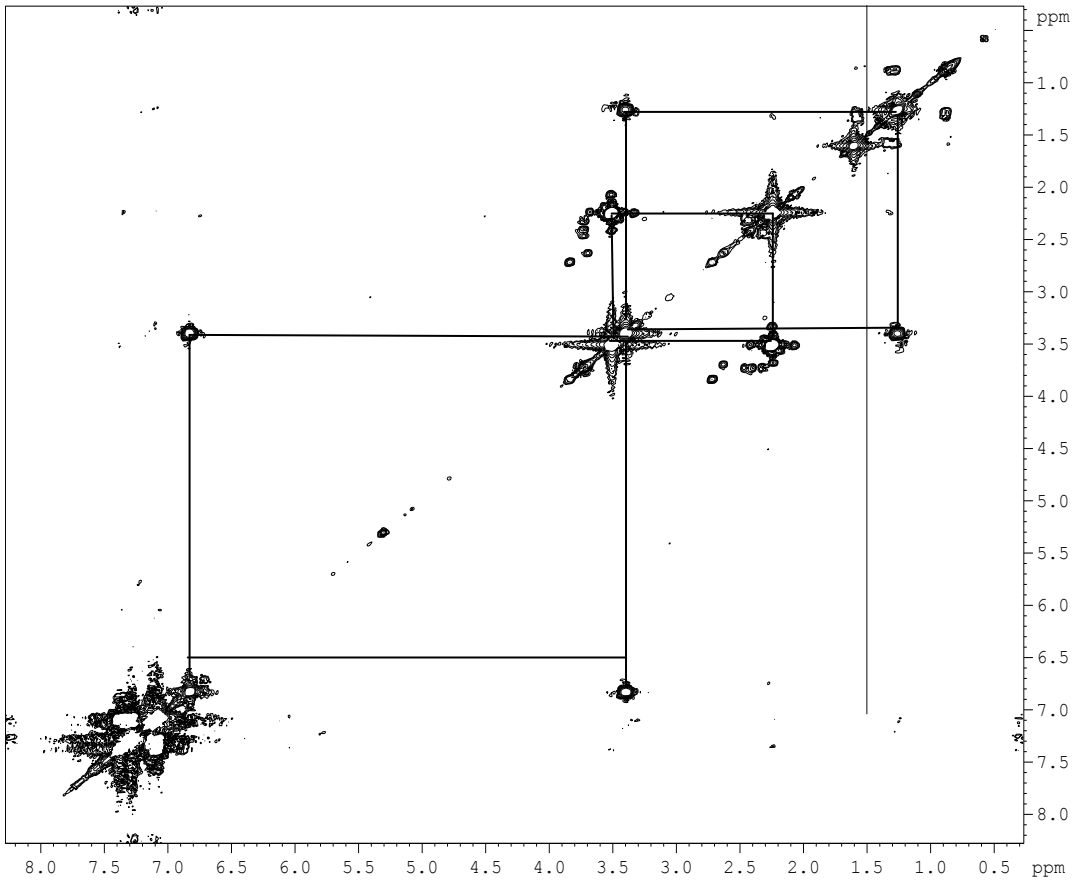

Figure A.1 ^{1}H-^{1}H COSY spectrum of **2.7b**

A.7 X-ray Crystallography

Generally preliminary investigations were undertaken by viewing the isolated crystals under a microscope at x100 magnification. This gave an indication of the stability of the dried crystal and quality for data acquisition. Intensity data sets of crystal structure determination were collected by University of Auckland, University of Canterbury and the National University of Singapore. Unless otherwise stated, were equipped with a Bruker SMART APEX II diffractometer equipped with a CCD area detector using MoKα radiation (λ = 0.71073 Å). The software SMART[2] was used for the collection of data frames, for indexing reflections, and to determine lattice parameters; SAINT[2] was used for the integration of the intensity of the reflections and for scaling; SADABS[3] was used for empirical absorption correction. The structures were solved using by direct method or Patterson (heavy atom) option of SHELXS-97[4]. Structure refinement of the data and reporting was carried out by SHELXL-97[5]. A final check on the crystallographic information file utilised PLATON[6]. All programmes were ran under the WINGX suite of programs[7]. The structures were refined by full-matrix least-squares based on F_o^2 (SHELXL-97[5]). The program Ortep3v2 (version 2.02)[8] or Mercury 2.3 (Cambridge Crystallographic Data Centre (CCDC) program) were used to view and generate the structures diagrams. Complete tables of bond lengths, bond angles, final position parameters and thermal parameters are presented on a CD (inside back cover) in the form of the CIF files.

A.8 References

1. L. J. Arnold, *J. Chem. Educ.*, 1992, **69**, 811.
2. SMART and SAINT, in *Software Reference Manuals, version 4.0, Siemens Energy & Automation Inc., Analytical Instrumentation* Madison, WI (USA), Editon, 1996.
3. G. M. Sheldrick, in *SADABS, a software for empirical adsorption correction* University of Göttingen, Göttingen, Germany, Editon edn., 1993.
4. G. M. Sheldrick, in *SHELXS-97 Programs for the Solution and Refinement of Crystal Structures*, University of Göttingen, Germany, Editon, 1997.

5. G. M. Sheldrick, in *SHELXL-97 Programs for the Solution and Refinement of Crystal Structures*, University of Göttingen, Germany, Editon, 1997.
6. A. L. Spek, *J. Appl. Cryst.*, 2003, **36**, 7.
7. L. J. Farrugia, *J. Appl. Cryst.*, 1999, **32**, 837.
8. L. J. Farrugia, *J. Appl. Cryst.*, 1997, **30**, 565.

Appendix II

List of Isolated Compounds

A .2 List of Isolated Compounds

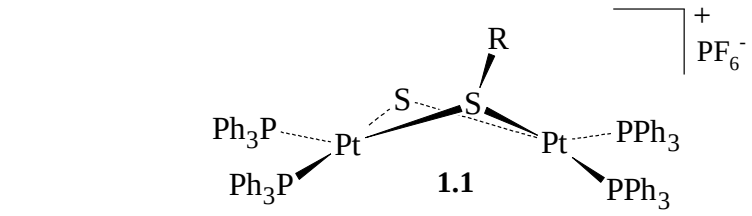

1.1

R =

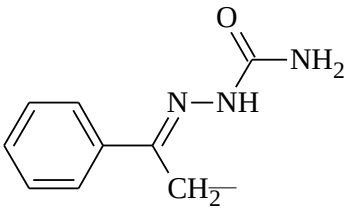

2.1b

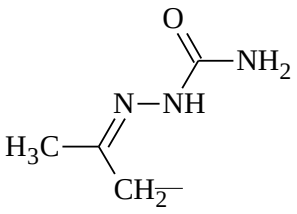

2.2b

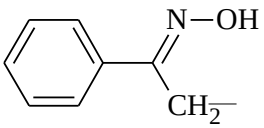

2.3b

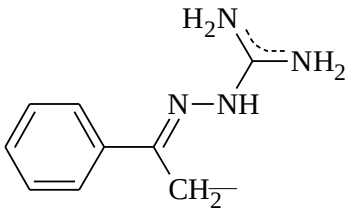

2.4b

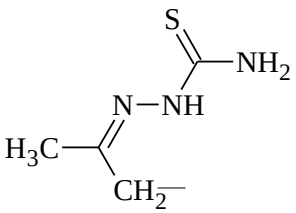

2.5b

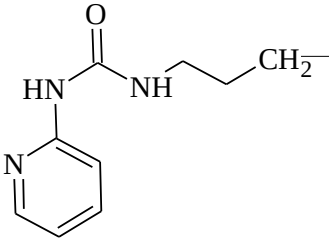

2.6b

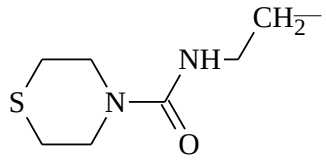

2.7b

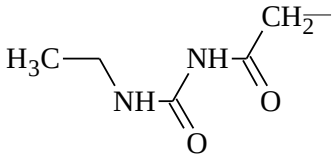

2.8b

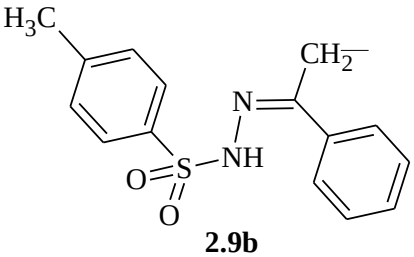

2.9b

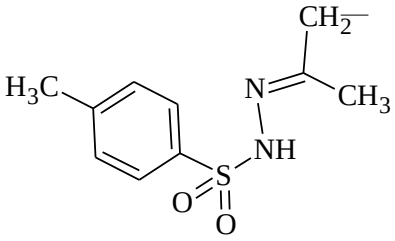

2.10b

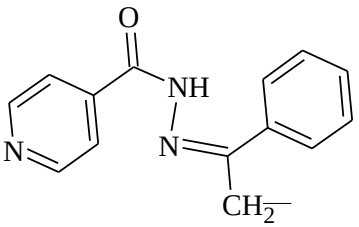

2.11b

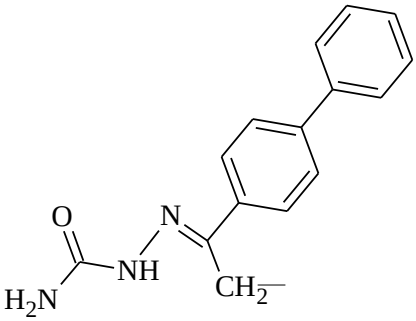

2.12b

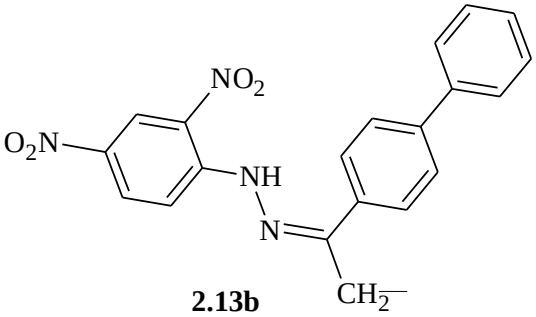

2.13b

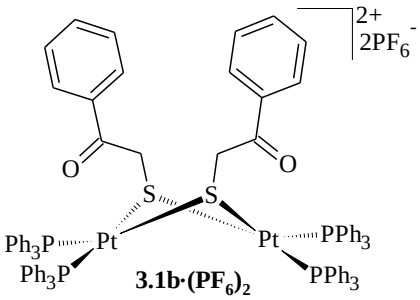

3.1b·$(PF_6)_2$

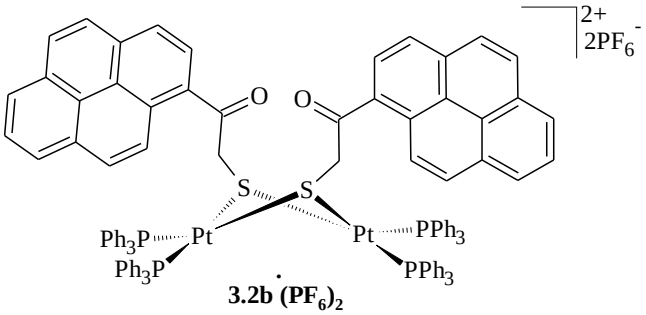

3.2b·$(PF_6)_2$

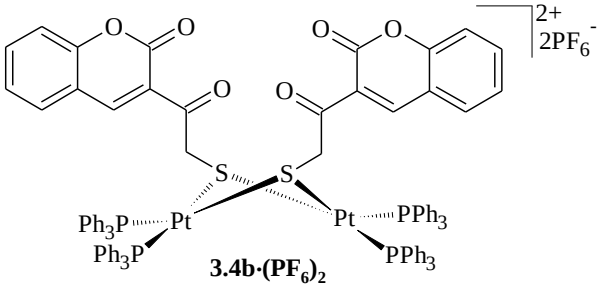

3.4b·(PF$_6$)$_2$

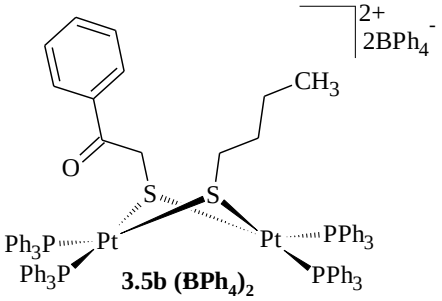

3.5b (BPh$_4$)$_2$

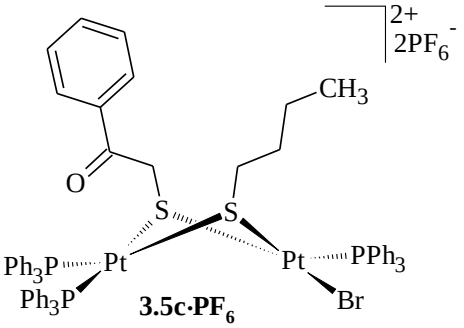

3.5c·PF$_6$

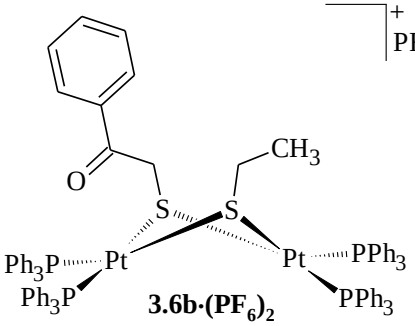

3.6b·(PF$_6$)$_2$

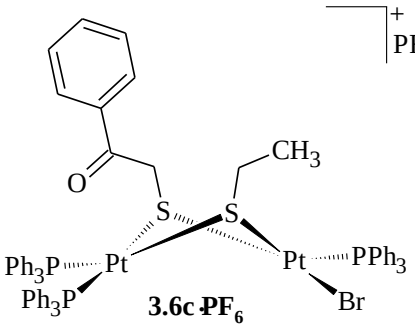

3.6c·PF$_6$

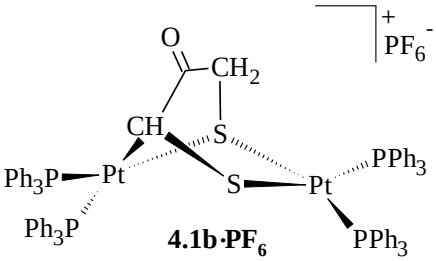

4.1b·PF$_6$

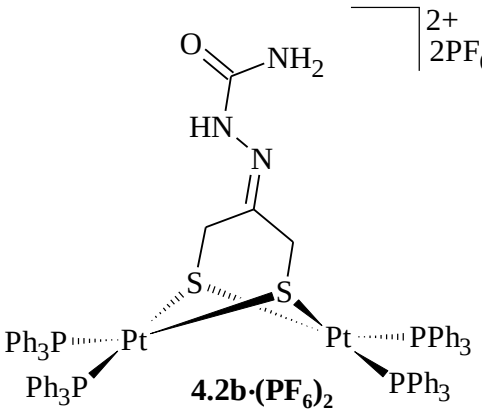

4.2b·(PF$_6$)$_2$

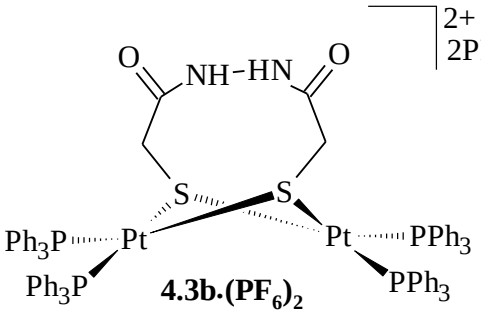

4.3b.(PF$_6$)$_2$

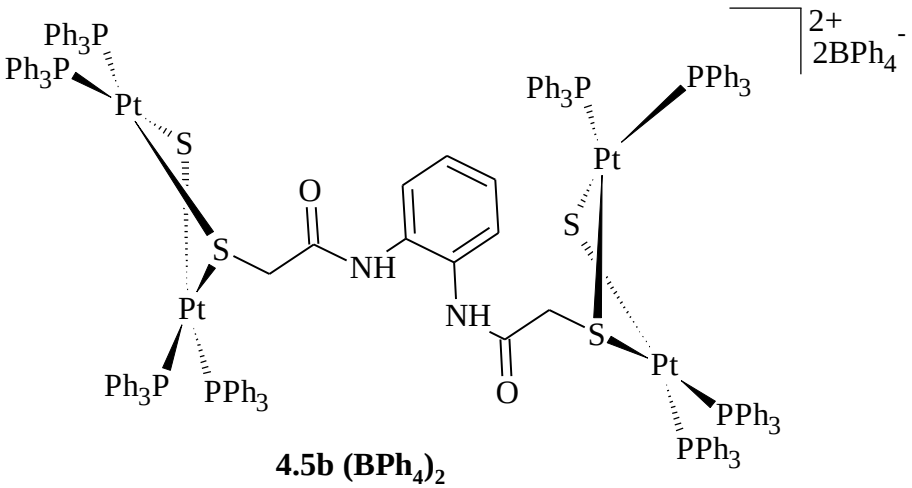

4.5b $(BPh_4)_2$

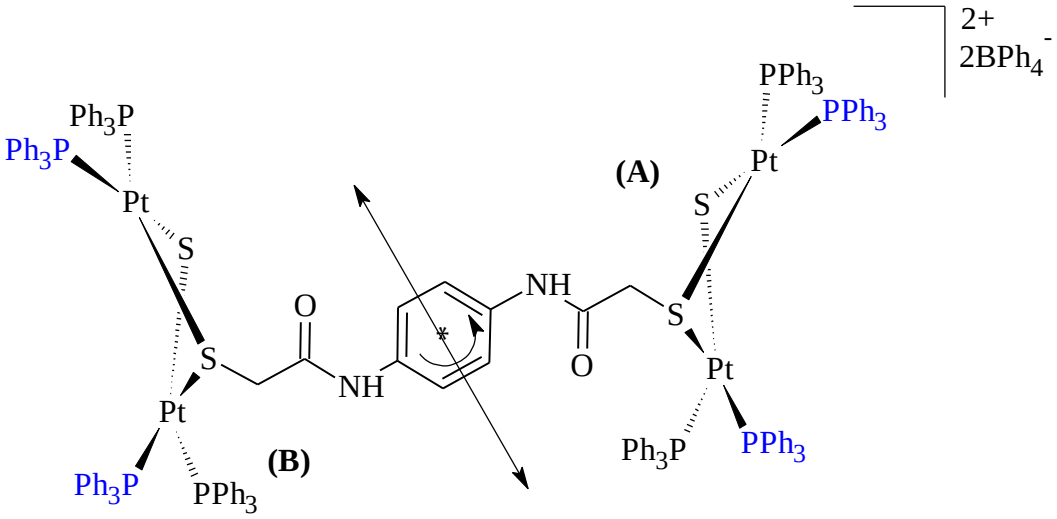

4.4b·$(BPh_4)_2$

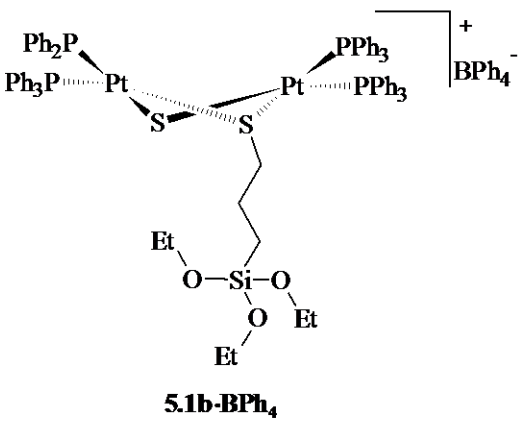

5.1b-BPh_4

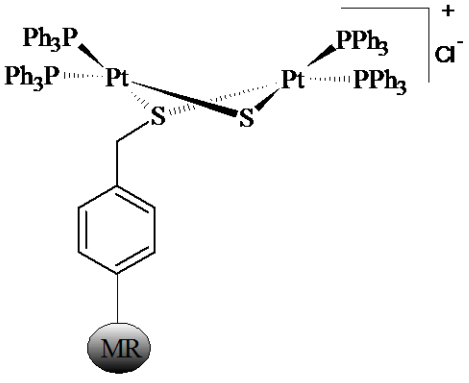

5.2b

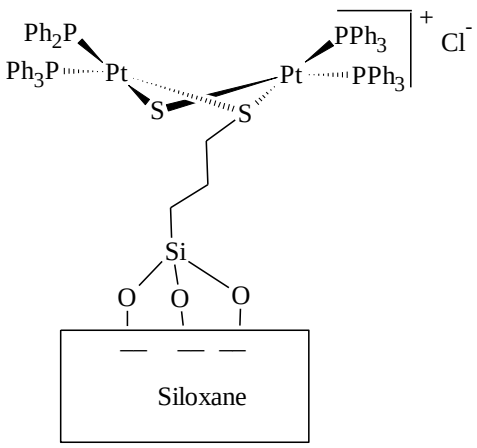

5.3b

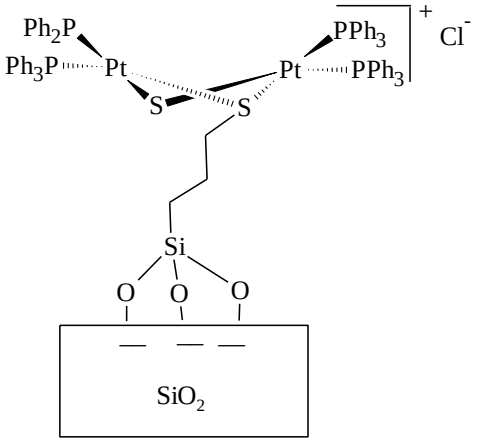

5.4b

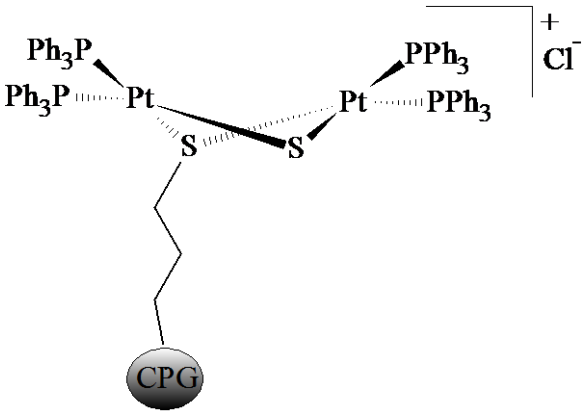

5.5b

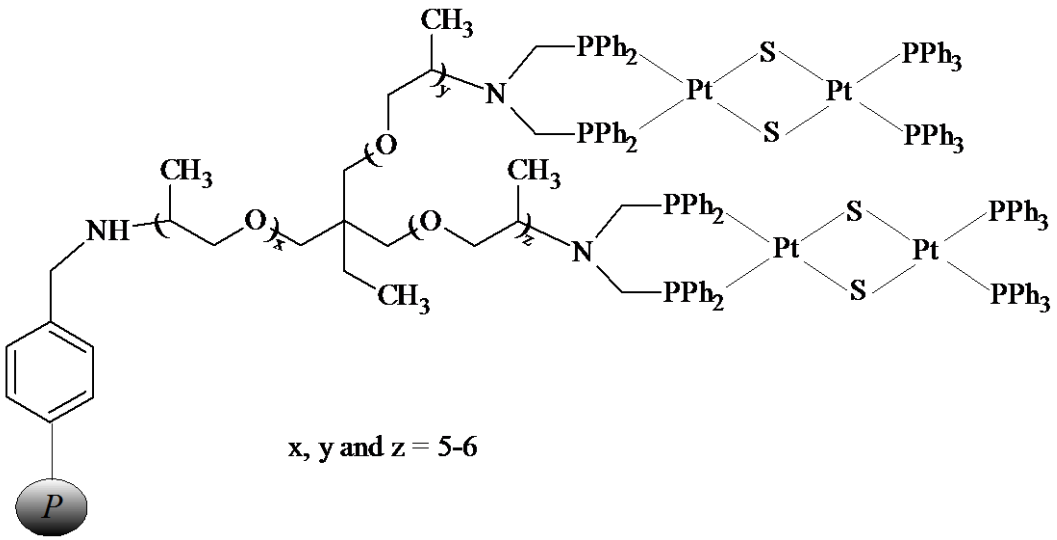

x, y and z = 5-6

5.7b

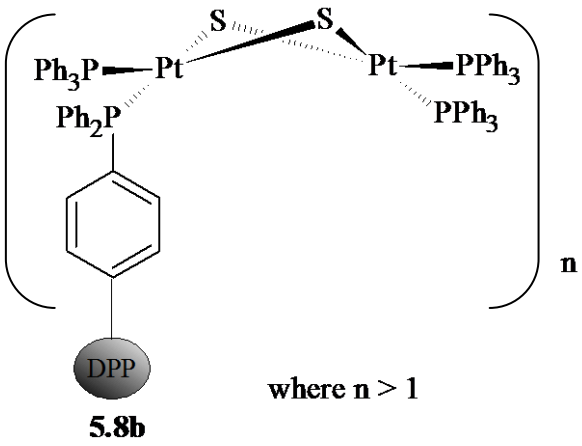

where n > 1

5.8b

Appendix III

List of Publications

1. **Further studies on the dialkylation chemistry of $[Pt_2(\mu\text{-}S)_2(PPh_3)_4]$ with activated alkyl halides $RC(O)CH_2X$ (X = Cl, Br)**
Ujam, Oguejiofo T , Henderson, William , Nicholson, Brian K , Hor, T S A
Parent Document: Inorganica Chimica Acta, Volume 376, 255-263
Category: Refereed Journal Articles
Year Published: 2011

2. **The reactivity of $[Pt_2(\mu\text{-}S)_2(PPh_3)_4]$ towards difunctional chloroacetamide alkylating agents: Formation of cyclized or bridged products**
Ujam, Oguejiofo T , Henderson, William , Nicholson, Brian K , Christopher M. Fitchett
Parent Document: Inorganica Chimica Acta, Volume 375, 220-227
Category: Refereed Journal Articles
Year Published: 2011

3. ***E/Z* isomerism in monoalkylated derivatives of $[Pt_2(\mu\text{-}S)_2(PPh_3)_4]$ containing 2,4-dinitrophenylhydrazone substituents**
Ujam Oguejiofo T, Henderson, William , Alistair L. Wilkins, Nicholson, Brian K
Parent Document: Journal of Coordination Chemistry, Volume 64, 2782–2790
Category: Refereed Journal Articles
Year Published: 2011

4. **Dinuclear platinum complexes with designer thiolate ligands from the monoalkylation of $[Pt_2(\mu\text{-}S)_2(PPh_3)_4]$**
Ujam, Oguejiofo T , Devoy, Sarah M , Henderson, William , Nicholson, Brian K , Hor, T S A
Parent Document: Inorganica Chimica Acta, Volume 363, 3558-3568
Category: Refereed Journal Articles
Year Published: 2010

5. **Electrospray Ionisation Mass Spectrometry (ESI-MS) directed multifunctional alkylation of $[Pt_2(\mu\text{-}S)_2(PPh_3)_4]$**
Ujam, Oguejiofo , Henderson, William , Nicholson, Brian K , Hor, T.S. A.
Parent Document: M5 5th Australian Organometallics Meeting
Category: Conference – Abstract
Year Published: 2010

6. **Electrospray Ionisation Mass Spectrometry (ESI-MS) monitored synthesis and characterisation of multifunctional alkylated derivatives of $[Pt_2(\mu\text{-}S)_2(PPh_3)_4]$**
Ujam, Oguejiofo T , Henderson, William , Nicholson, Brian K , Hor, T.S. A.
Parent Document: Inorganic Chemistry Conference (IC08)
Category: Conference – Abstract
Year Published: 2008